OMEE

Book of Abstracts

International Conference on

Oxide Materials for Electronic Engineering – fabrication, properties and applications

OMEE-2021

September 28 – October 2, 2021
Lviv, Ukraine

OMEE-2021

Ministry of Education and Science of Ukraine
Lviv Polytechnic National University

Book of Abstracts

International Conference on Oxide Materials for Electronic Engineering – fabrication, properties and applications

OMEE-2021

September 28 – October 2, 2021
Lviv, Ukraine

Lviv
Lviv Polytechnic Publishing House
2021

Міністерство освіти і науки України
Національний університет “Львівська політехніка”

Збірник тез

Міжнародної наукової конференції “Оксидні матеріали електронної техніки – отримання, властивості, застосування”

OMEE-2021

28 вересня – 2 жовтня, 2021
Львів, Україна

Львів
Видавництво Львівської політехніки
2021

УДК 521.315.61
О 64

Збірник тез Міжнародної наукової конференції “Оксидні матеріали електронної техніки – отримання, властивості, застосування” (ОМЕЕ-2021) / упор. М. В. Шпотюк. – Львів: Видавництво Львівської політехніки, 2021. – Режим доступу: http://science.lpnu.ua/omee-2021/book-abstracts-omee-2021 вільний. – Заголовок з екрана. – Мова укр. і англ..

О 64

ISBN 978-966-941-629-2

У збірнику подані тези доповідей Міжнародної наукової конференції “Оксидні матеріали електронної техніки – отримання, властивості, застосування” (ОМЕЕ-2021). Конференція присвячена актуальним проблемам технології отримання та дослідження структурних, оптичних, магнітних та електрофізичних властивостей оксидних матеріалів, а також можливості їх практичного застосування у пристроях електронної техніки та розроблення нових функціональних пристроїв на їх основі.

Для науковців та аспірантів, які працюють в галузі фізики оксидних матеріалів.

УДК 521.315.61

Відповідальний за випуск – М. В. Шпотюк
Усі матеріали подано в авторській редакції

ISBN 978-966-941-629-2

Preface

Dear Colleagues,

Welcome to the 6th International Conference on Oxide Materials for Electronic Engineering – fabrication, properties and applications (OMEE-2021) in Lviv, Ukraine, September 28 – October 2, 2021. Lviv Polytechnic National University has an honour to host this scientific meeting that continues the good tradition that has been commenced as a local workshop in Lviv, which gathered researchers and engineers of several educational and scientific institutions of our city engaged in technology, studying and practical developments of oxide materials for electronic engineering. Afterwards this tradition was continued as series of international scientific workshops. The first one, in 2007, was devoted to the memory of Prof. Andriy O. Matkovskii (1954-2004) who initiated these meetings. The extended subject matters as well as geography of participants of the second workshop in 2009 allowed thinking about new format of the OMEE meeting. Since 2012 this event was hold as an international conference. Thus, it is already the sixth international scientific forum on Oxide Materials for Electronic Engineering in Lviv Polytechnic National University. This meeting was supposed to take place in 2020, but the pandemic prompted us to change the dates of the conference. Also OMEE-2021 will be held in a mixed format due to the same circumstances – some of the keynote lectures will be presented online. But we are very pleased that even in these circumstances, more than 100 participants representing contributions from 34 scientific, educational and R&D institutions from 13 countries (Belarus, Estonia, Georgia, Germany, Hungary, Latvia, Poland, Portugal, Slovenia, Turkey, Ukraine, United Kingdom, USA) decided to participate in OMEE-2021 and have kept up this tradition. We are particularly pleased that 36 young scientists are participating in OMEE 2021 and have received a discounted participation fee owing to our sponsors as well as due to the keynote lecturers supported the participation of young researchers by paying a full fee. Experienced scientists and young researchers, experimentalists and theoreticians in different fields of chemistry and physics, technology and engineering will have a forum for direct and unimpeded discussion of their results and new trends, exchange of knowledge and ideas, joining their efforts in collaboration and multidisciplinary research. The current Conference Program covers the topics of material science and technology, chemistry and physics of solid state, structure peculiarities on different scales, interconnection of chemical composition, structure and properties of oxides, their modification under external influence, developments of new methods of study and new applications of oxide materials in variety fields of electronic engineering. This collection contains abstracts of contributions submitted to the OMEE-2021 Conference. I hope that the most of participants will present the investigations in the form of scientific papers, which will be published as an issue of *Acta Physica Polonica A* journal as a result of the conference. On behalf of the Local Organizing Committee and Lviv Polytechnic National University which hosts the OMEE-2021 Conference, I would like to thank to all participants, to co-organizing institutions − the Scientific Research Company "Electron-Carat" (Lviv, Ukraine), Institute of Physics of the Polish Academy of Sciences (Warsaw, Poland), as well as to the IMAGE Project of Horizon 2020 Programme, Lviv Convention Bureau and Programme “Scientific Lviv”, the International Diffraction Data Center (ICDD) (USA) and Seltok Photonics company (Kyiv, Ukraine), which financially supported the Conference. We are looking forward for successful meeting as well as a pleasant and memorable stay in the ancient Lviv.

OMEE Conference Chair  Sergii Ubizskii, Dr.Sc., Prof.

Conference Board

Organizers

Lviv Polytechnic National University (Ukraine)
Institute of Physics of the Polish Academy of Sciences (Poland)
NGO «Cultural Initiatives Support and Development Center»
Scientific Research Company "Carat" (Ukraine)

Supported by

IMAGE Project (#778156 – IMAGE – H2020-MSCA-RISE-2017)
Lviv Convention Bureau and co-financed by Programme "Scientific Lviv"

Sponsors

International Centre for Diffraction Data (ICDD), USA
Seltok Photonics, Ukraine

International Advisory Committee

D.K. Becker (Germany)
A. Belous (Ukraine)
U. Bismayer (Germany)
Yu. Bobalo (Ukraine)
M. Vakiv (Ukraine
R. Gladyshevskii (Ukraine)
Yu. Grin (Germany)
M. Leoni (Italy)
A. Suchocki (Poland)

Program Committee

M. Berkowski (Poland)
M. Godlewski (Poland)
P. Esquinazi (Germany)
M. Fontana (France)
H. Fritze (Germany)
E. Hristoforou (Greece)
A. Kamińska (Poland)
L. Kovacs (Hungary)
N. Kuleshov (Norway)
A. Luchechko (Ukraine)
M. Manfred (Germany)
V. Mykhaylyk (UK)
W. Paszkowicz (Poland)
A. Popov (Latvia)
A. Senyshyn (Germany)
I.M. Solskii (Ukraine)
G. Suchanek (Germany)
D. Sugak (Ukraine)
M.Takeshi (Japan)
S. Ubizskii (Ukraine)
L. Vasylechko (Ukraine)
A. Andrushchak (Ukraine)
Ya. Zhydachevskyy (Poland)
E. Zych (Poland)

Local Organizing Committee

S. Ubizskii (Chairman)
N. Martynyuk
U. Yakhnevych
O. Buryy
L. Kovalyk
V. Hreb
O. Pavlovska
M. Shpotyuk
D. Sugak
S. Turchak
L. Vasylechko

Abstracts

SECTION 1

TECHNOLOGY OF FUNCTIONAL MATERIALS FABRICATION

Oxides by Atomic Layer Deposition - from Applications in Nano-Electronics to Photovoltaics

M. Godlewski, R. Pietruszka, A. Seweryn, M. Ożga and B.S. Witkowski

Institute of Physics of the Polish Academy of Sciences PL-02668, Al. Lotników 32/46, Poland

Technology of Atomic Layer Deposition (ALD) was first introduced in Finland in 70s of XX century. The ALD was initially applied to deposit ultra-thin films of ZnS:Mn and dielectric films (so-called high-k oxides). Their properties were optimized for applications in thin film electroluminescence displays (TFEL). Later on several Rare Earth doped layers were also tested for the above application.

A real breakthrough in the ALD technology came with application of high-k oxides in nano-electronics. ALD-deposited ultra-thin films of HfO_2 replaced SiO_2/SiON as a gate oxide in Si-based field effect transistors. This was followed by use of ALD-deposited films in memories and transparent electronics.

Soon after several new applications of this deposition method were demonstrated. The latter is due to the fact that ALD-deposited materials show wide range of properties required for new applications, not only in electronics or in photovoltaics, as discussed, but, for example, in medicine, as well. On one hand perfect isolating films can be deposited by the ALD, but highly conducting films (metallic conductivity), can also be produced. Thus, films for range of applications can be prepared.

In the talk some of these new applications will be discussed together with discussion of materials properties, based on the results obtained in the ALD laboratory in the Institute of Physics of the Polish Academy of Sciences in Warsaw.

Acknowledgments. The present research was partly supported by the NCBR National Centre for Research and Development) project TECHMATSTRATEG1/347431/14/NCBR/2018.

Wide Band Gap Oxide Semiconductors for Electronics that Can Operate at High Temperature and High Power

A. Zakutayev

National Renewable Energy Laboratory, Golden, Colorado, USA

Oxide semiconductors have been widely used in many applications, such as transparent conductive electrodes in solar cells, and channel layers in transparent thin film transistors. Such applications require semiconductors with wide band gaps, suitable electronic doping, and good charge carrier transport, as materials properties. The same properties are also necessary for semiconductors used in electronic devices that can operate at high power, high frequency, and high temperature. Historically these applications have been dominated by carbide (SiC) and nitrides (GaN) wide band gap semiconductors. Recently gallium oxides (Ga_2O_3) has attracted great research attention for power electronic applications, because of high theoretical performance limit (Baliga's figure of merit), and due to availability of high-quality Ga_2O_3 single crystal substrates. However, Ga_2O_3 also faces several technical challenges for power conversion, such as low thermal conductivity and difficulty in *p*-type doping. These problems may not be as important for radio-frequency (RF) unipolar devices, and for high-temperature electronic applications. In fact Ga_2O_3 may have other advantages for electronics that operates at high temperature and in harsh environments, such as ultra-wide band gap (4.8 eV) and good thermal stability (resistance to further oxidation).

In this presentation, I will describe our ongoing experimental efforts to develop wide band gap oxide semiconductors for electronics that can operate at high temperature and high power. High-quality low-doping Ga_2O_3 layers are grown by molecular beam epitaxy (MBE) on single crystal Sn:Ga_2O_3 substrates across a wide range of growth conditions. The structural quality of the samples is characterized by skew asymmetric x-ray diffraction (XRD) at grazing incidence angles, to deconvolution the signals of the homo-epitaxial from that of the substrate. The resulting layers are processed into diodes using simple etching and metallization procedures to form Schottky and Ohmic contacts, as well as novel *p*-type oxide heterojunction partners. The diodes are characterized by current-voltage (J-V) and capacitance-voltage (C-V) measurements at room temperature to extract materials properties, and as a function of increasing temperature and operation time to demonstrate device reliability. The results indicate that these Ga_2O_3 devices are suitable for high-temperature electronic devices such as sensors and amplifiers.

In this presentation, I will also mention recent modeling efforts that support ongoing experimental developments. The results of techno-economic analysis of the manufacturing cost of Ga_2O_3 wafers will be presented, supporting their projected cost advantage compared to SiC and GaN [1] Finite element analysis of electrical and thermal performance of vertical Ga_2O_3 transistors reported in literature will be demonstrated, comparing MOSFET to FinFET device architectures [2]. The findings of first-principles computational search for wide band gap semiconductors with high figures of merit and large thermal conductivity will be discussed [3], highlighting new oxide material candidates (beyond Ga_2O_3) for power-electronic and high-temperature applications.

[1] Reese, S. B., Remo, T., Green, J., & Zakutayev, A. How Much Will Gallium Oxide Power Electronics Cost? *Joule* 3, 1 (2019)

[2] Kotecha, R., Metzger, W., Mather, B., Narumanchi, S., & Zakutayev, A. Modeling and Analysis of Gallium Oxide Vertical Transistors, *ECS Journal of Solid State Science and Technology*, 8, Q3202 (2019)

[3] Gorai, P., McKinney, R. W., Haegel, N. M., Zakutayev, A., & Stevanovic, V. A computational survey of semiconductors for power electronics, *Energy & Environmental Science* 12, 3338 (2019).

High-Temperature Oxidation of Ti-Al-C MAX Phases-Based Bulk Materials and Coatings, Variation of Their Electrical Conductivity

T.A. Prikhna[1], O.P. Ostash[2], A.S. Kuprin[3], V.Ya. Podhurska[2], T. Cabioc`h[4], T.B. Serbenyuk[1], M.V. Karpets[1], B. Matovic[5], S.S. Ponomarov[6], V.B. Sverdun[1], B.D. Vasyliv[2], V.E. Moshchil[1], G.N. Tolmachova[3], M.A. Bortnitskaya[3], P. Barvitskyi[1] and O.V. Matsenko[1]

[1]*V. Bakul Institute for Superhard Materials of the National Academy of Sciences of Ukraine, 2, Avtozavodskaya str., Kyiv, 04074, Ukraine (prikhna@ukr.net, serbenuk@ukr.net, vsverdun@ukr.net, mkarpets@ukr.net, ardna@ukr.net)*

[2]*Karpenko Physico-Mechanical Institute of the National Academy of Sciences of Ukraine, 5, Naukova str. Lviv, 79060, Ukraine (orest.ostash@gmail.com, podhurskavika@gmail.com, mechengin1111@gmail.com)*

[3]*National Science Center Kharkov Institute of Physics and Technology, 1, Akademicheskaya str., Kharkov, 61108, Ukraine (kuprin@kipt.kharkov.ua, tolmachovagn@kipt.kharkov.ua, SquirellS06@gmail.com)*

[4]*Institut PPRIME, Département de Physique et Mécanique des Matériaux, CNRS, Université de Poitiers, ENSMA UPR 3346, SP2MI, Téléport 2, Boulevard Marie et Pierre Curie, BP30179, 86962 Futuroscope Chasseneuil Cedex, France (thierry.cabioch@univ-poitiers.fr)*

[5]*Institute for Nuclear Sciences Vinca, University of Belgrade, P.Box. 522 11001 Belgrade, Serbia (mato@vin.bg.ac.rs)*

[6]*Institute of Semiconductor Physics of the National Academy of Sciences of Ukraine (NASU), 41, Nauky ave., Kyiv, 03028, Ukraine (s.s.ponomaryov@gmail.com)*

The, results of variations of structure in oxidizing atmosphere at high temperatures (after heating and thermocycling up to 600 – 1400 °C), and electrical conductivity (after long time heating at 600 °C) of MAX Ti_2AlC-, Ti_3AlC_2- and $(Ti,Nb)_3AlC_2$-based bulk materials with different porosity (prepared by synthesis in vacuum and/or by hot pressing) and coatings (vacuum-arc deposited) are presented. The characteristics of highly dense Ti-Al-C composite bulks and vacuum-arc deposited 6 μm thick coatings before and after heating at 600 °C in air for 1000 h were compared. High electrical conductivity ($\Delta m/S = 1.3 \cdot 10^6$ S/m) of the highly resistant toward oxidation ($\Delta m/S = 0.07$ mg/cm^2) Ti-Al-C coating was preserved after long-term heating in air. It was found that the specimen surface layers of MAX-phases Ti_3AlC_2 and Ti_2AlC based bulks and chromium-containing Crofer 22APU steel became semiconductors because of high-temperature long-term oxidation (at 600 °C). The vacuum-arc deposited Ti-Al-C coating revealed high oxidation resistance and electrical conductivity along with good mechanical characteristics, namely nanohardness H (10 mN)= 9.5±1.5 GPa, and Young's modulus E=190±10 GPa, which make it very promising for interconnects of solid oxide fuel cells (SOFCs).

Acknowledgements. The investigations were performed in the frames of the project NATO SPS G5773 "Advanced Material Engineering to Address Emerging Security Challenges" for 2020-2023, the project 03-03-20 of Ukrainian-Belorussian cooperation for 2020-2021, and the projects III-3-20 (0779), III-5-19 (0778), and II-5-19 (IHM-29/20) supported by the National Academy of Sciences of Ukraine.

Growth and Optical Properties of Ce^{3+} Doped $Y_{3-x}Ca_xAl_2Al_{3-x}Si_xO_{12}$ (x=0-0.5) and $Gd_{3-x}Ca_xGa_2Al_{3-x}Si_xO_{12}$ (x=0-0.3) Single Crystalline Films

V. Gorbenko[1*], T. Zorenko[1], A. Shakhno[1], S. Witkiewicz-Łukaszek[1], N. Majewska[2], T. Lesniewski[2], S. Mahlik[2] and Yu. Zorenko[1]

[1]*Institute of Physics of Kazimierz Wielki University in Bydgoszcz, 85090 Bydgoszcz, Poland*
[2]*Institute of Experimental Physics of University of Gdansk, 80-308 Gdańsk, Poland*
Corresponding author e-mail: gorbenko@ukw.edu.pl

In this work, we present the results on crystallization and investigation of the optical and photoelectrical properties of the single crystalline films (SCFs) of Ce^{3+} doped and singly Ca^{2+} and doubly Ca^{2+}-Si^{4+} co-doped of $Y_{3-x}Ca_xAl_2Al_{3-x}O_{12}$:Ce and $Gd_{3-x}Ca_xGa_2Al_{3-x}Si_xO_{12}$ (x=0-0.3) garnets, where x=0-0.5 and x=0-0.3, respectively. The SCFs were grown by the liquid phase epitaxy (LPE) method onto $Y_3Al_5O_{12}$ (YAG) and $Gd_3Ga_{2.5}Al_{2.5}O_{12}$ (GAGG) substrates, respectively, from the super-cooling melt–solution based on the PbO-B_2O_3 flux. The absorption, luminescence and photoelectrical properties of $Y_{3-x}Ca_xAl_2Al_{3-x}O_{12}$:Ce at x=0-0.5 and $Gd_{3-x}Ca_xGa_2Al_{3-x}Si_xO_{12}$:Ce at x=0-0.3 were compared with the properties of the reference YAG:Ce SCF sample.

The influence of the thermal annealing at 1300 °C in air and in 95% N_2 - 5% H_2 reducing atmosphere on the optical and photoelectrical properties of both types of SCFs was investigated as well. The results of this research can be useful for the development of luminescent materials for composite photovoltaic screens as well as for white LED converters based on the epitaxial structures of Ca^{2+}-Si^{4+} containing garnets, grown by LPE method.

Acknowledgements. The work was performed in the framework of 2019/33/B/ST3/00406 project.

Influence of Thermal Treatment on the Elimination of Impurities in ZnO Thin Films on Glass

P. Sedzicki[1], E. Nowak[2], M. Szybowicz[2] and B. Derkowska-Zielinska[1]

[1]*Institute of Physics, Faculty of Physics, Astronomy and Informatics, Nicolaus Copernicus University in Torun, Grudziadzka 5, 87-100 Torun, Poland*
[2]*Faculty of Materials Engineering and Technical Physics, Poznan University of Technology, Piotrowo 3, 60-965 Poznan, Poland*

We investigated the photoluminescence (PL) of ZnO sol-gel films. These films were coated on glass substrates using a spin-coating method and then annealed in the temperature range from 230℃ to 600℃ (see Fig. 1). The main purpose of the heat treatment was the elimination of organic waste products and the formation of a polycrystalline layer.

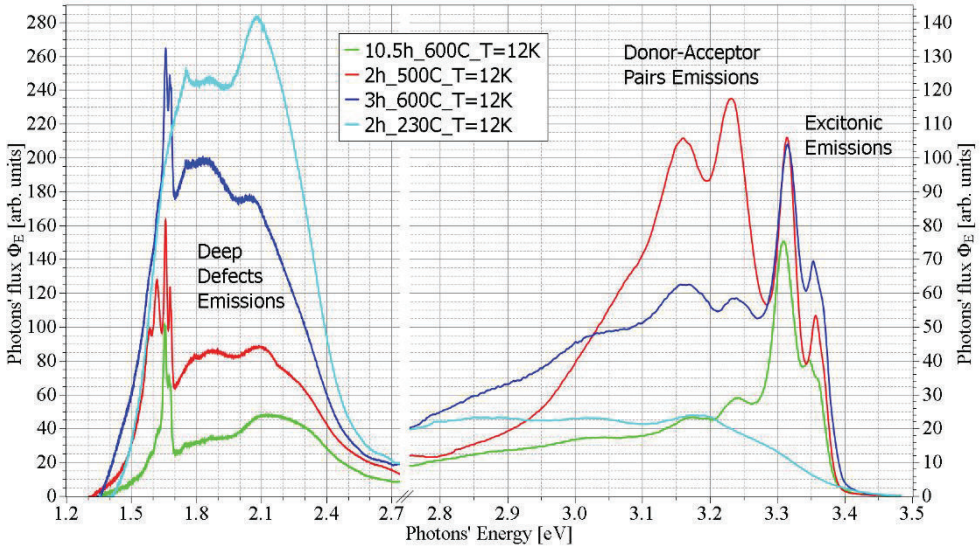

Fig. 1. Photoluminescence spectra of ZnO samples prepared with different annealing time and temperature. Spectra were collected at $T = 12$ K under constant laser excitation $\lambda_{EX} = 325$ nm. Axis break at $E = 2.7$ eV was used to zoom in the right-hand side of spectra, without additional renormalization.

In addition, the temperature dependence of photoluminescence was investigated. Gaussian deconvolution of photoluminescence was performed for spectra collected in the temperature range from $T = 12$ K to $T = 400$ K. This procedure provides insights into optically active defects formed in the samples and allows comparison between ZnO films prepared under different thermal conditions. We demonstrated that luminescence properties can be tuned by changing the annealing conditions of deposited sol-gel films. Moreover, the positions, broadening and amplitudes of the emission peaks were discussed in relation to specific defects such as zinc (and oxygen) vacancies or interstitials.

Our samples show significant differences in both the emission of the donor-acceptor pair and the emission of deep defects attributable to the annealing process. Higher temperatures and longer annealing times benefit excitonic emission, which is in good agreement with the literature. The activation energy of the individual dopants was also estimated based on spectral deconvolution.

Structural Properties of Transparent IGZO Thin Films Produced by Thermal Evaporation Technique

Atilgan ALTINKOK[1] and Murat OLUTAS[2]

[1]*National Defense University,Turkish Naval Academy, Department of Electrical and Electronics Engineering,, Istanbul, Turkey*
[2]*Abant İzzet Baysal University, Department of Physics, 14030 Bolu, Turkey*

The use of Transparent Conductive Oxide (TCO) thin films in technology has increased in the last decades. These materials have good electrical conductivity visible light transmittance simultaneously. TCOs have many technology applications such as thin film transducers (TFTs), conductive electrodes, capacitors, sensors, electrochemical devices. Although indium tin oxide (ITO) is the most widely used material among these materials, studies on N-type indium-gallium-zinc oxide (IGZO) that better electrical properties (electron mobility μ_{FE}>10 cm^2 /V.s) cm2 / Vs) have increased in recent years. In this study, IGZO thin films are produced which have a very homogeneous amorphous structure at room temperature under high vacuum by thermal evaporation system on glass substrates. Structural characterization was carried out by Atomic force microscopy, scanning electron microscopy on IGZO thin films for various thicknesses and annealing temperatures. Transmittance and thickness measurements were performed using UV-VIS spectroscopy and profilometer for the investigation of optical properties, respectively. It is seen that roughness is reduced when annealing temperature is increased.

Acknowledgements. This work was supported Giresun University Research Fund under project number FEN-BAP-A-230218-26.

Effect of $Pb(BO_2)_2$ Doping on Power Factor of $Bi_2Sr_2Co_{1.8}O_y$ Thermoelectric Ceramics

G.A. Mumladze[1], I.G. Kvartskhava[1], V.V. Zhghamadze[1], N.G. Margiani[1] and A.S. Kuzanyan[2]

[1]*Institute of Cybernetics of the Georgian Technical University*
[2]*The Institute for Physical Research of National Academy of Sciences of Armenia*

In this work, thermoelectric materials with composition $Bi_{2-x}[Pb(BO_2)_2]_xSr_2Co_{1.8}O_y$ (x=0, 0.075, 0.15, and 0.25) were prepared through the solid-state reaction method. Resistivity and Seebeck coefficient of the synthesized samples were measured in the temperature range 25-650°C, and the power factor was calculated. The preliminary results obtained show that doping of $Bi_2Sr_2Co_{1.8}O_y$ by lead borate — $Pb(BO_2)_2$ leads to the marked decrease of electrical resistivity, while not remarkably affecting the Seebeck coefficient. For x = 0.075-0.15 dopant content, 2.1-2.4 and 1.6-fold decrease of resistivity was observed compared to the reference sample at 25 and 650 °C, respectively. When x = 0.15, $Pb(BO_2)_2$-doped sample exhibits a power factor of 0.04 mW/m·K^2 with a Seebeck coefficient of 175 μV/ K and a resistivity of 80 mohm·cm at 650 °C.

Acknowledgment. This work was supported by Shota Rustaveli National Science Foundation (SRNSF) [FR-18-4976/Tuning the functional properties of Co-based thermoelectrics via doping and high-energy ball milling].

Improvement of $Bi_2Ca_2Co_{1.7}O_y$ Thermoelectric Properties by $Pb(BO_2)_2$ Doping

V.V. Zhghamadze[1], N.G. Margiani[1], A.I. Klyndyuk[2], G.A. Mumladze[1], A.S. Kuzanyan[3], I.G. Kvartskhava[1] and G.R. Badalyan[3]

[1]*Institute of Cybernetics of the Georgian Technical University;*
[2]*Belarusian State Technological University;*
[3]*The Institute for Physical Research of National Academy of Sciences of Armenia*

Thermoelectric materials with composition $Bi_{2-x}[Pb(BO_2)_2]_xCa_2Co_{1.7}O_y$ (x=0-0.225) were prepared using a solid-state reaction method within 750-795 °C temperature interval. Samples were characterized by powder XRD analysis and SEM technique. Resistivity and Seebeck coefficient were measured in the temperature range 25-650°C. Thermal conductivity was analyzed from 25 to 400 °C. Doping of $Bi_2Ca_2Co_{1.7}O_y$ by $Pb(BO_2)_2$ leads to the decrease of its electrical resistivity at x = 0.075-0.125 and thermal conductivity at x = 0.075-0.175. The optimal doping level of $Bi_2Ca_2Co_{1.7}O_y$ by $Pb(BO_2)_2$ is close to x = 0.125: sample with composition $Bi_{1.875}[Pb(BO_2)_2]_{0.125}Ca_2Co_{1.7}O_y$ possesses the highest values of power factor (0.094 mW/m·K^2 at 650 °C) and figure-of-merit (0.041 at 400 °C) which are 18 and 15 % larger, respectively, than for undoped $Bi_2Ca_2Co_{1.7}O_y$ ceramics. Obtained results suggest that the doping of $Bi_2Ca_2Co_{1.7}O_y$ by $Pb(BO_2)_2$ has to be considered as a promising route for enhancing its thermoelectric properties.

Acknowledgment. This work was supported by Shota Rustaveli National Science Foundation (SRNSF) [FR-18-4976/Tuning the functional properties of Co-based thermoelectrics via doping and high-energy ball milling].

Hydrothermal Synthesis, Structure and Luminescence of Cr^{3+}-Doped Stannates Li_2SnO_3, Na_2SnO_3 and Li_8SnO_6

V. Sydorchuk[1], V. Hreb[2], S. Ubizskii[2], S. Khalameida[1] and L. Vasylechko[2]

[1]*Institute for Sorption and Problems of Endoecology, NAS of Ukraine*
[2]*Lviv Polytechnic National University, 12 Bandera Str., 79013 Lviv, Ukraine*

Lithium and sodium stannates are of research interest due to their application in lithium ion batteries and matrices for preparation of luminescent materials. The crystal structure of these stannates is essential for their successful application. It is formed during synthesis and next treatments. High-temperature solid state and sol-gel techniques using complex reaction mixtures have been described previously in the literature for stannates preparation. The hydrothermal method reduces the temperature and simplifies the process due to the formation of hydroxostannates, which are precursors of stannates. It also allows to use of oxides and hydroxides as reagents instead of salts, makes it possible to eliminate the stage of washing the products. For synthesis of lithium and sodium stannates doped with 0.005 mol.% of chromium, we used a wet gel of SnO_2 as a tin source, which results in maximum contact of the reagents in the hydrothermal process and a reduction in its duration. Other components were added in reaction mixture as hydroxides. Temperature and duration of reaction were 250 ^oC and 5 h. As a result, DTA-TG and XRD data confirm formation of $Na_2Sn(OH)_6$ with rhombohedral structure and probably one of the forms of lithium hydroxostannate directly in hydrothermal reaction. Next subsequent heat treatment of the products at 500 ^oC and 600 ^oC for 2 h lead to gradual decomposition of the hydroxostannates and beginning of formation of anhydrous Li_2SnO_3 and Na_2SnO_3. Phase pure Li_2SnO_3:Cr and almost pure Na_2SnO_3:Cr materials are formed after further heat treatment of the powders at 800 ^oC and 900 ^oC, respectively; their structure is preserved up to higher annealing temperature of 1200 ^oC. Average grain size of Li_2SnO_3:Cr materials increases sharply from 7-9 nm after its formation at 500–600 ^oC up to 175–280 nm after additional heat treatment at 800 ^oC and higher temperatures. Simultaneously, a sharp reducing of the average microstrains values $<\varepsilon>$ is observed in the same temperature range. Precise structural parameters of both Li_2SnO_3:Cr and Na_2SnO_3:Cr series heat treated at different temperatures were evaluated from experimental XRD patterns by full profile Rietveld refinement. It was established that increase of heat treatment temperature affect on opposite way on the lattice parameters of chromium doped Li_2SnO_3 materials: a sharp decrease of the *a*-parameter between 800 ^oC and 900 ^oC is accompanied by simultaneous increase in the *b*- and *c*-parameters and monoclinic angle. It is evident, that the observed deviations reflect the complex processes of rearrangement of stacking faults of honeycomb structure and possible redistribution of cations in Li_2SnO_3:Cr structure. In contrast to abovementioned Li_2SnO_3 and Na_2SnO_3 stannates, this method does not allow to obtain phase of pure Li_8SnO_6 material – the amount of the desired phase does not exceed 40–50 wt. % after heat treatment of the product at 900-1000 ^oC.

In the excitation spectra of Li_2SnO_3:Cr there are two broad bands with maxima at 470 and 630 nm, which are associated with the $^4A_2 \rightarrow {}^4T_1$ and $^4A_2 \rightarrow {}^4T_2$ transitions in Cr^{3+} ions. The maximum intensity of photoluminescence at room temperature is observed in the spectral region of 640–800 nm. This wide luminescence band, which is typical for Cr^{3+} ions in octahedral positions, can be attributed to the $^4T_2 \rightarrow {}^4A_2$ radiative transitions. No luminescence of Cr^{3+} ions were detected in as-prepared Na_2SnO_3:Cr and Li_8SnO_6:Cr materials.

Acknowledgment: The work was supported by the National Research Foundation of Ukraine (grant no. 2020.02/0373).

Sol-Gel and Solid State Synthesis of Cation-Deficient Perovskites Formed in $CaTiO_3$-$La_{2/3}TiO_3$ Pseudo-Binary System

I. Lutsyuk[1], V. Hreb[1], S. Turchak[1], Ya. Zhydachevskyy[1,2], V.B. Mykhaylyk[3] and L. Vasylechko[1]

[1]*Lviv Polytechnic National University, Bandera 12, 79013, Lviv, Ukraine*
[2]*Institute of Physics of the PAS, Al. Lotników, 32/46, Warsaw, 02-668, Poland*
[3]*Diamond Light Source, Harwell Campus, Didcot, OX11 0DE, UK*

According to precise crystal structure investigation performed by means of X-ray synchrotron and neutron powder diffraction [1, 2], four type of cation-deficient perovskite structures were found in (1-x)$CaTiO_3$-$xLa_{2/3}TiO_3$ pseudo-binary system, depending on composition: *Pbnm* for $0 \le x \le 0.5$, *Ibmm* for $0.5 < x < 0.7$, *I*4/*mcm* for $0.7 < x < 0.9$, and *Cmmm* for $x \ge 0.9$. In addition, four kinds of temperature-induced phase transitions occur in this system at elevated temperatures, namely: *Pbnm–I*4/*mcm*, *Ibmm–I*4/*mcm*, *I*4/*mcm–Pm*3*m* and *Cmmm–P*4/*mmm* [1, 2]. The presence of high-temperature structural phase transitions in $CaTiO_3$–$La_{2/3}TiO_3$ system makes its attractive for a possible application in high-temperature fluorescent non-contact sensors with intrinsic temperature reference for calibration and verification of reliability. In order to prove this conception, two series of nano- and microcrystalline Cr-doped materials of six nominal compositions within $CaTiO_3$–$La_{2/3}TiO_3$ system were prepared by sol-gel synthesis and standard solid state technique:

Composition	Expected structure
$CaTi_{0.9995}Cr_{0.0005}O_3$	*Pbnm*
$La_{0.133}Ca_{0.8}Ti_{0.9995}Cr_{0.0005}O_3$	*Pbnm*
$La_{0.33}Ca_{0.5}Ti_{0.9995}Cr_{0.0005}O_3$	*Pbnm* or *Ibmm*
$La_{0.4}Ca_{0.4}Ti_{0.9995}Cr_{0.0005}O_3$	*Ibmm*
$La_{0.5}Ca_{0.25}Ti_{0.9995}Cr_{0.0005}O_3$	*I*4/*mcm*
$La_{0.6}Ca_{0.1}Ti_{0.9995}Cr_{0.0005}O_3$	*Cmmm*

Wet-chemical synthesis of nanocrystalline powders doped with Cr^{3+} ions was performed by standard citrate sol-gel route from $CaCO_3$, $La(NO_3)_3 \times 9H_2O$ and Ti(IV) tetrabutoxide as initial reagents. Obtained products were sequentially annealed at 700 °C, 800 °C, 900 °C, 1000 °C for 2h in order to improve phase purity and crystallinity of the materials. As it was proved by X-ray powder diffraction, crystallization of the desired mixed oxide materials with perovskite structure begins at 700 °C, however the traces of anatase and rutile TiO_2 phases remain even after annealing at 1000 °C.

In solid state synthesis of Cr-doped (1-x)$CaTiO_3$-$xLa_{2/3}TiO_3$ materials, corresponding oxide and carbonate precursors (La_2O_3, TiO_2, Cr_2O_3 and $CaCO_3$) taken in stoichiometric proportions according to nominal compositions were carefully mixed in agate mortar and annealed two times at 1200 °C for 6-10 h with intermediate regrinding of the products. According to XRD phase analysis, beside the desired perovskite phases as-obtained powders contain traces of initial TiO_2 and La_2O_3 oxides, as well as minor amount of $La_2(TiO_3)_3$ parasitic phase. Crystal structure peculiarities of two series of Cr-doped *A*-cation deficient perovskites (1-x)$CaTiO_3$-$xLa_{2/3}TiO_3$ and their luminescence properties are discussed.

Acknowledgment: The work was supported by the National Research Foundation of Ukraine (grant no. 2020.02/0373).

[1] V. Vashook, L. Vasylechko, N. Trofimenko, *et al*. *J Alloys Comp* 419 (2006) 271–280.
[2] Z. Zhang, G.R. Lumpkin, C.J. Howard, *et al*. *J. Solid State Chem.* 180 (2007) 1083–1092.

Unexpected Conductivity of Anionic and Cationic Polyelectrolyte Nanobrushes on Flat Ceramic Surfaces

O. Izhyk, N. Mitina, A. Zaichenko, K. Volianiuk, I. Grygorchak and O. Balaban

Lviv Polytechnic National University, * zaichenk@polynet.lviv.ua

Novel approach of the synthesis of polyelectrolyte nanoscale brushes possessing controlled electrophysical characteristics on flat ceramic surfaces was developed. It consists of covalent attachment of oligoperoxide metal complex macroinitiator or 4,4'-azobis (4-cyanopentanoic acid) (DAK-COOH) and consequent radical initiation of graft polymerization of 2-carboxyethyl acrylate (CEA) and 2-(diethylamino) methyl methacrylate (DMAEMA) providing formation of anionic or cationic polyelectrolyte brushes, respectively which are irreversibly tethered to the ceramic surface. Polymer brushes were studied using functional and element analyses, AFM and SEM techniques, impedance spectroscopy, and they are characterized by chemical stability, controlled grafting density and length. Li^+ cations were inserted into polymer brushes from lithium chloride solution to provide conductivity.

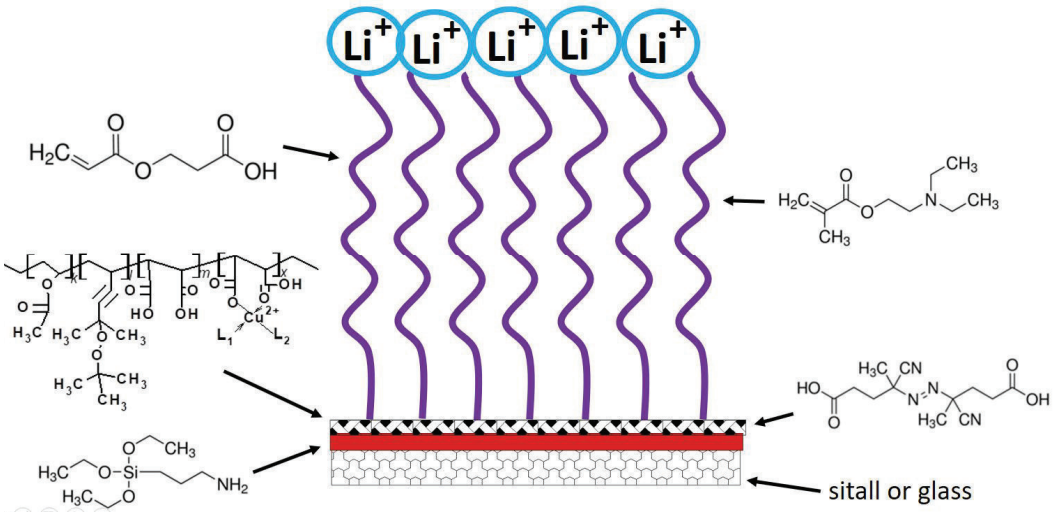

Fig. The schema of obtaining polymer nanobrushes conductive material.

AFM study confirms formation of polyelectrolyte nanolayers with thickness in a range of 20 - 30 nm for poly(CEA) and poly(DMAEMA). The results of impedance measurements show that conductivity of polymer brushes appear even before processing by lithium chloride. Polyelectrolyte brushes without included Li^+ cations also contribute into total conductivity, evidently, due to proton transfer conductivity. In general, we have got increasing of conductivity in five times and incorporation of lithium positive charges leads to two orders of conductivity enhancement. High dielectric permittivity values in the low frequency range (and simultaneously at low values of the electric loss angle tangent) indicate that the synthesized material is capable to store energy at the quantum level. Thus, this material is effective in quantum batteries manufacturing.

The Peculiarities of Experimental Determination of the Acousto-Optic Efficiency of Oxide Crystals

T. Voronyak[1,2], D. Vynnyk[2,3], N. Andrushchak[2], I. Stasyshyn[1], I. Senko[2] and A. Andrushchak[2]

[1]*Karpenko Physico-Mechanical Institute of the NAS of Ukraine, Lviv, Ukraine*
[2]*Lviv Polytechnic National University, Lviv, Ukraine*
[3]*Scientific Research Company Electron-Carat (SRC 'Carat'), Lviv, Ukraine*

One of the experimental methods used to investigate the acousto-optic properties of solids, mainly for the determination of the elastic-optic coefficients and acousto-optic figure-of-merit M_2, is based on the Bragg diffraction phenomenon [1]. The peculiarity of this method is the use of ultrasonic waves with frequencies of 100-300 MHz. The essence of the used technique consists of measuring the intensity of a light beam diffracted on the ultrasonic wave in the investigated material and comparing the obtained value of the intensity with the one of the light diffracted in the material with known photoelastic properties. The experimental equipment for this technique was first developed and applied by Smith and Korpel [2]. Then the method was subsequently refined by Dixon and Cohen, who made it possible to use both longitudinal and transversal ultrasonic waves [3]. During the experiment, short ultrasonic pulses enter into the buffer. The buffer in our case is the Bragg cell with the light-sound waveguide made from the material with known characteristics (mainly fused silica). A plane-parallel sample of the investigated material is attached to the free surface of the buffer by a special adhesive. The ultrasonic wave propagates along the normal to the interface between the buffer and the sample and partially reflects on it. The wave entering the investigated sample reflects from the free surface of the sample and again enters the buffer.

However, it is known that the propagation of transversal ultrasonic waves in many oxide crystals (TeO_2, $CaWO_4$, $LiNbO_3$, etc.) is accompanied by their walk-off, i.e., by the deviation of the propagation direction from the normal to the surface from which the wave was excited [4]. Moreover, the parallelism of opposite faces of investigated samples is often unsatisfactory. It leads to the additional deviation of the wave from the normal after reflection from the free surface of a sample. If these two factors are not considered, the measurements following the Dixon-Cohen method will be either incorrect (obtained results will be under-valued) or completely impossible. Thus the interferometric control of the geometry of the samples and the determination of the walk-off angles have to be preliminarily done for all actual (planned) geometries of acousto-optic interaction [5].

The authors proposed techniques and schemes of the experimental set-up, which allow realizing this preliminary control. The approbation of the Dixon-Cohen method taking into account the walk-off angles of ultrasonic waves, was carried out on the examples of $CaWO_4$ and $LiNbO_3$ crystals.

[1] T.S. Narasimhamurty, Photoelastic and electro-optic properties of crystals. New York, Plenum, 1981.
[2] T. Smith, A. Korpel, Measurement of light-sound interaction efficiencies in solids. IEEE J. Quantum Electron., 1965, V. 1, P. 283-284.
[3] R.W. Dixon, M. G. Cohen, A new technique for measuring magnitudes of photoelastic tensors and its application to lithium niobate. Appl. Phys. Lett., 1966, V. 8, P. 205-207.
[4] V. Voloshinov, N. Polikarpova, Acousto-optic investigation of propagation and reflection of acoustic waves in paratellurite crystal. Appl. Opt., 2009, V. 48, P. C55-C66.
[5] A.S. Andrushchak, T.I. Voronyak, O.V. Yurkevych, N.A. Andrushchak, A.V. Kityk, Interferometric technique for controlling wedge angle and surface flatness of optical slabs. Opt. Laser Eng., 2013, V. 51, P. 342-347.

Investigation of the Electrophysical Properties of Dense Anodic Aluminum Oxide Films

V. Shulgov

Belarusian State University of Informatics and Radioelectronics (BSUIR)

In the process of the electrochemical anodizing aluminum, dense (barrier) and/or porous alumina films can be formed depending on the composition of the electrolyte. Dense (barrier-type) oxide films are formed when aluminum is anodized in neutral solutions (pH = 5 – 7) that negligibly slight dissolve aluminum oxide.

Porouse alumina films are widely used in microelectronics for the manufacturing switching plates, multiterminal VLSI packages, multichip modules, etc [1]. Dense anodic alumina films (AAF) as thick as up to 1000 nm can be used as a dielectric layer in capacitors, isolation layers in the multilevel interconnection system, a top protective layer of a passive part of hybrid integrated circuits, etc. [2]. To date, studies into the formation process of dense AAF and their behavior are the subject of extensive literature. However, a diversity of dense oxide functionnalities in the microelectronic technology, specificity of microminiaturization problems, an increase in the reliability requirements to the devices necessitate more thorough and detailed knowledge about the features of the anodic alumina. Special research should be done into the alumina characteristics to ensure their effective use for realizing specific design-technological targets.

This article discusses the studies into the anodization kinetics and structural composition of dense oxides obtained in the presence of surfactant additives. As a surfactant, we used organic compounds of the alcohol class, which were used in the study of porous AAF [3]. The influence of surfactants on the anodic oxidation kinetics of aluminum was studied by taking polarization curves. The structure and chemical composition of anodic films were studied by secondary ion mass spectroscopy (SIMS).

Studies have shown that the surfactant addition to electrolytes for the dense aluminum anodization allows controlling the penetration depth and the concentration of electrolyte anions in the oxide as well as the width of the homogeneous oxide range that, in turn, allows changing electrophysical characteristics of aluminum dense oxides. Specifically, surfactant additives increase the dielectric insulation resistance and breakdown voltage of the films. A slight decrease in the specific capacity of the AAF is observed. The dielectric losses in the films obtained in electrolytes with and without surfactant additives practically do not differ.

The following conclusions can be drawn from the study performed:

– A film of natural oxide has a significant effect on the kinetics of aluminum dense anodization. The cathodic polarization of the samples before anodizing allows layers of natural oxide to be removed;

– The introduction of a surfactant from the alcohol class into the electrolyte for aluminum anodizing leads to inhibition of the surface of the growing oxide film, while the rate of chemical dissolution of dense alumina decreases;

– The presence of surfactant molecules in the double electric layer leads to the formation of Al_2O_3 films more stable in composition;

– The electrophysical properties of dense AAF improve.

[1] Surganov V., Mozalev A. Microelectronic Engineering 37/38 (1997) PP.329-334.
[2] Takada T. Mat. Res. Soc. Symp. 1993. Vol. 284. P. 371.
[3] Shulgov V. Acta Physica Polonica A. 2018. Vol. 133. N4. PP.767-770.

Diffusion of Cobalt Ions into Crystals of Non-Stoichiometric Magnesium Aluminate Spinel $MgO{\cdot}xAl_2O_3$

O.O. Vovk, S. Nizhankovskiy, Yu. Siryk and P. Mateichenko

Institute for Single Crystals NAS of Ukraine, 60 Nauky Ave., Kharkiv, 61001, Ukraine
ovovk@isc.kharkov.ua

Magnesium-aluminate spinel $MgO{\cdot}xAl_2O_3$ (MALO) in the form both of crystals and ceramics possess excellent chemical, thermal, dielectric, mechanical, and optical properties. These properties make MALO an attractive material for manufacturing substrates, optical windows, transparent armor, and IR sensors. When doped with transition metals MALO, both stoichiometric composition ($MgAl_2O_4$, x=1) and non-stoichiometric ($MgO{\cdot}xAl_2O_3$, $1 < x \leq 3$) is a promising matrix for the manufacture of laser active media (Cr, Ti, etc.) and doped with Co^{2+} ions also for passive Q-switching [1,2].

The present work deals with the investigation of the conditions for introducing the cobalt ions into the MALO crystal by gas phase diffusion at high-temperature annealing. For example, it is known that Cr ions can be introduced into stoichiometric $MgO{\cdot}Al_2O_3$ crystals under significant pressure (up to 2 GPa) during annealing at 1100-1250 ^oC [3].

We assume that using non-stoichiometric spinel $MgO{\cdot}xAl_2O_3$ enriched with alumina activates the diffusion processes of Co^{2+} ions into the MALO crystal lattice due to the appearance of the cationic vacancies of V_{Mg2+} that increases the diffusion rate of Co^{2+} ions.

MALO single crystals grown by horizontal directed crystallization method in the molybdenum crucibles under a reducing gas media have been used to carry out the study. The crystals of different stoichiometry with x ranged from 1 to 2.7 have been utilized. The temperature intervals of the phase stability of MALO depending on the degree of non-stoichiometry have been determined to adapt to our conditions according to the results of annealing of the samples with different x and analysis of the phase diagram of the $MgO\text{-}Al_2O_3$ system. It was found that increasing x lifts the lower temperature of the phase stability $MgO{\cdot}xAl_2O_3$. MALO with x>1.4 is stable under annealing at the temperature higher than 1400^{o}C, while compositions with x>1,46 and x>1,63 keep stability at the temperatures higher than 1450^{o}C and 1500^{o}C, respectively. The annealing at the lower temperatures corresponded to these x causes the decomposition of the MALO phase onto the spinel enriched with magnesium in comparison with the initial composition and Al_2O_3.

To investigate the diffusion of Co^{2+} ions into MALO, the tablets of Ø 5 mm and thickness of 1 mm have been prepared from the grown crystals with x from 1 to 1.63. The tablets and Co_3O_4 powder were placed in a closed container and were annealed at the temperature of 1300-1500 ^oC for 24 h in air. It was found that increasing both annealing temperature and stoichiometry coefficient x significantly increases the layer thickness of Co ions penetrated crystal body, at x=1,67, the spinel tablet contains cobalt across its thickness.

The diffusion coefficients of cobalt into MALO at different temperatures and stoichiometry as well as efficient activation energy were calculated based on the obtained data.

[1] Ruikun Wu, J.D. Myers, M.J. Myers etc. Co^{2+}:$MgA1_2O_4$ Crystal Passive Q-Switch Performance At 1.34, 1.44 and 1.54 micron, In Solid State Lasers IX, Richard Scheps, Editor, 42 Proceedings of SPIE Vol. 3929 (2000).

[2] D.P. Jiang, Y.Q. Zou, L.B. Su etc. A Co^{2+}-doped alumina-rich $Mg_{0.4}Al_{2.4}O_4$ spinel crystal as saturable absorber for a LD pumped Er: glass microchip laser at 1535 nm, Laser Phys. Lett. 8, No. 5, 343–348 (2011).

[3] C. Freda, B. Celata, G. Andreozzi etc. Cr diffusion in $MgAl_2O_4$ synthetic spinels: preliminary results, Geophysical Research Abstracts, Vol. 14, EGU2012-5313-3, 2012.

Zinc-Iridium Oxide Thin Films Fabrication and Properties

V. Skvortsova, M. Zubkins, R. Kalendarev, H. Arslan and J. Purans

Institute of Solid State Physics, University of Latvia, Latvia

A wide variety of metal oxide materials with different electrophysical properties and values of the band gap covering the entire range of the solar spectrum makes it possible manufacturing multilayer film heterostructures for the most efficient use of solar radiation. Currently, there is an active search for new promising materials for transparent electronics. The most interesting are metal oxide compounds such as zinc oxide, tin dioxide, in their pure form being n-type semiconductors. In particular, because of their cheap technology, as well as due to the fact that these compounds are transparent and wide-gap (3.2 eV for ZnO and 3.54 eV for SnO_2) semiconductors, they can be used in wide temperatures range in products of transparent electronics. Doped ZnO thin films are promising n-type transparent-conducting oxide (TCO) materials. The preparation of p-type ZnO thin films is an important stage in the development of transparent electronics. Several precious-metal-based transparent oxides have also shown *p*-type conductivity, including polycrystalline ZnM_2O_4 (*M*= Ir, Rh, Co) films [1-3]. The aim of the study is to develop Zinc-Iridium Oxide thin films deposition process and investigate films physical properties.

Zinc-iridium oxide thin films in the wide Ir concentration range were deposited on glass, Ti, Si and polyimide tape substrates by reactive DC magnetron co-sputtering in an $Ar+O_2$ atmosphere. Two sets of samples were deposited. The sets differed both in the Ir concentration range and in the deposition parameters and geometry. The first set of the ZnO-Ir samples was deposited with a relatively low Ir concentration, increasing it gradually to accurately investigate the changes of the structure and properties of deposited films. The second set was deposited in a wide Ir concentration range (up to 66 %) so that the Zn/Ir concentration ratio matches the $ZnIr_2O_4$ compound.

The investigations of the Zn-Ir-O thin films with various concentrations of iridium deposited by reactive DC magnetron sputtering have shown that the observed absorption spectrum bands are associated with iridium ions with different valence states (3+, 4+ and 5+).

It is shown that increase of the Ir concentration in thin films changes the lattice structure from nano-crystalline to X-ray amorphous.

The resistivity of the heated films is slightly lower compared to the non-heated films in the Ir concentration range from 20 to 40 at. %. An increase in the concentration of iridium in both heated and unheated films changes the sign of the Seebeck coefficient from negative to positive.

[1] H. Ohta, H. Mizoguchi, M. Hirano, S. Narushima, T. Kamiya, H. Hasono, *Appl.Phys.Lett.* **82,** 823(2003).
[2] M. Dekkers, G. Rijnders and D. H. A. Blank, *Appl. Phys. Lett.* **90,** 021903 1-3 (2007).
[3] H. J. Kim, I. Song, C. H. Sim, D. Kim, Y. Kim, E. Ihm and W. K. Choo, *J. of Appl. Phys.* **95,** 7387 (2004).

Optical Properties of $MgAl_2O_4$ Crystals Grown by Iridium-Free Technology

S. Nizhankovskyi, A. Kozlovskyi, O. Vovk, N. Sidelnikova and Yu. Siryk

Institute for Single Crystals, STC "Institute for Single Crystals", National Academy of Sciences of Ukraine, Kharkiv, Ukraine

Aluminum-magnesium spinel crystals $MgAl_2O_4$ (MALO) are widely used in electronics, optics and research [1]. An important advantage of MALO crystals is the possibility of doping with transition metal ions, which opens up prospects for their use in optical devices, in particular, in laser technology [2]. To date, MALO crystals are usually obtained by the Czochralski method [3]. Existing technologies of the growth of MALO crystals use very expensive iridium crucibles, the melting point of which is only slightly higher than the crystallization temperature of spinel. Therefore, the service life of an iridium crucible is only a few processes. To solve these problems, it is necessary to develop iridium-free technology for growing crystals using other materials for the crucible.

In this report we demonstrate results of using iridium-free technology for growing crystals MALO. The crystals MALO for the first time were grown by horizontal directional crystallization method (HDCM) [4] in molybdenum crucible under an argon atmosphere. It was carried out investigation of the optical absorption of the grown crystals. The optical absorption spectra of MALO crystals grown by HDCM in a reducing medium exhibit absorption bands (267 nm and 325 nm) caused by complexes of defects formed by oxygen vacancies and cations located in anti-sites. It is shown that annealing of crystals in an oxidizing environment leads to the elimination of these absorption bands and an improvement in the optical properties of the grown crystals.

[1] I. Ganesh. // INT MATER REV, 58, No 2, pp. 63 – 112 (2013)
[2] Anis Jouini, Akira Yoshikawa, Al. Brenier, Tsuguo Fukuda, G. Boulon Phys. stat. sol. (c) 4, No.3, pp. 1380-1383 (2007)
[3] G.H. Sun, Q.L. Zhang, J.Q. Luo, W.P. Liu, X.F. Wang, S. Han, L.L. Zheng, W.M. Li, D.L. Sun. // Mater. Chem. Phys., 204, pp. 277-281 (2018).
[4] S.V. Nizhankovskyi, A.V. Tan'ko, N.S. Sidelnikova, G.T. Adonkin., Crystal res. and tech., 50, No.3, pp. 223-229 (2015).

Theoretical Study of the Effectiveness of Radiation Coloring of the Thallium-Containing Fluorite Crystals

V. Salapak[1], S. Kachan[1,*], O. Nahurskyy[1], I. Pirko[2] and L. Salapak[2]

[1]*Lviv polytechnic National university, 12 Bandera street, Lviv 79013, Ukraine*
[2]*Ukrainian National forestry university, 103 gen. Chuprynka street, Lviv 79057, Ukraine*
[*]*sikach@gmail.com*

By their radiation properties, $SrCl_2$-Tl^+ crystals are similar to fluorite crystals doped with alkali metals or oxygen. As in fluorite crystals, the boundary concentration of color centers in $SrCl_2$-Tl^+ crystals is of the order of 10–20% of the dipole concentration in the crystal upon irradiation of the crystal at 90 K and increases several times with increasing temperature.

A significant difference between the $SrCl_2$-Tl^+ crystals, on the one hand, and the MeF_2-Me^+ and MeF_2-O^{2-} crystals, on the other hand, is that there is no illumination effect of ionizing radiation in the region of room temperature and the crystal reaches the threshold radiation sensitivity: upon irradiation of the crystal, almost all the IVDs present in the crystal, due to the localization of charge carriers, turn into color centers. The absence of the illumination effect of X-rays on color centers is due to the fact that the Tl^{2+}- and $Tl^0(2)$-centers are electrically neutral with respect to the lattice.

In the present paper, the parameters of radiation sensitivity of the thallium -doped fluorite crystals were calculated in a one-dimensional model. The boundary concentrations of the color centers as a function of the concentration of the thallium impurity in the fluorite crystal were defined. The table shows the calculation data of the parameters of the $SrCl_2$-Tl^+ – crystals' radiation sensitivity.

c	l	ω_1	ω_2	ω_3	c_1/c_0	n_1, cm^{-3}	c_2/c_0	n_2, cm^{-3}	c_2/c_1
0.50	6a	0.100	0.40	0	0.200	$5\cdot10^{18}$	1.0	$2.5\cdot10^{19}$	5.0
0.10	10a	0.069	0.37	0	0.170	$8.5\cdot10^{17}$	1.0	$5.0\cdot10^{18}$	5.9
0.01	21a	0.032	0.36	0	0.082	$4.1\cdot10^{16}$	1.0	$5.0\cdot10^{17}$	12.0

Note: c – molar concentration of the thallium ions in the crystal; l – average distance between impurity ions in the crystal framework; a – parameter of the ion chain; $c_0 = 0.5c$ - molar concentration of IVD-pairs (impurity-vacancy dipoles) in the crystal; c_1 – boundary concentration of color centers emerging during the irradiation of the crystal at $T<130$ K; c_2 – boundary concentration of color centers emerging in the crystal during its irradiation at $T>130$ K; n_1 – boundary density of color centers emerging at the stage of color saturation of the crystal being irradiated at $T<130$ K; n_2 – boundary density of color centers emerging at the stage of color saturation of the crystal being irradiated at $T>130$ K; c_0 – IVD-pairs concentration in the crystal before the irradiation.

As evidenced by the data presented in the table, at the low-temperature irradiation of the crystal, the possibility ω_1 of color centers emergence is lower than the probability ω_2 of their destruction during irradiation. Accordingly, the color centers concentration c_1 is considerably lesser than IVD concentration c_0. Conversely, if the crystals are being irradiated at the room temperature, ω_1 is greater than ω_3. Hence, at the stage of color saturation of the crystal, the concentration of the color centers exceeds the IVD concentration. As the thallium content reaches 0.5 mole, the color centers concentration runs up to 10^{19} cm^{-3} which is by order of magnitude greater than that in *KCl* crystals. Because of the high radiation sensitivity of the doped fluorite crystals, they are a promising material for micro- and nanoelectronics.

The Effect of Sintering Temperature on Crack Growth Resistance Characteristics of Yttria-Stabilized Zirconia Determined by Various Test Methods

V. Kulyk[1], Z. Duriagina[1,2], B. Vasyliv[3], T. Kovbasiuk[1], P. Lyutyy[1], V. Vira[4] and V. Vavrukh[1]

[1]*Department of Materials Science and Engineering, Lviv Polytechnic National University, 12 S. Bandera str., Lviv 79000, Ukraine, E-mail: kulykvolodymyrvolodymyrovych@gmail.com*
[2]*Department of Materials Engineering, The John Paul II Catholic University of Lublin, 14 Racławickie Al., Lublin 20-950, Poland*
[3]*Department of Hydrogen Technologies and Alternative Energy Materials, Karpenko Physico-Mechanical Institute, 5 Naukova str., Lviv 79060, Ukraine*
[4]*Department of Department of Strength of Materials and Structural Mechanics, Lviv Polytechnic National University, 12 S.Bandera str., Lviv 79000, Ukraine*

Zirconium oxide commonly called "zirconia" (ZrO_2) is widely used for applications in high-temperature structural materials. Zirconia is often more useful in its phase stabilized state. Upon heating, zirconia undergoes disruptive phase changes. By adding small percentages of yttria, these phase changes are eliminated, and the resulting yttria-stabilized zirconia (YSZ) material has superior thermal, mechanical, and electrical properties. Products made of YSZ ceramics are characterized by high strength and crack growth resistance. Such mechanical behavior of YSZ ceramics is a reason of their applications in many industry fields instead of conventional metallic alloys. That is why these materials are used for manufacturing products and components of hydrogen and ammonia reformers, air heaters, fired heaters, cracking furnaces, etc. According to the needs and corresponding qualities required, the products are to be thermal shock resistant, wear and corrosion resistant, highly-insulated, and possess high strength and crack growth resistance.

In this work, YSZ ceramics sintered at various temperatures have been studied. The series of beam specimens of ZrO_2 ceramics stabilized with 6, 7, and 8 mol% Y_2O_3 were prepared using a conventional sintering technique. Three sintering temperatures were used for each series: 1450, 1500, and 1550 °C. Sintered specimens were grinded and polished to reach a good surface quality. Two different mechanical tests were performed: fracture toughness test by the indentation method and single-edge notch beam test under three-point bending.

Based on the obtained fracture toughness data for tested variants of material it was found that both the yttria percentage and sintering temperature affect the mechanical behavior of the ceramics. It is known that in the case when the sufficient amount of the metastable tetragonal phase is present, the tetragonal to monoclinic phase transformation can occur under the action of an applied stress, magnified by the stress concentration at a crack tip. This is followed by retardation of crack growth due to putting the crack into compression. As a result, the fracture toughness can increase significantly. The maximum transformation toughening effect was revealed for ZrO_2–6 mol% Y_2O_3 ceramics. Based on X-ray diffraction analysis the phase balance of each composition was substantiated. In addition, the microstructure and fracture surface analyses allowed us to conclude that transformation toughening of such ceramics strongly depends on the sintering mode and is related to changes in the fracture surface morphology.

Chemically Synthesized Binary Pd-Co Alloys: Structural and Magnetic Properties

Dogan Kaya[1], Idris Adanur[2], Mustafa Akyol[3], Faruk Karadag[2] and Ahmet Ekicibil[2]

[1]*Cukurova University, Vocational School of Adana, Department of Electronics and Automation, Adana, Turkey*
[2]*Cukurova University, Faculty of Art and Sciences, Department of Physics, Adana, Turkey*
[3]*Adana Alparslan Turkes Science and Technology University, Faculty of Engineering, Department of Materials Science and Engineering, Adana, Turkey*

Nanoparticles (NPs) have received considerable attention because of their remarkably different properties, such as enhancing catalytic, electronic, optical, and magnetic properties from those of their bulk materials [1]. For these purposes alloying noble metals with low-cost *3d* metals (such as Fe, Co, Ni, Cu, *etc*.) is a successful method that modify structural, enhances catalytic, control magnetic properties, and reduces the production costs for catalysis, magnetoresistive sensor technology, data recording media, and optoelectronic [2].

In this study, Pd-Co based magnetic alloy nanoparticles were prepared by the modified polyol process and stabilized by polyvinylpyrrolidone (PVP) and 3-aminopropyl-trimethoxysilane (APES) capping agents and further reduction of metal salts with sodium borohydride ($NaBH_4$) at high temperature to form desired NPs [3]. We have a detailed investigation of the effect of Pd concentration in the Pd-Co alloy NPs on structural and magnetic properties. XRD and Rietveld refinement analyses were confirmed that the multiphase structures of fcc-PdCo, fcc-Co, and hcp-Co phases coexist at low Pd loading samples. Over %50 of Pd loading resulted in a single fcc-PdCo phase with reduced lattice parameter to 4.0079 Å and $d_{(111)}$-space to 2.31 Å. TEM and SEM images reveal well dispersed and uniformly distributed NPs with an average particle sizes of below 7 nm. The elemental compositions and the characteristic OH, CH, CO stretching peaks of capping agents were confirmed by EDS and FT-IR spectrums, respectively. $M(T)$ and $M(H)$ curves revealed that there are multi magnetic phase transitions in the Pd-Co structure as a function of Pd loading from superparamagnetic to ferromagnetic phase or back to superparamagnetic phase by reducing the temperature from 300 K to 5 K. We observed that the blocking temperature (T_B) could not be detected due to 5% Pd loading below 300 K, while it reduced up to 55 K at high Pd loading of 62%. The coercive field (H_c) was increased to ~1900 Oe for $Pd_{0.62}Co_{0.38}$ sample due to the smallest particle size as 5.26 nm. The highest amount of Co resulted in maximum saturation magnetization (M_s) up to 65.5 emu/g for 5% Pd concentration. We measured the M_r/M_s ratios were less than 0.5, which is due to the internal stress that results in the uniaxial magnetic anisotropy in the structure. The maximum K_{eff} and $\mu_{f.u.}$ values were found to be over 12.9 $\times 10^6$ erg/cm^3 and 0.72 μ_B at 5 K for 5% Pd concentration, respectively.

[1] R.C.P. Oliveira, M. Sevim, B. Šljukić, C.A.C. Sequeira, Ö. Metin, D.M.F. Santos, Mesoporous graphitic carbon nitride-supported binary MPt (M: Co, Ni, Cu) nanoalloys as electrocatalysts for borohydride oxidation and hydrogen evolution reaction, Catal. Today, 357 (2019) 291-301.

[2] V. Abdelsayed, G. Glaspell, M. Nguyen, J.M. Howe, M. Samy El-Shall, Laser synthesis of bimetallic nanoalloys in the vapor and liquid phases and the magnetic properties of PdM and PtM nanoparticles (M = Fe, Co and Ni), Faraday Discuss., 138 (2008) 163-180

[3] D. Kaya, I. Adanur, M. Akyol, F. Karadag, A. Ekicibil, Detailed investigation of structural and magnetic properties of multiphase binary Pd-Co alloys prepared by modified polyol process, J. Alloys Compd., 876 (2021) 160157.

SECTION 2

MATERIALS FUNDAMENTALS: CRYSTAL STRUCTURE, DEFECTS, INTERACTIONS

Diffraction Computed Tomography and Its Applications

A. Senyshyn[1], V. Kochtetov[1], M.J. Mühlbauer[1,2], A. Schökel[3] and M. Hofmann[1]

[1]*Heinz Maier-Leibnitz Zentrum (MLZ), Technische Universität München, Lichtenbergstr. 1, 85748 Garching, Germany*
[2]*Institute for Applied Materials (IAM), Karlsruhe Institute of Technology (KIT), Hermann-von-Helmholtz-Platz 1, D-76344 Eggenstein-Leopoldshafen, Germany*
[3]*Deutsches Elektronen Synchrotron (DESY), Notkestr. 85, 22607 Hamburg, Germany*

There is a variety of questions and applications (e.g. medical, engineering, materials science) where non-destructive visualisation of the sample interior is needed. Radiography - a 2D visualisation technique based on the imaging of white beam, when attenuated by the partially absorbing sample, is one of the most straightforward approach. Its major drawback, however, is the loss of information in one (in beam) direction, which can lead to misinterpretation of the images. A new technique to overcome this disadvantage was developed based on inverse Radon transform in the 1970s called "Computerized transverse axial tomography" (CAT or CT). By acquiring projection images from different sample orientations, a 3D volume can be reconstructed using dedicated computer algorithms.

Right after first implementation the CT was used for medical applications and further expanded to wood technology, palaeontology, soil science and industrial applications. Although X- and gamma-rays are most commonly used types of the incident radiation in computed tomography, the protons, neutrons and heavy particles (*e.g.* ions) can be used as a source. "Alternative" to X-rays radiation sources are used as complementary information enhancing contrast and sensitivity, which is certainly limited for the X-ray case. Analysis of phase of X-ray beam (based on the observation of interference patterns between diffracted and undiffracted waves) enables the increase of sensitivity to variations of density and chemical content, e.g. improved soft tissue contrast *etc*. However, the phase-contrast imaging is essentially more time consuming than conventional attenuation-based imaging, thus making CT data collection unreliably long. To further improve elemental sensitivity Bragg-edge diffraction imaging with neutrons or energy-selective imaging with X-ray photons is often used.

Alternative way to increase sensitivity to density variations and chemical composition as well as to improve discrimination of chemically and morphologically similar but structurally distinct phases the accounting for scattering effects in the radiography and tomography has a vital importance. This pawed the way to diffraction CT – an experimental technique combining X-ray Diffraction with Computed Tomography by XRD-CT [1], where similar to traditional X-ray CT, the sample is scanned by a pencil-beam, but the diffraction picture is collected instead of the attenuation of X-rays in the transmitted beam. Prominent progress has been achieved during the last decades in increasing spatial and temporal resolution. Studies applying XRD-CT for structural analysis of energy materials, biological samples, catalysts and fuel cells have been already reported [2].

In the current contribution we report the applications of XRD-CT to studies of lithium distribution in commercial cylinder-type Li-ion batteries as well as the implementation and first results of ND-CT (Neutron Diffraction with Computed Tomography) experiments using monochromatic thermal neutrons.

[1] Harding, G., Kosanetzky, J. & Neitzel, U. (1987). *Med Phys* **14**, 515-525.
[2] Beale, A. M., Jacques, S. D. M., Gibson, E. K. & Di Michiel, M. (2014). *Coordination Chemistry Reviews* **277-278**, 208-223.

Quantitative Description of Oxygen Non-Stoichiometry in Mixed Ionic and Electronic Conductors Based on a Non-Ideal Solution Approach

Y. Naumovich

Institute of Power Engineering, Department of High Temperature Electrochemical Processes (HiTEP)
Mory 8, 01-330 Warsaw, Poland
CTH2 - Center for Hydrogen Technologies, Institute of Power Engineering, Augustowka 36, Warsaw, 02-981, Poland

Quantitative estimations of oxygen non-stoichiometry in complex oxides with mixed ionic and electronic conductivity (MIECs) is a keystone element of the insight in to properties and efficiency of such materials. MIECs are basic materials for fabrication of the high-temperature solid state electrochemical devices. They are used for fabrication of the electrodic layer (cathodes of solid oxide fuel cells and anodes of the solid oxide electrolyzers) and as membranes for separation of the oxygen and for partial oxidation of the light hydrocarbons. Oxygen non-stoichiometry is a guiding feature of the MIECs. It typically changes with temperature and partial pressure (or chemical potential) of the oxygen in the environment and such dependences are known as $p(O_2)$-T-δ diagrams. Alteration of the non-stoichiometry governs such properties of the MIEC as electronic and ionic conductivity, and it also impacts thermal expansion through isothermal chemical expansion term. The present overview describes techniques, which allow elaborate models for quantitative estimation of the equilibrium partial pressure of the oxygen on MIEC with specified oxygen content and at the specified temperature. These models are based on statistical thermodynamics for crystalline solids as background and also included assumptions related to the nature of the electronic sub-system and related point defects. A crystal lattice of the MIEC is considered as the non-ideal solution, where some reference state of the lattice should be chosen as solvent and solutes are point defects, which may interact one with another due to Coulombic forces or local distortions. Among simulated $p(O_2)$-T-δ diagram, foresaid models outcome equilibrium concentrations of the point defects, involved in equilibration with environment. As result, modelling of the $p(O_2)$-T-δ diagrams allows to estimate and to analyze transport properties of the MIECs, like ionic conductivity or oxygen permeability in case of surface limitations. Modelling of the $p(O_2)$-T-δ diagrams was performed on various solid solutions, including material with perovskite, brownmillerite and Ruddlesden-Popper structures. Models were validated using experimental $p(O_2)$-T-δ data sets and used for analysis of the ionic transport in oxides with perovskites($La_{1-x}Sr_xCoO_{3-\delta}$ and $LaGa_{0.65}Mg_{0.15}Ni_{0.20}O_{3-\delta}$) and Ruddlesden-Popper ($La_2NiO_{4+\delta}$) structure. The aforementioned approach is under elaboration for high-temperature electrochemical objects (SOFC, SOEC and SOFEC electrodes, oxygen separation and POX membranes, *etc.*). However, it might be expanded on other crystalline materials, for which an impact of the point defects interactions on practically-important properties is sufficient.

Acknowledgements. These studies were supported by FCT/FEDER, (Portugal), project PTDC/CTM-CER/114561/2009 and by National Science Centre (Poland), project 2018/30/M/ST8/00675.

Foray into Non-Contact Luminescence Cryothermometry Enabled by Oxides

V.B. Mykhaylyk

Diamond Light Source, Harwell Campus, UK

Luminescence thermometry is a non-contact technique that utilises the temperature-dependent variation of emission characteristics in selected luminescence materials for temperature monitoring. Accurate temperature sensing in the way that does not require physical contact is a key requirement for the systems operating in a harsh environment where the contact with the object is restricted due to it requiring isolation, shielding, or because it is not stationary. Extending the application of the luminescence thermometry towards cryogenic temperatures relies upon identification of further materials with luminescence properties suitable for temperature sensing in this temperature range. The main interest for such application represents the systems where thermally induced processes of particle exchange between excited levels and thermal quenching require low activation energy that can then translate in the tangible changes of a luminescence parameter with temperature.

In this work we carried out systematic studies of the temperature-induced changes in the luminescence of Cr^{3+} doped oxides (Al_2O_3, Ga_2O_3, $YAlO_3$), tungstates AWO_4 (A=Ca, Sr, Zn, Cd) and molybdates $AMoO_4$ (A=Ca, Sr, Cd) over the 4.5-300 K temperature range. The responsivity of the luminescence characteristics that can be used for the non-contact measurements of temperature i.e. luminescence intensity ratio, wavelength shift and decay time constant, is examined and the chief features influencing thermometry over the cryogenic temperature range are identified. This is complemented by comprehensive analysis and interpretation of thermometric properties of the crystals under study. We applied pertinent theoretical models to explain the observed temperature dependences by the changes in the dynamics of exited levels population due to i) thermalization, ii) electron-phonon interaction, iii) nonradiative multiphonon relaxation and iv) thermal depopulation of higher states. It is shown that the intensity ratio of R-lines of Cr^{3+} at low temperatures is predominantly controlled by process (i) responsible for redistribution of populations between the upper and lower levels. The process (ii) is the cause of wavelength shift while the explanation of the temperature change of decay rate requires to take into account combined effect of all processes i)-iv). We will show that these models provide adequate interpretation of the processes as can be judged from the high quality of fits obtained for the measured temperature dependences of luminescence intensity ratio, wavelength shift and decay time constant in the crystals under study. The results of the fits yielded a number of quantitative parameters of which further analysis allowed to establish how the energy structure of the emission centre and phonon dynamics in different hosts influence the luminescence properties and what effect it has upon the different modes of non-contact luminescence temperature sensing. Finally, we will assess the performance of different materials and methods of temperature sensing used in cryothermometry.

Characterization of Radiation-Induced Point Defects via EPR and Optical Spectroscopy in Oxides

Aleksandr Lushchik

Institute of Physics, University of Tartu, W. Ostwald Str. 1, 50411 Tartu, Estonia

Insufficient tolerance to intentional irradiation and even prolonged stay in harsh radiation environment is a serious limitation for the use of wide-gap materials with a certain functional property for different applications. At present, the search for materials with optical/diagnostics window capabilities in a wide spectral region is an urgent task within the programs of the EUROfusion consortium. Several wide-gap oxides, in particular MgO, Al_2O_3 and $MgAl_2O_4$ are considered as promising candidates for the use in harsh environment of DEMO fusion reactor.

In general, the functionality of optical materials is strongly influenced by the accumulation of stable defects (interstitial-vacancy Frenkel pairs and their aggregates) formed under irradiation. For this reason, the investigation and understanding of the mechanisms of defect creation, accumulation with dose/fluence and subsequent thermal annealing play a crucial role. Note that the characteristics of the main point defects – F^+ and F centers (one or two electrons in the field of an oxygen vacancy) have been thoroughly studied in irradiated and additively coloured oxides, while the complementary defect – single interstitial oxygen – remains the most "invisible/hidden" primary Frenkel defect in wide-gap metal oxides. The creation of Frenkel defects in cationic sublattice is studied/understood insufficiently as well.

The processes of radiation damage caused by fast neutrons, 100-keV protons or ~GeV heavy ions have been studied in MgO, Al_2O_3 and $MgAl_2O_4$ crystals by means of several methods (optical absorption, photo- and cathodo-luminescence, EPR) [1-6]. The analysis of the EPR signal angular dependencies at different microwave power allowed to reveal neutron-induced defects, which are ascribed to the hole localized at regular oxygen ion nearby a different cation defect ($MgAl_2O_4$ [1,2]) or to a tentative single oxygen interstitial (Al_2O_3). The pulse annealing of the EPR signal of these defects was compared to that of radiation-induced optical absorption (RIOA, decomposed into Gaussian components) in the same crystals in order to elucidate the correlation between the paramagnetic centers and relevant elementary absorption bands.

The accumulation of F-type centers under oxide irradiation by protons ($MgAl_2O_4$ [3]) or swift ions (MgO [4], Al_2O_3) with fluence varying by three orders of magnitude has been investigated. The thermal annealing of RIOA in oxides has been analyzed in terms of the diffusion-controlled bimolecular reactions between F-type centers and complementary interstitial oxygen ions [5,6]. The behavior of the kinetic parameters has been discussed in terms of Meyer-Neldel rule known in chemical kinetics of condensed matter (see, e.g., [6]). A tentative scenario of the irreversible annealing of neutron-induced defects (involving both anion and cation sublattice) in $MgAl_2O_4$ and Al_2O_3 single crystals has been proposed.

[1] A. Lushchik, S. Dolgov, E. Feldbach et al., Nucl. Instrum. Meth. B 435, 31-37 (2018).
[2] V. Seeman, E. Feldbach, T. Kärner et al., Opt. Mater. 91. 42-49 (2019).
[3] E. Feldbach, I. Kudryavtseva, K. Mizohata et al., Opt. Mater. 96, 109308 (2019).
[4] G. Baubekova, A. Akilbekov, E. Feldbach et al., Nucl. Instrum. Meth. B 463, 50-54 (2020).
[5] G. Baubekova, A. Akilbekov, E.A. Kotomin et al., Meth. B 462, 163-168 (2020).
[6] A.I. Popov, A. Lushchik, E. Shablonin et al., Nucl. Instrum. Meth. B 433, 93-97 (2018).

Thermochemical Expansion: Constraints for the High-Temperature Processing and Operation of Perovskite-Related Oxides

Aleksey Yaremchenko

CICECO - Aveiro Institute of Materials, Department of Materials and Ceramic Engineering, University of Aveiro, 3810-193 Aveiro, Portugal
ayaremchenko@ua.pt

Perovskite-like and perovskite-related oxides based on variable-valence transition metals may exhibit substantial changes in oxygen content in the course of temperature cycling or under variation of oxygen chemical potential at elevated temperatures. This gives rise to a chemical contribution to the thermal expansion (chemical expansion/contraction or chemical strain) originating mainly from the accompanying changes in the average oxidation state of transition metal cations and, consequently, their ionic radii. Excessive dimensional changes caused by the chemical expansion impose constraints to the applicability of functional oxides at elevated temperatures and under variable redox conditions (due to thermomechanical instability or incompatibility with other materials) and also complicate the processing of oxide ceramics at high-temperatures. Another unfavourable phenomenon is microcracking caused by a strongly anisotropic expansion of crystal lattice. Microcracking has a negative impact on the quality and mechanical properties of ceramics and is responsible for significant hysteresis in dimensional changes and variations of functional properties on thermal cycling.

This talk gives an overview of representative study cases including selected perovskite-like systems (donor-doped $SrTiO_3$, $(Ba,Sr)Co_{0.8}Fe_{0.2}O_{3-\delta}$, $LaCrO_3$- and $LnMnO_3$-based compositions) and perovskite-related Ruddlesden-Popper phases based on $Ln_2NiO_{4\pm\delta}$.

Revealing the Luminescence Mechanisms in Li_2MoO_4 Scintillation Crystals by Complex Experimental and Computational Studies

Yu. Hizhnyi[1], S. Nedilko[1], V. Chornii[1,2], I. Tupitsyna[3], O. Dubovik[3] and G. Yakubovskaya[3]

[1]*Taras Shevchenko National University of Kyiv, 64/13 Volodymyrska st., Kyiv,Ukraine*
[2]*National University of Life and Environmental Sciences of Ukraine, 15 Geroiv Oborony st., Kyiv, Ukraine*
[3]*Institute for Scintillation Materials NAS of Ukraine, 60 Nauky ave., Kharkiv, Ukraine*

The lithium molybdate crystals Li_2MoO_4 have been considered as perspective scintillation materials for cryogenic scintillation bolometers. The Li_2MoO_4 crystals were characterized by relatively low scintillation light yield but they have an excellent separation between β-like and α events, at the level required for a high sensitive $0\nu2\beta$ decay search. Understanding of peculiarities of the luminescence processes in Li_2MoO_4 is a very important step for elaboration of crystals with optimal scintillation characteristics.

This report presents cumulative results of computational and experimental studies which improve understanding of the mechanisms of luminescence and excitation energy transfer in Li_2MoO_4 crystals. The studies cover the data about growth and characterization of samples with various concentrations of point defects, post-growth treatment of the samples, optical absorption and luminescence spectroscopy, TSL measurements as well as the data concerning electronic band structure calculations of Li_2MoO_4 crystals conyaining various defects.

The lithium molybdate charge was obtained by a solid-state synthesis technique from MoO_3 (99.5% or 99.9 % purity) and Li_2CO_3 (99.5 % or 99.99 % purity) powders. Single crystals of Li_2MoO_4 were grown by the Czochralski technique in a Pt crucible at room atmosphere or dry air. Precise ratios of the crystal constituents and concentrations of trace impurities were studied by X-ray fluorescence elemental analysis and mass-spectrometry technique. Morphology of the samples was studied using scanning electron microscopy technique. The luminescence characteristics under photo- and X-ray excitations, the IR and optical transmission spectra, TSL characteristics of the grown Li_2MoO_4 samples were measured and analyzed.

Calculations of the electronic structure of Li_2MoO_4 crystals with defects were carried out using the DFT-based plane-wave pseudopotential method implemented in the CASTEP package [1] in the super-cell approach using geometry optimization. The super-cells were constructed as 1x2x2 multiplication of the unit cell of the crystal and comprised 72 formula units of Li_2MoO_4 (in the defectless case). Several most probable kinds of point defects and defect combinations were modeled in the super-cells: natural vacancies and vacancy complexes (V_O, V_{Li}, V_O+V_{Li}, Vo+2V_{Li}), the Li cation substitutions $Me(II)_{Li}$ (Me(II) = Be, Mg, Ca, Sr, Ba, Zn,) and Al_{Li}, other alio- (Tc_{Mo}, Nb_{Mo}, F_O, N_O) and isovalent substitutions (Na_{Li}, K_{Li}, W_{Mo}, Cr_{Mo}), interstitial defects Zn_i and incorporated species MoO_3, H_2O, CH_3 and OH. The partial densities of states, the linear optical properties (including absorbance and reflectance spectra) and defect transition levels (defect ionization energies) were calculated and analysed.

The influence of studied point defects on the luminescence and energy transfer processes in Li_2MoO_4 crystals was discussed on the ground of obtained experimental and calculation results. The origin of shallow charge carrier traps was revealed in analysis of calculated ionization energies of most common defects existing in lithium molybdate. The mechanism of high hygroscopicity of Li_2MoO_4 grown samples was explained, too.

[1] M. C. Payne, M. P. Teter, D. C. Allan, et al. // Rev. Mod. Phys. 64 (1992) 1045–1097.

Synthesis and Luminescence Properties of Pure and Doped with Europium(III) $A_{0.5x}Bi_{1-0.5x}Mo_xV_{1-x}O_4$ (A – Na, K) Compounds

V. Chornii[1,2], V. Boyko[1], S.G. Nedilko[2], O. Petrenko[2], V. Prokopets[2], K. Terebilenko[2] and M. Slobodyanyk[2]

[1]*National University of Life and Environmental Sciences of Ukraine, 15 Geroiv Oborony st., 03041, Kyiv, Ukraine*
[2]*Taras Shevchenko National University of Kyiv, 64/13 Volodymyrska st., 01301, Kyiv, Ukraine*

Bismuth-containing oxides are of great interest due to perspectives of their application as luminophores, laser active media, scintillating materials, etc. The crystal structures and spectroscopic properties of the $A^IBi(M^{VI}O_4)_2$ (here A^I – Li, Na, K, Cs, and M^{VI} – Mo, W) binary compounds have been intensively studied. These compounds were considered to be of the scheelite - related structure. The key feature of this crystal structure is random distribution of A^I and Bi atoms over the same crystallographic positions, while M^{VI} is more likely to be found in slightly distorted tetrahedra. The bismuth cations and molybdate molecular anions determine the edges of electronic bands of the crystals: the Bi *s* and O *p* electronic states dominate at the top of valence band when Bi *p* and Mo *d* forming bottom of the conduction band. Much attention has been also paid to study of the rare-earth (RE) doped bismuth molybdates and tungstates and it was found that doping with vanadium increased absorption of the light in UV – violet spectral range and absorbed energy could be transferred to the RE ions.

Synthesis of the $A_{0.5x}Bi_{1-0.5x}Mo_xV_{1-x}O_4$ (A – Na, K) samples was performed by solid state technique in this work. Analytically pure A_2CO_3, Bi_2O_3, MoO_3, V_2O_5 and Eu_2O_3 were taken as starting materials without further purification. Stoichiometric amounts of the reagents were thoroughly mixed in an agate mortar into fine powders. At the first stage, the mixtures have been calcinated at 550 °C for 2 h to get rid of carbon dioxide. Then, the resulting powders have been mixed with a drop of ethanol, thoroughly reground and sintered at 600 for 5 h, 700 °C for 8 h, and 750 °C for 8 h with intermediate regrinding after each temperature in covered alumina crucibles. The purity of the polycrystalline products and phase composition of the obtained mixtures have been controlled and identified using powder X-ray diffraction. The IR- spectra were measured on a PerkinElmer Spectrum BX FTIR spectrometer in the frequency range 400–4400 cm^{-1} using the sample pressed with KBr. The SEM studies were performed at JEOL JCM-6000 NeoScope Benchtop microscope. The photoluminescence (PL) studies under excitations in the UV and visible regions were carried out at 77 and 300 K temperatures. The diffraction spectrometer MDR-23 was used for registration of the PL emission and excitation spectra. The radiation of the Xenon-arc lamp (150 W) was used for the PL excitation.

The solid solutions $x(M^I_{0.5}Bi_{0.5}MoO_4)$-$(1-x)BiVO_4$ crystallize tetragonal with the space group $I4_1/a$ and are related to the $CaWO_4$ scheelite structure. The cationic site corresponds to dodecahedral oxygen environment, while Mo and V are tetrahedral coordinated. The band gap values were estimated from UV-Vis diffuse reflectance spectra and are in 2.28 – 2.67 eV and 2.33 – 2.72 eV range for $Na_xBi_{1-x}Mo_{2x}V_{1-2x}O_4$ and for $K_xBi_{1-x}Mo_{2x}V_{1-2x}O_4$ series, respectively. Two the PL bands of intrinsic emission with maxima near 620 and 705 nm have been observed under band-to-band excitation at liquid nitrogen temperature. The doped with Eu^{3+} samples reveal intensive PL emission related with $^5D_0 \rightarrow {}^7F_J$ f-f electronic transitions in these RE ions under excitation both into absorption bands of molybdate host and Eu^{3+} ions. The conclusion was made about perceptiveness of the studied materials using as red luminophores.

Temperature Dependence of Nickel Oxide Wetting with Liquid Tin

I. Shtablavyi[1], R. Ovsianyk[1], S. Mudry[1], B. Venhryn[2], Yu. Pashko[1] and Yu. Kulyk[1]

[1]*Ivan Franko National University of Lviv, Kyryla i Mephodia Str. 8, Lviv 79005, Ukraine*
[2]*Lviv Polytechnic National University, S. Bandery Str. 12, Lviv 79013, Ukraine*

Powder wettability plays a significant role in many applications, such as coatings, dispersions, powder processing, such as granulation and other practical uses. Such significance has driven scientists to develop ways to evaluate the wettability of powders with liquid metals [1-3]. Typically, the wettability of solid surfaces is estimated via measuring the angle formed by the liquid under study on a certain solid surface.

One of the most common method of measuring the wetting angle is the sessile drop method [4], when a drop of liquid is placed on the surface and the wetting angle is measured directly at the contact boundary of the three phases (liquid, solid and vapour). For powder samples, this method requires compacting the powder into the disk using high pressure and then measuring the wetting angle by the fluid under investigation. Another way to use the sessile drop method is to deposit a layer of investigated powder on the substrate and then measure the wetting angle.

These two methods of sample preparation were used to study the wetting of nickel and nickel oxide by liquid tin. The wetting process was investigated in the temperature range of 450-1250 K. It was established that below the temperature of 1034 K the tin does not wet the pressed nickel oxide, and at the temperature of 1034 K there is an intense chemical interaction of nickel oxide and tin. The uncompressed powder of nickel oxide is not wetted with tin up to a temperature of 1000 K. With further heating, the wetting angle sharply decreases.

The result of the interaction of liquid tin with nickel oxide was investigated by X-ray diffraction and scanning electron microscopy.

[1] A. Alghunaim, S. Kirdponpattara, B.Z. Newby, Techniques for Determining Contact Angle and Wettability of Powders, *Powder Technology* **287** (2016) 201–215, https://doi.org/10.1016/j.powtec.2015.10.002.

[2] N. Eustathopoulos, Wetting by Liquid Metals – Application in Materials Processing: The Contribution of the Grenoble Group, *Metals* **5** (2015) 350–370, https://doi.org/10.3390/met5010350.

[3] E. Nowak, G. Combes, E.H. Stitt, A.W. Pacek, A comparison of contact angle measurement techniques applied to highly porous catalyst supports, *Powder Technology* **233** (2013) 52–64, https://doi.org/10.1016/j.powtec.2012.08.032.

[4] L. Susana, F. Campaci, A.C. Santomaso, Wettability of mineral and metallic powders: Applicability and limitations of sessile drop method and Washburn's technique, *Powder Technology* **226** (2012) 68–77, https://doi.org/10.1016/j.powtec.2012.04.016.

Optical Absorption of the Transparent Spinel Ceramics after High Energy Electron Irradiation and Thermal Annealing

Yu.G. Kazarinov[1,2], V.T. Gritsyna[2] and S.P. Gokov[1]

[1]*NSC Kharkiv Institute of Physics and Technology NAS of Ukraine 1, Akademicheskaya St. 61108, Kharkiv, Ukraine*
[2]*V.N. Karazin Kharkiv National University, 4 Svoboda Sq.,61022 Kharkiv, Ukraine*

Due to unique combination of dielectric, optical and mechanical properties, magnesium aluminates spinel is recommended for application as a component for many technological applications. Recently the production of the transparent optical ceramics was developed that stimulate its application as armor and optical windows for automobile, planes and missiles, which can undergo to different types of irradiation. We intend to present the results of our investigations of optical properties of spinel ceramics after irradiation with high energy electrons and subsequent thermal annealing.

Spinel ceramics were prepared by a conventional hot-pressing technique. Slices of 0.7 mm in thickness were cut from ceramic disk and polished to optical finish. Irradiation was provided at the linear accelerator with electron energy of 16 MeV and current density of 2.5 μA/cm^2 in the range of fluences Φ=4.2·10^{16}–3.3·10^{17} el/cm^2. Measurements of the optical absorption spectra were provided using a single beam spectrophotometer in the wavelength range of 186-960 nm at room temperature.

Using the deconvolution of the experimental spectra into Gaussians we observed the numerous absorption bands which can be divided in two photon energy ranges hv<4 eV and hv> 4 eV. In the visible range of absorption spectra the bands of maxima at 2.2, 2.8, 3.4, and 3.8 eV were obtained, some of them were identified with hole centers at native and radiation induced cationic vacancies. The high photon energy bands at 4.15, 4.75, and 5.26 eV are related to electron centers formed on the anionic vacancies [1].

The intensity of the radiation induced absorption bands in the visible range practically was saturated at the lowest the electron fluence. The fluence dependence of radiation induced number of electron centers (area of absorption bands) demonstrates the linear dependence in the measured fluence range of different slopes: $N(F^+)=a_1+2.8\Phi$ and $N(F)=a_2+8.5\Phi$, where a_1 and a_2 are absorption coefficient of pristine samples. It was revealed that the value of ratio $N(F)/N(F^+)$ grows in dependence on the electron fluence. At the maximal fluence the number of F-centers is twice time larger to compare with that of F^+-centers. Such value of ratio for electron irradiated spinel ceramics is consistent with that for neutron irradiated spinel single crystals [2]. Because both F^+- and F-centers are formed by capturing one or two electrons on the same radiation created anionic vacancies efficiency formation of F^+ centers to compare with that of F-centers is governed by electronic processes.

The annealing of radiation induced optical absorption was performed in air by heating sample on metal surface to given temperature in a step of 50K, exposure at this temperature for 60 sec, and cooling to room temperature together with heater for the optical measurements. The dependence of radiation induced absorption on annealing temperature demonstrate the higher thermal stability of F^+-center to compare with that of the F-centers.

[1] J.-M. Constantini, G. Lelong , M. Guillaumet, S. Takaki, K.Yasuda. J. Appl. Phys. 124 (2018) 245901.
[2] A. Lushchik, S. Dolgov, E. Feldbach, R. Pareja, A.I. Popov, E, Shablonin, V. Seeman. Nucl. Instrum. Methods B 435 (2018) 31-37.

Formation of p-Type NiO Thin Films on Different Substrates: Structural, Electrical, Optical, and Magnetic Properties

Dogan Kaya[1], Hafize Seda Aydınoğlu[2], Ebru Şenadım Tüzemen[3,4] and Ahmet Ekicibil[5]

[1]*Department of Electronics and Automation, Vocational School of Adana, Cukurova University, 01160, Adana, Turkey*
[2]*Department of Medical Services and Techniques, Program of Opticianry, Vocational School of Healthcare, Sivas Cumhuriyet University, 58140, Sivas, Turkey*
[3]*Nanophotonics Research and Application Center, Sivas Cumhuriyet University, 58140, Sivas, Turkey*
[4]*Department of Physics, Faculty of Science, Sivas Cumhuriyet University, 58140, Sivas, Turkey*
[5]*Department of Physics, Faculty of Art and Sciences, Cukurova University, 01330, Adana, Turkey*

Metal oxide materials have received considerable attention recently due to their high sensitivity, fast response/recovery times, low power consumption and low production costs in the applications such as gas sensors, optical devices, thin-film transistors, etc. [1] In this study, we have investigated high-quality p-type NiO semiconductor thin film using the thermal evaporation method by annealing Ni layer at 450 °C for 2.5 h. The formation of NiO film on different natures of substrates; glass, sapphire, Si(100), InP, and GaAs [1,2] have been characterized by x-ray diffraction (XRD) analysis, scanning electron microscopy (SEM) images, and Hall-effect measurements. The structural properties of NiO film were determined as a cubic phase with space group of *Fm-3m* by XRD analysis that revealed two possible formations; with (sapphire, InP, and GaAs) and without (glass and Si(100)) Ni-surface interaction. Due to the annealing process, Ni ions diffuse into the sapphire, InP, and GaAs substrates, and the secondary phases of NiAl, Ni_xP/Ni_2InP, and $NiAs/Ni_2GaAs$ were formed. SEM images managed to determine the average film thickness and the reduction of the film thickness revealed a possible Ni-surface interactions. The optical transparency was obtained at approximately 94% and 89% transmittance in the range of 300-800 nm for the NiO film on sapphire and glass substrates, respectively. The direct optical band gap of NiO film on glass and sapphire substrates were calculated by Tauc's equation and found to be 3.63 eV and 3.67 eV, respectively. We were confirmed a p-type characteristic of the NiO film on glass and sapphire substrates by Hall-effect measurements [2].

[1] C. Glynn, C. O'Dwyer, Solution Processable Metal Oxide Thin Film Deposition and Material Growth for Electronic and Photonic Devices, Advanced Materials Interfaces, 4 (2017) 1600610.
[2] D. Kaya, H.S. Aydınoğlu, E. Şenadım Tüzemen, A. Ekicibil, Investigation of optical, electronic, and magnetic properties of p-type NiO thin film on different substrates, Thin Solid Films, 732 (2021) 138800.

Luminescence and Energy Transfer Processes in $LuNbO_4$:Bi,Eu

V. Tsiumra[1,2], M. Baran[3], A. Kissabekova[4,5], A. Krasnikov[4], A. Lushchik[4], Ya. Zhydachevskyy[1,6], L. Vasylechko[6] and S. Zazubovich[4]

[1]*Institute of Physics, Polish AS, Al. Lotników 32/46, 02-668 Warsaw, Poland*
[2] *Ivan Franko National University of Lviv, Kyryla and Mefodiya 8a, Lviv 79005, Ukraine*
[3]*Institute of Electronic Materials Technology, Wólczyńska 133, 01-919 Warsaw, Poland*
[4]*Institute of Physics, University of Tartu, W. Ostwaldi 1, 50411 Tartu, Estonia*
[5]*L.N. Gumilyov Eurasian National University, Nur-Sultan, Kazakhstan*
[6]*Lviv Polytechnic National University, Bandera 12, 79013 Lviv, Ukraine*

The interest in Bi^{3+}-doped compounds increased drastically in recent years due to their possible applications as scintillator and phosphor materials suitable for X-ray screens, white light-emitting diodes, solar cells, dosimeters, etc. The compounds co-doped with Bi^{3+} and different trivalent rare-earth (RE^{3+}) ions were found to be potentially applicable as spectral converters for solar cells and solid-state light sources of new generation, so-called white light-emitting diodes (WLED), owing to strong absorption in the ultraviolet spectral region, intense broad visible Bi^{3+}-related emission bands, and effective $Bi^{3+} \rightarrow RE^{3+}$ energy transfer, resulting in the appearance of the luminescence covering a wide spectral range from blue to red.

Recently, a detailed and systematic investigation of the Bi^{3+}-related luminescence in $YNbO_4$:Bi, $LuNbO_4$:Bi, and $GdNbO_4$:Bi microcrystalline powders with different Bi^{3+} contents was carried out [1]. Two broad visible Bi^{3+}-related emission bands were observed in the emission spectrum of the Bi^{3+}-doped niobates. The analysis of temperature dependences of their decay time and the values of the corresponding relaxed excited states (RES) parameters allowed us to conclude their exciton-like origin. The higher-energy emission was ascribed to an exciton localized around a single Bi^{3+} ion. The lower-energy emission, showing the superlinear dependence on the Bi^{3+} content, was ascribed to the radiative decay of an exciton localized around a dimer $\{Bi^{3+}–Bi^{3+}\}$ center. The absence of the ultraviolet emission, arising from the radiative decay of the triplet RES of a Bi^{3+} ion, and the exciton-like origin of the visible Bi^{3+}-related emissions indicate that the triplet RES of both the Bi^{3+} ion and the $\{Bi^{3+}–Bi^{3+}\}$ dimer are located inside the conduction band of the investigated niobates.

In this work, six samples of the $LuNbO_4$:Bi,Eu microcrystalline powders with the same Bi^{3+} content (2%) and different Eu^{3+} concentrations (varying from 0.2 to 8%) are synthesized and analyzed by the XRD method. The luminescence characteristics of the $LuNbO_4$:Bi,Eu powder are investigated by the steady-state and time-resolved luminescence spectroscopy methods in a wide temperature range (4.2–500 K) and compared with the characteristics of the undoped and Bi^{3+}-doped $LuNbO_4$. It is found that owing to the complete overlap of the intrinsic and Bi^{3+}-related emission bands with the absorption bands of Eu^{3+} ions, an effective energy transfer from the host and Bi^{3+}-related exciton-like states to Eu^{3+} takes place in $LuNbO_4$:Bi,Eu resulting in the appearance of the luminescence in the 1.7–3.5 eV energy range. The shortening of the Bi^{3+}-related luminescence decay time with the increasing Eu^{3+} concentration allows us to conclude the nonradiative (resonance) energy transfer mechanism in $LuNbO_4$:Bi,Eu. The CIE color coordinates and the luminescence quantum yield values are determined. Possible application of the $LuNbO_4$:Bi,Eu phosphor in WLED is discussed.

The work was partially supported by the National Research Foundation of Ukraine under Grant no. 2020.02/0373.

[1] M. Baran, K. N. Belikov, A. Kissabekova, A. Krasnikov, A. Lushchik, E. Mihokova, V. Tsiumra, L. Vasylechko, S. Zazubovich, Ya. Zhydachevskyy, J. Alloys and Compounds 859, 157800 (2021).

Photoinduced Effects in the Single Crystals of PbO – MoO_3 System

D. Bondar, T. Bochkova, M. Trubitsyn and M. Volnyanskii

Laboratory of Active Dielectric Crystals, Dept. of experimental physics, Oles Honchar Dnipro National University, prosp. Gagarina 72, Dnipro, 49010, Ukraine

Acoustooptics is a most promising field of application for the crystals of PbO – MoO_3 family. Lead molybdate ($PbMoO_4$) is widely used due to broad spectral range and high acousto-optical characteristics. Well developed technology for growing $PbMoO_4$ crystals of acceptable quality is an important favorable factor. Double lead molybdate (Pb_2MoO_5) have not yet been widely used in acousto-optical devices mainly owing to lack of affordable technology for growth of high-quality crystals. Nevertheless Pb_2MoO_5 is an optically biaxial crystal with high and strongly anisotropic acousto-optical parameters, which open up the perspectives of its applications in fundamentally new acousto-optical devices. A significant drawback of these acousto-optical materials is light yellow coloration and dependence of optical absorption on external influences (UV irradiation, annealing in various atmospheres).

$PbMoO_4$ and Pb_2MoO_5 have a different crystal structure. Lead molybdate possess the scheelite-type structure (tetragonal space group $I\ 4_1/a$). The lattice of Pb_2MoO_5 belongs to monoclinic system with a space symmetry group $C\ 2/m$. At the same time, both crystals contain the characteristic molecular anionic tetrahedra $(MoO_4)^{2-}$ with almost the same Mo – O distance.

In the abstract we report the data on study of $PbMoO_4$ and Pb_2MoO_5 single crystals grown by Czochralski method. Variation of the growing conditions, composition stoichiometry and doping with impurities were used to modify the crystals properties.

Study of electrical and optical properties of both crystals revealed a number of photoinduced phenomena. In particular, photodielectric effect consisted in the appearance of permittivity ε and conductivity σ anomalies under influence of UV radiation. The anomalies grew in amplitude for higher radiation dose, disappeared after annealing at 700 K and could be restored by repeated irradiation. In both crystals, the observed anomalies were detected as nearly symmetrical ε(T) peaks that significantly differed from typical Debye-type stepwise temperature behavior. In addition it was shown that UV radiation changed absorption optical spectra and led to photochromic effect. The nature of the observed phenomena was discussed with the help of recent EPR studies of lead molybdate and tungstate crystals.

It was suggested that UV radiation induced the defects with electric dipole moments giving rise to ε and σ anomalies in an AC field. The photoinduced dipole defects were associated with photoelectrons captured by molybdenum ions within tetrahedra distorted by oxygen vacancy $(MoO_3)^-$. Distorted $(MoO_3)^-$ tetrahedron acquired electric dipole moment produced by excess charges of captured by Mo photoelectron and oxygen vacancy V_O. Thermally activated V_O hopping through the vertexes of $(MoO_3)^-$ complex was accompanied by reorientation of the dipole moment.

The effect of growing conditions, doping, and high temperature annealing on the properties of crystals $PbMoO_4$ and Pb_2MoO_5 were also discussed.

Four-Component Perovskites in the *A*–*R*–Fe–O Systems at 1200°C (*A* – Alkaline-Earth, *R* – Rare-Earth Metal)

O. Zaremba, V. Hrytsan and R. Gladyshevskii

Ivan Franko National University of Lviv,
Kyryla i Mefodiya St. 6, UA-79005 Lviv, Ukraine

The analysis of data about *A*–*R*–Fe–O systems [1] indicated on the formation of four-component $(A,R)FeO_3$ perovskites in the vast majority of cases. In the Ca–*R*–Fe–O systems the compounds exist for *R* = light rare-earth metal (except Pm and Eu) and Dy, that belong to $CaTiO_3$ or $GdFeO_3$ structure type. Similar situation is observed in Sr–*R*–Fe–O systems: the $(Sr,R)FeO_3$ phases are formed for *R* = light rare-earth metal (except Pm) and Dy, that can be described by $CaTiO_3$, $GdFeO_3$, $LaAlO_3$, $Ba(Pb_{0.5}Bi_{0.5})O_3$ or $Sr(Fe_{0.5}Ru_{0.5})O_3$ structures. Regarding Ba–*R*–Fe–O systems, there is information about the formation of 1:1:3 phases with most REMs (except Pm, Eu, Dy, Ho) and all of them belong to the $CaTiO_3$ type. We noticed that the phases described above differ not only in structures, but also in the conditions of existence and *A*/*R* ratio what was a reason for systematic study of the $AFeO_3$–$RFeO_3$ cross-sections.

$A_{0.5}R_{0.5}FeO_3$ samples were obtained by multi-stage solid-state synthesis from alkaline-earth metal carbonates, rare-earth metal and iron(III) oxides. At the beginning reagents were mixed and heated at 1000°C during 24 h for decomposition the carbonates. Then they were ground, pressed into tablets and sintered again. Finally, all samples were annealed at 1200°C during 8 h. X-ray powder diffraction data were used for phase and structural analysis.

Under conditions of our investigation the existence of tetrary $A_{0.5}R_{0.5}FeO_3$ phases with $CaTiO_3$-type perovskite structure was confirmed for *R* = Pr and Nd in the Ca–*R*–Fe–O systems and *R* = Pr, Nd, Sm and Eu in the Sr–*R*–Fe–O systems only (tables 1,2).

Table 1 Results of phase analysis of $A_{0.5}R_{0.5}FeO_3$ samples, annealed at 1200°C

№	Nominal composition	Phase composition	ST	PS	SG	Content, wt.%
1	$Ca_{0.5}Pr_{0.5}FeO_3$	$Ca_{0.5}Pr_{0.5}FeO_3$	$CaTiO_3$	*cP*5	*Pm*-3*m*	100
2	$Ca_{0.5}Nd_{0.5}FeO_3$	$Ca_{0.5}Nd_{0.5}FeO_3$	$CaTiO_3$	*cP*5	*Pm*-3*m*	100
3	$Sr_{0.5}Pr_{0.5}FeO_3$	$Sr_{0.5}Pr_{0.5}FeO_3$	$CaTiO_3$	*cP*5	*Pm*-3*m*	100
4	$Sr_{0.5}Nd_{0.5}FeO_3$	$Sr_{0.5}Nd_{0.5}FeO_3$	$CaTiO_3$	*cP*5	*Pm*-3*m*	100
5	$Sr_{0.5}Sm_{0.5}FeO_3$	$Sr_{0.5}Sm_{0.5}FeO_3$	$CaTiO_3$	*cP*5	*Pm*-3*m*	100
6	$Sr_{0.5}Eu_{0.5}FeO_3$	$Sr_{0.5}Eu_{0.5}FeO_3$	$CaTiO_3$	*cP*5	*Pm*-3*m*	100

Table 2 Refined composition and cell parameters of $A_{0.5}R_{0.5}FeO_3$ tetrary perovskites

№	Phase	*a*, Å	*b*, Å	*c*, Å	R_B
1	$Ca_{0.47(2)}Pr_{0.53(2)}FeO_3$	3.8501(3)	–	–	0.081
2	$Ca_{0.46(2)}Nd_{0.54(2)}FeO_3$	3.8486(4)	–	–	0.097
3	$Sr_{0.54(3)}Pr_{0.46(3)}FeO_3$	3.8783(4)	–	–	0.095
4	$Sr_{0.51(3)}Nd_{0.49(3)}FeO_3$	3.8752(4)	–	–	0.095
5	$Sr_{0.45(2)}Sm_{0.55(2)}FeO_3$	3.8651(4)	–	–	0.094
6	$Sr_{0.46(1)}Eu_{0.54(1)}FeO_3$	3.8653(2)	–	–	0.047

[1] P. Villars. K. Cenzual (Eds.). Pearson's Crystal Data – Crystal Structure Database for Inorganic Compounds. Release 2017/18. ASM International. Materials Park. OH. 2017.

Electrochemical Synthesis of $Li_yCa_{1-x}Nd_xMnO_3$ Solid Solution

V. Kordan, O. Zaremba and P. Demchenko

Ivan Franko National University of Lviv,
Kyryla i Mefodiya St. 6, UA-79005 Lviv, Ukraine

$Ca_{1-x}Nd_xMnO_3$ solid solution belongs to perovskite family, the investigation of which is actual taking into account the variety of their applications. It is characterized by orthorhombic $GdFeO_3$ structure (Pearson symbol *oP*20, space group *Pnma*).

Ceramic samples were synthesized by solid-state reaction starting from corresponding quantities of $CaCO_3$, Nd_2O_3 and Mn_2O_3 powders in two stages at 1000 and 1200°C, respectively. X-ray diffraction data of nominal and Li-containing samples were obtained using STOE STADI P automatic diffractometer (Cu $K\alpha_1$-radiation). The composition of samples before and after electrochemical lithiation was controlled by X-ray fluorescent spectroscopy (ElvaX Pro spectrometer) and energy-dispersive X-ray spectroscopy (electron microscope Tescan VEGA3 LMU; analyzer Oxford Instruments Aztec ONE system with X-Max^{N}20 detector). Electrochemical lithiation was carried out in galvanostatic mode (2-electrode prototype "Swagelok-cell") at 0.5-1.0 mA/cm^2. Studied samples were used as cathode, whereas commercial metallic lithium was applied as anode. 1M solution of $Li[PF_6]$ salt in a mixture of aprotic solvents (dimethyl carbonate and ethylene carbonate in ratio 1:1) served as electrolyte.

The composition of $Ca_{0.5}Nd_{0.5}MnO_3$ and $Ca_{0.5}Nd_{0.5}MnO_3$ samples was confirmed by spectral methods. Insertion of Li into voids of oxide phase takes place during discharge process at potential below 3.5 V. The compositions of Li-containing solid solutions are $Li_{0.057}Ca_{0.5}Nd_{0.5}MnO_3$ [1] and $Li_{0.091}Ca_{0.3}Nd_{0.7}MnO_3$ (1.14 and 1.82 at. % Li), correspondingly. X-ray phase and structural analysis (see pictures) showed the formation of phases with increased unit cell (see tables) and appearance of amorphous halo (the by-products of reaction between of electrode surface and electrolyte).

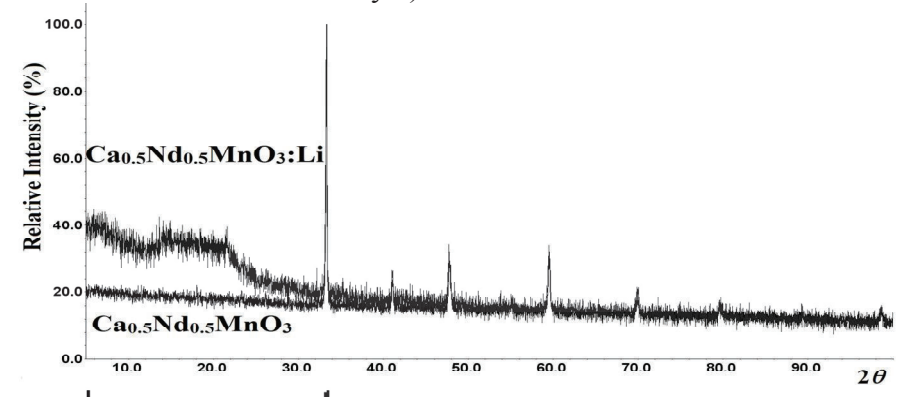

$Li_{0.057}Ca_{0.5}Nd_{0.5}MnO_3$	
a, Å	5.3953(12)
b, Å	7.5908(17)
c, Å	5.3766(11)
V, Å^3	**220.20(8)**

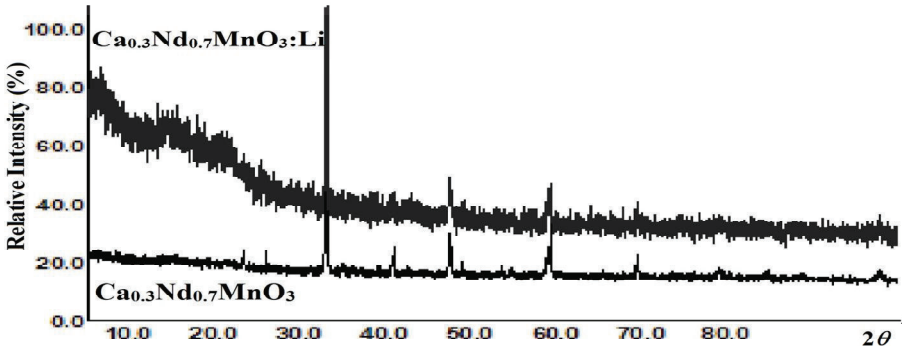

$Li_{0.091}Ca_{0.3}Nd_{0.7}MnO_3$	
a, Å	5.4623(14)
b, Å	7.652(2)
c, Å	5.4102(12)
V, Å^3	**226.14(10)**

[1] Kordan V., Zaremba O., Demchenko P. XVIII Scient. Conf. "Lviv Chemical Reading - 2021". P. H32.

Ionic and Electronic Transport in Acceptor-Doped $PrVO_4$

Rui G. Pinto[1], Blanca I. Arias-Serrano[1,2] and Aleksey A. Yaremchenko[1]

[1]*CICECO - Aveiro Institute of Materials, Department of Materials and Ceramic Engineering, University of Aveiro, 3810-193 Aveiro, Portugal*
[2]*Leibniz Institute for Plasma Science and Technology, 17489 Greifswald, Germany*

$LnVO_4$ orthovanadates attract attention as prospective materials for electrochemical applications, in particular, as redox-reversible electrode components for solid oxide fuel cells (SOFC) [1,2]. One important advantage of $LnVO_4$-derived components of SOFC anodes is their good resistance to carbon deposition and sulphur-containing impurities which is critical for hydrocarbon-fueled SOFCs. The present work is focused on the impact of the acceptor-type substitution by calcium on the electrical transport properties of zircon-type orthovanadate $PrVO_4$ under oxidizing conditions.

Undoped $PrVO_4$ and calcium-substituted $Pr_{1-x}Ca_xVO_{4-\delta}$ (x = 0.02-0.20) were prepared by conventional solid-state route and sintered at 1300ºC for 5 h in air. The prepared materials were characterized by XRD, SEM/EDS, thermal analysis, and measurements of electrical properties in controlled atmospheres. XRD demonstrated the formation of phase-pure solid solutions with tetragonal zircon-type structure for up to 5 at.% of calcium in Pr sublattice, while SEM/EDS suggest a lower solubility due to the presence of Ca-V-O phase impurities. $Pr(Ca)VO_4$ ceramics showed semiconducting behavior under oxidizing conditions at 400-900ºC. Within the solubility range, doping with calcium increases the total conductivity. The ionic and electronic contributions at 700-900ºC were assessed by the modified e.m.f. technique. The electronic conductivity is *p*-type and decreases with reducing $p(O_2)$. At lower temperatures, the total conductivity was found to be higher in wet atmospheres compared to dry conditions, thus implying a significant contribution of protonic transport at temperature below 550ºC. The redox behavior of $PrVO_4$-based ceramics on isothermal cycling between air and 10%H_2-N_2 was studied by impedance spectroscopy, thermogravimetry and XRD analysis.

[1] L. Adijanto, V.B. Padmanabhan, R. Küngas, R.J. Gorte, J.M. Vohs, J. Mater. Chem. 22 (2012) 11396.
[2] E.V. Tsipis, M.V. Patrakeev, V.V. Kharton, N.P. Vyshatko, J.R. Frade, J. Mater. Chem. 12 (2002) 3738.

Theoretical Estimation of Compositional Variations in Glass-Transition Temperature of Chalcogenide Glass Systems from Stochastic Agglomeration Theory and Covalent Bond Approach

M. Shpotyuk[1] and O. Shpotyuk[2,3]

[1]*Lviv Polytechnic National University, 12, Bandera str., Lviv, 79013, Ukraine*
[2]*O.G. Vlokh Institute of Physical Optics, 23, Dragomanov str., Lviv, 79005, Ukraine*
[3]*Jan Dlugosz University in Czestochowa, 13/15, al. Armii Krajowej, Czestochowa, 42200, Poland*

The glass-transition temperature T_g is one of most important thermodynamic characteristics of network-forming vitreous substances like chalcogenide glasses (ChG). Those, compositional changes in T_g values and their interrelation with materials-specific parameters defined by covalent bond approach such as mean coordination number Z, energy of covalent bonding of glassy network, etc. play a crucial role. First essential attempt to estimate T_g theoretically was done by Ke. Tanaka [1] derived simple relationship between T_g and mean coordination number Z for ChG and molecular materials with hydrogen bonding covering the range of $1 \le Z \le 2.7$. Almost a quarter century ago, Tichý and Tichá [2], employing the covalent bond approach derived simple linear master equation for glass transition temperatures T_g in dependence on the overall mean bond energy E. Nevertheless, they applied incorrect energy calculating formalism and therefore obtained wrong equation.

M. Micoulaut [3] proposed to estimate glass-transition temperature T_g in multinary ChG under the combination of covalent bond approach and stochastic agglomeration theory. Within this approach, the enhanced connectivity follows from increased number of equivalent structural states within the network accessible under glass transition. Unfortunately, this approach was unsuccessful owing to application the incorrect algorism of overall mean bond energy calculation described in [2].

We developed the universal relationships realistically predicting the compositional trends in the glass-transition temperature T_g for chalcogen-riched binary and ternary ChG derived from the revised covalent bond approach combining with the stochastic agglomeration theory. The master equation was shown to be obtained in the following form:

$$\frac{T_g}{T_{g0}} = 1 + A\left(E - E_0\right),$$

where T_{g0} and E_0 are glass-transition temperature and overall mean bond energy of pure for elemental ChG (such as S, Se, Te). The slope A depends on the type of ChG-building atoms being compositionally invariant for all binary and "symmetric" ternary ChG.

[1] K. Tanaka, *Solid State Commun.* **54** (1985) 867.
[2] L. Tichý, H. Tichá, *J. Non-Cryst. Solids* **189** (1995) 141.
[3] M. Micoulaut, *C.R. Chimie* **5** (2002) 825.

Growth, Optical Properties and Conductivity of the Lithium Heptagermanate Crystals Doped with Rare - Earth and 3d Ions

M. Trubitsyn[1], M. Koptiev[1], M. Volnianskii[1], S. Nedilko[2], V. Scherbatskii[2], M. Androulidaki[3], A. Papadopoulos[3] and A. Manousaki[3]

[1]*Oles Honchar Dnipro National University, prosp. Gagarina 72, Dnipro, 49010, Ukraine*
[2]*Taras Shevchenko National University of Kyiv, Volodymyrska Str., 64/13, Kyiv 01601, Ukraine*
[3]*Institute of Electronic Structure & Laser, Foundation for Research & Technology Hellas (FORTH) Crete, Greece*

The lithium heptagermanate crystals $Li_2Ge_7O_{15}$ (LGO) were grown and studied in the contributed paper. It is known that the structure of the noted crystals as well as structure of other crystals of the Li_2O-$x$$GeO_2$ family is formed by Ge-O tetrahedra and octahedra which are linked by the vertexes and edges. Presence of germanium- oxygen complexes enables doping the Li_2O-$x$$GeO_2$ crystals with transition group 4f and 3d ions of various valences [1]. The Ge-O polyhedra of the crystal create three-dimensional framework of the lattice that favors high mobility of the Li ions along the structural channels. It was shown that conductivity σ of $Li_2Ge_7O_{15}$ crystals was strongly anisotropic and can be changed in a wide range by doping with a small amount of Cr and Mn. Later we studied electrical properties of $Li_2Ge_7O_{15}$:Cu, Al. It was concluded that trivalent dopants (Cr^{3+}, Al^{3+}) substituted for Ge^{4+} hosts and increased σ strongly. The effect was explained by appearing lithium interstitials (A_{Li}) which compensated excess charge of the dopants and contributed to conductivity. In contrast, divalent impurity (Mn^{2+}) substituted for Li^{+} hosts, produced excess Li vacancies (V_{Li}) and decreased σ.

On can hope that doped Li_2O-$x$$GeO_2$ crystals can be also used as optically active media for various applications. Study of the doping influence on optical spectra and electrical conductivity may give valuable information on the crystal structure and the properties on atomic level. In the paper we report the data on crystal growth and study of optical properties and conductivity of the lithium heptagermanate $Li_2Ge_7O_{15}$ crystals (LGO) doped with some rare-earth and 3d ions.

The $Li_2Ge_7O_{15}$ single crystals doped with Eu, Gd, Cr, Mn, Cu, Al ions were grown by Czochralskii method. The dopants were added to initial chemical reagents (Ge and Li oxides) before mixing and synthesis of the charge. The doped with mentioned ions $Li_2Ge_7O_{15}$glasses were prepared by the melts quenching.

Electrical properties were measured in AC field by using LCR meter Keysight E4980AL and E7-10 bridge. The diffraction spectrometers DFS-12 and MDR-23 were used for registration of the photoluminescence (PL) emission and excitation spectra at room and cryogenic temperatures. The radiation of the Xenon-arc lamp (150 W) was used for the PL excitation.

All the samples under study were characterized with PL in visible range of the light. Three types of luminescence were found regarding spectral shape, intensity and decay of the PL. First, there were wide band low intensity luminescence inherent in un-doped crystals. Second, that was the PL inherent in LGO crystals doped with RE ions, and third, that was the PL caused by radiation *f-f* transitions in the intrinsic shell of the RE ions. Composition and intensity of the PL bands depends on the dopants concentration, type and morphology of the samples.

Influence of dopant on conductivity and optical properties was compared for doped single crystalline and amorphous $Li_2Ge_7O_{15}$.

[1] Trubitsyn M.P., Volnianskii M.D., Obaidat Yahia AH. Ionic conduction in $Li_2Ge_7O_{15}$ crystals doped with Cr and Mn ions. - Physics of the Solid State. – 2008. – V. 50, No 7. – P. 1234-1237.

Influence of Dy^{3+} on Luminescence Spectra Emission of $CaSO_4$ under X-Ray Excitation

T. Çavdar[1], V. Güçkan[2], Ö. Yiğit[2], Z. Yeğingil[2] and K. Kurt[1]

[1]*Mersin University Science and Letter Faculty Physics Department Mersin Turkey*
[2]*Çukurova University Science and Art Faculty Physics Department Adana Turkey*

Luminescence spectra of undoped and Dy^{3+} doped $CaSO_4$ have been studied under x-ray excitation at room temperature. Undoped CaSO4 has two wide emissions, prominent in the red region and relatively weak in the UV region. Doped CaSO4, on the other hand, has six peaks from the UV to IR region. The emission of 385nm might be attributed to anion vacancies of host materials and also can be seen in undoped material too. The emissions of 479nm, 578nm, 670nm, 750nm and 840nm belong to Dy^{3+} transition from $^4F_{9/2}$ to $^6H_{15/2}$, $^6H_{13/2}$, $^6H_{11/2}$, $^6H_{9/2}$ + $^6F_{11/2}$ and $^6H_{7/2}$ + $^6F_{9/2}$ respectively.

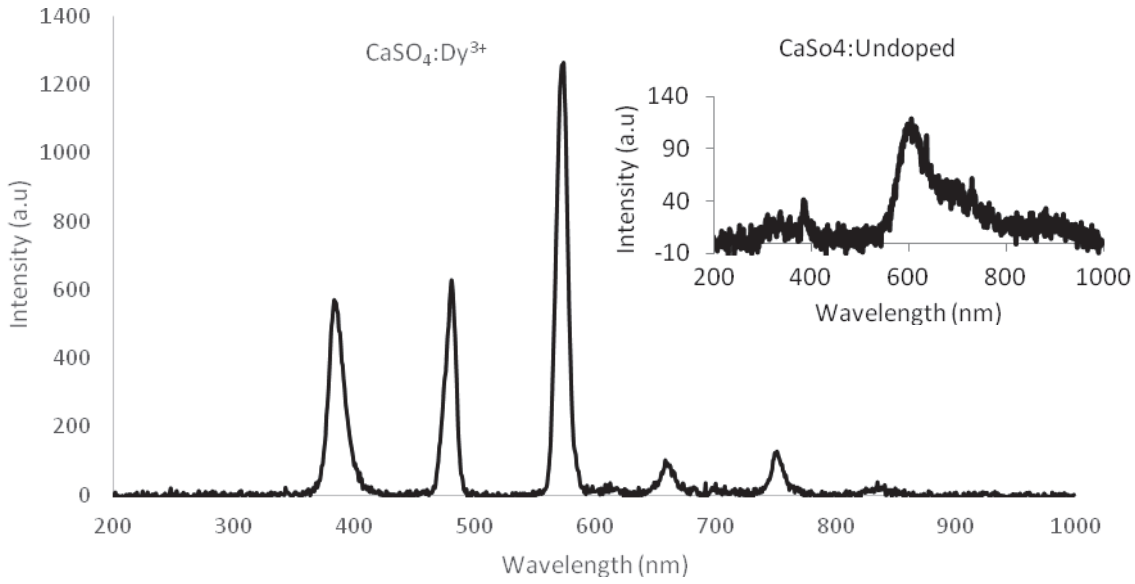

Fig. Luminescence spectra of Dy^{3+} doped and undoped $CaSO_4$ under X-Ray excitation

Acknowledgements. This research is supported by NATO through the project SPS G5647. We acknowledge gratefully the financial supports of NATO.

[1] G.H. Dieke, Spectra and energy levels of rare earth ions in crystals, New York: Interscience, 1968.

Features of Experimental Determination of the Coefficient of Acousto-Optical Quality of Crystalline Materials

D. Vynnyk, B. Venhryn, A. Ratych, I. Yidak and A. Andrushchak

Lviv Polytechnic National University, S. Bandery Str. 12, Lviv 79013, Ukraine

One of the main parameters of acousto-optical devices is the efficiency of acousto-optical interaction. For the diffraction efficiency of acousto-optical interaction in the case of interaction of plane acoustic and optical waves, the following relation is obtained [1] (Bragg diffraction case):

$$\eta = \sin^2 \frac{\pi}{\lambda} \sqrt{\frac{M_2 P_a l}{2h}}, \qquad (1)$$

here λ is the wavelength of incident optical radiation, l is the interaction length of optical and acoustic rays, h is the size of the optical beam, P_a is the power of the acoustic wave propagating in the acousto-optical material, M_2 is the parameter of acousto-optical quality of this material:

$$M_2 = \frac{p_{ef}^2 n^6}{\rho V^3}, \qquad (2)$$

where p_{ef} is the effective elastic-optical coefficient for this material; n, ρ, V are refractive index, density, and velocity of acoustic wave propagation, accordingly, for this material. Formula (1) is valid for the case: $\cos\Theta_B \approx 1$, where Θ_B is the Bragg angle of incidence.

It follows from (1) that the larger the value of M_2, the smaller the value of the consumed acoustic power P_a is required to obtain a certain value of the diffraction efficiency η at different constant parameters. Therefore, the calculation of M_2 and its experimental determination are important tasks for acousto-optics.

The most common method of experimental determination of M_2 is the method of comparing the acousto-optical properties of the reference and test materials (the Dixon-Cohen method). This paper is devoted to the analysis of the Dixon-Cohen method for the determination of M_2 in order to form complete conditions under which this method can be applied without significant errors both in the case of Bragg diffraction and in the case of Raman-Nat diffraction. Cases, when these conditions are violated are also considered. Thus, the paper takes into account the effect of acoustic wave attenuation in the test material on the value of the measured coefficient of acousto-optical quality M_2, and also considers cases of strong interaction of acoustic and light fields in the test material and obtained formulas for calculating M_2. The proposed approach significantly simplifies the experimental determination of M_2 in the case of strong interaction. In addition, the paper considers a generalization of the Dixon-Cohen method in the case when the transmission of optical radiation by the investigated and reference samples is different from 100%.

[1] Goutzoulis A.P., Pape D.R. Design and Fabrication of Acousto-Optic Devices. – New York: *Marcel Dekker*, 1994, 497 p.

Structure and Luminescence Properties of Cr-Doped $CaAl_4O_7$ and $CaGa_4O_7$ Crystalline Phosphors

V. Hreb[1], V. Stadnik[1], S. Ubizskii[1], A. Kondyr[1], A. Luchechko[2], Ya. Zhydachevskyy[1,3] and L. Vasylechko[1]

[1] *Lviv Polytechnic National University, Lviv, S. Bandera St, 12, 79013, Ukraine,*
[2] *Ivan Franko National University of Lviv, Universytetska St., 1, Lviv, 79000, Ukraine*
[3] *Institute of Physics of the PAS, Al. Lotników, 32/46, Warsaw, 02-668, Poland*

Near-infrared phosphors are showing great advantages compared to traditional NIR light sources, such as high efficiency, energetic savings, and being environmentally friendly. The phosphors doped with transition metal ions, in particular, Mn^{4+} or Cr^{3+}, which have broadband excitation in UV and visible spectral region and deep red emission, can be a weighty alternative to phosphors activated by rare-earth ions. At the same time, calcium aluminates and gallates doped with chromium ions have interesting luminescence and afterglow properties under UV and X-ray irradiation, varying according to the octahedral crystalline surroundings of the Cr^{3+} ions [1,2].

A combined sol-gel solution combustion method was used for the synthesis of $CaAl_4O_7$ and $CaGa_4O_7$ nanocrystalline powders doped with Cr^{3+} ions. Their structural and photoluminescent properties were compared depending on the annealing temperature of the powders in the range 800-1300°C. Crystallization of the phases $CaAl_4O_7$:Cr and $CaGa_4O_7$:Cr occurs after annealing of the samples for 4 hours at 900°C and 800°C respectively. The values of structural parameters, including unit cell sizes, coordinates, and atomic displacement parameters, were obtained from experimental powder diffraction patterns by the Rietveld refinement method.

Characteristic photoluminescence of Cr^{3+} ions in $CaAl_4O_7$:Cr with narrow *R*-lines (electronic transitions $^2E \rightarrow {}^4A_2$) is observed under the excitation in the vicinity of 420 and 550 nm. The intensity of this red luminescence is determined by the excitation wavelength and annealing temperature. The obtained excitation and emission spectra of Cr^{3+} ions indicate the existence of two different Cr^{3+} centers in octahedral coordination in $CaAl_4O_7$:Cr. The photoluminescence excitation spectra of the $CaGa_4O_7$:Cr nanopowders in the visible spectral region are typical for Cr^{3+} ions. At the same time, the broad band of luminescence, which can be attributed to radiative $^4T_2 \rightarrow {}^4A_2$ transitions in Cr^{3+} activator ions, is dominated in the $CaGa_4O_7$:Cr, unlike $CaAl_4O_7$:Cr.

Acknowledgments: The work was supported by the National Research Foundation of Ukraine (grant no. 2020.02/0373).

[1] Jun'an Lai, Jianbei Qiu, Qi Wang,Dacheng Zhou, et al., *Inorg. Chem. Front*., 7 (2020) 2313-2321.
[2] Jungkyu Park, Gunha Kim, Young Jin Kim, *Ceramics International,* 39 (2013) S623-S626.

Influence of Synthesis Conditions on Luminescence Properties of Cr/Er/Yb Co-Doped $LiGa_5O_8$ Spinel-Type Phosphors

V. Hreb[1], I. Lutsyuk[1], A. Luchechko[2], Ya. Zhydachevskyy[1,3] and L. Vasylechko[1]

[1]*Lviv Polytechnic National University, Lviv, S. Bandera St, 12, 79013, Ukraine,*
[2]*Ivan Franko National University of Lviv, Universytetska St., 1, Lviv, 79000, Ukraine*
[3]*Institute of Physics of the PAS, Al. Lotników, 32/46, Warsaw, 02-668, Poland*

Among the crystal hosts, which in combination with the co-doping by transition ions and rare earth elements are currently considered as the most promising for long-lasting afterglow in the deep red or near-infrared ranges, there are materials with a spinel structure. At the same time, the size and dispersion of particles are extremely important for biomedical applications of such phosphors [1,2].

This paper presents the research results of the phase composition, crystal structure, and luminescent properties of crystal phosphors based on $LiGa_5O_8$ spinel, co-doped with Cr^{3+}, Er^{3+}, and Yb^{3+} ions. The phosphors with different ratios of activators, namely 1:1:3, 1:1:5, 1:1:7, were obtained by three methods, including solid-state synthesis, arc melting, and low-temperature sol-gel synthesis.

Single-phase microcrystalline samples were obtained after annealing of compressed powders into tablets at 1200°C. The content of the spinel phase in the samples obtained by the arc melting method was 95-98% for different concentrations of activators. The sol-gel synthesis technique allowed obtaining phase-pure samples at a treatment temperature of powders of 700°C for all three combinations of activator ions concentrations. Precise determination of unit cell parameters and atomic coordinates for all samples obtained by different methods was performed using the Rietveld refinement method.

The photoluminescence excitation spectra as well as photoluminescence spectra of Cr^{3+} ions in $LiGa_5O_8$:Cr,Er,Yb samples in the visible spectral region are typical for Cr^{3+} ions in octahedral coordination. All the studied samples, except for the samples obtained by the arc melting method, show an intense up-conversion luminescence of Er^{3+} ions in the red spectral region (650-700 nm) and low-intense - in the green spectral region (525-575 nm) when excited in the Yb^{3+} ions absorption band by 980 nm. An intense afterglow was detected for all $LiGa_5O_8$:Cr,Er,Yb samples after UV excitation.

The influence of synthesis conditions on the luminescence properties and long-lasting afterglow, as well as the mechanisms of excitation energy transfer, are discussed.

Acknowledgments: The work was supported by the National Research Foundation of Ukraine (grant no. 2020.02/0373).

[1] Y. Cheng, K. Sunb, P. Ge., *Opt. Mat.,* 83 (2018) 13–18.
[2] W. Huang, X. Gong, R. Cui, X. Li, L. Li, X. Wang, C. Deng., *J. Mater. Sci.: Mater.* 29 (2018) 10535–10541.

Electronic Structure and Magnetic Properties of $SmCo_{0.5}Cr_{0.5}O_3$ from First Principles

V. Shved, V. Hreb and L. Vasylechko

Lviv Polytechnic National University, 12 Bandera Street, 79013 Lviv, Ukraine

The recent investigations of multiferroicity in the rare earth chromites RCrO$_3$ have attracted a lot of interest to these compounds. The rare earth cobaltites RCoO$_3$ are famous for the spin crossover and the magnetic and transport features highly depended on spin state transitions. In this work, we used the first principles calculations to obtain the electronic and magnetic properties of mixed samarium cobaltite–chromite $SmCo_{0.5}Cr_{0.5}O_3$ by means of ABINIT software package.

In strongly correlated materials, such as RCoO$_3$ and RCrO$_3$ perovskites, LDA and GGA approximations are not able to correct the electron self-interaction problem, as a consequence the resulting band gap would be dramatically underestimated. Therefore, for an adequate description of highly localized 3d and 4f electrons, the hybrid exchange-correlation functional PBE0 was adopted. The projector augmented wave method was employed to describe the ion-electron interactions. The valence electrons were treated as follows: $5s^25p^66s^25d^14f^5$ for Sm, $3s^23p^64s^13d^7$ for Co, $3s^23p^64s^13d^5$ for Cr, $2s^22p^4$ for O, respectively. The Monkhorst-Pack grid of 6×6×4 was used to integrate the Brillouin zone. For the basis of plane waves the energy cut-off was set at about 500 eV. The lattice constants and atomic coordinates of orthorhombic $SmCo_{0.5}Cr_{0.5}O_3$ obtained from X-ray synchrotron diffraction measurements were used for the calculations.

In $SmCo_{0.5}Cr_{0.5}O_3$ the calculated band gap is indirect, the conduction band minimum is located at Γ point and the valence band maximum occurs at S point. The obtained gap value is 1.29 eV. The bottom of the conduction band is generally derived from Co d, Cr d and O p states. The top of the valence band originates from hybridized Cr d and Co d states. The states in the conduction band ranging from 2.38 to 4.07 eV have mainly Sm f contribution.

At low temperatures $SmCoO_3$ is a non-magnetic material with a low spin state of Co^{3+} ions [1]. In contrast to $SmCoO_3$, $SmCrO_3$ exhibits the canted G-type antiferromagnetic ordering below Neel temperature (197 K) [2]. According to our calculations of the total ground state energy, the antiferromagnetic configuration has the lowest energy and is the most stable in $SmCo_{0.5}Cr_{0.5}O_3$. The calculated local magnetic moment of Co^{3+} in $SmCo_{0.5}Cr_{0.5}O_3$ is insignificant, proving that Co^{3+} ions are in the low spin state, similar to the parent $SmCoO_3$ material [1]. The calculated magnetic moment per Cr^{3+} ion is 2.56 μ_B, which agrees well with the theoretical value of 2.798 μ_B obtained for the "pure" $SmCrO_3$ chromite in Ref. [3]. The antiferromagnetic properties of $SmCo_{0.5}Cr_{0.5}O_3$ can be explained mainly by the magnetic interactions of Cr^{3+} ions. Recently the antiferromagnetic behaviour of the related Fe, Mn-doped $SmCrO_3$ materials was experimentally revealed by means of magnetization measurements [4].

[1] B. Raveau, Md. Motin Seikh, Handbook of Magnetic Materials (2015).
[2] Z. Xiang, J. Xu, Y. Huang, S. Ge, Y. Cui, *Prog. Nat. Sci-Mater.* **28** (2018) 609-613.
[3] J. Ding, L.Wen, H. Li, H. Hao, Y. Zhang, *J. Am. Ceram. Soc.* **102** (2019) 267-274.
[4] J. Zhang, S. Wang, L. Yuan, Ch. Hou, *Chem. Res. Chin. Univ.* **34** (2017) 1-7.

Influence of Electron Beam Alloying on Structure and Properties of Cast Aluminium Surface

Krzysztof Labisz[1*], Regita Bendikienė[2] and Jarosław Konieczny[1]

[1]*Silesian University of Technology, Faculty of Transport, Department of Railway Transport, ul. Krasińskiego 8, 40-019 Katowice, Poland*
[2]*Kaunas University of Technology, Faculty of Mechanical Engineering and Design, Department of Production Engineering Studentų st. 56, LT-51424 Kaunas, Lithuania*
**Corresponding author. E-mail address: krzysztof.labisz@polsl.pl*

One of modern methods for surface layer engineering in currently surface electron beam treatment, where to the matrix material there are introduced small amount of alloying additions into the surface layer in form of ceramic particle powders with different properties influencing the surface layer appliance possibilities.

It was possible to produce a layer consisting of the heat affected zone, transition zone and remelted zone, without cracks and defects as well as has with a slightly higher hardness value compared to the non remelted material. The electron beam current was chose as 30 to 35 mA and implicated by one process speed rate in a range of 15-20 mm/s.

The investigation helps to use the electron beam treatment technique for feeding of ceramic powder particles into the surface of light alloys. The process used is selective electron beam melting (SEBM). Similar to selective laser melting (SLM), SEBM belongs to the powder bed AM methods. SEBM, which uses an electron beam as heat source, shows significant advantages over SLM.

This study was conducted to determine an effect of SiC powder addition on structure and mechanical properties as well the and structure changes occurred during the rapid solidification process. As the main findings there was found that, the obtained surface layer is without cracks and defects as well as has a comparably higher hardness value compared to the non remelted material. The hardness value increases according to the electron beam power used so that the highest power applied gives the highest hardness value in the remelted layer.

In this work, periodic macro-cellular structures with dense struts are successfully fabricated from an aluminium brass by selective electron beam melting (SEBM). The process window for the SEBM of the Cu–Al alloy is developed. The microstructure and the mechanical properties of the Cu–Al samples are studied.

Also the distribution of the SiC particles is good, but the particles are mainly present in the upper part of the surface layer. The hardness value increases in general according to the electron beam power used so that the highest power applied gives to highest hardness value in the remelted layer. The main goal of this work is to investigate and determine the effect of SEBM remelting and alloying on the cast Al-Si-Cu cast aluminium alloy structure to recognise the possibility for application in real working conditions mainly for light metal constructions as well as in many branches of the industry.

The Spin-Polarized Electronic Structure in the Crystal ZnTe:Cr without and with a Cationic Vacancy

S.V. Syrotyuk

Lviv Polytechnic National University, S. Bandera str. 12, Lviv, Ukraine

This work is devoted to the study of the electronic structure of ZnTe cubic zinc blende crystal doped with transition Cr element. All calculations were performed using the ABINIT program [1] on the projector augmented waves (PAW) [2] basis. The basic PAW functions were obtained by means of the AtomPAW program [3]. All the calculation have been performed for a supercell containing 64 atoms.

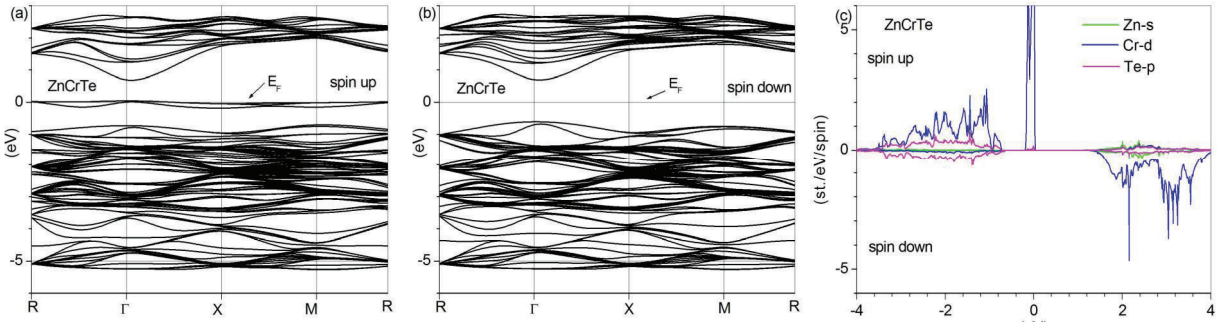

Fig. 1. Electronic structure of a crystal ZnTe:Cr.

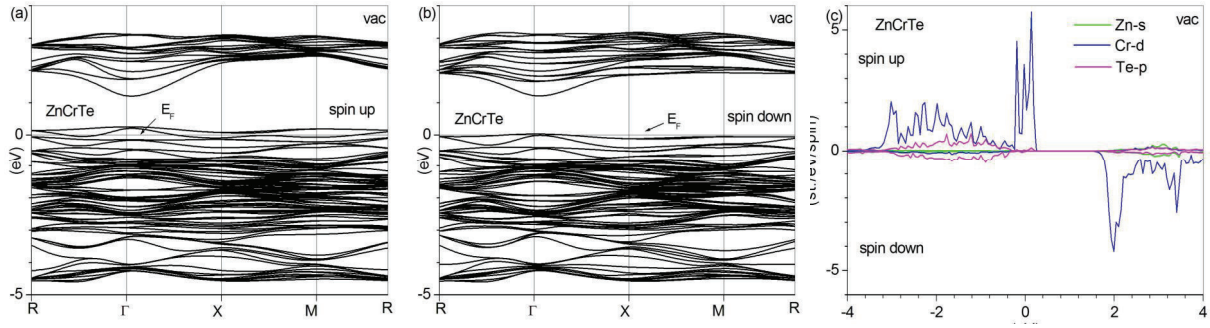

Fig. 2. Electronic structure of a crystal ZnTe:Cr with cationic vacancy.

Fig. 1a shows that the 3d electrons with spin up are present at the Fermi level. As can be seen from the Fig. 2a, introduction of a cationic vacancy into the crystal leads to the immersion of the Fermi level in the valence band. Fig 1b shows that the crystal for electrons with the spin up is the semiconductor, but for spin down the Fermi level is located in the upper part of the valence band (Fig. 2b). The comparison of Figures 1c and 2c reveal the significant redistribution of the 3d electrons caused by cationic vacancy. The magnetic moment of the supercell equals to $4.0\,\mu_B$ and $3.17\,\mu_B$, without and with a cationic vacancy, respectively. For the spin-down electrons the minimum optical and fundamental gaps equal to 1.21 eV for a crystal without a vacancy.

[1] X. Gonze, et al., Comput. Phys. Commun. 205, 106 (2016).
[2] P.E. Blöchl, Phys. Rev. B. 50, 17953 (1994).
[3] N.A.W. Holzwarth, A.R. Tackett, G.E. Matthews, Comput. Phys. Commun. 135, 329 (2001).

Influence of Lanthanides on Luminescence Spectrum Emission of BeO under X-Ray Excitation

K. Kurt, T. Çavdar and Ö. Yiğit

Mersin University Science and Letter Faculty Physics Department Mersin Turkey

In this study, lanthanides doped BeO were prepared pellet form for dosimetry investigation. Each sample measured luminescence spectrum emission under x-ray excitation in room temperature for investigating influence of lanthanides. The luminescence emission of BeO monitored broadband from 200nm to 400nm for each samples. Narrow emission lines were seen between 400nm and 950nm. The main emission from host material start from UV region up to 400nm. Other emission, which has narrow lines, might belong to Impurities. The emission of host material at UV region attributed to F and F^+ colour centres. F and F^+ colour centres emissions suppressed the contribution of lanthanides.

.

[1] WERZ, B. HENDERSON and J. E. «Defects in the Alkaline Earth Oxides.» (Advances in Physics) 17:70, no. 749-855 (1968).

[2] Yukihara, Eduardo G. «Luminescence properties of BeO optically stimulated luminescence (OSL) detectors.» (Radiation Measurements) 46, no. 6-7 (2011).

SECTION 3

NANOPARTICLES, NANO-CERAMICS AND NANO-COMPOSITES

Advanced Magnetic Nanostructures for Biomedical Applications

A.I. Tovstolytkin[1], O.I. Nakonechna[1], I.V. Sharay[1], A.V. Bodnaruk[2], V.M. Kalita[2,3], S.M. Ryabchenko[2], Yu.Yu. Shlapa[4], S.O. Solopan[4] and A.G. Belous[4]

[1]*Institute of Magnetism of the NAS of Ukraine and MES of Ukraine, 36-b Vernadsky Blvd., Kyiv 03142, Ukraine*
[2]*Institute of Physics of the NAS of Ukraine, 46 Nauky Ave., Kyiv 03028, Ukraine*
[3]*National Technical University of Ukraine "Igor Sikorsky Kyiv Polytechnic Institute", 37 Peremohy Ave., Kyiv 03056, Ukraine*
[4]*V.I. Vernadskii Institute of General and Inorganic Chemistry of the NAS of Ukraine, 32/34 Palladina Ave., Kyiv 03142, Ukraine*

Artificial magnetic nanostructures have generated a new trend in the field of advanced materials, particularly due to their multiple technological and biomedical applications [1]. Among these applications, magnetic resonance imaging (MRI), targeted drug delivery and magnetic hyperthermia (MHT) are the most promising ones [2]. In MRI, which is a non-invasive technique for the diagnosis of diseases, magnetic nanoobjects are used as contrast enhancement agents. In MHT, which is a thermal treatment of cancerous cells in conjugation with chemotherapy and radiotherapy, nanoparticles and more complex nanostructures are used as heat mediators.

Hyperthermia takes advantage of higher sensitivity of tumor tissue to heat and typically involves heating of affected organ to 42 – 45 °C. MHT allows minimizing side effects by the localized heating of only desired parts of the organism. The method involves introduction of magnetic nanoobjects into the desired part of the organism and heating them with an alternating magnetic field .

Substituted manganites $(La,Sr)MnO_3$ are of interest in this context due to easy tunable composition-dependent T_C and relatively large magnetic moment at room temperature [3]. The other promising mediators are core-shell nanoparticles and sophisticated artificial magnetic nanostructures, since they promise tunability of a number of important characteristics [4].

In recent years, considerable attention has been focused on multifunctional nanostructures, in which the above mentioned diagnostic (MRI) and therapeutic (MHT) capabilities are combined together [5]. Such a possibility to combine the therapeutic effect generated by the heat release with the enhanced contrast in the MRI is extremely appealing since it would provide the possibility to monitor the effect of the applied hyperthermia therapy. To this end, the nanostructures, which display temperature-dependent magnetic moments near the human body temperature, are of especial interest for MRI-based thermometry that can provide temperature maps.

In this work, the technological, physical and medical aspects concerning the prospects of the use of the above nanoobjects as self-controlled mediators of MHT and/or temperature-dependent MRI contrast agents are reviewed. The mechanisms behind their intriguing behavior are analyzed. The ideas and steps to achieve further progress in this direction are discussed.

[1] A. Belous, A. Tovstolytkin, S. Solopan, and O. Fedorchuk, "Synthesis , Properties and Applications of some Magnetic Oxide Based Nanoparticles and Films," vol. 133, no. 4, pp. 1006–1012, 2018.
[2] E. A. Vitol, V. Novosad, and E. A. Rozhkova, "Microfabricated magnetic structures for future medicine: from sensors to cell actuators," *Nanomedicine*, vol. 7, no. 10. pp. 1611–1624, Oct-2012.
[3] V. M. Kalita *et al.*, "Mechanisms of AC losses in magnetic fluids based on substituted manganites," *Phys. Chem. Chem. Phys.*, vol. 17, no. 27, pp. 18087–18097, 2015.
[4] S. O. Solopan *et al.*, "Core/shell architecture as an efficient tool to tune DC magnetic parameters and AC losses in spinel ferrite nanoparticles," *J. Alloys Compd.*, vol. 788, pp. 1203–1210, 2019.
[5] Z. Li *et al.*, "Magnetically amplified photothermal therapies and multimodal imaging with magneto-plasmonic nanodomes," *Appl. Mater. Today*, vol. 12, pp. 430–440, 2018.

Lithium Niobate: from Single Crystals to Nanocrystals

L. Kovács, K. Lengyel, L. Kocsor, L. Péter and G. Corradi

Wigner Research Centre for Physics, Budapest, Hungary

Single crystal $LiNbO_3$ was first grown more than 50 years ago [1]. Since that time thousands of papers have been published dealing with its outstanding ferroelectric, acoustic, nonlinear optical, holographic etc. properties and demonstrating its countless realized or potential applications. It was about a quarter of century ago, when the first $LiNbO_3$ crystals grown with stoichiometric composition [2] gave a new impulse to its never-ending investigation. Different applications require different undoped or doped systems of bulk, thin film, or nanocrystal forms. In the present talk I'll show two examples, (i) incorporation of dopants into stoichiometric crystals, and (ii) properties of $LiNbO_3$ nanocrystals prepared by high-energy ball-milling.

Dopants are generally used to tailor the crystal properties for a given application. So called optical damage resistant dopants such as Mg, Zn, Sc, In, Zr, Hf, or Sn are required for high-intensity laser applications, transition metals such as Fe, Mn, Cu, or Ni in contrast increase the photorefractive sensitivity, while rare-earth dopants Nd, Er, Yb etc. serve as laser activators or active centers in coherent quantum optical experiments [3]. To understand the effect of dopants the incorporation mechanism and/or the substitution site in the crystal have to be known. Our earlier and recent IR absorption studies identified the stretching vibration of hydroxyl ions in $M_{Nb}^{n+} - OH^-$ type complexes, where all these dopants (M) occupy a Nb site. This unambiguously showed that in stoichiometric crystals above a threshold concentration depending on the ion's valence state these cation dopants partially substitute at Nb sites, in contrary to concentrations below the threshold, where they can only be found on Li sites [4].

As a first step in the investigation of nano-crystalline $LiNbO_3$ systems, undoped samples have been prepared by a "top-down" method starting from single crystals and ground by the high-energy ball-milling technique [5]. The resulting particle size has a broad distribution in the range of a few hundred nanometers. During the milling process the material suffers partial reduction that leads to a balanced formation of bipolarons and polarons yielding gray color together with Li_2O segregation on the open surfaces. Upon high temperature oxidation, the volatile Li_2O phase and the polarons get eliminated and the Li deficiency is accommodated by the formation of a more stable $LiNb_3O_8$ shell. Darker or brownish color appearing upon high temperature reduction is caused by the preferential formation of bipolarons. The Li_2O loss was observed to increase with the growing total surface of the particles. The average thickness of the non-ferroelectric surface segregate corresponds to a few molecular layers forming the passivating shell of the particles. These findings provide a comprehensive explanation of the physicochemical behavior of the system during grinding and annealings.

This research was supported by the National Research, Development and Innovation Fund of Hungary within the Quantum Technology National Excellence Program (Project No. 2017-1.2.1-NKP-2017-00001)

[1] K. Nassau, H. J. Levinstein, G. M. Loiacono, *J. Phys. Chem. Solids* **27**, 983 (1966).
[2] K. Polgár, Á. Péter, L. Kovács, G. Corradi, Zs. Szaller, *Journal of Crystal Growth* **177**, 211 (1997).
[3] Y. Sun, C. W. Thiel, R. L. Cone, R. W. Equall, R. L. Hutcheson, *Journal of Luminescence* **98**, 281 (2002).
[4] L. Kovács, L. Kocsor, É. Tichy-Rács, K. Lengyel, L. Bencs, G. Corradi, *Opt. Mat. Express* **9**, 4506 (2019).
[5] L. Kocsor, L. Péter, G. Corradi, Z. Kis, J. Gubicza, L. Kovács, *Crystals* **9**, 334 (2019).

Properties and Application of Nanopowders of Polyvalent Iron Oxides Obtained by Electroerosion Dispersion

T. Prikhna[1], M. Monastyrov[1], O. Prysiazhna[1], B. Halbedel[2], V. Moshchil[1] and P. Brvitskyi[1]

[1]*V. Bakul Institute for Superhard Materials of the National Academy of Sciences of Ukraine (NASU), 2, Avtozavodskaya Str., Kiev 07074, Ukraine*
[2]*Department of Inorganic-Nonmetallic Materials, Technische Universität Ilmenau, POB 10 05 65, D-98684 Ilmenau, Germany*

Iron oxide nanoparticles have considerable interest in many fields of research and application, such as their strong magnetic moment, biocompatibility and magnetoelectric properties: biomedical sciences (diagnostics and therapy), ferrofluids, catalysis, colored pigments, high-density magnetic recording, printer toners, wastewater treatment and absorption of electromagnetic waves, etc.

In the present study iron oxide polyvalent nanopowders were obtained using developed by us efficient and cheap method of electroerosion dispersion (EED) [1, 2] in plasma of extra clean iron granules (for medical application) or steel shavings (for technical and animal husbandry applications). According to X-ray study with Rietveld refinement the iron oxide nanopowders (with density $\rho = 5.175$ g/cm^3) prepared from steel shavings contain iron in different oxidation states and approximately in the following amounts: magnetite (Fe_3O_4) – 41 wt.% (the main phase), metallic iron (Fe) – 40 wt.% , wustite (FeO) – 19 wt. %. Using cerimetry, it was found that the content of Fe^{2+} in the EED powder is 53.83 ± 1.23 wt.%. This value is greater than the theoretical proportion of Fe^{2+} in magnetite, which is 24.12 wt.%, i.e. this result confirms that the powder also contains iron in another oxidation state (so we refer to the powder as Fe-O). The particle sizes of magnetite powders are in the range from $D_{10.3}$ = 3.6 to $D_{90.3}$ = 11.8 microns. The TEM image confirms that they are aggregates, and shows that the primary particles of the iron oxide powder are smaller than 50 nm (TEM image with a magnification of 99,000). Particles smaller than 20 nm are also observed. The main shape is spherical. The electromagnetic properties of the EED powder enable a microwave absorption similar to *hexaferrite powders* and larger to commercially available iron oxide powder *Magsilica*®. However, the EED powder is simply producible [2].

The Fe-O nanopowders have been used by us as fillers for the manufacture of materials that provide absorption in a wide range of frequencies and for wastewater treatment from ions of heavy metals. They occurred to be effective in medicine (Technical Conditions ТУ-У 10.9-41540468-001: 2020 "Dietary additives based on a mixture of powders of polyvalent nanodisperse oxides, Lysofferin"), animal husbandry (ТУ-У 10.9-41540468-002: 2020 "Feed additives based on a mixture of powders of polyvalent nanodisperse iron oxides for veterinary medicine, Nano-Fe"), and agriculture. Dietary additive "Lysofferin" provides oxygen saturation of blood of patients with COVID, increase in hemoglobin after chemotherapy, and showed positive dynamics in the treatment of Parkinson's and Alzheimer's diseases.

[1] Monastyrov, M. K., Prikhna, T.A., Mamalis, A.G., Gawalek W., Talanchuk, P.M., Shekera, R.V. Electroerosion dispersion-prepared nano- and submicrometre-sized aluminium and alumina powders as power-accumulating substances. *Nanotechnology Perceptions*. **4**(2008) 179–187.

[2] Monastyrov, M., Prikhna, T., Halbedel, B., Kochetov, G., Marquis, F., Mamalis, A. Electroerosion dispersion, sorption and coagulation for complex water purification electroerosion waste recycling and manufacturing of metals, oxides and alloys nanopowders. *Nanotechnology Perceptions.* **15**(2019) 48 □ 57.

Structure and Properties of Micro and Nanostructured Cellulose Films Incorporated with Oxides and Carbon Particles

S. Nedilko[1], O. Alekseev[1], V. Barbash[3], V. Chornii[1,2], K. Krolenko[1], M. Lazarenko[1], S. Revo[1], M. Schegeda[1] and V. Scherbatskii[1]

[1]*Taras Shevchenko National University of Kyiv, 64/13 Volodymyrska st., 01601-Kyiv, Ukraine*
[2]*National University of Life and Environmental Sciences of Ukraine, 5 Geroiv Oborony st., 03041-Kyiv, Ukraine*
[3]*National Technical University of Ukraine "Igor Sikorsky Kyiv Polytechnic Institute", Prospect Peremogy, 37, 03056-Kyiv, Ukraine*

There are many examples of development of devices, which use materials elaborated on the base of cellulose. Those are sensors, drives, flexible electronics components, etc. The cellulose properties can be modified by substitution of its hydroxyl groups with some functional groups such as specific acids, chlorides, oxides or dyes with the aim to enrich some characteristics or to obtain new properties [1 - 3]. Nevertheless, cellulose and derived materials are not often used or studied as optical systems or systems where optical phenomena can be inquired. The development of solar radiation dosimeters consisting of organic dye and titanium oxide as a photocatalyst printed on the cellulose substrate is one of the few examples. Cellulose fibers containing specific luminescent compounds as markers and simultaneously as effective modifiers for textile products, papers and plastic is other example. It is also common knowledge that cellulose is a very effective sorbent. Despite of the fact that synthetic sorbents based on polyethylene, propylene and other polymers show better performance than cellulose, they are not eco-friendly in comparison to cellulose.

The aim of this work was to develop and to study the composites based on three types of micro/nanostructured cellulose and filled with some oxides, especially luminescent ones. Those were synthetic microcrystalline cellulose (MCC) - 1), as well as nanocellulose of plant - 2) and of bacterial origin - 3). Carbon nanoparticles such as carbon nanotubes and graphene were added to the composites for modification of their structural, mechanical and optical properties.

The samples were characterized using X-ray powder diffraction (XRD), scanning electron microscopy (SEM), thermogravimetry, differential scanning calorimetry, optical reflectance, ellipsometry, light scattering, FTIR, Raman and luminescence spectroscopy. Some mechanical characteristics such as hardness and tensile strength were measured too.

The correlations between structural, morphological and physical properties characteristics of composites were found and discussed. The data were analyzed and they have confirmed the perspectives of the studied composites for practical applications.

[1] S. Pradhan. A.K. Brooks, V.K. Yadavalli. Nature-derived materials for the fabrication of functional biodevices. *Materials Today Bio*. – June 2020. - https://doi.org/10.1016/j.mtbio.2020.100065.
[2] K. Nelson, et al. American process: Production of low cost nanocellulose for renewable, advanced materials applications. Springer (2016) p. 267-302.
[3] S. Hokkanen, E. Repo, T. Suopajärvi, H. Liimatainen, J. Niinimaa and M. Sillanpää, Adsorption of Ni(II), Cu(II) and Cd(II) from aqueous solutions by amino modified nanostructured microfibrillated cellulose, *Cellulose*, 21 (2014) 1471-1487.

Pulsed Laser Deposition of Luminescent Downshifting Coatings on Silicon Solar Cells

O. Chukova[1], S.A. Nedilko[1], S.G. Nedilko[1], T. Voitenko[1], M. Androulidaki[2], K. Savva[2], E. Stratakis[2], H.S. Rahimi Mosafer[3], R. Minikayev[3] and W. Paszkowicz[3]

[1]*Taras Shevchenko National University of Kyiv, Volodymyrska Str., 64/13, Kyiv 01601, Ukraine*
[2]*Institute of Electronic Structure & Laser (IESL) of Foundation for Research & Technology Hellas (FORTH), Heraklion 711 10 Crete, Greece*
[3]*Institute of Physics, Polish Academy of Sciences, al. Lotnikow 32/46, PL 02-668 Warsaw, Poland*

Luminescent converters, in particular, luminescent down-shifting materials can be widely applied in the modern techniques. The most known their application is coating of luminescent lamps and light emitting diodes used for obtaining of white light emission. A new possible application has attracted research interest for last years. There are luminescent converters (downshifters) for improvement of efficiency of incident light harvesting by solar cells. It is known that theoretical limit of energy transformation efficiency for single-junction silicon photovoltaic cell is about 31%. Application of luminescent converters was proposed to reduce solar energy losses associated with spectral mismatch of solar cells sensitivity and energy distribution in the solar spectrum. Inorganic luminescent oxides are perspective candidates for this role due to their excellent thermal, mechanical and optical properties.

Luminescent materials based on RE-doped orthovanadates are widely used for various science and technology purposes because the orthovanadates are characterized by high absorption in a wide spectral range (from UV to yellow light), by effective energy transfer from host to the RE ions, and by intensive emission. Within our previous research, we have found optimal conditions of synthesis that allow for achievement of high intensity of luminescence of the $La_{1-x}Eu_xVO_4$ nanoparticles synthesized by sol-gel method. We have also developed vanadate nanoparticles with enhanced light harvesting from violet spectral range using heterovalence substitutions of RE ions with alkali earth cations. So, we have developed materials exhibiting luminescent properties suitable for luminescent downshifting applications. The next important task is to retain high optical characteristics of oxide nanoparticles at their deposition on various substrates. It is important to prevent loses of luminescent characteristics of nanoparticles with their incorporation in films and various coatings.

Pulsed laser deposition (PLD) is a promising method to save luminescent properties of the applied materials, because this method does not require any additional chemical agents nor matrices for dispersion of nanoparticles, neither heavy metal nor organic solvents. In the present work we report results of the PLD experiments with the RE^{3+}-doped $LaVO_4$ vanadate nanoparticles on silicon solar cell. Applied vanadate nanoparticles were synthesized by aqueous nitrate-citrate sol-gel method using citric acid as a complexing agent. The PLD of nanoparticles was carried out in a vacuum camera using KrF excimer laser with λ_{ex} = 248 nm.

The transparent films of $La_{1-x-y}Eu_yCa_xVO_4$ orthovanadate nanoparticles were successfully applied on surfaces of silicon solar cells and various silicon substrates. Then structure and optical properties of the films were studied. The $La_{0.8}Eu_{0.1}Ca_{0.1}VO_4$ films have demonstrated intensive luminescence effectively excited from the 250 – 400 nm spectral range that pointed their perspective to be used for luminescent downshifting of the incident solar light.

This work has received funding from Ministry of Education and Science of Ukraine and from the EU-H2020 research and innovation program under grant agreement No 654360 having benefited from the access provided by FORTH, Crete, Greece within the framework of the NFFA-Europe Transnational Access Activity.

Synthesis of CeO_2 Nanoparticles by Precipitation in the Solutions and Their Physical-Chemical Properties

Yu. Shlapa, S. Solopan, I. Timashkov and A. Belous

V. I. Vernadskii Institute of General and Inorganic Chemistry of the NAS of Ukraine, prosp. Palladina, 32/34, Kyiv, 03142

Nanosized CeO_2 can find application in different fields of science and technology [1]. The interesting feature of this material is the presence of Ce^{4+} ions in nano-state as well as Ce^{3+} ions. It makes CeO_2 of particular interest for biomedical applications, because they can exhibit antioxidant properties due to the co-existing of Ce^{4+} and Ce^{3+} ions at the nanoparticles (NPs) surface [2], which is necessary for the treatment of neurodegenerative and oncological diseases, sepsis, the effects of mass irradiation when using weapons of mass destruction etc [3]. It is important to note that the concentration of Ce^{3+} ions increases with the growing the NPs size, however, for NPs less than 2 nm Ce^{4+} completely transforms to Ce^{3+}. For promising medical application is significant to synthesize CeO2 NPs, which would be able to form stable aqueous suspensions even without any additional stabilizers. Therefore, one of the most important chemical issues is a development of the synthesis conditions of CeO_2 NPs with sizes up to 10-15 nm, which will be able to provide the high level of antioxidant properties.

The aim of this study was synthesis of nanosized CeO_2 particles by precipitation in aqueous/alcohol solutions and investigation of their crystallographic and electrocinetic properties.

A number of CeO_2 NPs were synthesized by precipitation in aqueous/alcohol solutions using i-propanol (0, 25, 50, 75 and 90%). Physical-chemical properties of NPs were investigated by means of XRD and DLS methods, main parameters were summarized in Table.

Table. Physical-chemical parameters of CeO_2 NPs

No of sample	Alcohol concentration (%)	Level of crystallinity (%)	$d_{Sherrer}$ (nm)	d_{WH} (nm)	D_{hydro} (nm)	ζ-potential (mV)
Ce1	0	80	14.5	14.7	70.7	+40,9
Ce2	25	79	13	13.2	135.2	+41,5
Ce3	50	72	11.2	11.4	144.8	+41,6
Ce4	75	69	10	10.2	147.6	+42,0
Ce5	90	65	6.8	7.0	149.1	+42,9

According to obtained data it was established that synthesized CeO_2 NPs had the crystalline size in the range of 6-15 nm. It was shown that change of the ratio of H_2O/i-propanol gave the possibility to control the NPs size: crystalline diameter and level of crystallinity of NPs decreased with growing the alcohol concentration in the solution. It was established that all synthesized NPs formed high-stable aqueous suspensions without additional stabilizers as it was evidences by the high positive values of ζ-potential. Synthesized CeO_2 NPs are interesting and promising for potential application in medical purposes.

[1] Sun, C. W.; Li, H.; Chen, L. Q. Energy Environ. Sci. 2012, 5 (9), 8475−8505

[2] Celardo, I.; De Nicola, M.; Mandoli, C.; Pedersen, J. Z.; Traversa, E.; Ghibelli, L. ACS Nano 2011, 5 (6), 4537−4549.

Inbaraj, B. S.; Chen, B.-H. Asian J. Pharm. Sci. 2020 doi.org/10.1016/j.ajps.2019.10.005

Phase Transformations at the Synthesis of Organic-Inorganic Perovskites $CH_3NH_3PbI_3$

P.V. Torchyniuk[1], O.I. V'yunov[1], V.O. Yukhymchuk[2], O.M. Greshchuk[2] and A.G. Belous[1]

[1]*V.I. Vernadsky Institute of General and Inorganic Chemistry of the NAS of Ukraine, Palladina ave., 32/34, Kyiv - 03142, Ukraine*
[2]*V. Lashkaryov Institute of Semiconductor Physics of the NAS of Ukraine, Prospect Nauky, 45, Kyiv - 03028, Ukraine*

One of the main sources of renewable energy today is solar energy. Among new materials for the efficient conversion of solar energy into electrical are organic-inorganic perovskites, which demonstrate the high efficiency of energy conversion 25.2% [1]. They are an unusual class of materials that combine the advantages of organic and inorganic semiconductors, namely, large optical absorption, high mobility of charge carriers and the variation in the band gap with chemical composition [2]. However, organic-inorganic perovskites are characterized by significant shortcomings that do not allow them to be introduced into mass production today, namely properties degradation over time. Therefore, the cause of this degradation and the means of its prevention is being sought. Today one of the widely used formation methods of thin perovskite films is the deposition of a solution of PbI_2 and CH_3NH_3I compounds in different solvent DMF, DMSO, GBL, NMP onto the substrates. Depending on the solvent nature and the ratio of PbI_2 and CH_3NH_3I, films with different morphology, structural, optical and electrical properties are formed. Our previous investigations have shown that complexes (PbI_3^-, PbI_4^{2-}) are formed as a result of chemical interaction of the organic cation, the coordinating solvent and inorganic components. Such complexes differently affect the properties of perovskites [3]. At the same time, the processes of the formation of intermediates, which can significantly affect the properties of perovskites, are still insufficiently studied. Therefore, the purpose of this work was to investigate the processes of the formation of intermediate compounds at the synthesis of perovskite films $CH_3NH_3PbI_3$ at different ratios of starting reagents, PbI_2 and CH_3NH_3I.

Solutions in DMF of the initial reagents, PbI_2 and CH_3NH_3I in different ratios (1:1, 1:2, 1:3) were used for the synthesis of organic-inorganic perovskites. The formation of perovskite and intermediate compounds was determined by X-ray diffractometry (XRD) and Raman spectroscopy (RS). XRD shows that perovskite $CH_3NH_3PbI_3$ formed by different schemes depending on the ratio of initial reagents: (1) via the formation of three intermediate compounds $(CH_3NH_3)_3(DMF)PbI_5$, $(CH_3NH_3)_2(DMF)_xPbI_4$, $(CH_3NH_3)_2(DMF)_2Pb_3I_8$ (1:1); (2) via the formation of four intermediate compounds $(MA)_2(DMF)_2Pb_2I_6$, $(CH_3NH_3)_2(DMF)_2Pb_3I_8$, $(CH_3NH_3)_3(DMF)PbI_5$, $(CH_3NH_3)_2(DMF)_xPbI_4$ (1:2) and (3) via the formation of two intermediate compounds $(CH_3NH_3)_3(DMF)PbI_5$ and $(CH_3NH_3)_2(DMF)_xPbI_4$ (1:3). These results correlate well with RS, which confirmed the formation of the above-mentioned intermediate compounds at certain substrate temperatures. In addition, RS established the presence of DMF solvent molecules in samples in the temperature range from room temperature to 45 °C (for ratio of initial reagents 1:1), to 90 °C (1:2), and to 30 °C (1:3).

[1] National Renewable Energy Laboratory, Best Research-Cell Efficiencies. http://www.nrel.gov/ncpv/images/efficiency_chart.jpg

[2] Saba, M., Quochi, F., Mura, A., & Bongiovanni, G. (2016). Excited state properties of hybrid perovskites. *Accounts of chemical research*, *49*(1), 166-173.

[3] Belous, A., Kobylianska, S., V'yunov, O., Torchyniuk, P., Yukhymchuk, V., & Hreshchuk, O. (2019). Effect of non-stoichiometry of initial reagents on morphological and structural properties of perovskites $CH_3NH_3PbI_3$. *Nanoscale research letters*, *14*(1), 4.

Sol-Gel Combustion Synthesis, Crystal Structure and Luminescence of Cr- and Mn-Doped $SrAl_4O_7$ Nanopowders

V. Stadnik[1], V. Hreb[1], Ya. Zhydachevskyy[1,2] and L. Vasylechko[1]

[1]*Lviv Polytechnic National University, 12 Bandera Street, 79013 Lviv, Ukraine, vitalii.y.stadnik@lpnu.ua*
[2]*Institute of Physics, Polish Academy of Science, Warsaw, Poland*

Aluminates of alkaline earth elements with the structure of melilite MAl_4O_7 are promising for applications in white light sources (WLEDs), fluorescent lamps, optical amplifiers, radiant displays, solid-state lasers, radiation dosimetry, sensors, and radiographs. Recently, a number of publications have appeared on the synthesis of compounds doped with rare-earth elements (Eu, Dy, Nd, Sm), bismuth, as well as some transition elements such as Cr, Mn and Cu [1-2].

A combined sol-gel solution combustion method was used to synthesize nanocrystalline $SrAl_4O_7$ powders doped with Cr^{3+} and Mn^{4+} ions. In this method following substances were used: $Sr(NO_3)_2{\cdot}4H_2O$ or $SrCO_3$; $Al(NO_3)_3{\cdot}9H_2O$; $Cr(NO_3)_3{\cdot}9H_2O$, $Mn(NO_3)2{\cdot}4H_2O$, citric acid $C_6H_8O_7$ (CA) and ethylene glycol (EG) in an amounts: n(EG) : n(CA) : $n(\Sigma(Me^{(n+)}) = 8 : 2 : 1$. A 25 % NH_4OH solution was used to neutralize the final mixture and achieve the desired pH of the solution. Dopant concentrations varied from 0.05 to 5.0 at.%. Evolution of phase composition, crystal structure and microstructural parameters of nanocrystalline $SrAl_4O_7{:}xCr^{3+}(Mn^{4+})$ phosphors on the synthesis conditions was investigated by X-ray powder diffraction and, selectively, by the scanning electron microscopy. It was established that average crystallite size of $SrAl_4O_7$:xCr powders varied from 65 to 110 nm, depending on heat treatment temperature and dopant concentration.

For $SrAl_4O_7{:}xCr^{3+}$ samples, the luminescence excitation spectrum, recorded at 693 nm, shows excitation from 250 nm to 650 nm, with three maxima at wavelengths of ~330, 420, and 560 nm and is attributed to intracenter transitions in chromium ions. Two broad maxima in the visible spectrum region 420 and 560 nm correspond to the $^4A_2 \rightarrow {}^4T_1$ and $^4A_2 \rightarrow {}^4T_2$ transitions in Cr^{3+} ions. The dominant narrow luminescence lines (*R*-lines) at about 693 nm corresponds to the transitions from the splited (4.4 meV at RT) metastable level ^2E to the ground state $^4A_2$. The intensity of photoluminescence increases with increasing annealing temperature. In the case of $SrAl_4O_7{:}xMn^4$, the excitation spectra have two maxima located around 320 nm and 460 nm, which correspond to the transitions $^4A_2 \rightarrow {}^4T_1$ and $^4A_2 \rightarrow {}^4T_2$ in Mn^{4+} ions. Photoluminescence spectrum of Mn^{4+} extends from 600 to 750 nm with a double maximum at about 652 nm, which is attributed to $^2E \rightarrow {}^4A_2$ transitions in Mn^{4+} ions, is characteristic for Mn^{4+} ions occupying octahedral positions in oxides.

The $SrAl_4O_7$ samples simultaneously doped by Cr^{3+} and Mn^{4+} ions reveal the combined photoluminescence of both the Cr^{3+} and Mn^{4+} centres. Such double doping allows an efficient excitation of the phosphor in whole UV-visible range and broadening of the complex emission spectrum in the deep-red range at 600-750 nm.

The work was supported by the National Research Foundation of Ukraine (grant no. 2020.02/0373).

[1] J. Lai, J. Qiu, Q. Wang et al., *Inorg. Chem. Front.* **7** (2020) 2313.
[2] V.T. Jisha. *Acta Ciencia Indica* **XLII**(2) (2016) 105.

Development of the Borate Glasses Incorporated with La-Vanadate Nanoparticles

O. Chukova[1], S.A. Nedilko[1], S.G. Nedilko[1], T. Voitenko[1], A. Manousaki[2] and A. Papadopoulos[2]

[1]*Taras Shevchenko National University of Kyiv, Volodymyrska Str., 64/13, Kyiv 01601, Ukraine*
[2]*Institute of Electronic Structure & Laser (IESL) of Foundation for Research & Technology Hellas (FORTH), Heraklion 711 10 Crete, Greece*

Oxide micro/nanoscale composite materials, such as oxide glass ceramics, are promising for the newest luminescent coatings (LC) elaboration. Currently, development of such types of LCs is in the initial stage, but some advantages of the glass-ceramics LCs have been already described.

Development of new LCs glass-ceramics composites in the present work is based on vanadate nanoparticles incorporated into borate-vanadate glass matrices. Vanadate component were chosen with the aim to achieve the best binding between glass matrix and incorporated crystalline nanoparticles.

Borate-vanadate glass-ceramics composites were synthesized by melt quenching procedure from calculated amounts of V_2O_5, Li_2CO_3 and H_3BO_3. Concentration of vanadate component was varied from 3 to 40 mass. %. The reagents were grinded, mixed and placed in porcelain crucibles, then melted in the air at 700 ^{0}C in a muffle furnace. After melting, the samples were quickly quenched using non-magnet metal plates.

Some of the samples were incorporated with the Eu,Ca-doped $LaVO_4$ luminescent vanadate nanoparticles synthesized by sol-gel method. Phase compositions of the synthesized samples were determined using Shimadzu 2000 X-ray diffractometer ($Cu_{K\alpha}$ - radiation with a Ni filter). The diffraction patterns were taken at a step 2 deg/min. The microstructure of the samples was studied with a scanning electron microscope (SEM) JEOL JSM-7000F. Reflectance spectroscopy of the samples was performed using Perkin Elmer Lambda 950 spectrometer. The photoluminescence (PL) was excited at 405, 478 and 532 nm laser radiation or at 325 nm radiation of the powerful Xenon lamp, and the PL spectra were registered using DFS12 monochromator (grating 600 grooves/mm, slit on 50 micron and FEU-79 photomultiplier).

Using the Kubelko-Munch transformations of reflection spectra, we have estimated the band gap of synthesized vanadate-borate glass composites by determining of tangent versus photon energy to the F^2 curve, where $F = (1-R)^2/2R$, R is the reflection spectrum. The obtained band gap values for glass containing 40, 25, 4 and 3% of vanadium oxide were 1.976, 2.265, 2.477 and 2.542 eV, respectively. Therefore, we consider the samples with 3 and 4 % of the vanadium oxide as sufficiently transparent and they should be promising for optical applications. Therefore, just these concentrations of vanadium oxide were used for preparation of the glass-ceramics incorporated with $LaVO_4$:Eu,Ca particles. The composite samples have shown luminescent properties those are characteristic for the corresponded pure nanoparticles.

This work has received funding from Ministry of Education and Science of Ukraine and from the EU-H2020 research and innovation program under grant agreement No 654360 having benefited from the access provided by Institute of Electronic Structure & Laser (IESL) of Foundation for Research & Technology Hellas (FORTH) in Heraklion, Crete, Greece within the framework of the NFFA-Europe Transnational Access Activity.

Features of Obtaining Polymer Composites Based on Disperse Oxides and Vinyl Polymers

V. Dutka and Ya. Kovalskyi

Ivan Franko National University of Lviv, Ukraine
E-mail: volodymyr.dutka@lnu.edu.ua

Polymer-mineral composites (PMC) have unique properties. The filler in a mineral composite polymer can perform many functions by providing the resulting material of specific properties. An effective method for obtaining PMC is a radical polymerization in the presence of disperses mineral oxides. The highly developed surface of the mineral filler due to the adsorption of the monomer and the peroxide radical initiator will affect the parameters of the polymerization process and to change molecular weights and molecular weight distribution of the polymer (MWD) formed under these conditions. The mineral filler may affect the speed of the thermal decomposition of peroxide compounds that are used to initiate the polymerization, which in turn will change the polymerization parameters.

In our study, adsorption of some peroxide compounds and polymerization of vinyl monomers in the presence of disperse oxides, namely α-PbO, β-PbO, PbO_2, Fe_2O_3, SiO_2, Cr_2O_3, TiO_2 was studied. As the initiators of the polymerization, benzoyl peroxide (PB), sebacic acid oligoperoxide (OPS), *tert*-butyl hydroperoxide (HTB), and didecanoicdiperadpinate (DP) were used. The work was used as monomers - styrene (ST), methyl acrylate (MA), methyl methacrylate (MMA), butyl acrylate (BA) and butyl methacrylate (BMA). Investigation of the polymerization rate in the presence of radical polymerization initiators shows that, depending on the nature of disperse oxide, the polymerization process can accelerate or inhibit compared to a homogeneous system. During the study of polymerization in the collapsible dilatometer, such a stirring rate of the polymerization mixture is chosen so that the particles of disperse oxide are evenly distributed in the reaction medium. In all polymerization experiments, the process led to ~10% degree of monomer conversion. Upon achieving such a degree of conversion on the surface of disperses oxide, a shirt of the macromolecules of the polymer was formed and in the future, the filler did not affect the polymerization process. The study of the rate of thermolysis of peroxide initiators in the polymerization environments indicates that the filler can lead to a growth rate constant or not affecting this process. Polymerization in filled systems takes place in a solution of monomer and on the surface of disperses oxide. The surface of the disperse oxide participates in the reaction of the breakdown of growing polymer radicals and the process of initiating polymerization.

The molecular weight of polymers obtained in the presence of mineral disperse oxides is smaller than in polymers obtained in homogeneous systems. In particular, in the presence of a disperse Cr_2O_3, MWD of ST is bimodal, indicating the participation of the surface of the oxide in the formation of a polymer. The degree of grafting of the polymer macromolecules is found to the surface of disperses oxides. The amount of macromolecules grafted to the surface of the oxide depends on the nature of the peroxide initiator and monomer.

Interaction of Chromate Oxyanions with Carbon Nanostructures: TD-DFT Calculations of Excited Electronic States and Possibility of the Optical Monitoring

Yu. Hizhnyi, S. Nedilko and V. Borysiuk

Taras Shevchenko National University of Kyiv, 64/13 Volodymyrska st., Kyiv, Ukraine

One of the most promising methods of water purification from heavy metals is their adsorption on artificial adsorbents. The search for new adsorption materials to create effective cleaning schemes is an important scientific and technological task. Materials based on carbon nanostructured materials, in particular CNTs, are also considered as promising adsorbents of heavy metals. Among other adsorbents, CNTs are characterized by a number of different important properties due to their large surface area and the generally high adsorption capacity of the carbon surface to many toxic molecules [1].

Application of optical monitoring procedures for the adsorption process of heavy metal anions, in particular chromate anions on carbon nanotubes, can significantly improve an efficiency of cleaning methods and promote the creation of new effective environmental protection technologies. In this report, the principal possibility of optical monitoring of adsorption (in particular, detection of the fact of adsorption itself) of chromate anions on the surface of carbon nanostructures was analysed. The analysis was based on the results of theoretical calculations of the oscillator strengths of electronic transitions and corresponding optical spectra of various forms of chromate anions (CrO_4^{2-}, $Cr_2O_7^{2-}$ and $HCrO_4^{-}$) and chromate molecular complexes ($M^I_2CrO_4$, M^I = Li, Na, K and $M^{II}CrO_4$, M^{II} = Zn, Cd, Hg) on the surface of pure and B(N)-doped carbon nanotubes CNT(5,5) and graphene sheets.

The calculations were carried out at the Time-Dependent Density Functional Theory (TD-DFT) within molecular cluster approach. The geometry-optimized calculations were carried out using Gaussian 09 software package [2]. Excited electronic states of chromate anions and molecular complexes in “free” and adsorbed configurations were calculated using the two-level ONIOM-2 approach [3]. In this approach, the system with optimized geometry was divided into two regions, the quantum mechanical (QM) and the molecular mechanical (MM). The QM region comprised the atoms of the anions, while the MM region comprised all atoms of carbon nanostructure. The electronic embedding was used in order to take into account electrostatic interaction between the QM and MM regions, i.e., the atoms of the QM region were treated by TD-DFT calculations, while the atoms of the MM region were treated as partial charges contributing to the quantum-mechanical Hamiltonian.

It was found that the calculated optical spectra of chromate anions and molecular complexes adsorbed on the surface of carbon nanostructures significantly changed in comparison with the corresponding spectra of the anions in "free" state. Therefore, the optical absorption and reflectance spectroscopies have to be considered as promising methods for monitoring of the adsorption processes of chromate anions on the surface of carbon nanostructures.

[1] Jung, C., Heo, J., Han, J., Her, N., Lee, S. J., Oh, J. & Yoon, Y. (2013). Hexavalent chromium removal by various adsorbents: powdered activated carbon, chitosan, and single/multi-walled carbon nanotubes. *Separation and Purification Technology*, 106, 63-71.

[2] M. J. Frisch, G. W. Trucks, H. B. Schlegel, et al, Gaussian 09, Gaussian: Wallingford, CT, 2009.

[3] Dapprich S, Komáromi I, Byun KS, Morokuma K, Frisch MJ (1999) A new ONIOM implementation in Gaussian98. Part I. The calculation of energies, gradients, vibrational frequencies and electric field derivatives. *J Mol Struct THEOCHEM* 461–462, 1–21.

Bifunctional Polymer-Magnetite Composites

R. Filipsonov[1], G. Martynyuk[2], S. Malynych[1] and O. Aksimentyeva[3]

[1]*Hetman Petro Sahaidachnyi National Army Academy*
[2]*Rivne State Humanitarian University*
[3]*Ivan Franko National University of Lviv*
e-mail: filipsonov.ruslan@gmail.com

Nowadays, the studies connected to the search for available materials that absorb (or scatter) electromagnetic radiation, especially those, which can be used in the defense technologies for antiradar coatings have become very important [1]. Composite materials containing dielectric or semiconductor nanoparticles of a particular shape as well as periodical micro- and nanostructures capable of spatial redistribution of scattered electromagnetic radiation in desired directions are perspective for that task. The goal of our present work is fabrication of bifunctional composite coating with antiradar and anticorrosive properties. Iron oxides, magnetite or Fe_3O_4 in particular are especially interesting among other components due to their ability to absorb electromagnetic waves of near IR and microwaves ranges [1]. Carbon threads or carbon nanotubes inclusions in magnetite-based composites may provide a synergetic effect, i.e. enhance electromagnetic energy absorption and improve anticorrosive properties on metal surface. We suggest to explore organic compounds based on conductive conjugated polymers along with magnetite immersed into epoxy resin matrix as an effective coating [2]. Dispersed magnetite Fe_3O_4 in a form of spherical particles with the diameter of 0.6–1.2 μm capable of not only absorb but also scatter electromagnetic radiation served as magnetic filler for composites. The magnetite colloidal dispersion was stabilized via surfactants that results in the formation of self-assembled molecular aggregates and provides overall stability of the system [3]. Prepared polymer composites were characterized by X-ray and EDAX-analysis, Raman spectroscopy, thermogravimetric, mechanical and thermo-mechanical techniques. Variation in the size of Fe_3O_4 particles and their concentration in the composites does not affect the period of elementary cell of magnetite and has a complex effect on the magnetic susceptibility, microhardness and thermomechanical properties of magnetite–polymer composite. It was found that composite containing magnetic microparticles and particles of polyaniline doped with sulfuric acid in 1:1 ratio exhibits the strongest microwave absorption. At the same time this optimal composition provides high microhardness and anticorrosive properties of the coating on the surface of steel. On the basis of obtained results method of composite formation with special purpose would be developed.

[1] Borisov Yu.I. Dynamics of Radioelectronics-3. - Moscow, Technosphere, 2009. - P. 276-279 (in Russian).
[2] Filipsonov R., Malynych S., Aksimentyeva O., Martynyuk G. Composite polymer coatings for special purpose //VII International scientific-technical conference «The modern technologies of polymer materials obtaining and processing» Book of abstracts, Lviv, November 06–08, 2019. – P.42.
[3] Aksimentyeva O. I., Savchyn V. P., Dyakonov V. P. et al. Modification of polymer-magnetic nanoparticles by luminescent and conducting substances// Mol. Cryst. Liq. Cryst. 2014. Vol. 590. P. 35–42. DOI: 10.1080/15421406.2013.873646.

Nanocatalysts for Carbon Monoxide Oxidation Based on the Acid Modified Polyphase Aluminosilicate Support and Contained Palladium(II) and Copper(II) Salts

T.L. Rakitskaya, T.A. Kiose and Yu.I. Popruha

Faculty of Chemistry and Pharmacy, Odessa I.I. Mechnikov National University.
St. Dvoryanskaya 2, 65082, Odessa, Ukraine. E-mail: tlr@onu.edu.ua

Basalt tuff (BT) from Rivnens'ka Oblast' (Ukraine) was used as a support ($\bar{S}$) for nanocatalysts contained palladium(II) and copper(II) salts as base components. XRD, SEM, FT-IR spectroscopy, and pH-metry were used for characterization of natural basalt tuff (N-BT), its acid modified forms (H-BT), and palladium-copper catalysts based on theses supports (K_2PdCl_4–$Cu(NO_3)_2$–KBr/$\bar{S}$). All the catalysts under study have the same composition i.e. $C_{Pd(II)} = 2.72\times10^{-5}$, $C_{Cu(II)} = 2{,}2\times10^{-5}$, and $C_{Br^-} = 1{,}02\times10^{-4}$ mol/g. The catalyst samples (10 g each) were tested in a flow-type unit at an inlet CO concentration in the gas-air mixture (GAM) of 300 mg/m^3, a GAM volume flow rate of 1 L/min, its RH of 76 % and temperature of 20 °C. Both natural and chemically modified basalt tuffs contain the following phases: clinoptilolite (CLI), mordenite (MOR), montmorillonite (Mont) and also α-quartz and hematite. Crystallite sizes of the phases are in the range from 9 to 90 nm. Treatment of N-BT samples with 3M solutions of HNO_3, H_3PO_4, H_2SO_4, and $C_6H_8O_7$ and their subsequent impregnation with solutions of palladium(II) and copper(II) salts result in slight structural changes only in the Mont phase. No new phase was detected. SEM images of the sample surface confirm the presence of morphotypes characteristic of CLI, MOR, and Mont phases. It has been found that the catalytic activity of the Pd(II)-Cu(II)/3H-BT-0.5 compositions depends not only on the acid treatment duration (its optimal value is 0.5 h) but also on the nature of acids (Figure). It can be seen that, at the same conditions of support modification, the catalysts obtained demonstrate the steady state mode of carbon monoxide oxidation with outlet CO concentrations, C^f_{CO}, lower than MPC_{CO}. Forms of the kinetic curves at initial periods of the reaction are different and depend on the acid nature: C^f_{CO} is lower than MPC_{CO} only for the catalyst samples based on supports treated with nitric (curve 1) and citric (curve 3) acids. These two catalytic compositions are applicable in the case of devices intended for respiratory protection against carbon monoxide.

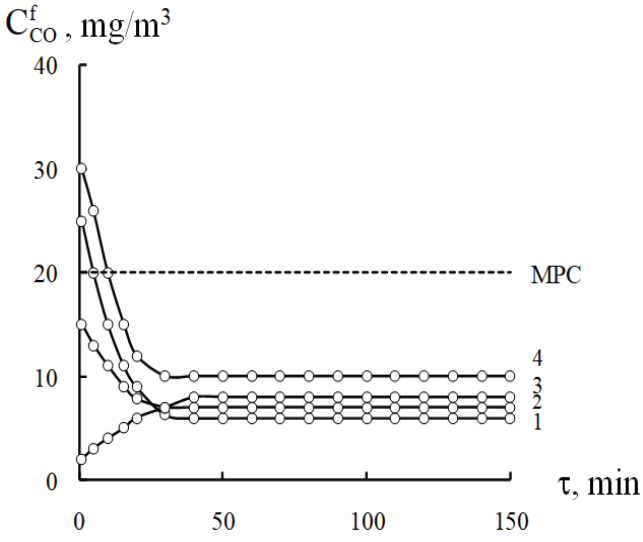

Fig. Time dependences of C^f_{CO} for CO oxidation with air oxygen over Pd(II)-Cu(II)/3H-BT-0.5 samples in the case of support treatment with different acids: HNO_3 (1), H_3PO_4 (2), $C_6H_8O_7$ (3), and H_2SO_4 (4)

Synthesis, Phase Transformations of Polymorphous Nanooxidic Forms of Iron and Their Interaction with Sulfur Dioxide

T.L. Rakitskaya, A.S. Truba, A.P. Nazar, T.A. Kiose and V.Y. Volkova

Faculty of Chemistry and Pharmacy, Odessa I.I. Mechnikov National University, 2,St. Dvoryanskaya, 65082, Odessa, Ukraine. E-mail: tlr@onu.edu.ua

Polymorphous forms of iron(III) (α-Fe_2O_3, γ-Fe_2O_3, Fe_3O_4, α-FeO(OH), and β-FeO(OH)) are characterized by different activity in the reaction with sulfur dioxide and their positions in the known activity series are not single valued due not only to their phase compositions but also to their obtaining methods. Besides that, there are no systematic investigation concerning the influence of the structure and morphology of iron oxidic forms on the kinetics of their reaction with SO_2 in the presence of air oxygen and at ambient temperatures.

Sample	Phase (content, %)	D, nm	τ_{MPC}, min	$Q_{sp}\cdot10^4$, moles of SO_2 per gram
IS-Fe-300	γ-Fe_2O_3 (100)	7.4	-	0
IIS-Fe-20	α-FeO(OH) (100)	15	-	1.06
IIS-Fe-110	α-FeO(OH) (100)	15	2	1.1
IIIS-Fe-110	Fe_3O_4 (49.6)	38	60	7.42
	γ-FeO(OH) (39.1)	9		
	α-FeO(OH) (11.3)	9		
IVS-Fe-200	α-FeO(OH) (78.7)	15	60	9.82
	α-Fe_2O_3 (21.3)	6		
VS-Fe-110	Semicrystalline mixture	-	110	11.12
IS-Fe-500	α-Fe_2O_3 (99)	16	-	0
	γ-Fe_2O_3 (1.0)	11		
IIS-Fe-500	α-Fe_2O_3 (100)	38	-	0.18
IVS-Fe-500	α-Fe_2O_3 (100)	30	-	1.3
VS-Fe-500	α-Fe_2O_3 (100)	64	120	10.4

Monophase iron oxide samples (α-Fe_2O_3, γ-Fe_2O_3, and α-FeO(OH)) and also mixtures of iron oxides with different phase compositions i.e. Fe_3O_4, γ-FeO(OH), α-FeO(OH), and α-FeO(OH), α-Fe_2O_3, were obtained by a precipitation method with variation of the nature of iron salts, precipitators as well as drying and calcination temperatures. The samples were identified by XRD, SEM, and FT-IR spectroscopy methods. The samples were also tested in the reaction with sulfur dioxide at an initial SO_2 concentration in the gas-air mixture (GAM) of 150 mg/m^3, a GAM volume flow rate of 16.6 cm^3/s, its RH of 76 % and temperature of 20 °C. Data concerning phase compositions of the samples, their crystallite sizes and reactivity in the reaction with SO_2 are summarized in Table. All the samples except for VS-Fe-110 obtained by a sol-gel method are crystalline with the typical morphology. Protective properties of four samples and, particularly, a time of protective action, τ_{MPC}, were found to increase in the order IIIS-Fe-110 = IVS-Fe-200 < VS-Fe-110 < VS-Fe-500. A specific amount of SO_2 entered into the reaction, Q_{sp}, depends on the sample phase compositions. As can be seen, a reactivity for the α-Fe_2O_3 phase formed by thermal transformation of different iron precursors is unequa: Q_{sp} changes from 0 to 10.4×10^{-4} moles of SO_2 per gram. Interaction of SO_2 with iron(III) nanooxides in air does not result in formation of new phases. The FT-IR spectra give evidence of the formation of surface sulfite and bisulfite forms from SO_2 adsorbed.

Hybrid Solid Electrolyte Based on the Combination of $Li_{1.3}Al_{0.3}Ti_{1.7}(PO_4)_3$ Ceramic and Liquid Solution with $LiPF_6$ for Li-Ion Batteries

I. V. Lisovskyi[1], S. A. Solopan[1], A. G. Belous[1] and V. G. Khomenko[2]

[1]*V.I. Vernadsky Institute of General and Inorganic Chemistry, NAS of Ukraine, 32/34 Academic Palladin Avenue, Kyiv 03142, Ukraine*
[2]*Kyiv National University of Technologies and Design, 2 Nemyrovycha-Danchenka Street, Kyiv 01011, Ukraine*

Lithium-ion batteries (LIB) have long been an integral part of every modern person's life. They are widely used in various electronic devices such as smartphones, cameras, laptops and more. Due to its high energy density, LIBs are considered promising power supplies for electric vehicles. However, due to the use in modern LIBs polymer separators saturated with liquid electrolyte, there are a number of problems, namely: the threat of electrolyte leakage, fire hazard, in addition, such systems are characterized by a narrow operating range of temperature and electrochemical stability [1, 2]. Therefore, solid-state batteries, which do not contain flammable components and have potential advantages in gravimetric and volumetric energy density, operating temperature range and safety compared to LIB, are of great interest.

The main disadvantage of existing solid-state lithium batteries based on inorganic materials is the low conductivity of the solid electrolyte (~ 10^{-5}-10^{-7} S/cm) [3]. In addition, it is well known that a high interfacial resistance is usually observed at the solid electrolyte/cathode interface [4]. However, Al-substituted lithium titanium phosphate $Li_{1.3}Al_{0.3}Ti_{1.7}(PO_4)_3$ (LATP) with NASICON structure is characterized by high ionic conductivity (~ 10^{-3}–10^{-4} S/cm) at room temperature, which makes it promising candidate for use in solid state batteries [5].

To increase the level of LIBs` safety, we proposed a hybrid solid electrolyte based on a porous ceramic matrix LATP impregnated with 1M solution of LiPF6 in a mixture of solvents ethylene carbonate, diethyl carbonate and dimethyl carbonate (1:1:1). The specific capacity of the cathode material in the elements with a hybrid electrolyte is 140.5 and 138.2 mAh/g at an electrolyte thickness of 0.8 and 1.6 mm, respectively. The obtained result is not significantly inferior to the models of LIB with liquid electrolyte (145.6 mAh/g). The proposed hybrid electrolyte solves the problems of lithium-ion batteries associated with electrolyte leakage, as the liquid electrolyte is immobilized exclusively in the pores of the ceramic matrix, and fire hazard, due to preventing the formation of lithium dendrites in the interelectrode space.

[1] Duh Y. S., Chen Y. L., Kao C. S. Thermal stability of ethylene carbonate reacted with delithiated cathode materials in lithiumion batteries // J. Therm. Anal. Calorim. – 2017. – 127, № 1. – P. 995–1007.
[2] Hess S., Wohlfahrt-Mehrens M., Wachtler M. Flammability of Li-ion battery electrolytes: flash point and self-extinguishing time measurements // J. Electrochem. Soc. – 2015. – 162, № 2. – P. A3084.
[3] Manthiram A., Yu X., Wang S. Lithium Battery Chemistries Enabled by Solid-State Electrolytes. Nat. Rev. Mater. 2017. 2 (4): 1.
[4] Wu B., Wang S., Evans IV W.J., Deng D.Z., Yang J., Xiao J. Interfacial behaviours between lithium ion conductors and electrode materials in various battery systems. J. Mater. Chem. A. 2016. 4 (40): 15266.
[5] Aono H., Sugimoto E., Sadaoka Y., Imanaka N., Adachi G.Y. Ionic conductivity of solid electrolytes based on lithium titanium phosphate. J. Electrochem. Soc. 1990. 137 (4): 1023.

Dynamic Dielectric Function of Two-Dimensional Electron Gas

C. Tovstyuk

Department of Electronics and Information Technology, Lviv Polytechnic National University

In this paper we investigate the dynamic dielectric function of two-dimensional electron gas which is effect by exchange correlation by holes in quantum nanostructure GaAlAs/GaAs/GaAlAs. For our investigations we used the results obtained in [1], where the different approximations (random phase, Hubbard approximation and self-consistent local field correction) where compared.

We calculated the temperature dependence of real part of dielectric function for electrons with different momenta and different frequencies (energies). As we found out for electron with large momenta (about the second half of Brillouin zone) $Re\ \varepsilon$ is almost independent function frequencies (ω =1, corresponds to Fermi level) and temperature (up to the room temperature). For small momentum of electron we obtained different dependences.

- A serial of functions which are almost independent on ω (for electron with q = 0.2 and q = 0.5 at room temperature)
- A serial of functions which are almost independent on temperature for small momenta, for example for $q = 0.2$, $\omega = 0.2$; $\omega = 0.25$; for $q = 0.17$, $\omega = 0.2$; $\omega = 0.45$; for $q = 0.15$, $\omega = 0.2$; $\omega = 0.4$.
- A serial of functions which are slowly and monotony increasing with the temperature for small momenta. For example for $q = 0.15$, $\omega = 0.25$; for $q = 0.17$, $\omega = 0.35$; for $q = 0.2$, $\omega = 0.4$; $\omega = 0.45$.
- A serial of functions which are slowly and monotony decreasing with the temperature for small momenta. For example for $q = 0.15$, $\omega = 0.3$; for $q = 0.17$, $\omega = 0.25$ and $= 0.3$; for $q = 0.2$, $\omega = 0.3$; $\omega = 0.35$.
- Some cases, when $Re\ \varepsilon$ has got slightly non-monotony dependences on temperature. For example for $q = 0.15$, $\omega = 0.35$; for $q = 0.17$, $\omega = 0.4$; for $q = 0.2$, $\omega = 0.45$.

Different temperature dependences of $Re\ \varepsilon$ denote that the frequency dependence is a strongly non-monotonic function. We passed our calculations for room temperatures, to follow the influences of electron quasi-momentum and frequencies. For small momenta we obtained a family of non-monotonic functions with singularity, typical for generalized functions. To the left of singularity (for small frequencies) we get the function almost independent on ω with the values overcoming the asymptotic, typical for the right side of singularity. After the singularity our function increases rapidly and moves to the asymptotes (1 for our dimensionless calculations). It means that as a fact we get some higher values of Re ε for small ω. Such conclusion is in good agreement with the well known facts that layered systems are effective for low energies [2].

But for $q = 0.17$ we obtained different dependences for $Re\varepsilon(\omega)$: constant and negative for small frequencies, switching into positive region after its singularity and decreasing to ω = 1 for high frequencies. Actually such dependences for $Re\varepsilon(\omega)$ are typical for polaritons in solids. It means that there are particular electromagnetic waves, propagating only on the surface of two-dimensional layer.

[1] S. A. Hashemizadeh, R. Vahdat, Journal of Nanostructures, 2013, V. 3, P. 415-419.
[2] C.C. Tovstyuk, Chem. Met. Alloys, 2011, V. 4, P. 58-62.

Sol-Gel Synthesis of $ZnAl_2O_4$, $MgGa_2O_4$ and $LiGa_5O_8$ Nanopowders Co-Doped with Cr^{3+}, Er^{3+} and Yb^{3+} Ions

I. Lutsyuk[1], V. Hreb[1], A. Zelinskiy[2] and L. Vasylechko[1]

[1] *Lviv Polytechnic National University, Bandera 12, 79013, Lviv, Ukraine*
[2] *Ivan Franko National University of Lviv, Universytetska 1, Lviv, 79000, Ukraine*

Low-temperature citrate sol-gel method was used for a synthesis of series of nanocrystalline luminophores based on $MgGa_2O_4$, $ZnAl_2O_4$ and $LiGa_5O_8$ spinel materials, co-doped with different concentrations of Cr^{3+}, Er^{3+} and Yb^{3+} ions. In contrast to the traditional high-temperature solid-state synthesis, the applied method allowed to obtain phase-pure nanopowders of all three types of spinel materials at a minimal heat treatment temperature of 700 °C (Fig.). In the case of $ZnAl_2O_4$-based series, the average crystallite size increases from ~33 nm after initial crystallization at 700 °C up to 73-75 nm in the materials heat treated at 1200 °C. Much smaller particles with a size of 5-11 nm are initially formed in the case of crystal phosphors based on $MgGa_2O_4$ and $LiGa_5O_8$ spinels.

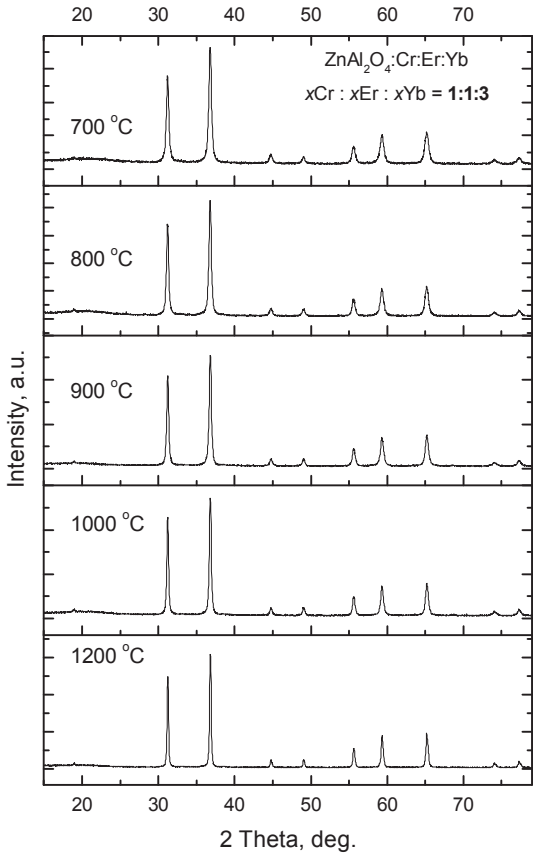

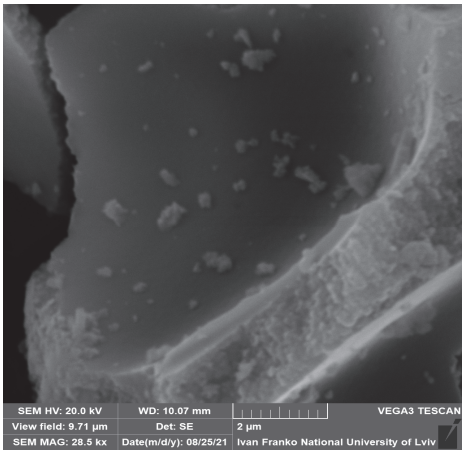

XRD patterns of the $ZnAl_2O_4$:Cr/Er/Yb powders showing evolution of crystal and microstructure after heat treatment at different temperatures (left column) and SEM of the powder annealed at 800 °C.

Crystal structure peculiarities of three series of Cr/Er/Yb co-doped spinel type materials based on $MgGa_2O_4$, $ZnAl_2O_4$ and $LiGa_5O_8$ and their evolution with the heat treatment temperature of the powders are discussed.

Acknowledgment: The work was supported by the National Research Foundation of Ukraine (grant no. 2020.02/0373).

Porous Silicon Surface Modified and Incorporated by ZnO

M. Rudko[1,3], P. Parandiy[2] and B. Turko[3]

[1]*Scientific-Technical and Educational Center of Low Temperature Studies, Dragomanova St., 50, 79005 Lviv, Ukraine,*
[2]*Ivan Franko National University of Lviv, Electronics and Computer Technology Department, 50, Dragomanova St., Lviv, 79005, Ukraine*
[3]*Ivan Franko National University of Lviv, Physics Department, 50, Dragomanova St., Lviv, 79005, Ukraine*

The influence of formation conditions on the surface morphology and spectra of photoluminescence (PL) of porous silicon (PS) are researched. The photoluminescence (PL) and photoluminescence excitation spectra (PLE) and electron and atomic force microscopy were investigated. The results of low-dimension electro-chemically and chemically etched PS, ZnO - PS heterostructures studies, obtained by chemical etching method and formation of ZnO nanoclusters on the PS surface (deposition method and solution gas transport reactions) are represented.

One of the way on nanomaterials creation with improved functional properties is a combination of different nature substances on molecular, nano- and submicron levels [1], in particular, with the nanostructured conductive inorganic semiconductor matrix. Prospects for the application of various porous structures, in particular based on silicon are founded on the properties of these structures in relation to detecting substances and quantum size effect [2].

Samples surface morphology study obtained by chemical etching was carried out on scanning probe microscope SolverNEXT by atomic force microscopy (AFM) and using REMMA-102-02 Scanning Electron Microscope-Analyzer. The photoluminescence spectra were measured using double-aperture spectrometer SDL-1 at the nitric temperature, PLE spectra of all prototypes were carried out at room temperature on spectral device SM 2203, monochromator MDR-6, connected with photosensor modules. The sample was excited by GaN laser (405 nm) and N_2 laser (337 nm). The sample was placed in a closed loop helium cryostat, equipped with a cryocooler DE-202A and a temperature regulator Cryocon 32.

The PL spectrum at T = 77 K showed a wide range of PS PL 400-960 nm with three bands in the 450-630 nm, 630-700 nm and 750-950 nm (in the near infrared region) in accordance with maxima 518 nm, 655 nm and a broad peak 850-925 nm. PS PL spectra obtained on various single-crystal substrates, methods and different excitation wavelengths found differences in the values of intensity and maximum of PL position.

The photoluminescence spectrum of PS incorporated by ZnO sample, measured at T = 13 K, is characterized by three intensive overlapping bands with the maxima at 500 nm, 615 nm and 670 nm in the visible region. It was found that the decay kinetics of these three overlapping bands of photoluminescence at T = 13 K consists of two components - fast and slow.

[1] Aksimentyeva O.I., Monastyrskyi L.S., Savchyn B.M // Modec.Cryst.&Liq.Cryst., 2007, Vol.467.- C.73-83.
[2] Canham L.T. Appl. Phys. Lett.-1990.-57.- P.1046-1048

Synthesis and Characterization of $CuMn_2O_4$ Nanoparticles: a Potential Semiconductor for Photoelectric Devices

M. Enhessari[1] and A. Salehabadi[2]

[1]*Department of Chemistry, Naragh branch, Islamic Azad University, Naragh, Iran*
[2]*School of Industrial Technology, Universiti Sains Malaysia, 11800 Penang, Malaysia*

$CuMn_2O_4$(copper manganese oxide) nanoparticles was successfully synthesized via a sol-gel method using its respective metal cations sources i.e., Cu^{2+} and Mn^{2+} in an appropriate complexing agent (stearic acid). The structural analysis of the crystalline phase indicates the formation of a series of sharp peaks with particle size about 39 nm. The excitation threshold of photoluminescence (PL) indicated that the $CuMn_2O_4$ is a medium material in photoluminescence applications. The band gap energy (Eg) equal to 1.4 eV calculated from DR spectra, revealed that $CuMn_2O_4$ can be used as a semiconducting material in photoelectrical devices.

Vibrating sample magnetometer (VSM) analysis of the nanostructures indicates moderate ferromagnetic properties. Examination of the dielectric properties by the LCR meter indicates the semiconducting property of the nanostructure. The highest conductivity increase was in the frequency of 308 MHz equal to 70.7 μS. Therefore, the $CuMn_2O_4$ nanostructures are potential candidates in fuel cells, telephones, loudspeakers and transformers due to their properties and convenience, non-toxic and environmentally friendly production methods.

[1] Enhessari M (2013). Synthesis, characterisation and optical band gap of $Cr_{1.3}Fe_{0.7}O_3$ nanopigments. Pigment & Resin Technology 42(4): 347–352.
[2] Enhessari M, Shaterian M, Esfahani MJ and Motaharian MN (2013). Synthesis , characterization and optical band gap of La_2CuO_4 nanoparticles. Materials Science in Semiconductor Processing. Elsevier 16(6): 1517–1520.

SECTION 4

MATERIALS FOR SENSING AND CATALYSIS

Nonstoichiometry and Chemical Expansion of Cerium Oxide Based Thin Films

H. Fritze[1], H. Wulfmeier[1], T. Defferiere[2], S. Schröder[1] and H. L. Tuller[2]

[1]*Institute of Energy Research and Physical Technologies, Clausthal University of Technology, Germany*
[2]*Department of Materials Science and Engineering, Massachusetts Institute of Technology, Cambridge, USA*

Nonstoichiometry in oxides governs many key materials properties including electronic and ionic conductivity, oxygen and cation diffusion and chemical expansion. The latter can be utilized for the development of a new generation of high-temperature actuators. Contrary, related mechanical stress in e.g. fuel cells results in limited lifetime and needs to be avoided. Therefore, the focus of this paper is the investigation and correlation of nonstoichiometry and chemical expansion taking cerium oxide based solid solutions as model materials. In this context, thin films are of special interest since they enable fast operation due to short transport paths for ions and, simultaneously, miniaturization of devices.

Oxygen nonstoichiometry □ in thin-film $CeO_{2-□}$ and $Pr_{0.1}Ce_{0.9}O_{2-□}$ (PCO) is determined at elevated temperatures and controlled oxygen partial pressures using resonant nanobalances. The latter consist of y-cut CTGS ($Ca_3TaGa_3Si_2O_{14}$) piezoelectric resonators, operated in the thickness shear mode at about 5 MHz where they show a mass resolution of about 50 ng [1]. A decrease of the oxygen partial pressure from 0.2 to 10^{-8} bar at 700°C results in changes of the nonstoichiometry from 0.02 to 0.05 which is in good agreement with previously reported oxygen nonstoichiometry data derived from chemical capacitance studies [2]. Below about 10^{-5} bar, the nonstoichiometry approaches a plateau which is attributed to the full reduction of Pr to the trivalent state. The chemical expansion of PCO films is determined up to 800°C by laser Doppler vibrometry. The method enables detection of nanometer displacements, provided that displacement frequencies are above 0.1 Hz. The PCO films are deposited on yttrium stabilized zirconia (YSZ) substrates operated in the electrochemical oxygen pump mode to periodically adjust the oxygen activity within the PCO film. A maximum displacement of about 150 nm at the center of the substrate plate (film: thickness 1.35 µm, substrate: diameter 10 mm, thickness 0.5 mm) is found during application of a periodic 0.1 Hz pumping voltage at 800°C. Recalculation for substrate and film parameters used for nanoscale electrochemomechanical spectroscopy [3] results in good agreement at 600 and 650°C where the application temperatures of both methods overlap (Fig. 1). The correlation of nonstoichiometry and chemical expansion is discussed.

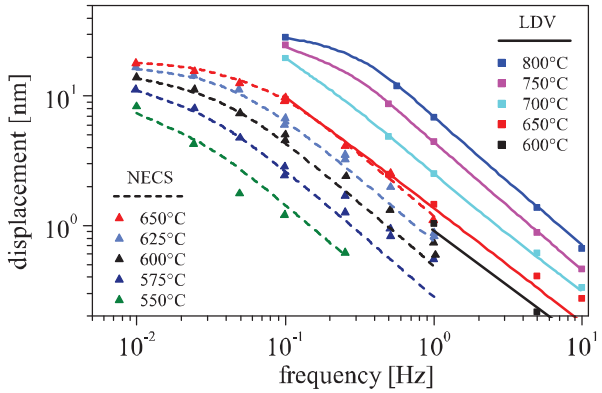

Fig. 1. Displacement of PCO coated YSZ substrates determined by LDV at high temperatures (squares and solid lines) in comparison to NECS data at medium temperatures [3] (triangles). Further, the fit of a first-order transfer function to the displacement as presented in [3] is shown (solid lines).

[1] S. Schröder, H. Fritze, S. Bishop, D. Chen, H.L. Tuller, Appl. Phys. Lett. **112** (2018) 213502.
[2] D. Chen, S. R. Bishop, and H. L. Tuller, Chem. Mater. **26** (2014) 6622.
[3] J. G. Swallow, J. J. Kim, J. M. Maloney, D. Chen, J. F. Smith, S. R. Bishop, H. L. Tuller, K. J. Van Vliet, Nat. Mater. **16** (2017) 749.

Contributions to Acoustic Loss in Piezoelectric CTGS ($Ca_3TaGa_3Si_2O_{14}$) Resonators

Yu. Suhak[1], W. Johnson[2], A. Sotnikov[3], H. Schmidt[3], B. Sorokin[4] and H. Fritze[1]

[1]*Institute for Energy research and Physical Technologies, Clausthal University of Technology, Goslar, Germany*
[2]*National Institute of Standards and Technology, Boulder, CO, USA*
[3]*SAWLab Saxony, Leibniz Institute for Solid State and Materials Research Dresden, Dresden, Germany*
[4]*Technological Institute for Superhard and Novel Carbon Materials, Troitsk, Moscow, Russia*

Piezoelectric single crystals of the langasite ($La_3Ga_5SiO_{14}$, LGS) family are promising materials for sensing applications in harsh environments and could be used for a variety of purposes including mass detection, temperature, pressure and gas sensing. The sensing principles of such piezoelectric resonators are based on the resonance frequency shifts that arise from external factors, such as varying temperature or mass load. In order to increase the sensing resolution of such devices, it is essential to maximise the resonant quality factor (Q-factor) or, correspondingly, to understand and minimise the acoustic loss. Catangasite ($Ca_3TaGa_3Si_2O_{14}$, CTGS) is a langasite isomorph that possesses reasonably high piezoelectric coefficients, exhibits no phase transformation below its melting temperature (1370 °C) and shows substantially lower losses at elevated temperatures, comparing to LGS.

This work includes investigations of room temperature acoustic loss in CTGS in the GHz frequency range and of temperature dependent loss up to 900 °C in the MHz frequency range. The crystals for this study were grown by Fomos Materials (Moscow, Russia) and IKZ (Berlin, Germany). The measurements in GHz range were carried out by means of $Al_{0.7}Sc_{0.3}N$ thin film piezoelectric transducers that are deposited on the CTGS samples to realize High overtone Bulk Acoustic Resonator (HBAR) structures. The high temperature measurements were performed using Y-cut CTGS resonators, operated in the thickness-shear mode (TSM). Resonant ultrasound spectroscopy on Pt-electroded samples [1] as well as non-contacting tone-burst excitation technique on samples without electrodes [2] were applied.

The study revealed that a superposition of several physical mechanisms, including phonon-phonon interactions (Akhiezer relaxation), point-defect relaxations and conductivity-related relaxation determines the losses in CTGS. Fig. 1 shows the overall Q^{-1} of CTGS as well as the separate loss contributions.

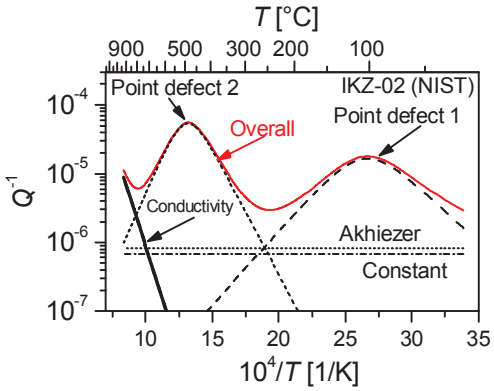

Fig. 1. Q^{-1} of a CTGS resonator, operated in TSM as a function of temperature, and separate contributions to Q^{-1}

[1] H. Fritze, *High-temperature bulk acoustic wave sensors*, Meas. Sci. Technol., **22** 12002 (2011).
[2] W. L. Johnson, M. Schulz, H. Fritze, *High-temperature electroacoustic characterization of Y-cut and singly-rotated $Ca_3TaGa_3Si_2O_{14}$ resonators*, IEEE Trans. Ultrasonics **61** 1433-1441 (2014).

High-Temperature Stable Thin-Film Oxide Electrodes for Langasite and Catangasite Resonators

H. Wulfmeier, R. Feder, L. Zhao and H. Fritze

Clausthal University of Technology, Institute of Energy Research and Physical Technologies, Am Stollen 19 B, D-38640 Goslar, Germany

The availability of high-temperature and chemically stable devices for monitoring and controlling of high-temperature processes is a key requirement for efficient and environmentally friendly industrial production or energy conversion. Piezoelectric resonators based on materials with the $A_3BC_3D_2O_{14}$ structure like langasite (LGS, $La_3Ga_5SiO_{14}$) or catangasite (CTGS, $Ca_3TaGa_3Si_2O_{14}$), fulfil these requirements provided that stable electrodes are available. However, at elevated temperatures, degradation of commonly used metal electrodes may affect the performance of the piezoelectric resonators. Thin-film noble metal electrodes of platinum, rhodium, iridium or their alloys are operational at temperatures up to e.g. 900 °C in case of platinum [1]. Typical degradation mechanisms include oxidization, agglomeration or evaporation of the metal films [2]. Oxide electrodes are expected to overcome these concerns. Further, problems arising from differences in thermal expansion between electrode and piezoelectric resonators could be minimized if the resonator and electrodes consist of identical or similar materials. Accordingly, the objective of this work is to create nearly monolithic resonators. A critical aspect, however, is the low electrical conductivity of oxide films in comparison to metal electrodes. Doping of the oxide films is expected to result in sufficiently high conductivities.

The present work focuses on two major aspects: (I) The growth of high-quality undoped and doped LGS thin-film electrodes by pulsed laser deposition (PLD) and (II) the characterization of the resulting nearly monolithic resonator devices.

Homo- end hetero-epitaxial films are grown by PLD. High substrate temperatures (450–750 °C) are applied to obtain crystalline films. Ga evaporation during thin-film deposition as occurring here is a common phenomenon. It is compensated by an increased p_{O2} (10^{-3}–10 Pa) in the deposition chamber and by an increased Ga content in the PLD targets whose Ga content is three times as high in comparison to stoichiometric LGS. Crystallinity and stoichiometry of the films are confirmed by X-ray diffraction and secondary neutral mass spectrometry (SNMS). Detailed information on the variation of the growth parameters are given in [3].

Based on optimized growth parameters for the undoped films, Sr-doped LGS thin films are grown. Here, 33 % of La in the target composition is substituted by Sr. The film conductivity is increased by one order of magnitude compared to nominally undoped bulk LGS. Keyhole-shaped Sr-doped LGS electrodes are deposited on both sides of CTGS resonator blanks. CTGS and LGS single crystals exhibit comparable lattice constants. Therefore, doped LGS electrodes on CTGS crystals form nearly monolithic films, as confirmed by XRD. The great advantage of CTGS resonators is their significant lower conductivity compared to LGS. This combination enhances the conductivity difference between doped LGS electrodes and the resonator material even more. The resonance behaviour of such nearly monolithic resonators is evaluated in the temperature range from 600 to 1000 °C and compared to that of CTGS resonator blanks. These resonators show stable operation and high resonator quality factors of 1200 even at 1000 °C, for details see [4].

[1] D. Richter, M. Schulz, S. Sakharov, Z.J. Davis, H. Fritze: Mater. Res. Soc. Symp. Proc., **1519**, mrsf12-1519-mm03-29, 2013.
[2] S.L. Firebaugh, K.F. Jensen, M.A. Schmidt: J. Microelectromech. Syst., **7**, 128-135, 1998.
[3] H. Wulfmeier, R. Feder, L. Zhao, H. Fritze: MRS Advances, **4**, 523-529, 2019.
[4] H. Wulfmeier, R. Feder, L. Zhao, H. Fritze: Journal of Sensors and Sensor Systems, **9**, 14-25, 2020.

Non-Stoichiometry of Thin-Film $Ce_{1-x}Zr_xO_{2-\delta}$ Characterized by a Resonant Nanobalance

I. Kogut[1], A. Wollbrink[1], C. Steiner[2], R. Moos[2] and H. Fritze[1]

[1]*Institute for Energy Research and Physical Technologies, Clausthal University of Technology, Am Stollen 19B, 38640 Goslar, Germany*
[2]*Department of Functional Materials, University of Bayreuth, Universitätsstraße 30, 95440 Bayreuth, Germany*

Due to the large oxygen storage capacity of cerium oxide ($CeO_{2-\delta}$), stemming from a strong and reversible dependence of its non-stoichiometry δ on the partial oxygen pressure (p_{O2}), this material is widely used in three way catalytic converters, in particular, for exhaust gas aftertreatment of gasoline combustion engines, as well as in gas sensors and for hydrogen generation [1, 2]. In ceria-based mixed-oxide compounds, e.g. $Ce_{1-x}Zr_xO_{2-\delta}$ (CZO) solid solutions, the reduction efficiency and gas storage capacity are expected to be further enhanced [3]. However, the effect of the oxygen deficiency on the catalytic activity of such solid solutions has not yet been fully understood, since the existing data and models are limited to very narrow non-stoichiometry ranges and relatively high oxygen partial pressures. Moreover, data for thin-film CZO, which may differ from those for the bulk material, are rare. A reliable direct access to non-stoichiometry in broader ranges would be beneficial for explaining the kinetics and mechanisms of defects formation and their influence on electrical transport and catalytic activity in CZO.

In this work, high-precision measurements of oxygen non-stoichiometry δ in thin-film $Ce_{1-x}Zr_xO_{2-\delta}$ with x = 0, 0.2, 0.33, 0.5, 0.67 and 1 are performed *in situ* with a resonant nanobalance [4] in the temperature range of 300–1200 K and at controlled oxygen partial pressures ranging from 0.2 to 10^{-20} bar. Thin layers (ca. 2 µm) of CZO were deposited by pulse laser ablation on both faces of high-temperature stable $Ca_3TaGa_3Si_2O_{14}$ (CTGS) *Y*-cut piezoelectric resonators operated in the thickness-shear mode (TSM, ~5 MHz). Then, the change in the resonance frequency (f_r) of CTGS resonator is proportional to the added load of CZO layer, and the mass change of the latter is derived from an additional shift in f_r using a physical model for TSM resonators [5]. The achieved mass resolution during the experiments was estimated to be about 7 ng/Hz at 900 °C, which infers a high suitability of the developed method for thermogravimetric analysis of micro- and nanoscale materials. The oxygen non-stoichiometries δ corresponding to observed mass losses in $Ce_{1-x}Zr_xO_{2-\delta}$ were calculated. At 900 °C and $p_{O2} = 3\times10^{-14}$ bar the preliminary δ values of 0.037 for pure CeO_2, 0.12 for $0.2 \le x < 0.5$ and 0.22 for $0.5 \le x \le 0.67$ are found. The obtained non-stoichiometry is analyzed with consideration of the *in situ* measured high-temperature electrical conductivity of $Ce_{1-x}Zr_xO_{2-\delta}$ at variable oxygen partial pressures.

[1] M. Mogensen, N. M. Sammes, G. A. Tompsett, Physical, chemical and electrochemical properties of pure and doped ceria, *Solid State Ionics* 129 (2000) 63-94.
[2] O. Deutschmann, J.-D. Grunwaldt, Abgasnachbehandlung in mobilen Systemen: Stand der Technik, Herausforderungen und Perspektiven, *Chemie Ingenieur Technik* 85 (2013) 1-24.
[3] D. Chen, Y. Cao, D. Weng, H. L. Tuller, Defect and Transport Model of Ceria-Zirconia Solid Solutions: $Ce_{0.8}Zr_{0.2}O_{2-\delta}$ - An Electrical Conductivity Study, *Chem. Mater.* 26 (2014) 5143-5150.
[4] S. Schröder, H. Fritze, S. Bishop, D. Chen, H.L. Tuller, Thin-film nano-thermogravimetry applied to praseodymium-cerium oxide films at high temperatures, *Appl. Phys. Lett.* 112 (2018) 213502.
[5] H. Fritze, High-temperature bulk acoustic wave sensors, *Meas. Sci. Technol.* 22 (2011) 12002.

TiO_2-Nanotubes-Based Reactors for Highly Efficient Photocatalytic and Photoelectrocatalytic Degradation of Organic Compounds

M. Čeh[1,2], L. Suhadolnik[1] and Ž. Marinko[1,3]

[1]*Nanostructured Materials, Jožef Stefan Institute, Jamova 39, Ljubljana, Slovenia*
[2]*Center for Electron Microscopy and Microanalysis, Jožef Stefan Institute, Ljubljana, Slovenia*
[3]*Jožef Stefan International Postgraduate School, Jamova 39, Ljubljana, Slovenia*

Titanium dioxide (TiO_2) is well known material for its photocatalytic applications due to its appropriate band-gap value, nontoxicity, low price and chemical inertness. This is why TiO_2 can also be used for catalytic degradation of persistent organic compounds in waste waters. The aim of our research was to synthesise highly active TiO_2 nanostructures and use them as catalytic materials in especially designed photocatalytic as well as photoelectrocatalytic reactors [1,2]. There are many synthesis routes that can produce nano-sized TiO_2, however only the process of anodic oxidation of metal titanium (wire, foil, mesh) yields two-dimensional ordered arrays of TiO_2 nanotubes that are firmly attached to the metallic titanium substrate. This enables the use of such TiO_2 arrays for photocatalytic as well as photoelectrocatalytic studies of degradation of organic pollutants in waste waters. Firm contact of TiO_2 nanotubes with titanium metal substrate namely enables the process of photoelectrocatalysis since the composite TiO_2/Ti can be directly used as an electrode material. Furthermore, the strong adhesion of ingrown TiO_2 nanotubes into the titanium substrate prevents possible release of TiO_2 particles into liquid after the purification process thus preventing subsequent pollution of purified liquid.

In our work we have systematically studied the influence of various experimental parameters of anodic oxidation process (electrolyte composition, applied potential, surface preparation of metal titanium, time of anodization, thermal treatment, etc.) on TiO_2 nanotubes structure and morphology (length, crystallinity, crystal structure, inner and outer diameter, etc.). Microstructural examination of such TiO_2 nanostructures after thermal annealing at 450°C for 1h using various electron microscopy techniques (SEM, TEM, ED, EDX, WDX) showed that the nanotubes were polycrystalline in nature with nano-grains ranging from only a few nm up to app. 10 nm, exhibiting anatase crystal structure. The inner and outer diameter of the nanotubes ranged from 50 to 60 nm and from 100 to120 nm, respectively. Thus prepared TiO_2 nanotubes arrays were incorporated into specially designed photocatalytic and photoelectrocatalytic (micro)reactors. In order to study efficiency of our catalytic systems, degradation of phenol was studied [3,4], as well as real waste waters containing synthetic dye [5]. For all tested organic compounds it was found out that complete or partial degradation of organic compounds was successful. Furthermore, kinetic studies and mechanisms of degradation were also obtained for selected compounds. Even after prolonged degradation tests of organic compounds the TiO_2 nanotubes showed only minor changes in surface morphology and subsequent activity.

[1] M. Krivec, K. Žagar, L. Suhadolnik, M. Čeh, G. Dražić, ACS Appl. Mater. Interfaces 2013, 5, 9088−9094
[2] L. Suhadolnik, M. Krivec, K. Žagar, G. Dražić, M. Čeh, Journal of Industrial and Engineering Chemistry 47 (2017) 384–390
[3] L. Suhadolnik, A. Pohar, B. Likozar, M. Čeh, Chemical Engineering Journal 303 (2016) 292–301
[4] L. Suhadolnika, D. Lašič Jurković, B. Likozar, M. Bele, S. Drev, M. Čeh, Applied Catalysis B: Environmental, Volume 257, 15 November 2019, 117894
[5] L. Suhadolnik, A. Pohar, U. Novak, B. Likozar, A. Mihelič, M. Čeh, Journal of Industrial and Engineering Chemistry 72 (2019) 178–188

3D-Printed Scintillators with Inorganic Powders for X-Ray Imaging

T. Sibilieva[1], A. Boyarintsev[1], B. Grinyov[1], A. Krech[1], T. Nepokupnaya[1], I. Nevliudov[2] and I. Razumov-Fryziuk[2]

[1]The Institute for Scintillation Materials of National Academy of Sciences of Ukraine, 60 Nauky Ave., 61072, Kharkov, Ukraine
[2]Kharkiv National University of Radio Electronics, 14 Nauky Ave., 61166, Kharkiv, Ukraine

This work is devoted to the development of 3D-printed scintillators with inorganic powders for X-ray imaging. The development of 3D printing of inorganic scintillation layers will allow mobile creation of thin layer detectors for registration of soft x-ray radiation.

Scintillation filaments with 50-75%wt inorganic powders of ZnSe:Al, GOS:Pr, GaGG:Ce and CsI:Tl were made using PMMA plastics as binder medium. The size of grains was 1-15 μm.

Composite scintillation films were printed using developed filaments on a 3d-printer CreateBot F-430. The thickness of the samples was from 0.10 mm to 0.30 mm. The area of the films was 100x45 mm.

The best results for 3D-printed samples were obtained with a thickness of 0.15 mm, 1-15 μm grains size and 60%wt content of inorganic powders. Spatial resolution for these 3d-printed composite films base on ZnSe:Al, GOS:Pr, GaGG:Ce or CsI:Tl powders were form 3.15 lp/mm and to 3.35 lp/mm. Obtained results are in good correlation with the data for industrial samples.

The developed scintillation films for X-ray imaging are effective for registration of soft X-ray radiation (20 - 90 keV). It is also possible to print composite scintillators simultaneously with a reflector and an absorber, which opens up new possibilities for use.

Guest-Tuned Spin Crossover in Metal-Organic Frameworks

Yu. Klysko and S. Syrotyuk

Department of Semiconductor Electronics, Lviv Polytechnic National University, S. Bandera str., 12, Lviv 79013, Ukraine

The MOF-74 is a group of porous coordination polymers containing divalent metals and 2,5-dihydroxybenzene-1,4-dicarboxylate. The structure of the metal-organic frameworks (MOF) is characterized by infinite M-O chains in hexagons vertices. These columns are connected by organic linkers creating 1d pores with a radius around 12 Å. The unit cell contains 54 atoms and is described by space group R-3 [148], and the Bravais lattice is rhombohedral (hR).

Previous study says that MOF-74 has ferromagnetic (FM) short-range (across a metal-oxide chain) and antiferromagnetic (AFM) long-range ordering (antiparallel alignment of the chains) [1].

We have carried out the self-consistent calculation of electronic and magnetic properties for Fe-MOF-74 with small molecule organic (ethylene, acetylene, ethanol, acetic acid etc) and inorganic (carbon mono- and dioxide, chlorine, bromine etc) impuruies. Both FM and AFM states have been considered. The AFM configuration describes antiparallel alignment of neighbour chains, and the corresponding space group is rhombohedral, R-3 [148], with magnetic group (-3)′ containing six elements.

We have performed the ground state calculation within GGA-PBE, implemented in ABINIT [1] code, using projector augmented wave (PAW) basis [2]. Then Wannier functions and Hamiltonian have been extracted in order to evaluate exchange parameters, using Green's function approach, implemented in the TB2J code. The temperature dependence of the magnetic moment and susceptibility have been obtained using the MULTIBINIT code implemented in the ABINIT package.

[1] P.D.C. Dietzel, Y. Morita, R. Blom, H. Fjellvåg. Angew. Chem. Int. Ed. 2005, 44, 6354.
[2] X. Gonze et al. Comput. Phys. Commun. 2016, 205, 106.
[3] P. E. Blöchl, Phys. Rev. B. 1994, 50, 17953.
[4] Xu. He, N. Helbig, M. J.Verstraete, E. Bousquet. Comput. Phys. Commun. 2012, 264, 107938.

Sensitive Elements of Gas Sensors Based on Poly-*o*-Toluidine/Silica Nanoparticles Composite

Yu. Horbenko[1], B. Tsizh[2,3], M. Dzeryn[2], I. Olenych[1], O. Aksimentyeva[1] and V. Bogatyrev[4]

[1]*Ivan Franko National University of Lviv, Lviv, Ukraine;*
[2]*Stepan Gzytsky Lviv National University of Veterinary Medicine and Biotechnologies,Lviv, Ukraine;*
[3]*Kazimierz Wielki University in Bydgoszcz, Bydgoszcz, 85-064, Poland;*
[4]*O. O. Chuiko Institute of Surface Chemistry NAS of Ukraine, Kyiv, Ukraine*

Conducting polymers have received considerable interest attributed to their unique electrical, chemical, and physical properties, reasonable price, simple preparation, small dimensions and large surface area. Thus, they have been broadly researched for applying in supercapacitors, solar cells, batteries, biochemical applications, electrochromic devices and sensors [1]. Using conductive polymers as sensitive material in sensors production provides numerous advantages such as high sensitivity, short response time, room temperature operation, and the possibility of tuning both chemical and physical properties by using different substituents [2]. Combining conducting polymers with other components especially nanomaterials such as inorganic oxides, due to the synergistic effects, can improve some characteristics like high electrical conductivity and large surface area. Poly-*o*-toluidine (PoT) is one of the most promising conducting polymers. It is known humidity sensing by PoT/TiO_2 nanocomposite films [3]. Moreover, the authors reported earlier that the introduction of modified silica nanoparticles helps stabilize the resistivity of polyaniline nanocomposites in high humidity and enhance their sensitivity to hydrogen chloride vapors [4]. In both these cases in situ chemical oxidation polymerization was used, but electrochemical approach to prepare new polymer composites can easily control the conductivity, compound state, morphology, and thickness of its.

So, in this research, the thin films of conducting polymer composites of PoT with incorporated silica nanoparticles were electrochemically deposited on optical transparent substrates, covered with semiconductor SnO_2 layer under cyclic voltammetric conditions. It has been used modified with phosphorus (III) chloride nanoparticles of SiO_2, grade P-2.1, developed at the O. O. Chuiko Institute of Surface Chemistry NAS of Ukraine.

The influence of gas vapours (HCl, H_2S, NH_3) on the PoT/ P-2.1 absorption spectra was studied. It has been found, that only ammonia molecules cause appearance of two additional peaks of optical absorption – at 450 and 600 nm, thus polymer composite can be used as sensitive elements of optical sensors for selective detection of NH_3. In addition, it has been established that specific surface resistance of obtained PoT/P-2.1 thin films significantly increases under the action of H_2S and NH_3 gases – in 2 and 26 times respectively. Based on the obtained data, the possibility of using electrodeposited thin films of poly-o-toluidine/modified silica nanocomposite in gas sensors production, both optical and resistive, for monitoring the state of environments in real conditions of atmosphere, is shown.

[1] S. A. Alqarni,, M. A. Hussein, et al, *BioNanoSci.* (2020) doi:10.1007/s12668-019-00708-x.
[2] Y. Wang, A. Liu, *Polym. Int*. 69 (2020) doi: 10.1002/pi.5907.
[3] T. Zhou, X. Xie, et al, *Polym. Bull. 73* (2015) doi:10.1007/s00289-015-1509-y.
[4] Yu. Yu. Horbenko, B. R. Tsizh, O. I. Aksimentyeva, I. B. Olenych, V. M. Bogatyrev, M. R. Dzeryn, *Scientific Messenger LNUVMB. Series: Food Technologies*. 21 (2019) doi: 10.32718/nvlvet-f9106.

Cr-Doped Solid Solutions $La(Ga_{1-x}Al_x)O_3$ and $(La_{1-x}Sr_x)(Al_{1-x}Ti_x)O_3$ for Possible Luminescence Temperature Sensor Application

V. Hreb[1], I. Lutsyuk[1], K. Blazhivskyi[1], Ya. Zhydachevskyy[1,2], V.B. Mykhaylyk[3] and L. Vasylechko[1]

[1]*Lviv Polytechnic National University, Bandera 12, 79013, Lviv, Ukraine*
[2] *Institute of Physics of the PAS, Al. Lotników, 32/46, Warsaw, 02-668, Poland*
[3]*Diamond Light Source, Harwell Campus, Didcot, OX11 0DE, UK*

The strategy of exploiting the wide tenability of the phase transition temperature of oxide perovskites to design a new class of non-contact cryogenic luminescent sensor of thermometer with intrinsic temperature reference for calibration and verification of reliability are carefully studied. Based on the results of previous studies, there are strong indications that the most likely class of materials with good temperature sensitivity and phase transition in the temperature range of interest are oxide perovskites. A great advantage represented by the perovskite structure is the possibility to tune the phase transition temperature by using the cation substitution. Furthermore, Cr-doped $YAlO_3$ has recently been tested for the luminescence sensing of temperature [1] and this finding prompted studies of other materials of this family that fits exceptionally well the overall concept. To verify the possibility to finely control the phase transition temperature in the Cr-doped perovskites, we selected two promising systems based on rare-earth (RE) aluminates, gallates and titanates which undergo different types of structural phase transitions below room temperature, namely $La(Ga_{1-x}Al_x)O_3$ and $(La_{1-x}Sr_x)(Al_{1-x}Ti_x)O_3$. According to our own results and the literature data [2 and refs. herein], the first-order structural phase transition $R\bar{3}c \leftrightarrow Pbnm$ is predicted below RT in the mixed aluminate-gallate system $La(Ga_{1-x}Al_x)O_3$ at certain compositions between x=0.07 and 0.25. Other kind of LT structural transitions is antiferroelastic phase transition from the cubic *Pm*3*m* to tetragonal *I*4/*mcm* structure occurring in $SrTiO_3$ at T=105 K. The change of local symmetry of octahedral sites and configuration of hosting BO_6 (*B*=Al/Ga/Ti) octahedra occurred at the phase transitions will influence the crystal field parameters and characteristics of Cr^{3+} emission.

In order to prove this conception, two series of nano- and microcrystalline powders of solid solutions $La(Ga_{1-x}Al_x)O_3$ (x = 0.15, 0.19) and $(La_{1-x}Sr_x)(Al_{1-x}Ti_x)O_3$ (x = 0.1, 0.2, 0.3, 0.4, 0.5, 0.6) doped with Cr^{3+} ions were obtained by arbitrage methods of sol gel synthesis and solid state reaction technique. Impact of cation substitution in these mixed oxide perovskite systems on the structure and temperature of phase transitions, as well as on the luminescence characteristics of the materials has been studied and their potential as candidates for practical application is discussed.

Acknowledgment: The work was supported by the National Research Foundation of Ukraine (grant no. 2020.02/0373) and by the Polish National Science Centre (project no. 2018/31/B/ST8/00774).

[1] V.Mykhaylyk, H. Kraus, Y. Zhydachevskyy, V. Tsiumra, A. Luchechko, A. Wagner, A. Suchocki. Multimodal non-contact luminescence thermometry with Cr-doped oxides. Sensors 20 (2020) 5259.
[2] L. Vasylechko, A. Senyshyn, and U. Bismayer, Perovskite-Type Aluminates and Gallates. In K.A. Gschneidner, Jr., J.-C.G. Bünzli and V.K. Pecharsky, editors: *Handbook on the Physics and Chemistry of Rare Earths*, Vol. 39, Netherlands: North-Holland, 2009, pp. 113-295.

Effect of Mechanochemical and Microwave Modification of SnO_2 Nanomaterials on Properties of Hydrogen Sensors

I. Matushko[1], S. Khalameida[2], M. Samsonenko[2], V. Sydorchuk[2], L. Oleksenko[1], N. Maksymovych[1] and O. Khyzhun[3]

[1]*Taras Shevchenko National University of Kyiv, Department of Chemistry*
[2]*Institute for Sorption and Problems of Endoecology, NAS of Ukraine*
[3]*I.M.Frantsevich Institute for Problems of Materials Science, NAS of Ukraine*

Nowdays tin dioxide is one of the most perspective materials to create adsorption semiconductor gas sensors purposed to control air ambient. Morphology and structure-adsorption properties of the semiconductor materials using for the sensor creation greatly effect on the gas sensitive properties of the sensors. Since high temperature calcination is a necessary stage for fabrication of the sensors based on SnO_2 it can lead to enlargement of the particles of the sensor material, a decrease in its specific surface, a change in porous structure of the material, and, consequently, to a degradation in the parameters of the sensors created on their base, its surface morphology and can influence on the sensor properties. It is known [1] that modification of oxides under hydrothermal conditions allows to create larger-porous and more uniform structure that does not sinter to high temperatures, while maintaining a sufficiently high specific surface area and lesser crystallite size.

We subjected precipitated SnO_2 to mechanochemical and microwave treatments in aqueous medium (MChT and MWT, respectively) i.e. under hydrothermal conditions. Indeed, preliminary MChT and MWT of SnO_2 material contribute to noticeable increase in the specific surface area for annealed at 450°C samples: from 44 m^2/g for initial sample without any treatment to 60 and 84 m^2/g for modified samples, respectively. The obtained specific surface area gain is due to the fact that the modified samples have a larger mesopore size as well as contain macropores and therefore sinter to a lesser extent during annealing. Besides, the size of the crystallites determined using XRD and TEM data decreases from 15 nm for the initial sample to 7-10 nm for the samples after mechanochemical and microwave treatments.

The aim of the work is to study the effect of MChT and MWT of the material of the gas sensitive layer on the base of SnO_2 of adsorption-semiconductor sensors on their sensitivities to hydrogen.

The sensor of size 2x2x0.3 mm consisted of a ceramic plate with a heater on one side of the plate and measuring contacts on the opposite side of the plate. A sensitive layer of the semiconductor nanomaterial obtained after the MChT and MWT of SnO_2 was placed between the contacts. Then the obtained nonmodified sensors were calcinated at high temperature (up to 620 ^{0}C) in air. Cobalt oxide, a well-known catalyst of hydrogen oxidation, was also introduced into these layers by the impregnation method before the sensor high temperature treatment.

It was found that introduction of cobalt additives to the sensor nanomaterial increases the sensor response to 40 ppm of hydrogen. The Co-containing sensor with gas sensitive layer made with semiconductor material after the microwave treatment had the greater sensor response to hydrogen than the sensor with the material after the treatment in the aqueous medium mechanochemical treatment only. The obtained results are consistent with data of the larger specific surface area of the material after the microwave treatment (84 m^2/g) than mechanochemical one (60 m^2/g).

[1] J. Skubiszewska-Zieba, S. Khalameida, V. Sydorchuk.. Colloid Surf A Physicochem Eng Asp 2016 (504) 139-153.

Modification of Zn-Al Hydrotalcite as Potential Photocatalyst

V. Sydorchuk, S. Levytska, L. Kotynska and L. Kuznetsova

Institute for Sorption and Problems of Endoecology, NAS of Ukraine

The layered double hydroxides (LDHs), particularly hydrotalcites, are versatile materials used including the solution of environmental problems, for example as photocatalysts. There are two variants of their use: as pristine LDHs or as mixed oxide compositions after calcinations of LDHs. In both cases, materials must have certain properties in order to be effective photocatalysts: first of all, an optimal porous and crystalline structure, electronic characteristics. We applied the hydrothermal and mechanochemical treatments (HTT and MChT, respectively) of Zn/Al hydroxide to regulate these parameters both for the as-prepared sample and for the oxide composition obtained by calcining it. Zn/Al hydroxide with Zn/Al ratio 3 of composition $Zn_6Al_2(OH)_{16}CO_3 \cdot 4H_2O$ was prepared by precipitation at pH 8 and subjected to HTT and MChT in the form of wet gel and dried xerogel. Such approach has not previously been used to modification of Zn/Al hydroxide although was effective for other oxides. Then modified samples were calcined at 500-800°C for preparation of mixed oxides.

According to XRD data, as-precipitated sample has hydrotalcite structure with basal spacing 0.865 nm (in literature – 0.895 nm) which is also confirmed by DTA-TG and FTIR results. MChT in air partially destroys hydrotalcite structure without formation of other phases while milling in water only modifies it. Thus, position of reflex from (003) plane is shifted from 2Θ =10.23° to 2Θ =11.27° which is corresponds to a decrease in basal spacing to 0.786 nm. The latter is accompanied by development of porous structure, obviously, due to formation of additional mesoporosity: the specific surface area increases by 3 times, reaching 106 m^2/g, and the pore volume is almost 4 times (to 0.27 cm^3/g).

On the contrary, elevation in HTT temperature leads to decomposition of hydrotalcite: if its structure is improved at a temperature of 150°C, then it is partially destroyed at 200°C, and zinc oxide is formed at 250°C. Samples hydrothermally modified in the form wet gel have high value of mesopores – about 0.70-0.75 cm^3/g and specific surface area 50-67 m^2/g.

The changes in phase composition and crystal structure, which are observed due to MChT and MWT, are accompanied by changing the electronic characteristics determined from UV-Vis spectra. Thus, all modified samples are characterized by stronger absorption in the visible region compared to initial sample. Besides, significant hypsochromic shift occurs for samples subjected to HTT. As a result, the narrowing of band gap E_g is observed: from 3.2 eV (initial sample) to 2.8-2.9 eV (hydrothermally treated samples). Both these effects should enhance the photocatalytic activity of modified samples under visible irradiation. Indeed, initial sample is practically non-active in process of photocatalytic degradation of safranin T (as model substrate) in aqueous medium under these conditions. At the same time, sample subjected to dry milling at 300 rpm which has the bang gap 3.1 eV becomes active: rate constant of degradation $K_d = 1.8\ 10^{-5}\ s^{-1}$. The sample, modified by HTT in the form of gel at 200°C, possesses the maximal activity ($K_d = 3.4\ 10^{-5}\ s^{-1}$) since it simultaneously has E_g = 2.9 eV and high value of specific surface area - 67 m^2/g.

Therefore, mechanochemical and hydrothermal treatments allow to vary the physical-chemical characteristics of hydrotalcite. In particular, the samples, which are oxide-hydroxide compositions, were prepared by HTT of gel at low temperature. These compositions absorb visible light and possess photocatalytic activity under these conditions.

Sorption of Lead on Na-Modified Transcarpathian Clinoptilolite

V.O. Vasylechko[1,2], G.V. Gryshchouk[1], Ya.M. Kalychak[1], R.E. Gladyshevskii[1], I.P. Navrotska[1] and S.R. Bagday[1]

[1]*Faculty of Chemistry, Ivan Franko National University of Lviv, Kyryla and Mefodiya St. 6, 79005 Lviv, Ukraine*
[2]*Department of Natural Sciences and Environment Protection, Lviv University of Trade and Economics, Samchouk St. 9, 79011 Lviv, Ukraine*

Lead is a broad-spectrum toxicant. As the permitted Pb concentration is very low, during the analysis of samples, even with the application of state-of-the-art methods, there is a need for preliminary preconcentration, removal and/or separation of Pb trace amounts. The purification of waters and soils from this toxic element, and the regeneration of Pb from technological waste solutions, need to be considered. The solution to this problem is mainly connected with the use of efficient sorbents of Pb, in particular natural zeolites. The main characteristics of these natural oxide nanomaterials are resistance to aggressive environments, high sorption capacity and selectivity, ability to sorb trace amounts of substances, availability and low cost, possibility of regeneration and modification. Usually the Na-form of a zeolite exhibits higher sorption capacity towards heavy metals than its natural form.

The sorption properties of Na-modified Transcarpathian clinoptilolite towards trace amounts of Pb(II) were investigated by solid-phase extraction under dynamic conditions. The maximum sorption capacity of Na-clinoptilolite was observed in neutral solutions of Pb(II) (pH 7.0). Trace amounts of Pb(II) in such solutions are mainly present in the unhydrolized cationic form Pb^{2+} (~90 %), and partly as the cationic hydroxocomplex $PbOH^{+}$ (~10 %). This gives information about the ion-exchange mechanism of Pb(II) sorption on Na-clinoptilolite. The sorption capacity of the Na-clinoptilolite decreases significantly with increasing concentration of Pb(II) in the solution. This is probably caused by the decrease of the amount of Pb^{2+} and $PbOH^{+}$ and the simultaneous increase of polynuclear cation hydroxocomplexes with increasing Pb(II) concentration.

The sorption properties of Na-clinoptilolite depend on the preliminary thermal treatment, but the maximal sorption capacity was exhibited by uncalcined samples of the sorbent. An increase of the temperature of the preliminary thermal treatment of Na-clinoptilolite to 120 °C caused a significant decrease of the sorption capacity. At this temperature the elimination (evaporation) of water, present as a wet surface layer, took place in Transcarpathian clinoptilolite, which, probably, caused a decrease of the sorption efficiency of the samples towards cationic forms of Pb(II). Under optimal conditions, the maximum sorption capacity of Na-clinoptilolite towards Pb(II) reached 56 mg/g, which is 5.2 times higher than the corresponding sorption capacity of the natural form of this zeolite [1]. The best desorbents of Pb(II) from Na-clinoptilolite are 0.5 M NaCl, 0.5 M KCl and 2.5 M HNO_3. These desorbents remove 95–100 % of sorbed Pb(II). It was established that a (500–3000)-fold excess of main water components does not influence the maximum sorption capacity of Na-clinoptilolite towards Pb(II).

A preconcentration method of Pb(II) in nanogram amounts in the solid-phase extraction mode during atomic absorption analysis of natural waters has been proposed.

[1] Vasylechko V., Gryshchouk G., Neroda I. Adsorption of Pb(II) on Transcarpathian clinoptilolite // Visnyk Lviv. Univ. Ser. Khim. – 2009. – N 50. – P. 177-187.

Oxide-Hydroxide Layers on the Surface of Al-Gd-Ni(Fe) Amorphous Alloy Ribbons and Their Capacitive Properties

Khrystyna Khrushchyk, Lidiya Boichyshyn

Faculty of Chemistry, Ivan Franko National University of Lviv
khrushchyk.chem@gmail.com

Recently, amorphous metal alloys (AMA) are of interest as functional materials with great potential for application due to their physicochemical characteristics, such as high ability to thermoplastic formation, high oxidation rate, corrosion and electrochemical properties. One of the main advantages of AMA is its low viscosity in the area of super cooled liquid. Therefore, AMA can be used as a thermoplastic material or binder for various purposes [1]. For example, in [1] it was reported that amorphous Al-based alloys are promising materials for the formation of electrodes with high conductivity in silicon solar cells. It should be noted that the conductivity of electrodes with AMA based on aluminum depends on the structural state of the oxide layers that are formed on the surface due to contact with the environment or heating. The formation of the oxide layer affects the physicochemical properties of amorphous alloys, such as adhesion, microhardness, ductility and electrical conductivity before and after crystallization. Accordingly, a heat-resistant amorphous oxide is formed on the surface of amorphous aluminum alloys, which has a decisive influence on the oxidative stability of the amorphous alloy at high temperatures. The authors [1] report that during the annealing of the amorphous alloy $Al_{87}Ni_3Y_{10}$ a layer of amorphous oxide 100 nm thick is formed, and on the surface of pure crystalline aluminum [2] the thickness of the amorphous oxide layer is 4 nm. The presence of yttrium in the amorphous oxide layer inhibits the diffusion of oxygen ions. Therefore, a slight doping in the oxide layer can significantly affect the heat resistance of the amorphous oxide layer. From this point of view, it is necessary to study the effect of alloying elements in the amorphous Al-Gd-Ni(Fe) system on the formation of oxide layers. The results of the research showed that oxide-hydroxide layers are formed on the surface of AMA $Al_{87}Gd_5Ni_4Fe_4$ and $Al_{87}Y_1Gd_4Ni_4Fe_4$, which were examined by scanning electron microscopy (Tescan Vega 3 LMU) and electrochemical impedance spectroscopy (Auto Lab). Oxide layers are formed on the surface of AMA due to annealing at temperatures of 645 K and 647 K for 15, 30, 45, 60 minutes. It is shown that the doping of Gd and Fe leads to the formation of dense non-defective oxide layers. According to the results of electrochemical impedance spectroscopy, the electrical circuit of the interphase AMA / oxide / 0.3% NaCl solution was modeled. The resistance of charge transfer across the phase boundary was determined, as well as the thickness of the oxide-hydroxide layers formed in the aqueous solution. The type of treatment (electrochemical oxidation, annealing) affects the capacitive characteristics of the AMA / oxide system, the number and nature of charge carriers from hole to electronic.

[1] K.C. Kim, K.R. Lim, E.S. Lee, W.T. Kim, A. Gebert, J. Eckert, D.H. Kim, Thermal stability of amorphous oxide in $Al_{87}Ni_3Y_{10}$ metallic glass, Corros. Sci. 77 (2013) 1–5.

[2] F. Reichel, L.P.H. Jeurgens, G. Richter, E.J. Mittemeijer, Amorphous versus crystalline state for ultrathin Al_2O_3 overgrowths on Al substrates, J. Appl. Phys. 103 (2008).

Electrical Properties of Lithium-Sodium Tetragermanate Single Crystal

A.O. Diachenko, M.P. Trubitsyn, M. Volnianskii and D.V. Volynets

Laboratory of Active Dielectric Crystals, Oles Honchar Dnipro National University, prosp. Gagarina 72, Dnipro, 49010, Ukraine

Lithium-sodium tetragermanate $LiNaGe_4O_9$ (LNG) belongs to a family of germano-germanate crystals. By now, some information has been accumulated about structural, elastic and dielectric properties of LNG crystals. A special attention was paid to physical anomalies accompanying phase transition to ferroelectric phase, while peculiarities of LNG electric properties have not been investigated in details. In the abstract we report the results of studying temperature-frequency dependencies of permittivity ε and conductivity σ. The data obtained for LNG single crystals are compared with the results measured for LNG glass. Influence of long- and short-range ordering on ionic transport is discussed.

LNG single crystals were grown from the melts by Czhochralskii method. LNG glasses were prepared by quenching the melts [1]. The samples were coated by silver electrodes. Electrical properties were measured in AC field in the interval 300 ÷ 800 K, frequency was varied in the range 20 Hz ÷ 2 MHz. The measurements were performed by using bridges E7-10 and Tesla BM-507.

It was observed that ε of LNG single crystal showed broad step- like anomalies for all three crystallographic directions and most significant increase of ε was detected along [001] axis. The observed anomalies were typical for thermal dipole polarization processes. Above 450 K σ of LNG single crystal became strongly anisotropic. Conductivity was maximal along [001] axis and exceeded conductivity along [100] and [010] axes in approximately 30 times. In the interval 500÷600 K the experimental data σ(1/T) along [100] and [010] axes deviated from the straight line that together with the step- like anomalies of ε(T) could be attributed to dipole relaxation processes. It was assumed that along [001] such deviation was not visible owing to high temperature increase of σ which masked contribution of dipole relaxation. It was shown that conductivity in glassy LNG was higher in a few orders in comparison with σ of a single crystal. The results obtained were discussed on the basis of the features of LNG structure.

The crystal structure of LNG is formed by Ge-O octahedral and tetrahedral groups linked by polyhedral vertexes and edges. Light Li and Na ions occupy the positions within channels formed by Ge-O framework and are mobile enough to move in an external electric field. In the [100] direction, there are zig-zag channels containing Na sites. In the [010] direction there are two types of the channels, one of which containes Li sites and another one – regular Na sites. In the [001] direction there are the channels with Li sites. The highest contribution to conductivity was attributed to mobile Li ions moving through the structural channels along [001] axis. Relatively slow Li motion along [010] axis could result from significant attraction with oxygen anions which formed the walls of the more broad structural channels. Accounting the structural features, Na ions transport was assumed as negligible.

[1] Volnyanskii M., Nesterov O., Trubitsyn M. Devitrification of the Li_2O – $x(GeO_2)$ glass. - Ferroelectrics.- 2014.- V.466, No. 1. – P.126-130.

SECTION 5

MATERIALS FOR QUANTUM AND OPTO-ELECTRONICS AND DETECTORS OF RADIATION

Development of Advanced Composite Scintillators and LED Converters Based on the Epitaxial Structures of Garnet Compounds

V. Gorbenko[1], A. Markovskyi[1], Y. Syrotych[1], S. Witkiewicz-Lukaszek[1], T. Zorenko[1], J.A. Mares[2], M. Nikl[2], O. Sidletskiy[3], S. Nizhankovskiy[4], K. Kamada[5], A. Yoshikawa[6] and Yu. Zorenko[1*]

[1]*Institute of Physics, UKW in Bydgoszcz, Powstańców Wielkopolskich str., 2, 85-090 Bydgoszcz, Poland*
[2]*Institute of Physics, AS Czech Republic, Cukrovarnicka str., 10, 16253 Prague, Czech Republic*
[3]*Institute for Scintillation Materials, NAS of Ukraine, av. Nauky, 60, 61001 Kharkiv, Ukraine*
[3]*Institute for Single Crystals, NAS of Ukraine, Ukraine*
[4]*Institute for Materials Research, Tohoku University, 2-1-1 Katahira, Aoba-ku, Sendai 980-8577, Japan*

This report presents the review of our last results in the development of multilayered composite luminescent materials based on the single crystalline films (SCFs) and single crystals (SCs) of garnet compounds using the liquid-phase epitaxy (LPE) growth method for application in the environment radiation monitoring, microimaging technique and industrial lighting.

The main task of our research is connected with the creation of ***multilayered*** **composite scintillators** of phoswich-type (phosphor sandwich) based on SCFs and SCs of garnet compounds for simultaneous registration of different types of ionizing radiations (particles and quanta) in mixed ionization fluxes [1-4]. Such composite scintillators present the *three-layer epitaxial structures containing* two SCF scintillators grown „step-by-step" using the LPE method onto substrates from SC scintillators. Films and crystal parts of composite scintillators were fabricated from "the best as possible" effective scintillation materials on the basis of Ce^{3+}, Pr^{3+} and Sc^{3+} doped $Lu_3Al_5O_{12}$ garnets [1, 2] (case of homoepitaxial growth) and the Ce^{3+} doped $R_3B_5O_{12}$ (R=Lu, Gd, Tb; B=Al, Ga) mixed garnets (case of heteroepitaxial growth) [3, 4] with various scintillation decay kinetics due to the different types of dopants [1, 2] and various garnet content [3, 4].

The report presents also last results on fabrication of LuAG:Ce SCF/LuAG:Pr SCF/ LuAG:Sc SC, YAG:Ce SCF/TbAG:Ce SCF/$Gd_3Al_{2.5-2.3}Ga_{2.3-2.7}O_{12}$:Ce SC and TbAG:Ce SCF/ $Gd_3Al_{3-2.5}Ga_{2-2.5}O_{12}$:Ce SCF/ $Gd_3Al_2Ga_3O_{12}$:Ce SC composite scintillators using LPE method as well as the results of investigation of their luminescent and scintillation properties. The testing of the mentioned prototypes of tree layered composite scintillators for simultaneous registration of α- and β-particles and γ-quanta was performed and the obtained results were analysed for the optimization of their scintillation figure-of merit.

The report presents also the review of the results in the development of two-layered composite converters for WLED based on the SCFs of (Gd, Lu,Tb) Al_5O_{12}:Ce garnets, grown by the LPE method onto YAG:Ce SC substrates [5, 6]. The results of investigation of structural, luminescent and photoconversion properties (color coordinates, color rendering index, luminous efficacy) of different composite converters based on the mentioned SCFs and SCs were presented.

Acknowledgements: The work was performed in the framework of Polish NCN 2018/31/B/ST8/03390 and 2017/25/B/ST8/02932 projects and Polish PNAAE PPN/ULM/2020/1/00298 project as well as partially supported from the Operational Programme Research, Development and Education financed by European Structural and Investment Funds and the Czech Ministry of Education, Youth and Sports (Project No. SOLID21 CZ.02.1.01/0.0/0.0/16_019/ 0000760) and Czech Science Foundation project 21-17731S.

[1] S. Witkiewicz-Lukaszek, V. Gorbenko, T. Zorenko and others, IEEE TNS, 65 (2018,) 2114-2119.
[2] S. Witkiewicz-Lukaszek, V. Gorbenko, T. Zorenko and others, Optical Materials, 2018 (84) 593-599.
[3] J.A. Mares, S. Witkiewicz-Lukaszek, V. Gorbenko and others. Optical Materials, 96 , (2019), 109268.
[3] S. Witkiewicz-Lukaszek, V. Gorbenko, T. Zorenko and others, Crystal Growth & Design 18 (2018) 842.
[4] S. Witkiewicz-Lukaszek, V. Gorbenko, T. Zorenko and others, CrystEngComm, 2018, 20**,** 3994-4002.
[5] A. Markovskyi, V. Gorbenko, T. Zorenko, Y. Zorenko and others, CrystEngComm, 23 (2021) 3212.,
[6] A. Markovskyi, V. Gorbenko, T. Zorenko and others, pss RRL, 2021, https://doi.org/10.1002/pssr.202100173.

Oxide Composite Scintillation Materials for High-Energy Radiation Detectors

N. Galunov[1,2], Ya. Gerasimov[1], N. Karavaeva[1], A. Krech[1], T. Gorbacheva[1], I. Khromiuk[1], D. Kofanov[1], L. Levchuk[3] and V. Popov[3]

[1]*Institute for Scintillation Materials, National Academy of Sciences of Ukraine, 60 Nauky Ave., 61072, Kharkiv, Ukraine*
[2]*V.N. Karasin Kharkiv National University, 4 Svobody Sq., 61022, Kharkiv, Ukraine*
[3]*National Science Center ''Kharkiv Institute of Physics and Technology'', 1 Akademichna Str., 61108, Kharkiv, Ukraine*

A large number of experiments carried out at charged particle accelerators indicate that the radiation dose accumulated by the detectors and, in particular, by the scintillation materials contained in them, is significant. For example, in experiments at the Large Hadron Collider (LHC), the radiation dose for scintillation detectors can reach 10 Mrad and will increase in the future. In this connection, the search for new radiation-resistant scintillation materials is especially important.

Irradiation can significantly alter the characteristics of the scintillator material. The aim of this work was to study the features of possible radiation damage and transformations in composite scintillators under the action of ionizing radiation. Composite scintillators, which are transparent non-luminescent gel-compositions containing grains of scintillation oxide single crystals, have been investigated. A comparative analysis of the spectra of the relative light yield, transmission, and luminescence, as well as their dependence on the accumulated dose for various composite scintillators, has been carried out. Possible mechanisms of radiation changes occurring in scintillators under irradiation are proposed, and the influence of these processes on the radiation resistance of composite scintillators is analyzed.

In our previous works, we investigated composite scintillators based on a transparent gel composition containing single crystal grains of inorganic oxide crystals (GSO: Ce, GPS: Ce, Al2O3: Ti, YSO: Ce, and YAG: Ce). The gel composition was not only a binding material for scintillation grains. It was both a light-collecting medium in which a total scintillation signal from various grains was forming as well as a coating that protected scintillation grains from the effects of chemically active components of the atmosphere. At large cumulative doses of D, we observed a previously undescribed effect of scintillator cracking.

In this work, as in previous works in this series, we irradiated composite scintillators on a linear electron accelerator. The electron energy was 10 MeV. We irradiated for a low (0.2 Mrad/h) and a high dose rate (1500 Mrad/h). At the low dose rate, cracking occurs at lower D values (about 100–200 Mrad) than under irradiation with the high dose rate (up to 500 Mrad). The luminescent characteristics of the scintillator changed insignificantly until the gel composition fixing single-crystal grains cracked. After the destruction of the gel composition, an abrupt deterioration in the properties of the sample was occurring. Additional studies have allowed us to show that nitrogen compounds, including nitric acid, can appear in the irradiation zone under the influence of radiation. The scintillator in the irradiation zone can either begin to expand under the influence of heating or (and) to crack when exposed to aggressive atmospheric components. The analysis we carried out in the work proves that, at the low dose rate, nitrogen-containing compounds forming in the irradiation zone have a decisive influence on the effect of scintillator cracking. At the high dose rates, the main effect that leads to the cracking of scintillators is their heating, occurring under the influence of radiation.

Thermal Annealing of Point Defects in Irradiated Functional Ceramics for Nuclear Applications

A.I. Popov[1,*], E.A. Kotomin[1], V.N. Kuzovkov[1] and A. Lushchik[2]

[1]*Institute of Solid State Physics, University of Latvia, 8 Kengaraga, Riga, LV-1063 Latvia*
[2]*Institute of Physics, University of Tartu, W. Ostwald Str. 1, 50411 Tartu, Estonia*
[*]*Corresponding author (popov@latnet.lv)*

Radiation-resistant oxide insulators (MgO, BeO, Al_2O3, $MgAl_2O_4$, etc.) are important materials for use in fusion reactors. It is very important to predict / model not only the kinetics of diffusion-controlled accumulation of defects under neutron irradiation, but also the long-term evolution of the defect structure, including thermal annealing of defects after irradiation.

After introducing some basics on the radiation point defects in halides, binary oxides and oxide perovskites [1] as well as the mechanisms of point defect and metal colloid formation in additive/thermochemically reduced samples or under fast energetic particle irradiation (neutron, ion, proton, electron), *we will review the current understanding of their thermal annealing.*

We will shortly describe recently developed and successfully applied [2-4] theoretical approach based on the formalism of the correlation functions, describing spatial distribution of both similar (F-F centers) and dissimilar defects (Frenkel pair of defects: F center – an interstitial Oi ion) which allows us to study defect kinetics and aggregation much better than generally accepted rate equations or simple first order kinetics. Thus, the kinetics of the F-type center thermal annealing after electron, heavy ions or neutron irradiation was treated as the bimolecular process with equal concentrations of the complementary F and Oi defects. It is controlled by the interstitial oxygen ion mobility, which is much higher than that of the F centers. It is demonstrated how the shape of the F-annealing curves is determined by the two control parameters: migration energy Ea and effective pre-exponential factor, and strongly depends on irradiation fluence and other conditions.

The appropriate migration energies were obtained from available in literature annealing kinetics for electron, neutron and ion irradiated MgO, Al_2O_3, $MgAl_2O_4$, $Y_3Al_5O_{12}$, BeO, ZnO, YSZ, PLZT etc. The results obtained are used for evaluation of the interstitial oxygen migration parameters and compared with available ab initio calculations. Comparison with another type of experiments, such as F-type center annealing in TCR samples, will be also given for MgO, BeO and YSZ. This allows us to find the activation energies for the F center migration.

Special attention is paid to:

(1) dose effects on F center annealing in neutron and fast electron irradiated MgO and MgF_2;

(2) a detailed comparison of diffusion-controlled F center thermal annealing in neutron, electron and heavy-ion irradiated MgO, MgF_2, Al_2O_3, BeO, $Y_3Al_5O_{12}$;

(3) thermal transformation and modification of F and F_2 centers during their thermal annealing.

[1] A.I. Popov, E.A. Kotomin, J. Maier, *Nucl. Instr. Meth. B* **268** (2010) 3084.
[2] E.A.Kotomin, V.N. Kuzovkov, A.I. Popov, R. Vila, *Nucl. Instr. Meth. B* **374** (2016) 107.
[3] E.A. Kotomin, V.N.Kuzovkov, A.I. Popov, J.Maier, R.Vila, *J. Phys Chem A* **122** (2018) 28.
[4] V.N. Kuzovkov, E.A. Kotomin, A.I. Popov, *J. Nucl. Mat.* **502** (2018) 295.

The Different Magnetoresistance Mechanisms of $Sr_2FeMoO_{6-\delta}$ Ceramics

G. Suchaneck[1], E. Artiukh[2] and G. Gerlach[1]

[1]*TU Dresden, Solid State Electronics Laboratory, 01062 Dresden, Germany*
[2]*SSPA "Scientific-Practical Materials Research Centre of NAS of Belarus", 220072 Minsk, Belarus*

$Sr_2FeMoO_{6-\delta}$ (SFMO) double perovskite is a promising candidate for room-temperature spintronic applications since it possesses a half-metallic character (with theoretically 100% spin polarization), a high Curie temperature of about 415 K, and a low-field magnetoresistance (LFMR) [1]. A typical synthesis route of SFMO ceramics includes:

- Chemical synthesis, for instance by solid state reaction or sol-gel processes.
- Grinding.
- Cold pressing.
- Long-term annealing at high temperatures in different environment.

Annealing below 900°C does not affect the iron/molybdenum B-site ordering. Here, magnetically distorted grain-boundaries possessing spin-glass properties were obtained. An exchange bias coupling between the core and the surface spins produces a pinned ferromagnetic layer at the interface which 'switches on' the intergranular tunnelling only when a critical magnetic field much larger than the coercive field of the ferromagnetic layer is applied. In result, the magnetoresistance (MR) shows a spin-valve behaviour. The exchange bias decreases gradually with increasing annealing temperature and finally disappears at 900ºC. SFMO ceramics annealed at around 900°C contain significant amounts of antiphase boundaries. An intragrain tunnel MR across the antiphase boundaries starts to dominate. This mechanism decreases with temperature disappearing at around 1500°C. Annealing above 1500ºC practically removes all the antiphase boundaries and only the conventional tunnel MR remains [2].

Thus, from a viewpoint of MR with regard to synthesis conditions, we have to deal not with one, but with very different magnetic materials.

In this work, we analyse the different conductivity and MR mechanisms of SFMO:

- Fluctuation induced tunnelling in low-temperature post-annealed SFMO ceramics [3].
- MR across antiphase boundaries [4].
- Extrinsic low-field MR due to grain boundaries [1].
- Intergranular MR caused by spin-polarized tunnelling [5].
- MR through $SrMoO_4$ tunnelling barriers [6].

We discuss consequences for a controlled SFMO ceramic fabrication and thin film deposition for the purpose of the proper magnetic property design of spintronic devices, first of all, magnetic field sensors and magnetoresistive random access memories.

[1] G. Suchaneck, et al., Phys. Status Solidi B 257 (2019) 1900312.
[2] A. Nag et al., IOP Conf. Ser: Mater. Sci. Eng. 46 (2013) 012001.
[3] G. Suchaneck, E. Artiukh, Phys. Status Solidi B 258 (2021) 2000629.
[4] G. Suchaneck et al. EMRS Spring Meeting 2021, Invited talk, J-III.5
[5] G. Suchaneck, E. Artiukh, Open ceram (2021) (in print).
[6] A. Gaur, G.D. Varma, Mater. Sci. Eng. B 143 (2007) 64-69.

YAG:Ce-Al_2O_3 Eutectics Grown by Horizontal Directed Crystallization as Luminescent Converter of White SSL Driven by High Power Laser Diodes

O.M. Vovk[1], S. Nizhankovskyi[1], P. Dluzewski[2], A. Kozłowska[3] and M. Chaika[4]

[1]*Institute for Single Crystals National Academy of Sciences of Ukraine, Kharkiv, Ukraine*
[2]*Institute of Physics Polish Academy of Sciences, Warsaw, Poland*
[3]*Institute of Electronic Materials Technology, Warsaw, Poland*
[4]*Institute of Low Temperature and Structure Research, Polish Academy of Sciences, Wroclaw, Poland*

Crystalline materials based on YAG:Ce are well adapted for luminescent converter of white solid state lighting (WSSL) driven by power laser blue diodes due to matching most requirements that apply to such convertors. Introduction of the scattering centres with thermal conductivity higher than YAG like Al_2O_3 enhances the convertor characteristics of these materials.

This work is devoted to characterization of YAG:Ce-Al_2O_3 eutectics grown by Horizontal Directed Crystallization (HDC) technique as materials for luminescent convertors for WSSL driven by blue laser diodes. The melt of Al_2O_3, Y_2O_3, CeO_2 was used to crystal growth. It was show that eutectic YAG:Ce-Al_2O_3 possess the pore free structure while in the intermediate compositions pores were detected. The morphology of this eutectics consists of mutual penetrated phase of YAG and Al_2O_3 in the form like "Chinese script" (Fig.1). The boundaries between these phases are well developed without pores and extra phases (Fig.2). It was established that the chromaticity coordinates and correlated colour temperature (CCT) of eutectics are independent from the power of blue laser diode (λem=445 nm) (LD) up to 3 W. But minor dependence of these parameters from LD power was revealed for the samples of different morphology. (YAG-Al_2O_3):Ce Chromaticity coordinates of the eutectics are located in vicinity of x=3.75, y=3.90 point on the CIE 1931 chromaticity diagram. CCT is arranged in 4100 –4600 K interval. The eutectic sample temperature under irradiation of 1 W optical power LD does not exceed of 55 □ for most samples. It was shown that the light homogeneity generated by eutectic convertor depends on sample morphology and the optimal structure was established.

It has been concluded that YAG:Ce-Al_2O_3 eutectics grown by HDC are prospective materials for luminescent convertors of WSSL driven by LD.

Fig.1. 3D view of the sample cut from YAG:Ce-Al_2O_3 eutectic crystal

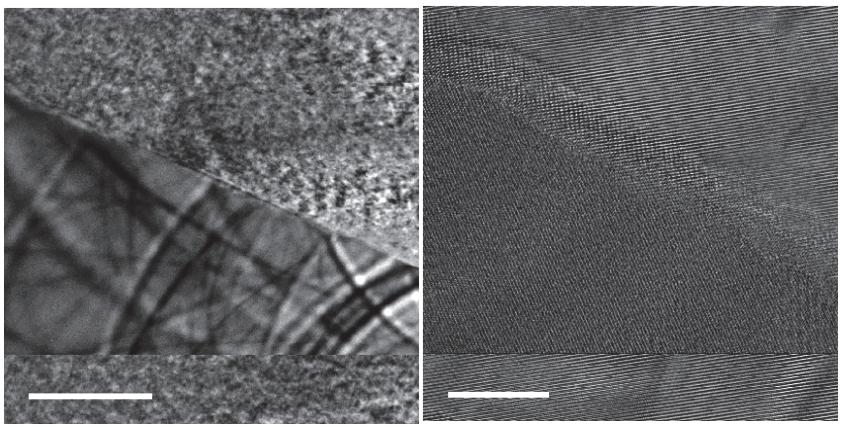

Fig. 2. TEM (a) and HRTEM (b) of the boundary in YAG:Ce-Al_2O_3 eutectic crystal

Scintillation Properties of Composite Scintillators Based on TAG:Ce Single Crystalline Films and GAGG:Ce Crystal Substrates

Y. Syrotych[1,2], V. Gorbenko[1], S. Witkiewicz-Łukaszyk[1], T. Zorenko[1], M. Kaczmarek[2], A. Yoshikawa[3], K. Kamada[3], J.A. Mares[4], M. Nikl[4], R. Kucerkova[4], A. Fedorov[5] and Yu. Zorenko[1]

[1]*Institute of Physics, Kazimierz Wielki University in Bydgoszcz, 85090 Bydgoszcz, Poland*
[2]*Mechantronics Department, Kazimierz Wielki University in Bydgoszcz, 85-074 Bydgoszcz, Poland*
[3]*Institute for Materials Research, Tohoku University, 2-1-1 Katahira, Aoba-ku, Sendai 980-8577, Japan*
[4]*Institute of Physics, Academy of Sciences of Czech Republic, 16200 Prague, Czech Republic*
[5]*SSI Institute for Single Crystals, National Academy of Sciences of Ukraine, 61178 Kharkiv, Ukraine*

This work presents results of growth and investigation of the scintillation properties of composite scintillators based on single crystalline films (SCFs) of $Tb_3Al_5O_{12}$:Ce (TAG:Ce) and $Tb_2GdAl_5O_{12}$:Ce (TGAG:Ce) garnets grown by the liquid phase epitaxy (LPE) method onto $Gd_3Ga_xA_{5-x}O_{12}$:Ce (x=2.3; 2.5; 3) single crystal (SC) substrates (later GAGG2.3; GAGG2.5:Ce and GAGG3:Ce SCs, respectively).

Recently, the TAG:Ce SCF/ GAGG2.5:Ce SC composite scintillator is developed using LPE method and successfully applied for simultaneous registration of α-particles and γ-quanta in the mixed ionizing fluxes [1]. Due to the fact that TAG:Ce SCF has a slower scintillation decay kinetics than that of GAGG2.5:Ce substrate [1, 2], the separation of scintillation signals, coming from the different components of composite scintillator, was performed using the differences in the decay times t_α and t_γ of their SCF and SC parts.

The LPE growth of TAG:Ce SCFs was successfully performed also onto GAGG2.3:Ce SC substrates. In such a way the two types of TAG:Ce SCF/ GAGG(2.3 and 2.5):Ce SCs composite scintillators were created and their luminescent and scintillation properties were investigated under excitation by α (^{239}Pu) and β (^{90}Sr) particles and γ (^{137}Cs) quanta. We have found that these composite scintillators possess comparable t_α/t_β and t_α/t_γ ratios and can be used for the simultaneous detection of α- and β-particles or α-particles and γ-quanta. The best t_α/t_β and t_α/t_γ ratios for these types of composite scintillators, being equal to 1.5-3, was achieved in the 0-3 μs interval.

Furthermore, when the Ga concentration in GAGG:Ce SC substrate increases from x=2.3-2.5 to 3.0, the strong acceleration of the scintillation decay kinetics is observed [3]. Therefore, the t_α/t_β and t_α/t_γ ratios for TbAG:Ce SCF/GAGG3:Ce SC composite scintillator in principle can be improved. However, the growth of TbAG:Ce SCF onto GAGG3:Ce substrates cannot be performed due to the large misfit (above 2%) between the lattice constants of SCF and substrate. For this reason, we used alloying of the large Gd cations in TbAG host what made it possible to grow the TGAG:Ce SCFs onto GAGG3:Ce substrate and create the respective composite scintillator as well. However, TGAG:Ce SCF possesses much faster scintillation response than that of TAG:Ce SCF counterparts. Due to this fact, the respective t_α/t_β and t_α/t_γ ratios are smaller than those in the case of TAG:Ce SCF/GAGG(2.3-2.5):Ce SC composite scintillators. Furthermore, the t_β/t_γ ratios for all the developed composite scintillators are small and insufficient for simultaneous separation of β-particles and γ-quanta in mixed ionization fluxes. For this reason, the LPE growth of three layered composite scintillators is proposed and possible mixed garnet compositions for this purpose are considered.

Acknowledgements: The work was performed in the framework of 2018/31/B/ST8/03390 project.

[1] S. Witkiewicz-Lukaszek, V. Gorbenko, T. Zorenko, K. Paprocki, O. Sidletskiy, A. Fedorov, R. Kucerkova, J. A. Mares, M. Nikl, Yu. Zorenko, CrystEngComm, 2018, 20, 3994.
[2] V. Gorbenko, T. Zorenko, S. Witkiewicz, K. Paprocki, O. Sidletskiy, A. Fedorov, P. Bilski, A. Twardak, Yu. Zorenko, Crystals, 2017, 7, 262.
[3] S. Witkiewicz-Lukaszek, V. Gorbenko, T. Zorenko, O. Sidletskiy, I. Gerasymov, A. Fedorov, A. Yoshikawa, J. A. Mares, M. Nikl, Yu. Zorenko, Crystal Growth & Design 2018, 18, 1834.

Study of Enhancement the TL/OSL Intensities of $KMgF_3$ Perovskites

V. Guckan[1*], V. Altunal[1], W. Abusaid[1], A. Ozdemir[2] and Z. Yegingil[1]

[1]*Cukurova University, Art Sciences Faculty, Department of Physics, 01330 Adana, TURKEY*
[2]*Kahramanmaras Istiklal University, Elbistan Vocational High School of Health Service, Elbistan, Kahramanmaras, Turkey*
[*]*Corresponding E-mail: veysiguckan@gmail.com*

In this study, we produced $KMgF_3$ perovskites doped with Eu and Yb lanthanides and Li alkali metals ($KMgF_3$:Eu,Yb,Li) at different molar concentrations in order to improve its luminescence sensitivity. In this systematic study, $KMgF_3$ perovskite samples were obtained by sol-gel method and the structural, morphological, luminescence and dosimetric properties were examined. Structural analysis, surface morphology and elemental analysis of the samples were performed by X-ray diffraction (XRD), scanning electron microscopy (SEM) and Energy Dispersive X-ray (EDS) methods. Optically Stimulated Luminescence (OSL), Thermoluminescence (TL) and Radioluminescence (RL) curves of $KMgF_3$ perovskites were recorded. To determine if $KMgF_3$:Eu,Yb,Li is structurally suitable for applications in dosimetry TL and OSL emissions of $KMgF_3$ were determined by step annealing and temperature dependence experiments. While OSL signals were observed to be reusable under constant laboratory conditions, OSL traps were found to be thermally stable up to 100 °C and sensitive to radiation dose over a linear dose range of 0.1 to 100 Gy. Only 4% decrease in OSL signal intensity was observed until a month storage after radiation exposure.

Acknowledgements. Financial assistance from the NATO SPS MYP under the research contract number G5647 and the Cukurova University Research Projects Development and Coordination Unit under contract numbers FDK-2018-10599 and FAY-2020-12932 and FBA-2020-13126 are gratefully acknowledged. This work is also supported by TÜBİTAK (The Scientific and Technological Research Council of Turkey) through the Doctoral Researcher Program 2211-C.

Electrothermal Properties in Highly Transparent and Resistive Thin Film of Thermally Evaporated Indium-Tin-Oxide

Atilgan ALTINKOK[1] and Murat OLUTAS[2]

[1]*National Defense University,Turkish Naval Academy, Department of Electrical and Electronics Engineering,, Istanbul, Turkey*
[2]*Abant İzzet Baysal University, Department of Physics, 14030 Bolu, Turkey*

Due to their excellent optical and electrical properties comprising high optical transparency, good electrical conductivity, and high infrared reflectance, semiconducting indium-tin-oxide (ITO) thin films are highly attractive materials among the transparent conductive oxide (TCO) films for optoelectronic device applications. In addition, the low electrical resistivity in the presence of the optical transparency makes this material as a well candidate for transparent thin film heater (TFH) applications such as defogging and deicing. Owing to the optical and electrical properties of the ITO films are strongly dependent on deposition techniques and conditions, the heating performance of the film in the TFH applications is also affected by these. In spite of the fact that high resistivity arising from a poor fabrication limits the utilizing of the thin film in the TFH applications, it can enable use it in some applications requiring high-voltage and low-current as a transparent coating material having poor thermal performance.

In this study, tin-doped indium oxide thin film was deposited by thermal evaporation method on glass substrate that is at room temperature. The structural, optical, electrical and electrothermal properties of the ITO thin film were investigated. Scanning electron microscope and x-ray diffraction spectroscopy were used for its structural analyses, whereas current-voltage and temperature-dependent resistivity measurements were carried out for the electrical characterization of the ITO thin film. In addition, the optical parameters of the thin film such including optical transmittance and energy gap were also determined. Furthermore, electrothermal properties of the ITO film were analyzed using infrared thermography method, voltage-temperature and temperature-time measurements. The heating performance of the thermally evaporated ITO thin film was also carried out as a function of time. It was observed that the prepared ITO thin film exhibits high optical transparency of 92.5% at 550 nm with highly resistive electrical characteristics, and it reaches to the steady-state temperature of ~64 °C in 5 min under the applied voltage of 300V.

Acknowledgements. This work was supported by the Research and Development Foundation of Abant İzzet Baysal University under project number 2016.03.02.1092 and Giresun University Research Fund under project number FEN-BAP-A-140316-55.

Alkaline Earth and Alkali Metals Impurities Effect on Optical and Scintillation Properties of YAG:Ce Single Crystals

Ia. Gerasymov[1], O. Sidletskiy[1,2], Ya. Boyaryntseva[1], S. Tkachenko[1], P. Arhipov[1], E. Galenin[1], D. Kurtsev[1], O. Zelenskaya[1], V. Alekseev[1], S. Witkiewicz-Lukaszek[2], T. Zorenko[2] and Yu. Zorenko[2]

[1]*Institute for Scintillation Materials of National Academy of Science of Ukraine, 60 Nauky ave., 61072 Kharkiv, Ukraine*
[2]*Institute of Physics Kazimierz Wielki at University in Bydgoszcz (UKW), 2 Powstańców Wielkopolskich str., 85-090 Bydgoszcz, Poland*

Search for new fast scintillators is a trend in modern scintillation materials science. This is due to the fact that, recently, there has been a trend towards an increase of the frequency of particle beams collisions [1] in accelerators, as well as a decrease of the dose load on a patient during PET diagnostics by increasing the scanning speed [2]. All this imposes new requirements on the scintillators speed. Among the variety of scintillation materials, oxide single crystals of rare-earth garnets, activated with cerium, demonstrate rather short decay times of luminescence and the ability to withstand significant dose loads. However, the luminescence associated with recombination on trivalent cerium ions in such matrices, although relatively fast but already insufficient for new applications. One of the ways to influence on the time characteristics of oxide scintillators is co-doping by the elements of the 1st or 2nd groups of the periodic table. Often, decreasing of the light output is the negative side of the such co-doping. Therefore, it is advisable to reduce the decay times of luminescence in scintillators with a high light output. Not so far in time, it was possible to achieve a high light yield in a seemingly long-studied commercial material - yttrium-aluminum garnet, activated by cerium and carbon, but the luminescence decay time of this material is still quite long [3].

This work presents the results of studies of YAG:Ce crystals co-activated with elements of the 1st (Li, Na, K) and 2nd (Mg, Ca, Sr, Ba) groups in different concentrations, grown in an reduction atmosphere preventing tungsten crucible damage. Crystals co-doped with calcium showed good results. In these samples, the decay time of the luminescence decreased in two times in comparison to YAG:Ce, but the light output decreases slightly.

[1] Burkhard Schmidt. The High-Luminosity upgrade of the LHC. Journal of Physics: Conference Series 706 (2016) 022002, p. 1-42.
[2] P. Lecoq. Pushing the Limits in Time-of-Flight PET Imaging. IEEE TRANSACTIONS ON RADIATION AND PLASMA MEDICAL SCIENCES, VOL. 1, NO. 6, NOVEMBER 2017. P. 473-485.
[3] O. Sidletskiy et al. Cryst. Growth Des. (2021) DOI: 10.1021/acs.cgd.1c00259

Development of Novel Film and Composite Color Converters for White LEDs Based on the Epitaxial Structures of $Lu_{3-x}Tb_xAl_5O_{12}$:Ce (x = 1-2) Garnet Using Liquid Phase Epitaxy Growth Method

A. Markovskyi[1,2], V. Gorbenko[1], K. Bartosiewicz, T. Zorenko[1], S. Nizhankovskiy[3], A. Fedorov[3] and Yu. Zorenko[1]

[1]*Institute of Physics, Kazimierz Wielki University in Bydgoszcz, Poland;*
[2]*Mechantronic Department, Kazimierz Wielki University in Bydgoszcz, Poland;*
[3]*Institute for Single Crystals, National Academy of Sciences of Ukraine, Ukraine*

Luminescence materials are indispensable components of phosphor-converted white LED (pc-WLED) devices. Therefore, the investigation and development of new pc-WLED phosphors are one of the most important and urgent challenges of advanced material science and technology. For the development of innovative high-power lighting sources, it is strongly needed the design and investigation of the new high structural quality and high-temperature stable planar converters in form of **single crystals (SC)** and **single crystalline films (SCF)**.

This research deals with the growth and investigation of structural, luminescence and photoconversion properties (color coordinates, color rendering index (CRI), luminous efficacy) of the (i) SCFs of Ce^{3+} doped $Lu_{3-x}Tb_xAl_5O_{12}$ (x = 1;1.5;2) mixed garnets, grown using the Liquid Phase Epitaxy (LPE) method onto undoped $Y_3Al_5O_{12}$ (YAG) substrates, and (ii) **composite film-crystal epitaxial structures** based on the $Lu_{1.5}Tb_{1.5}Al_5O_{12}$:Ce SCFs, LPE grown onto activated YAG:Ce SC substrates.

The trend lines on the CIE diagram were obtained for the $Lu_{3-x}Tb_xAl_5O_{12}$:Ce (x = 1;1.5;2) SCF converters by systematic variation of the Tb cations content and film thickness (Fig. a). The ideal white color was almost achieved for $Lu_{1.5}Tb_{1.5}$AG:Ce SCF converter with a thickness of 56 μm under 464 nm blue LED excitation. For this reason, this composition was used for the creation of $Lu_{1.5}Tb_{1.5}$AG:Ce SCF / YAG:Ce SC composite color converters (CCCs). The CCCs exhibit the broader emission due to the compensation of cyan valley by the additional YAG:Ce substrate emission, which allows obtaining a wide spectrum of WLEDs light with enhanced luminous efficacy in comparison with standard photoconverters. The combination of YAG:Ce SC substrates with $Lu_{1.5}Tb_{1.5}$AG:Ce SCFs with thickness in the 38-122 mm range enables tuning the white light tons from cold white/ daylight white (correlated color temperature (CCT) > 6000 K) to neutral white (6000 K > CCT > 3300 K). In this way, $Lu_{1.5}Tb_{1.5}$AG:Ce based film and composite film-crystal color converters exhibit a large promising potential for a planar phosphor converter in high-power WLEDs and in general for color tuning in solid-state lighting.

Acknowledgement. The work was performed in the frame of the Polish NCN 2017/25/B/ST8/02932 project.

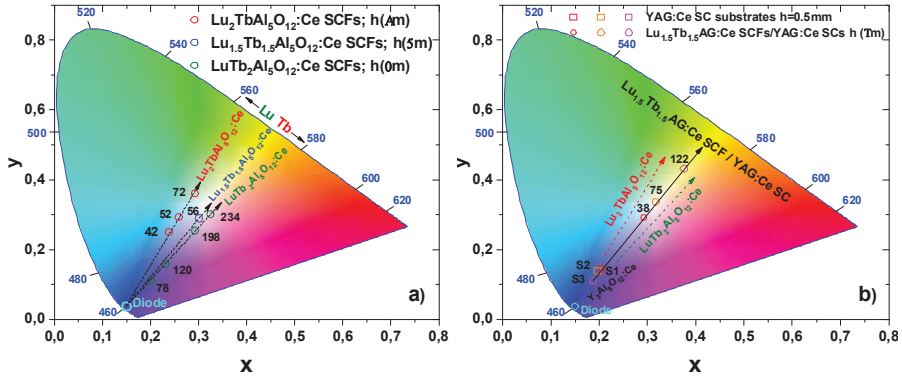

[1] N. Wei et al Appl. Phys. Lett. 101 (**2012**) 061902
[2] A. Markovskyi et al. J. Alloys Compd. 849 **(2020)** 155808
[3] J. Chen et al. Opt. Mater. Express 9 (2019) 3333.

Growth and Luminescent Properties of the Single Crystalline Films and Single Crystals of $Lu_{3-x}Gd_xAl_5O_{12}$:Ce Garnets

K. Bartosiewicz[1]*, V. Gorbenko[1], T. Zorenko[1],
M. Nikl[2], K. Kamada[3], A. Yoshikawa[3] and Yu. Zorenko[1]

[1]*Institute of Physics, Kazimierz Wielki University in Bydgoszcz, Powstańców Wielkopolskich str., 2, 85090 Bydgoszcz, Poland;*
[2]*Institute of Physics, Academy of Sciences of Czech Republic, Cukrovarnicka str., 10, 16200 Prague, Czech Republic*
[3]*Institute for Materials Research, Tohoku University, 2-1-1 Katahira, Aoba-ku, Sendai 980-8577, Japan*

The sets of the single crystalline films (SCFs) of undoped and Ce^{3+} doped $Lu_{3-x}Gd_xAl_5O_{12}$ x = 1-3 mixed garnets for undoped and x = 1-2.9 for Ce doped samples were successfully crystallized by the LPE method using $PbO-B_2O_3$ flux onto $Y_3Al_5O_{12}$ (YAG) substrates [1]. The phase stability and properties of the $Lu_{3-x}Gd_xAl_5O_{12}$:Ce films were compared with respective $Lu_{3-x}Gd_xAl_5O_{12}$ crystal grown from the melt by MPD method [2]. The lattice constant of $Lu_{3-x}Gd_xAl_5O_{12}$:Ce SCFs changed linearly starting from 11.9016 Å for LuAG to 12.102 Å for GdAG according to Vegard's law. The misfit m between SCF and YAG substrate depends on the Gd content and changes from 0.82% for LuAG SCF to 0.85% for GdAG. The Gd admixing in $Lu_{3-x}Gd_xAl_5O_{12}$:Ce SCFs result in the non-linear increasing of the crystal field strength in the dodecahedral positions of the garnet lattices (up to 20% at x = 2.9) and leads to the redshift of the Ce^{3+} emission band from 504 to 570 nm as well as to the non-linear change of decay time of the Ce^{3+} luminescence. The effective $Gd^{3+}\rightarrow Ce^{3+}$ energy transfer occurs in the $Lu_{3-x}Gd_xAl_5O_{12}$:Ce garnet under ionisation and direct excitation in the absorption bands of Gd^{3+} cations. The LY of $Lu_{3-x}Gd_xAl_5O_{12}$:Ce SCFs show a non-linear dependence on the Gd content (Fig. 1). The best LY under α–particles excitation (^{221}Am) is observed for LuAG:Ce and $Gd_{2.9}Lu_{0.1}Al_5O_{12}$:Ce SCFs. Such complicated character of the scintillation LY dependence in $Lu_{3-x}Gd_xAl_5O_{12}$:Ce SCFs with increasing the Gd^{3+} content is connected with the opposite influence of several factors: (i) the low energy shift of the Ce^{3+} emission; (ii) the shift of the onset of thermal quenching of the Ce^{3+} luminescence down to RT range; (iii) the better separation of Ce^{3+} emitting level inside garnet band gap at large (>2) Gd content; (iv) creation of Lu_{Al} antisite defects in the SCF; (v) the larger contamination of Pb^{2+} flux dopant in the Gd-containing SCFs in comparison with LuAG:Ce SCF.

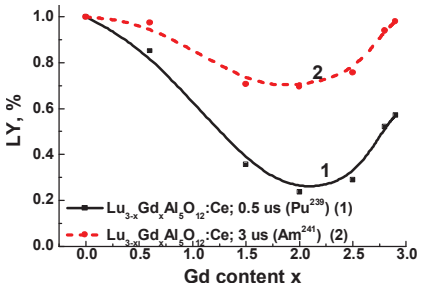

Fig. 1. Dependence of LY values on Gd content

Acknowledgements: Polish NCN 2018/31/B/ST8/03390 and 2020/39/D/ST3/02711, Czech OP RDE&MEYS SOLID21 CZ.02.1.01/0.0/0.0/16_019/0000760 and Japanese 2018SV11 ICC-IMR Tohoku University projects.

[1] Yu. Zorenko, et al. Mat. Res. Bull., 2015, 64, 355.
[2] K. Bartosiewicz, et al. Opt. Mater., 2018, 80, 98

Three-Layered Composite Scintillator Based on the Ce^{3+} and Sc^{3+} Doped YAG and LuAG Garnets for Simultaneous Registration of α-, β-Particles and γ-Quanta

S. Witkiewicz-Lukaszek[1*], V. Gorbenko[1], T. Zorenko[1], J.A. Mares[2], M. Nikl[2] and Yu. Zorenko[1]

[1]*Institute of Physics, Kazimierz Wielki University, Pow. Wielkopolskich 2, Bydgoszcz, 85090, Poland*
[2]*Institute of Physics, AS Czech Republic, 6253 Prague, Czech Republic*

The development of two-layered composite scintillators based on the single crystalline films (SCFs) and single crystals (SCs) of Ce^{3+} and Sc^{3+} doped LuAG garnet [1-3], opens also opportunity for constructing new types of three-layer composite scintillators for the registration of the different components mixed ionizing radiation (α– and β-particles and γ-quanta).

This work is dedicated to the growth of three-layered epitaxial structures YAG:Ce SCF/ LuAG:Sc SCF/LuAG:Ce SC and YAG:Ce SCF/LuAG:Ce SCF/LuAG:Sc SC using the Liquid Phase Epitaxy (LPE) method from a melt-solution based on the $PbO-B_2O_3$ flux and investigation of their scintillation properties. Special attention was paid to the ability of separating three various components of mixed ionizing radiation (α- and β- particles and γ-quanta) using differences in the scintillation decay kinetics of film and crystal part of such composite scintillators (Fig.1a).

Fig.1a shows the possibility of the simultaneous registration of these types of radiation by means of separation of the scintillation decay kinetics of SCF and crystal parts of such composite scintillators. The differences in the scintillation decay curves and decay time constants t_α, t_β and t_γ under ^{239}Pu (α–particles), ^{90}Sr (β-particles) and ^{137}Cs (γ-ray) excitations are characterized by the respective Figure of Merit (FOM) values calculated for the different intensity levels (1/e, 0.1, 0.05, 0.01) (Fig.1b). We have found that the best scintillation properties are observed in the YAG:Ce SCF/ LuAG:Ce SCF/LuAG:Sc SC epitaxial structures, especially for the cases of simultaneous registrations of α/γ and β/γ pairs.

Acknowledgments: The work was performed in the framework of Polish NCN 2018/31/B/ST8/03390 project and partially from the Operational Programme Research, Development and Education financed by European Structural and Investment Funds and the Czech Ministry of Education, Youth and Sports (Project No. SOLID21 CZ.02.1.01/0.0/0.0/16_019/ 0000760).

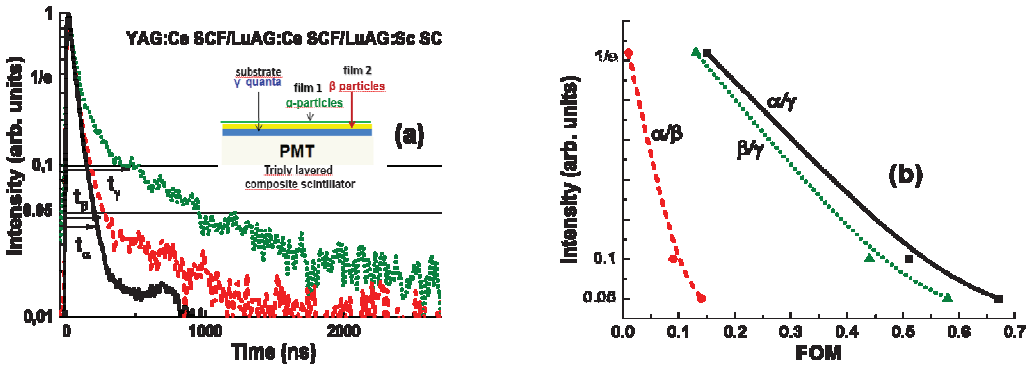

Fig.1. (a) - separation of the scintillation decay curves of YAG:Ce SCF/LuAG:Ce SCF/ LuAG:Sc SC composite scintillators under excitation by α- and β-particles and γ-quanta. (b) –FOM values under simultaneous registration of chosen two types of radiation.

[1] S. Witkiewicz-Lukaszek, e. a. *IEEE Transactions on Nuclear Science* 65 (2018) 2114 – 2119.
[2] S. Witkiewicz-Lukaszek, e. a. *Optical Materials* 84 (2018) 593-599.
[3] S. Witkiewicz-Lukaszek, e. a. *CrystEngComm* 22 (2020) 3713-3724.

High-Pressure Studies of Ce^{3+} Luminescence in Epitaxial $LuAlO_3$ Single Crystalline Film

Lev-Ivan Bulyk [a], Ajeesh Kumar Somakumar [a], P. Ciepielewski [a], Yu. Zorenko [b], Ya. Zhydachevskyy [a], I. Kudrjavtseva [c], V. Gorbenko [b], A. Lushchik [c] and Andrzej Suchocki [*,a]

[a] *Institute of Physics, Polish Academy of Sciences, Al. Lotnikow 32/46, 02-668, Warsaw, Poland*
[b] *Institute of Physics, Kazimierz Wielki University in Bydgoszcz, Powstańców Wielkopolskich str., 2, 85-090 Bydgoszcz, Poland.*
[c] *Institute of Physics, University of Tartu, W. Ostwaldi 1, 50411 Tartu, Estonia*

The absorption measurements in the near-UV region of YAP and LuAP crystals allowed us to establish an experimentally accurate value of the bandgap for $YAlO_3$ crystal at room temperature, which is equal to about 7.6 eV, assuming a direct type of bandgap. High-temperature luminescence efficiency of YAP:Ce, which thermal quenching begins at the temperature of about 650 K, locate the energy difference of the lowest excited *5d* level of Ce^{3+} 1.58 eV below the bottom of the conduction band. This value is affected by the temperature change of the bandgap, i.e., at low temperatures, the difference between the energy of the *5d* level and the bottom of the conduction band is larger. This conclusion correlates within the limits of error bars within the estimations of Dorenbos theory and DFT calculations.

Ce^{3+} luminescence quenching is not observed in LuAP crystals up to about 900 K. This results from a larger bandgap of LuAP compared to YAP.

The calculated downshift of the *3d* energy levels of Ce^{3+} does not agree with the energy for free Ce^{3+} calculated by Dorenbos from his theory. The difference can be reconciled if the downshift is calculated relative to the bandgap energy of YAP and LuAP. This approach also allows correlating observed changes of the energies of *3d* states under pressure in LuAP, related to the pressure-induced changes of the average cation-anion distances, assuming that the main changes of the bandgap are due to the increase of the bottom energy of the conduction band.

The other possibility might be related to the proposed in [1] pressure-induced shift of both *4f* and *5d* manifolds energies. This effect would lead to lack or very little dependence of the *4f* → *5d* transition energies versus pressure. This is somehow in contradiction to the Dorenbos model and common expectations that *5d* states are more influenced by the ligands than *4f*.

We suggest that the observed change of the pressure coefficients of the 5d → 4f Ce^{3+} luminescence bands is associated with pressure-induced structural transitions, occurring in the liquid-phase epitaxy grown layers at the pressure of about 10 GPa, and at higher pressures in micro-pulling down crystals. We relate that difference with certain unintentional dopants present in the micro-pulled down crystals. Similar changes of pressure coefficients of the Raman modes confirm this hypothesis.

Acknowledgments: This work was partially supported by the grant 2018/31/B/ST8/03390 of the Polish National Science Center.

[1] S. Mahlik, A. Lazarowska, J. Ueda, S. Tanabe and M. Grinberg, Phys. Chem. Chem. Phys., 2016, 18, 6683, PCCP 2019, 21, 2816

Determination of the Diffusion Incorporation Mechanism of Cu Ions into $LiNbO_3$ by Studying of Spatial Changes of Crystal Properties

U. Yakhnevych[1], D. Sugak[1,2], I.I. Syvorotka[1,2], O. Buryy[1] and S. Ubizskii[1]

[1]*Lviv Polytechnic National University, Lviv, Ukraine*
[2]*Scientific Research Company "Electron-Carat", Lviv, Ukraine*

Lithium niobate ($LiNbO_3$) plays a lead role among optoelectronic materials because of its outstanding multi-functionality expressed by electro-optic, nonlinear optic, acousto-optic, piezoelectric, photorefractive, pyroelectric, properties, etc. [1, 2]. In recent years, interest has been growing in modifying $LiNbO_3$ crystals properties by doping with metal ions. In particular, $LiNbO_3$ crystals doped with rare earth ions can be used as a laser material; Fe, Cu, or Mn are used to enhance photorefractive properties; while Mg and Zn ions are introduced to limit optical damage and, thus, to make the crystals are suitable for electro-optical modulation. One of the ways of such modification is diffusion. Doping by diffusion is an effective and practical method for improving material properties and widening material application.In turn, copper is an important place among the metal ions, which incorporate into LN crystal by diffusion. Firstly, this is due to the high diffusion coefficient of Cu in $LiNbO_3$, which is about 500 times higher than the one, for example, of Fe under the same conditions. No less important is the fact that the absorption bands caused by Cu^+ and Cu^{2+} ions in $LiNbO_3$ crystal are easy to distinguish by optical spectroscopy.

However, despite the great interest of scientists and an articles variety about the diffusion of metal ions in $LiNbO_3$, the diffusion incorporation mechanism of ions into the crystal is not fully understood. In view of this, we have proposed a new technique that allows studying the spatial distribution of incorporated ions by registration of the optical absorption, mechanical and pyroelectric properties in the directions perpendicular to the directions of diffusion (X, Y, or Z crystal-physics axes) [3, 4]. The structural properties of LN crystals doped with Cu ions were also additionally studied. On the basis of these investigations, we have offered a diffusion incorporation mechanism of ions that occurs in a crystal. We assumed that the spatial distribution of copper ions incorporated into $LiNbO_3$crystal is due to a complex process of ion exchange involving copper and lithium ions. In this case, the layer of the crystal adjacent to the surface is depleted by lithium ions and enriched by copper ions, which reduces the exchange diffusion coefficient in this layer. This leads to a difference in the probabilities of jumping of copper ions in opposite directions, which, in turn, is the reason of the observed shifts of the maxima of Cu^+ and Cu^{2+} ions concentrations from the crystal surface towards the crystal volume.

Acknowledgments: This work was supported by the project DB/MODUS (no. 0121U107736) of the Ukrainian Ministry of Education and Science.

[1] Wong K.K.: Properties of lithium niobate, INSPEC, London 2002.
[2] Volk T., Wöhlecke M.: Lithium niobate: defects, photorefraction and ferroelectric switching, Springer, Berlin 2009.
[3] Sugak D., Syvorotka I., Yakhnevych U., Buryy O., Levintant-Zayonts N., Savytskyy H., Bonchyk O., Ubizskii S.: Comparative investigations of nanohardness and impurity distribution profiles of lithium niobate single crystals diffusion doped by copper ions, *Crystal Research and Technology*. **54** (2019) 1900117(1)-1900117(7).
[4] Suchaneck G., Yakhnevych U., Eydam A., Sugak D., Syvorotka I.I., Haiduchok V., Ubizskii S., Gerlach G. Depth profiling of dopant concentration and pyroelectric properties of $LiNbO_3$ single crystals treated at high-temperature in the presence of metal ions, *Ferroelectrics*. **539** (2019) 146-152.

Luminescence Characterization of BeO:$Na_{5\%}$,$Ce_{0.01\%}$,$Er_{0.01\%}$ Ceramic

V. Altunal[1*], V. Guckan[1], A. Ozdemir[2], W. Abusaid[1], A. Ekicibil[1], F. Karadag[1] and Z. Yegingil[1]

[1]*Cukurova University, Art Sciences Faculty, Department of Physics, 01330 Adana, TURKEY*
[2]*Kahramanmaras Istiklal University, Elbistan Vocational High School of Health Service, Elbistan, Kahramanmaras, Turkey*
[*]*Corresponding E-mail: valtunal@cu.edu.tr*

In this work, we systematically produced the lanthanide (Ln)-doped BeO ceramics at different molar concentrations to improve the luminescence sensitivity of the material. The structural, morphological, luminescent and dosimetric characteristics of newly produced promising BeO based ceramic pellet, namely, BeO:$Na_{5\%}$,$Ce_{0.01\%}$,$Er_{0.01\%}$ was investigated by simultaneously comparing with commercialized BeO Thermalox 995 chips. The co-precipitation synthesis method was chosen to prepare our ceramics. The structural phase formations and morphologies have been analyzed by x-ray diffraction (XRD), scanning electron microscopy (SEM), and Energy Dispersive Xray (EDS) methods. BeO ceramic samples were characterized by Optically Stimulated Luminescence (OSL), Thermoluminescence (TL) and Radioluminescence (RL) techniques. To control the luminescence from our promising dosimeters for dosimetry applications, trap properties were identified by TL and OSL emissions, step-annealing, and temperature dependency experiments. The same luminescence mechanism in all cases (RL, TL, and OSL) was observed between 300 and 400 nm (i.e., 3-4 eV). The OSL signals were found to be thermally stable up to 150 °C, reusable under carefully controlled laboratory conditions, and sensitive to radiation dose with a linear dose range from 0.1 to 100 Gy. While an almost 7 % decrease is observed in the OSL signals of our product stored for 3 months after the radiation dose, the decrease in BeO Thermalox chips is 16 %. The results demonstrate that newly produced BeO ceramic is very encouraging for personal and medical dosimetry applications.

Acknowledgements. This work was supported by the NATO SPS MYP program under project number G5647 and Cukurova University Research Projects Development and Coordination Unit under the project numbers FDK-2018-10190, FAY-2019-11571, and FAY-2020-12932, FBA-2020-13126. The authors thank NATO and Cukurova University for supporting this research. We are grateful to Prof. Kasım Kurt and Tayfun Cavdar from Mersin University for RL emission measurements.

AMoRE: a Low Temperature Bolometric Experiment to Search for Double Beta Decay of ^{100}Mo with Molybdate Crystal Scintillators

N.V. Sokur

Institute for Nuclear Research of NASU, Kyiv, Ukraine

AMoRE is a project of large-scale experiment to search for neutrinoless double beta decay of ^{100}Mo by using low-temperature scintillation bolometric detectors with molybdate crystal scintillators with a dual heat and light readout. The first phase of the experiment AMoRE-Pilot, with 1.9 kg of calcium molybdate crystal scintillators produced from calcium depleted in the isotope ^{48}Ca, and molybdenum enriched in ^{100}Mo ($^{48depl}Ca^{100}MoO_4$), was completed in 2019 [1]. The second phase of the experiment, AMoRE-I, is running with approximately 6 kg of molybdate scintillators of different compound: lithium, sodium and calcium molybdates with a total mass of enriched ^{100}Mo ~3 kg. A goal of the AMoRE-I is further improvement of the detector performance in terms of background and energy resolution, and choice of a detector material for the final stage of the experiment, AMoRE-II, that is expected to operate a total detectors mass of 200 kg [2]. Preliminary results of the data analysis aiming at discrimination between beta and alpha events, rejection of randomly coinciding events and improvement of the detectors energy resolution will be presented.

[1] V. Alenkov et al., First results from the AMoRE-pilot neutrinoless double beta decay experiment, Eur. Phys. J. C 79 (2019) 791.

[2] V. Alenkov et al., Technical Design Report for the AMoRE 0□ □Decay Search Experiment, arXiv:1512.05957v1 [physics.ins-det].

Optical and Structural Properties of ZnO:Alq_3 Thin Layers Dispersed in Various Polymer Matrices

M. Sypniewska[1], R. Szczesny[2], L. Skowronski[3] and B. Derkowska-Zielinska[1]

[1]*Institute of Physics, Faculty of Physics, Astronomy and Informatics, Nicolaus Copernicus University in Torun, Grudziadzka 5, 87-100 Torun, Poland*
[2]*Faculty of Chemistry, Nicolaus Copernicus University in Torun, Gagarina 7, 87-100 Torun, Poland*
[3]*Institute of Mathematics and Physics, UTP University of Science and Technology, S. Kaliskiego 7, 85-796, Bydgoszcz, Poland*

In recent years, there has been a significant increase in interest of organic/inorganic hybrid composite materials, which due to their interesting physico-chemical properties, simplicity and low-cost of production technology provide a serious competition for traditional semiconductors (inorganic) materials currently used in optoelectronics. The use of such hybrid composite materials in organic light emitting diodes (OLEDs) provides high mobility, good stability and better luminescence efficiency compared to organic materials [1].

A thin layer made of mixing ZnO and Alq_3 (tris-(8-hydroxyquinoline)aluminum) meets the above requirements thus it can be used to produce white OLEDs. Zinc oxide (ZnO) is one of the II-VI compound semiconductors and it crystallizes in the cubic, zinc blende or hexagonal structure of the wurtzite [2]. ZnO has a direct energy band gap of about 3.37eV and a large exciton binding energy (60 meV), which provides more efficient exciton emissions at higher temperatures [3]. Due to its unique properties, ZnO is widely used in various optoelectronic devices [4]. Alq_3 is one of the most important organic semiconductor materials used in OLEDs as an electron-transport material and emitting layer. Alq_3 is a green emitter with PL peak wavelength in the range of 520 nm. In this material, the light emission originates from the ligand's electronic $\pi - \pi^*$ transition from the highest occupied molecular orbital (HOMO) to the lowest unoccupied molecular orbital (LUMO) [5].

In this work, we investigated the optical and structural properties of ZnO:Alq_3:polymer thin layers using UV-Vis and IR spectroscopies, spectroscopic ellipsometry as well as AFM and SEM/EDX. Photoluminescence (PL) properties were also analysed. ZnO:Alq_3 was dispersed in various polymer matrices such as polyvinylpyrrolidone (PVP), poly(methyl methacrylate) (PMMA) and poly(butyl methacrylate) (PBMA) and afterwards ZnO:Alq_3:polymer layers were deposited on silicon substrate using dip coating method. We found that the optical and structural properties of ZnO:Alq_3:polymer changed with the change of polymer matrix. Luminescence measurements showed that PL peak of ZnO:Alq_3:polymer was blue shifted with respect to Alq_3:polymer.

[1] G. Dasi, R. Ramarajan, K. Thangaraju, *Improved electron injection in spin coated Alq3 incorporated ZnO thin film in the device for solution processed OLEDs,*DAE Solid State Physics Symposium,060015 (2018)
[2] S. Ilican, Y. Caglar, M. Caglar, *Preparation and characterization of ZnO thin films deposited by sol-gel spin coating method,* Journal of optoelectronics and advanced materials **10**, 2578-2583 (2008).
[3] Ü. Özgür, Ya. I. Alivov, C. Liu, A. Teke, M.A. Reshchikov, S. Doğan, V. Avrutin, J. Cho, H. Morkoç, *A comprehensive review of ZnO materials and devices,* Journal of applied physics **98**, 041301-1 - 041301-103 (2005).
[4] S. Abed, H. Bougharraf, K. Bouchouit, Z. Sofiani, B. Derkowska-Zielinska, M.S. Aida, B. Sahraoui, *Influence of concentration of nano particles of Bi on the electrical and optical properties of ZnO thin films*, Superlattices and Microstructures **85**, 370-378 (2015).
[5] J.G. Mahakhode, S.J. Dhoble, C.P. Joshi, S.V. Moharil, *Blue-shifted photoluminescence of Alq3 dispersed in PMMA*, Bull. Mater. Sci. **34**, 1649-1651 (2011).

Luminescence Properties of the Sm^{3+} Centres in the Sm-Ag Co-Doped Glasses with $Li_2B_4O_7$ Composition

B.V. Padlyak[1,2], I.I. Kindrat[1], B. Kukliński[3], A. Drzewiecki[1], V.T. Adamiv[2] and I.M. Teslyuk[2]

[1]*University of Zielona Góra, Institute of Physics, 4a Szafrana Str., 65-516 Zielona Góra, Poland*
[2]*Vlokh Institute of Physical Optics, Department of Optical Materials, 23 Dragomanov Str., 79-005 Lviv, Ukraine*
[3]*University of Gdańsk, Institute of Experimental Physics, 57 Wita Stwosza Str., 80-308 Gdańsk, Poland*

Luminescent properties of the Sm-doped and Sm-Ag co-doped glasses with $Li_2B_4O_7$ (or $Li_2O–2B_2O_3$) basic composition are investigated and analysed. The $Li_2B_4O_7$ glasses doped with Sm and co-doped with Sm and Ag were obtained using standard glass technology [1,2]. Spectroscopic properties of the obtained $Li_2B_4O_7$:Sm and $Li_2B_4O_7$:Sm,Ag glasses were studied using measurements of optical absorption, electron paramagnetic resonance (EPR), photoluminescence (excitation, emission, decay kinetics), and quantum yield (QY) via an absolute method [2].

Optical absorption spectra exhibit absorption bands related with transitions from the ground $^6H_{5/2}$ state of Sm^{3+} ions to several excited states. Photoluminescence spectra of the Sm-doped glasses reveal emission bands, which correspond to the $^4G_{5/2} \rightarrow {}^6H_J$ (J = 5/2 – 13/2) transitions of Sm^{3+} ions. Luminescence excitation spectra, which show greater number of the Sm^{3+} bands with better resolution than the optical absorption spectra, also are analysed. Decay curves of the Sm^{3+} luminescence is characterised by exponential lifetimes slightly higher than 2.5 ms. The EPR study confirms presence of Ag species in the Sm-Ag co-doped samples. Photoluminescence emission and excitation spectra and luminescence decay kinetics of the Ag^+ ions and small non-plasmonic molecule-like silver (ML-Ag) nanoclusters also are observed and discussed.

Enhancement of Sm^{3+} luminescence in the $Li_2B_4O_7$:Sm,Ag glass has been observed. Measurements confirm the increasing of external QY of Sm^{3+} luminescence in 1.43 times in the Sm-Ag co-doped glass. Such enhancement of the luminescence is attributed to the excitation energy transfer from Ag^+ ions and ML-Ag nanoclusters to the Sm^{3+} ions as wells local-field effect induced by Ag nanoparticles. The obtained high QY of the Sm^{3+} luminescence shows that $Li_2B_4O_7$:Sm,Ag glass belong to promising luminescent materials.

[1] B.V. Padlyak, I.I. Kindrat, R. Lisiecki, V.T. Adamiv, I.M. Teslyuk, New effective luminescent materials based on the Sm-doped borate glasses, Adv. Mater. Lett. 8 (2017) 723–734.
[2] I.I. Kindrat, B.V. Padlyak, B. Kukliński, A. Drzewiecki, V.T. Adamiv, Effect of silver co-doping on enhancement of the Sm^{3+} luminescence in lithium tetraborate glass, J. Lumin. 213 (2019) 290–296.

Eutectic Composites in Al_2O_3–Y_2O_3 System Solidified by Horizontal Directed Crystallization Method

Yu. Siryk, O. Vovk, L. Gryn, A. Romanenko, V. Baranov and S. Nizhankovsky

Institute for Single Crystals, National Academy of Sciences of Ukraine, 60, Nauky Ave., Kharkiv, Ukraine
e-mail: lab15.oxydal@gmail.com

Developing modern solid-state lighting (SSL) driven by laser diodes (LD) significantly rising irradiation load on the phosphor's converter. The YAG:Ce is the widespread phosphor converter for SSL and its irradiation stability should be enhanced for such applications. Composites of Al_2O_3-YAG attract interest as the matrix of the phosphor converters due to their higher thermal conductivity to compare with pure YAG. Moreover, the particles of Al_2O_3 scatter the light in the converter body that increasing light output yield.

In the present work, the composites in the Al_2O_3-Y_2O_3 system have been investigated to determine the conditions for obtaining the eutectic Al_2O_3-YAG by the method of horizontally directed crystallization (HDC).

The palleted powder mixture of 81.5 mol.% Al_2O_3 (99,999%) and 18,5 mol.% Y_2O_3 (99,999%) have been used as raw materials for crystallization that was carried out on the installation "Horizont-3" in Mo crucible in the environment of Ar, CO, and H_2 at a total pressure of $1.3x10^5$ Pa at evaluated temperature and rate of solidification. As result, the samples of the different microstructure and the phase composition have been synthesized (see Figure).

It has been established that decreasing the rate of solidification from 30 mm/h (sample *a*) to 5 mm/h (sample *b*) causes the formation of Al_2O_3-$Y_3Al_5O_{12}$ eutectic morphology with a coarser structure. While the increasing the temperature of melt resulted in the formation of metastable eutectic of Al_2O_3-$YAlO_3$ (sample *c*) with the microstructure finer than that of sample *a*. This metastable eutectic can be easily transformed into Al_2O_3-$Y_3Al_5O_{12}$ by reheating above the phase transition with preserving the size of the microstructure (sample *d*) [1].

Thus, it has been shown that the eutectic composite of Al_2O_3-$Y_3Al_5O_{12}$ can be obtained by directed melt solidification using the HDC method. The morphology of such composites is governed by the modes of the melt solidifications. The eutectic composite of Al_2O_3-$Y_3Al_5O_{12}$ due to high thermal conductivity and scattering features can be considered as a promising host matrix for phosphor converter based on YAG:Ce for SSL driven by LD.

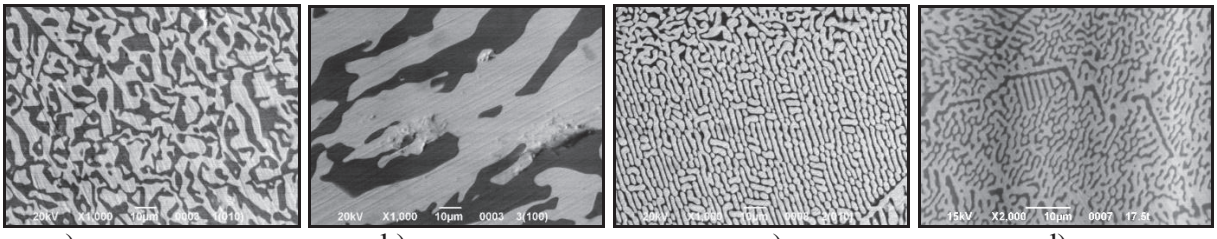

a) b) c) d)

Fig. SEM images of the microstructure of samples.
The dark phase - Al_2O, light phase - YAG in samples *a*), *b*), *d*), and YAP in sample *c*)

[1] T. Nagira, H. Yasuda, T. Sakimura, K. Yoshida, Solidification of Al_2O_3–YAG eutectic composites with off-metastable eutectic composition from undercooled melt produced by melting Al_2O_3–YAP eutectics, Journal of the European Ceramic Society, V. 32, 2012, 2137-2143.

$(Y,Gd)AlO_3$ Perovskite Solid Solution Single Crystals Doped with Mn and Hf Grown by the Czochralski and Floating Zone Methods

M. Głowacki[1], J. Fink-Finowicki[1], V. Stasiv[1], Ya. Zhydachevskyy[1,2], R. Diduszko[1,3], M. Berkowski[1] and A. Suchocki[1]

[1]*Institute of Physics, Polish Academy of Sciences, Al. Lotników 32/46, 02-668 Warsaw, Poland*
[2]*Lviv Polytechnic National University, Bandera 12, 79013 Lviv, Ukraine*
[3]*Tele and Radio Research Institute, Ratuszowa 11, 03-450 Warsaw, Poland*

Mn^{2+}-doped $YAlO_3$ (YAP) crystals have proven to be a good candidate for thermoluminescent (TL) or optically stimulated luminescent (OSL) dosimetry of ionizing radiation [1-2]. It was also shown that disordering the crystal lattice – inducing the occurrence of antisite defects – can significantly enhance thermoluminescence intensity of the material [1]. However there are still many unanswered questions about controlling this lattice disorder and maintaining manganese ions on 2+ oxidation state.

In this study a new approach to this problem will be presented. Gd^{3+} ions were introduced into the crystal matrix partially substituting Y^{3+} ions and Mn^{2+} oxidation state was stabilized by co-doping with Hf^{4+} ions. Single crystals of $(Y,Gd)AlO_3$ solid solution were grown using two different methods – by the Czochralski method from the iridium crucible in ambient atmosphere and by the floating zone method in air. During the presentation the growth conditions and crystal stoichiometry will be discussed. Results of structural and luminescence investigations will be presented.

Acknowledgements: The work was supported by the Polish National Science Centre (project no. 2018/31/B/ST8/00774) and by the NATO SPS Project G5647 as well as by the Ukrainian Ministry of Education and Science through the project DB/KINETYKA (No 0119U002249).

Fig. 1. Single crystal of $Y_{0.85}Gd_{0.15}AlO_3$: 0.05 at% Mn, 0.5 at% Hf grown by the Czochralski method.

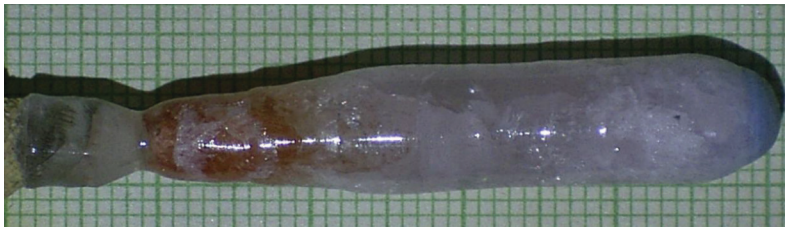

Fig. 2. Single crystal of $Y_{0.8}Gd_{0.2}AlO_3$: 0.05 at% Mn, 0.5 at% Hf grown by the floating zone method.

[1] Ya. Zhydachevskii, A. Suchocki, M. Berkowski, D. Sugak, A. Luchechko, S. Warchol, *J. Cryst. Growth* 310 (2008) 3219-3223.
[2] Ya. Zhydachevskii, A. Luchechko, D. Maraba, N. Martynyuk, M. Glowacki, E. Bulur, S. Ubizskii, M. Berkowski, A. Suchocki, *Radiat. Meas.* 94 (2016) 18-22.

Optical Properties and Electronic Structure of RAlO$_3$ (R = La, Gd, Y, Yb, Lu) Perovskite

Ya. Zhydachevskyy[1,2], Yu. Hizhnyi[3], S.G. Nedilko[3], M. Głowacki[1], P. Sybilski[1], M. Berkowski[1], S. Ubizskii[2] and A. Suchocki[1]

[1]*Institute of Physics, Polish Academy of Sciences, Warsaw, Poland*
[2]*Lviv Polytechnic National University, Lviv, Ukraine*
[3]*Taras Shevchenko National University of Kyiv, Ukraine*

Yttrium-aluminum perovskite ($YAlO_3$ or YAP) is well-known host material for solid-state lasers, scintillators and various kinds of converting and storage phosphors. YAP crystal possesses deformed perovskite-like structure with orthorhombic symmetry (space group D_{2h}^{16} – *Pbnm*). Other rare-earth-based aluminates and their solid solutions with the same type of structure (e.g. $LuAlO_3$, $GdAlO_3$, $YbAlO_3$ etc.) are also well known. Large amount of optical and luminescent properties of these crystals are determined not only by the specific doping creating energy levels inside the bandgap of the material, but also by presence of native and impurity trapping levels and their location (ionization energy) relative to conduction or valence bands.

The present work is devoted to systematic study of the electronic band-gap widths of RAlO$_3$ perovskites with various RE cations (R = La, Gd, Y, Yb, Lu). Both experimental and theoretical methods are applied to determine dependence of the band-gap width on type of the RE cation. The DFT-based theoretical calculations with use of the Plane-Wave Pseudopotential method were carried out in order to establish the electronic band structures of RAlO$_3$ crystals. Several kinds of the most common defects in RAlO$_3$ perovskites (cationic anti-site defects, oxygen vacancies and their complexes) were also considered in calculations.

Results obtained from the calculations for the studied materials are discussed and compared with corresponding experimental results for optical absorption in the VUV-UV range and TSL measured in the temperature range from 300 to 500 °C.

Acknowledgements: The work was supported by the Polish National Science Centre (project no. 2018/31/B/ST8/00774) and by the NATO SPS Project G5647 as well as by the Ukrainian Ministry of Education and Science through the project DB/KINETYKA (No 0119U002249).

Luminescent and Scintillation Properties of Sc^{3+} and La^{3+} Doped $LuAlO_3$ Crystals

W. Gieszczyk[1*], P. Bilski[1], A. Mrozik[1], V. Vistovskiy[2], A. Voloshinovskii[2], A. Fedorov[3], K. Paprocki[3], T. Zorenko[3*] and Yu. Zorenko[3]

[1]*Institute of Nuclear Physic, Polish Academy of Sciences, 313-42 Krakow, Poland*
[2]*SSI Institute for Single Crystals, National Academy of Sciences of Ukraine, 61178 Kharkiv, Ukraine*
[3]*Institute of Physics, Kazimierz Wielki University, 850-90 Bydgoszcz, Poland*

Isoelectronic impurities *(IIs)* with respect to core cations (e.g. La^{3+} and Lu^{3+} or Sc^{3+} and Al^{3+}) can effectively localize electrons and holes or excitons at the expense of non-Coulomb potential arising at substitution of core cation by *IIs* [1]. For this reason *IIs* are widely used to create the luminescence materials emitting in the UV range (250-350 nm) based on Al_2O_3-Lu_2O_3 oxide system of different structural types [1].

In this work, we present the results on crystallization and investigation of the luminescent and scintillation properties of $LuAlO_3$ (LuAP) crystals doped with Sc^{3+} and La^{3+} *IIs* as possible UV emitting scintillators. LuAP:La and LuAG:Sc crystals with different dopants concentration in the 0.2-5 and 0.2-6.9 mole % ranges, respectively, were grown from melt by the MPD method. The luminescent properties of LuAP:Sc and LuAP:La crystals were investigated by cathodoluminescence (CL) at 300 K, X ray excited luminescence (RL) at 300 and 77 K and thermoluminescence in the 320-600 K range.

We have found that under e-beam and X ray excitation the main emission bands of Sc^{3+} and La^{3+} doped in LuAP SCs are located in the UV range. The UV luminescence of LuAP:La crystals in the complex band peaked at 330 nm at 300 K results mainly from radiative de-excitation of an exciton bound with La_{Lu} centers. At low (77 K) temperature the complex emission band of LuAP:La crystals presents a superposition of two emission bands with various decay kinetics, attributed to the luminescence of different types of excitons *"localized at"* and *"bound with"* La_{Lu} centers. The short-wavelength component of the UV emission band located at 304 nm and decaying with lifetimes of t_1=480 ns and t_2=1885 ns is attributed to the luminescence of excitons localized at La_{Lu} centers, whereas the long-wavelength emission band located at 335 nm and decaying with lifetimes of t_1=680 ns and t_2=2125 ns are caused by the luminescence of an exciton bound with La_{Lu} centers.

The luminescence of LuAP:Sc crystals in the complex band in the UV range at low (77K) temperature is a superposition of several emission bands resulted from formation and radiative de-excitation of an exciton *"localized at"* and *"bound-with"* Sc_{Al} centers, respectively. The emission band peaking at 293 nm with the lifetimes of fast, middle and slow components of 95, 660 and 1825 ns, respectively, is attributed to the luminescence of excitons *localized at* Sc_{Al} centers, Meanwhile, the temperature stable at 300 K emission band peaking at 326 nm with lifetimes of fast, middle and slow components of 200, 1010 and 2010 ns, respectively, are caused by the luminescence of an exciton *bound with* Sc_{Al} centers. Such typical luminescence decay kinetics of La_{Lu} and Sc_{Al} centers, which are characterized by relatively fast (100-200 ns), middle (400-1010 ns) and the main slow (1825-2125 ns) components, indicates the creation of *triplet excitons*, connected with the mentioned centers.

The above mentioned results presuppose also the creation of the different trapping centers in LuAP crystals with the following recombination of free carries (electrons or holes) with La_{Lu} and Sc_{Al} centers. Allying the La^{3+} isoelectronic impurity in LuAP host results also in the appearance of TSL in the UV range with the low- and high-temperature peaks in TL glow curve at 380-385 K and 596-600 K. The energy of liberation of charge carriers from the respective traps is equal to 0.62-0.65 eV and 1-1.05 eV, respectively. Similarly to La^{3+} dopant, allying the Sc^{3+} impurity in LuAP host also results in the appearance of TSL in the UV range with respective high-temperature peaks in TL glow curves at 625-630 K with an energy of liberation of charge carriers of 1.29-1.35 eV.

Acknowledgements: The work was performed in the framework of 2016/21/B/ST8/03200 project.

[1] Yu. Zorenko, V. Gorbenko, T. Voznyak, T. Zorenko, M. Nikl, K. Nejezchleb. J. Lumin., 2008, 128, 595.

Luminescent Properties and Multi-Centres Formation in Ce-Doped $Ca_3Sc_2Si_3O_{12}$ Single Crystals

A. Shakhno[1,2], W. Gieszczyk[3], P. Bilski[3], T. Zorenko[1] and Yu. Zorenko[1]

[1]*Institute of Physics, Kazimierz Wielki University in Bydgoszcz, 85090 Bydgoszcz, Poland*
[2]*Mechantronics Department, Kazimierz Wielki University in Bydgoszcz, 85-074 Bydgoszcz, Poland*
[2] *Institute of Nuclear Physics, Polish Academy of Sciences in Krakow, 31345 Krakow, Poland.*

Today, white LEDs (WLEDs) are widely used for lighting applications due to their remarkable properties such as high efficiency, long lifetime and ecologically friendliness in comparison to the conventional light sources. Currently, the most known type of WLEDs is the combination of blue LED chip and yellow–emitting YAG:Ce photoconverters (pc). Although this garnet has a good thermal stability of the Ce^{3+} photoluminescence at high temperatures, nowadays alternative phosphors are still being sought for due to the lack of red emitting component in YAG:Ce pc [1]. $Ca_3Sc_2Si_3O_{12}$:Ce (CSSG:Ce) silicate garnet is one of the most interesting alternative phosphor to YAG:Ce that meets these requirements [2]. Possibility of practical application of these materials in the form of single crystals (SCs) and single-crystal films (SCFs) of these mixed garnets as lasers, cathodoluminescent materials, scintillators, and also white LED pc require detail study of the optical properties of these materials [2, 4].

In this work, the crystal of CSSG:Ce garnet was crystallized from the melt by a micro-pulling-down method in Ar atmosphere. The grown crystal was performed at a pulling rate of 1.5 mm/min using piece of Al_2O_3 crystal as a seed crystal. During the whole growth experiment, the volumetric flow rate of argon was around 20 l/min. The samples were characterized also by cathodoluminescence(CL) and photoluminescence (PL). The luminescent properties of CSSG:Ce crystal were compared with the reference YAG:Ce SC as well as with properties of CSSG:Ce single crystalline film and micro-powder counterparts [2,3].

We have observed the positive trends in variations of the CSSG:Ce SC spectroscopic properties due to the substitution of dodecahedral sites of garnet host by Ca^{2+} and octahedral positions by Sc^{3+} ions and the tetrahedral positions by Si^{4+} ions, which can be suitable for the development of pc-WLEDs [2].

We have also observed the formation at least two Ce^{3+} centers in the $Ca_3Sc_2Si_3O_{12}$:Ce crystals in their PL emission and excitation spectra and PL decay kinetics of the Ce^{3+} luminescence. This is mainly caused by the location of Ce^{3+} ions in the dodecahedral sites of Ca^{2+} and Y^{3+} cations with different crystal field strengths. Such Ce^{3+} multicenters in the mentioned dodecahedral positions of the garnet host possess additional local asymmetry due to the heterovalent substitution of the octahedral sites by Sc^{3+} ions and the tetrahedral sites by Si^{4+} ions. Based on the results of optical investigations, the luminescent characteristics of different Ce^{3+} based multicenter were estimated.

Acknowledgements: The work was performed in the framework of 2017/25/B/ST8/02932 project.

[1] S. Hu, C. Lu, G. Zhou, X. Liu, X. Qin, G. liu, S. Wang, Z. Xu, Ceramics International 42 (2016) 6935–6941
[2] I. Levchuk, A. Osvet, C.J. Brabec, M. Batentschuk, A. Shakhno, T. Zorenko, Y. Zorenko, Optical Materials 107 (2020) 109978.
[3] V. Gorbenko, T. Zorenko, S. Witkiewicz, K. Paprocki, A. Iskaliyeva, A.M. Kaczmarek, R. Van Deun, M.N. Khaidukov, M. Batentschuk, Y. Zorenko, Journal of Luminescence 199 (2018) 245–250.
[4] T. Kato, Y. Usui, G. Okada, N. Kawaguchi, T. Yanagida, Nuclear Instruments and Methods in Physics Research Section A: Accelerators, Spectrometers, Detectors and Associated Equipment 954 (2020) 161301.

Energy Transfer Processes in LuAG:Ce,Pr Single Crystalline Film Scintillators

A. Majewski-Napierkowski[1], P. A. Douissard[2], T. Martin[2], T. Zorenko[1], S. Witkiewicz-Łukaszek[1] and Yu. Zorenko[1]

[1]*Institute of Physics, Kazimierz Wielki University in Bydgoszcz, 85-090 Bydgoszcz, Poland*
[2]*ESRF- The European Synchrotron, 71, Avenue des Martyrs, 38043 Grenoble, France*

The single crystalline film (SCF) scintillating screens based on the different heavy oxide compounds are key part of high resolution X-ray detectors in the microtomography devices [1]. The Ce^{3+} and Pr^{3+} doped garnet compounds shows fast and efficient luminescence in the visible and UV ranges, respectively, due to the allowed 5d-4f transitions of these ions [2]. That makes them often used for the detection of high energy particles and X- or γ-rays [1, 2]. Among many heavy hosts, $Lu_3Al_5O_{12}$ (LuAG) garnet is also prospective SCF materials [3, 5], extending order of currently used SCF screens based on the $Gd_3Ga_5O_{12}$:Eu or Tb garnets [1] and Lu_2SiO_5:Tb orthosilicate [4].

This work is dedicated to the investigation of the energy transfer processes between Ce^{3+} and Pr^{3+} ions and their influence on the luminescent and scintillation properties of the LuAG:Ce,Pr SCFs, grown by Liquid Phase Epitaxy (LPE) method from overcooled melt-solution based on the PbO-B_2O_3 flux onto undoped LuAG substrates [5]. The concentration of CeO_2 and Pr_4O_7 activating oxides in the melt-solution was 10 and 1.5 mole % respectively. For study the energy transfer processes, the measurements of the absorption, cathodoluminescence, photoluminescence (PL) emission and excitation spectra as well as PL decay kinetics of LuAG:Ce and LuAG:Ce,Pr SCF samples were performed.

Based on obtaining results, we have shown presence of the direct $Pr^{3+} \rightarrow Ce^{3+}$ and backside $Ce^{3+} \rightarrow Pr^{3+}$ energy transfer processes in LuAG:Ce, Pr SCFs due to overlapping the respective 4f-5d and 4f-4f absorption and emission bands of Ce^{3+} and Pr^{3+} ions (Figure).

Apart decrease of the overall scintillation intensity, the Pr^{3+} alloying leads also to faster scintillation response and lower afterglow level of LuAG:Ce,Pr SCF scintillators with respect to LuAG:Ce SCF counterparts.

Acknowledgements: The work was performed in the frame of Polish NCN 2018/31/B/ST8/03390 project.

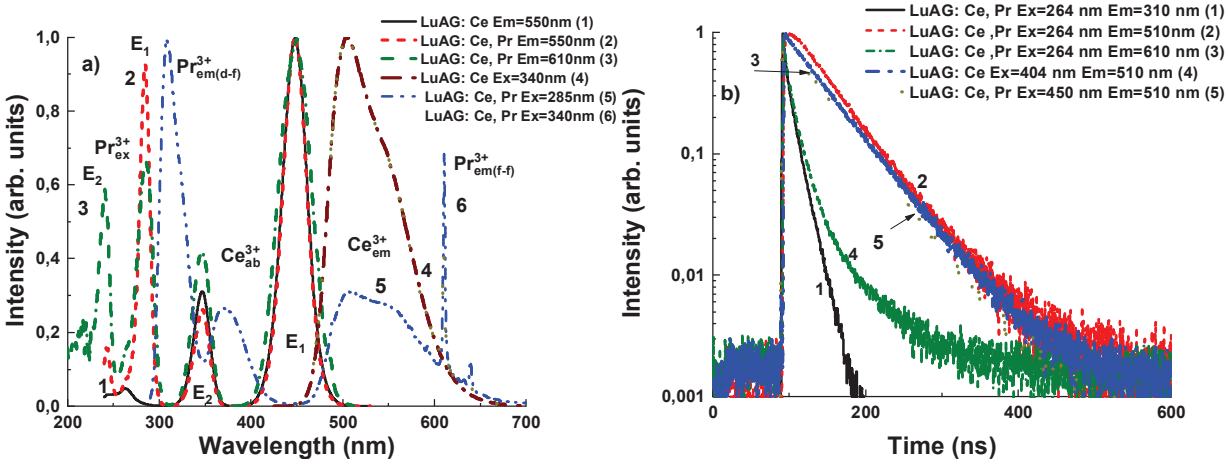

Fig. PL excitation and emission spectra (a) and decay kinetic (b) of LuAG:Ce and LuAG:Ce, Pr SCFs under registration of the Ce^{3+} and Pr^{3+} luminescence.

[1] T. Martin, A. Koch, Journal of Synchrotron Radiation, vol. 13, pp.180-194, 2006.
[2] P. Douissard, T. Martin; F. Riva, et al., IEEE Transactions on Nuclear Science, 63 (2016) 1726.
[3] M. Nikl, J. Tous, J. Mares, P. Prusa, E. Mihokova, K. Blazek, et al., Proc. SPIE, 7310 (2009) 731007.
[4] P. Douissard, T. Martin; F. Riva, et al., IEEE Transactions on Nuclear Science, 63 (2016) 1726.
[5] P.A. Douissard, A. Cecilia, T. Martin, V. Chevalier, M. Couchaud, et al., J. Synch. Radiation, 17 (2010) 571.

Recombination Luminescence of Zinc Tungstate Crystals Doped with Lithium, Terbium and Neodymium

L. Kostyk, V. Kapustyanyk, S. Novosad, I. Novosad and M. Rudko

Ivan Franko Lviv National University of Lviv, Ukraine

Zinc tungstate (wolframite-type crystals, space group *P2/c*) with a width of the band gap of $E_g \approx 4.6$ eV has a monoclinic crystalline structure of wolframite-type [1]. High energy resolution, low level of radioactive background and good signal resolution by particle types make $ZnWO_4$ suitable for searching for double beta decay of isotopes of zinc and tungsten, study of alpha decays of tungsten isotopes, as well as for use as a dark matter particle detector [2-4].

Results of comparative studies of the spectral-luminescence characteristics of $ZnWO_4$, crystals and $ZnWO_4$:Li, $ZnWO_4$:Tb, $ZnWO_4$:Nd samples after their long-term storage under laboratory conditions in an air atmosphere are analyzed in the paper.

For the present investigation the $ZnWO_4$ and $ZnWO_4$:Li crystals grown by the Czochralski method were used [1]. Doping impurities in the form of Li_2O, Tb_2O_3 and Nd_2O_3 oxides were entered into the charge in the amount of 0.5 - 1 mol.%. Samples in a thickness of 10-15 mm were obtained by cleaving the grown crystals in a (100) plane. Spectroscopic investigation of samples in the case of X-ray excitation was carried out in helium cryostat with the using a setup based on the MDR-12 diffraction monochromator.

Steady-state X-ray luminescence spectrum of $ZnWO_4$ at 90 K is represented by a non-elementary band with a maximum near 480 nm. With an increase temperature from 90 to 300 K, the emission of the $ZnWO_4$ sample decreases by about 30%, with a shift of its maximum up to 470 nm. The doping of $ZnWO_4$ with impurity mainly affects the intensity of X-ray luminescence and practically does not change the spectral composition of the radiation of the matrix.

X-ray luminescence (XRL) spectra of the investigated materials can be represented as a superposition of several partially overlapping basic elementary bands with maxima at about 440 nm (2.84 eV), 480 nm (2.59 eV) and a relatively weak band of 600 nm (2.04 eV). A typical intrinsic luminescence band with a maximum at 480 nm, which is dominant in the XRL spectrum, is caused by the radiative decay of self-trapped excitons of oxyanion complex WO_6^{6-}. The bands with a maximum at about 440 and 600 nm are associated with radiation in oxyanion groups, located near defective complexes containing cation and anion vacancies, respectively.

The TSL curve after X-ray excitation of $ZnWO_4$ crystal is characterized by a superposition of weak peaks at 107, 129, 152 and 170, 200 and 235 K of different intensities. Doping impurities leads to modification of the TSL curve of $ZnWO_4$ crystal. The TSL curve of the ZnWO4 doped with lithium is represented by a non-elementary intense peak at 129 K, lower-intensity peaks at 129 and 170 K, and two weak peaks in the 190-250 K region. The TSL curve of the ZnWO4: Tb crystal is characterized by a dominant peak at 131 K and low-intensity peaks at 197 and 234 K. A weak peak at 120 K is observed on the TSL curve of the ZnWO4: Nd crystal. The effect of these impurities on the luminescent properties of ZnWO4 was discussed.

[1] L.N. Lymarenko, A.E. Nosenko, M.V.Pashkovskii, D.-L.L. Futorskii, Effect of structural defects on the physical properties of tungstate, Lvov, 1978, 160 p. (in Russian).

[2] M.E. Globus, B.V. Grinyov, Inorganic scintillation crystals. New and traditional materials, Akta, Kharkov, Ukraine, 2001, 408 p. (in Russian).

[3] Belli P. Search for 2-beta processes in Zn^{64} with the help of $ZnWO_4$ crystal scintillator / P. Belli et. al. // Phys. Lett. B – 2008. – Vol. 658. – P. 193–197.

[4] Bavykina I. Development of cryogenic phonon detectors based on $CaMoO_4$ and $ZnWO_4$ scintillating crystals for direct dark matter search experiments / I. Bavykina et. al. // Optical materials. – 2009. – Vol. 31. – P. 1382–1387.

Luminescent Properties of $Zn_xCd_{1-x}WO_4$ Solid Solutions

N. Krutyak[1,2], V. Nagirnyi[2], D. Spassky[2,3] and B. Zadneprovski[4]

[1]*Physical Department, M.V. Lomonosov Moscow State University, Russia*
[2]*Institute of Physics, University of Tartu, Estonia*
[3]*Skobeltsyn Institute of Nuclear Physics, M.V. Lomonosov Moscow State University, Russia*
[4]*All-Russian Research Institute for Synthesis of Materials, Russia*

A wide range of scintillator applications sets demands for the improvement of existing and search of novel scintillation materials [1]. Alkali-earth and transition metal tungstates are of particular interest due to their attractive luminescent properties. Solid solutions (or mixed crystals) based on tungstates can combine the structural and luminescence properties of their constituents, thus advancing the performance of scintillation material. Since the values of the lattice parameters and cations ionic radii are close in $CdWO_4$ and $ZnWO_4$, these compounds can form a complete succession of solid solutions [2, 3]. The luminescent properties of $Zn_xCd_{1-x}WO_4$ crystals have been poorly studied so far. Here, we present the results of the study of the effect of cationic substitution on the luminescence properties of $Zn_xCd_{1-x}WO_4$ solid solutions. Such investigations conform with recent trends in radiation detector technologies where the most of the suggested novel scintillation materials belonged to mixed crystals.

A series of $Zn_xCd_{1-x}WO_4$ crystals were obtained by spontaneous crystallization from a solution of ZnO, CdO and WO_3 oxides in a NaCl melt. The cation composition of the crystals was varied from $x = 0$ to 1.0 with a step of 0.1. According to XRD analysis, all samples are characterized by a single phase of wolframite. Emission and luminescence excitation spectra, as well as temperature dependences of the luminescence were studied in the temperature range 77–500 K using a laboratory setup based on a LOT-Oriel MS-257 spectrograph.

It was found that in all the studied $Zn_xCd_{1-x}WO_4$ ($x = 0$–1) crystals, only intrinsic luminescence associated with the radiative decay of self-trapped excitons was detected. The dependence of the emission band shape and the position of the fundamental absorption edge on the concentration of substitutional cations **x** is demonstrated. The threshold of the excitation spectrum is shown to shift to the low-energy region when temperature is increased. At temperatures exceeding 250 K the intensity of intrinsic luminescence of $Zn_xCd_{1-x}WO_4$ crystals decreases due to temperature quenching. A linear dependence of the activation energy of the thermal quenching process on the concentration of substitutional cations is demonstrated. A comparative analysis of the obtained results with those for zinc-magnesium tungstate is carried out.

The research was performed within the project MOBJD613.

[1] Dujardin C. Inorganic scintillating materials // Techniques de L`Ingenieur. 2018. V. 1. P. 1-12.
[2] Dahlborg M.A., Svensson G. Structural Changes in the system $Zn_{1-x}Cd_xWO_4$, determined from single crystal data // Acta Chemica Scandinavica. 1999. 53 (12). P. 1103-1109.
[3] Zhang J. et al. Structural investigation and scintillation properties of $Cd_{1-x}Zn_xWO_4$ solid solution single crystals // CrystEngComm. 2015. 17 (18). P. 3503-3508.

Investigation of the Optical Activity of $Ca_3Ga_2Ge_4O_{14}$ Crystals

N. Ftomyn[1] and Y. Shopa[2]

[1]*Ivan Franko National University of Lviv, Faculty of Physics, Department of General Physics, 19 Drahomanov Street, 79005 Lviv, Ukraine, nazar.ftomyn@lnu.edu.ua*
[2]*Cardinal Stefan Wyszyński University in Warsaw, 5 Dewajtis Street, 01-815 Warszawa, Poland, i.shopa@uksw.edu.pl*

$Ca_3Ga_2Ge_4O_{14}$ crystals (space symmetry group $P321$, $Z = 1$) belong to family of langasite ($La_3Ga_5SiO_{14}$) and attract great interest of researchers as materials with a unique combination of physical properties. In is well known that the $Ca_3Ga_2Ge_4O_{14}$ crystals have complicated structure (these materials belong to the disordered systems). The studies of the optical activity are very important because this phenomenon is usually associated with some peculiarities of structural units of the investigated crystals.

As a matter of fact, that the HAUP-method (High-accuracy universal polarimeter) manifests itself as a most sensitive and universal for measuring optical effects. A value of the gyration tensor component g_{11} have already been measured for investigated systems at $\lambda = 780$ nm [1]. As a result, the aim of the present work is to determine the dispersion of the optical activity in the direction perpendicular to the optical axis of the $Ca_3Ga_2Ge_4O_{14}$ by means of HAUP-related polarimetric measurements at least for several fixed wavelength of light. The experiments were performed with the aid of a computer-controlled laser polarimeter ($\lambda = 532$ nm, 635 nm). The optical scheme of the polarimeter includes a minimal quantity of optical components: a polarizer, specimen and analyzer, thus forming the PSA system. The method involves the measuring the optical transmission of the PSA system. In the same time the optical parameters of investigated crystals (e.g., the optical rotatory power $\rho(\mathbf{k})$) may be calculated theoretically using the equation suggested in the study [2, 3]:

$$\rho(\mathbf{k}) = -\frac{e_{rij}k_r}{2nv}\,\mathrm{Im}\sum_{SS'}\left(C_{SS'}\right)_{ij} \qquad (1)$$

Here $\mathbf{k}$ denotes the wave vector, e_{rij} the Levi–Civita symbol, n the refractive index, v the unit-cell volume, δ_{ij} the Kronecker symbol, $C_{SS'}$ complex tensors, and S the index referred to different atoms in the crystalline structure.

Using dispersion of the electronic polarizability volumes calculated with the Lorentz–Lorenz formula, the spectral dependence of the optical activity in the direction perpendicular to the optical axis was calculated in the wide spectral region (400-800 nm).

Finally, the computations based on dipole-dipole interaction model [3] applied to determining the optical activity of $Ca_3Ga_2Ge_4O_{14}$ crystals will allow to compare the experimental results with theoretical calculations.

[1] Shopa Ya. Optical activity of $Ca_3Ga_2G_4O_{14}$ crystals: experiment and calculus / Ya. Shopa, N. Ftomyn, // Optica Applicata – 2013. – Vol. XLIII, No 2. – P. 217-228.
[2] Kaminsky W. Experimental and phenomenological aspects of circular birefringence and related properties in transparent crystals / W. Kaminsky // Rep. Prog. Phys. – 2000. – Vol. 63. – P. 1575–1640.
[3] Devarajan V. Theory and computation of optical rotatory power in inorganic crystals / V. Devarajan., A.M. Glazer // Acta. Cryst. – 1986. – A 42. – P. 560–569.

Refractive and Dilatometric Properties of Doped K_2SO_4 Crystals

R. Matviiv[1], V. Stadnyk[1], R. Brezvin[1], P. Shchepanskyi[1,2] and R. Kildiyarov[1]

[1]*Ivan Franko National University of Lviv, Str. Kyrylo and Mefodiy 8, 79005, Lviv, Ukraine,*
[2]*Jan Dlugosz University in Czestochowa, Al. Armii Krajowej 13/15, 42-200 Czestochowa, Poland*

Potassium sulfate (PS) crystals K_2SO_4 are typical representatives of dielectric ferroics that have a number of phase transitions with spontaneous deformation as order parameter. These crystals have specific physical properties allowing them to be used in electromagnetic radiation control devices. In order to expand the application capabilities of these crystals, it is necessary to modify their physical properties. One of the available methods of changing the properties of crystals is to introduce substitutional impurities. Therefore, the purpose of this work is to investigate the effect of Cu^{2+} transition metal impurity on the refractive and dilatometric properties of PS crystals.

The crystals studied were obtained by slow evaporation at constant temperature from an aqueous solution of salts of pure K_2SO_4 and $CuSO_4 \cdot 5H_2O$ copper sulfate crystalline hydrate with a mass 1.7% of the total mass of dissolved salts. The dispersion dependences of the refractive indices $n_i(\lambda)$ and the temperature-spectral changes of birefringence Δn_i (λ,T) were investigated by Obreimov interference-polarization methods. The introduction of impurity was established to significantly change the absolute value of Δn_i, without changing the character of the dispersion $|\partial\Delta n_x/\partial\lambda| > |\partial\Delta n_y/\partial\lambda| > |\partial\Delta n_z/\partial\lambda|$. However, a significant change in the magnitude of the Δn_i variance on the wavelength scale is observed. The refractive indices n_i decrease by approximately 0.001...0.002, while the relationship between their values and the dispersinal changes $n_z > n_x > n_y$, $dn_z/d\lambda > dn_x/d\lambda > dn_y/d\lambda$ remain unchanged. Since the refractive index n_x decreases the most (the *X*-direction corresponds to the direction perpendicular to the plane of the optical axes), the overall size and anisotropy of the optical indicatrix of the crystal decreases with the introduction of the impurity.

The thermal expansion $\Delta l/l_i$ of the doped PS crystals was measured using a quartz dilatometer. The largest temperature changes in the sample sizes were detected in the *a*-direction, which corresponds to the direction of the acute bisectrix of the angle between the optical axes. Here, the value $\Delta l/l_c$ after $T \sim 300$ K increases almost exponentially. Thermal expansion along the *b*- and *c*-directions is relatively slow and almost linear. The magnitudes of the linear expansion coefficients in these directions are almost equal to each other within the experiment error. The expansion along the *a*-direction is highly anisotropic compared to the *b*- and *c*-directions ones.

It is found that the introduction of impurities leads to a slight decrease in the value of $\Delta l/l_i$. These changes indicate that the copper impurity leads to the increasing of the structural units in the unit cell and to the increase in the rigidity in the doped crystal comparing to the nominally pure one. At the phenomenological level, these changes can be explained by the influence of internal stresses occurring in the doped crystal, which can be considered as similar to the influence of uniaxial or hydrostatic pressures.

Spatial Anisotropy of Electromechanical Coupling in $Li_2B_4O_7$ Crystals

D.M. Vynnyk[1], M.V. Kaidan[2], A.S. Andrushchak[2] and B.M. Strykhaluik[2]

[1]*Scientific Research Company ''Electron-Carat'', 202 Stryjska Str., 79031 Lviv, Ukraine*
[2]*Lviv Polytechnic National University, 12 S. Bandery Str., 79013 Lviv, Ukraine*
mykola.v.kaidan@lpnu.ua

In this research we study the electromechanical coupling coefficients in $Li_2B_4O_7$ crystals. The coefficient of electromechanical coupling - expresses the degree of connection between the electrical and mechanical properties of piezoelectric material and characterizes its ability to convert electrical energy into mechanical and on the contrary [1]: $k_m^2=P_a/P_e$, where P_a - power of acoustic wave developed by piezoelectric as a result of piezoelectric effect; P_e - electric power consumed by a piezoelectric material from the source, which generate the voltage.

For spatial anisotropy research we used an algorithm for constructing the indicative surfaces of electromechanical coupling coefficients for a particular direction of radius vector [2]. The proposed algorithm is a following: 1) choose the particular radius vector direction which coincides with the direction of acoustic waves propagation; 2) determine three speeds of acoustic waves by using the Green-Christophe's equation [1,2]; 3) determine the direction of each acoustic wave polarization by substituting the obtained values from the velocities in the Green-Christophe's equation; 4) determine the coefficient of electromechanical coupling to study its spatial distribution by substituting the values of radius vector direction ($\alpha_{r1}=\sin\theta\cos\varphi$, $\alpha_{r2}=\sin\theta\sin\varphi$, $\alpha_{r3}=\cos\theta$, where φ and θ- spherical coordinates) and the direction of acoustic wave polarization obtained in the previous step.

The indicative surfaces for coefficients of electromechanical coupling in $Li_2B_4O_7$ crystals have been obtained first time. These surfaces were constructed using piezoelectric stress constants [3-6], elastic constants [3-5, 7], density [3, 8] and dielectric constants [3-6, 8, 9].

On the basis of parameters from different articles, the directions of efficient use of $Li_2B_4O_7$ crystal for acoustic device have been determined. For the transverse polarization, the maximum coefficient of electrical communication is from 0.16 to 0.3, and for the longitudinal polarization from 0.36 to 0.42, depending on the different articles [3-9]. The maximum coefficient of electrical communication for the longitudinal polarization is in the direction of the axe X_3 (Fig). For the fast transverse acoustic waves of the maximum coefficient of electrical communication observes along the axis X_1, but with the slow of transverse acoustic waves of the maximum is on the plane X_1X_3 where the angle of deviation from the X3 axis is from 20.34 to 25.38 depending on the different articles [3-9]

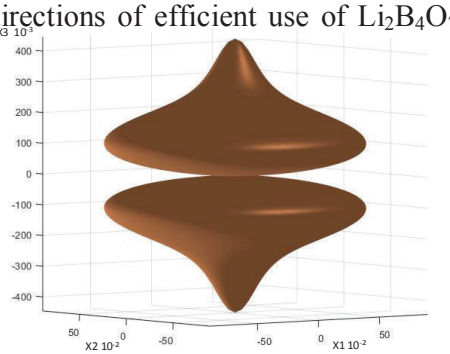

Fig. The surfaces for coefficients of electromechanical for the longitudinal polarization

[1] E. Dieulesaint, D.Royer: Elastic waves in solids: applications to signal processing. Chichester, J. Wiley, 1980.
[2] M.V.Kaidan, Herald Lviv Polytechnic National Univ «Radio electronics and telecommunications», 846, 185-193 (2016).
[3] L.Bohaty *et al.*, Cryst.Rest Technol, 24, P.1159 (1989).
[4] N.M. Shorrocks *et al.*, Proc. IEEE Ultras. Symp., 34, P.337 (1981).
[5] M. Adachi *et al.*, Proc. IEEE Ultras. Symp., P.228 (1985).
[6] J.Wang *et al.*, Chinese J.Acoust., 9 P.123 (1990).
[7] H.A.A.Sidek *et al.,* J.Phys. Chem.Comm., 51 P.457 (1990).
[8] T. Shiosaki *et al.*, Jpn J.Appl.Phys., 24 P. 25 Suppl. 24-1 (1985)
[9] K. Fukuta *et al.*, Jap.J.Appl.Phys., 22, Suppl. 22-2, P. 140 (1983)

Modulation of Terahertz Radiation by Bismuth Germanate Crystals

N. Andrushchak[1], D. Vynnyk[1], M. Melnyk[2], P. Bajurko[3], J. Sobolewski[3], V. Haiduchok[4], A. Andrushchak[1] and E. Yashchyshyn[3]

[1]*Lviv Polytechnic National University, 12 S. Bandery str., Lviv, 79013, Ukraine, email: nazariy.a.andrushchak@lpnu.ua*
[2]*Lviv Center for Space Research Institute of the National Academy of Sciences of Ukraine, 5A Naukova str., Lviv 79060, Ukraine, email: melnykmo@isr.lviv.ua*
[3]*Warsaw University of Technology, Pl. Politechniki 1, Warsaw 00-661, Poland, email: e.jaszczyszyn@ire.pw.edu.pl*
[4]*Scientific Research Company «Electron-Carat», 202 Stryysyka str., Lviv 79031, Ukraine, email: haiduchok@ukr.net*

Currently, the terahertz frequency range of electromagnetic radiation is of considerable interest [1], since terahertz waves are used in various fields of science and technology. For the effective development of the terahertz technique, a component base is required. One of the essential components is devices for controlling such parameters of the terahertz wave as amplitude, frequency, phase, polarization are the so-called modulators. Developing effective terahertz modulators is quite a challenge. This is partly due to the difficulty of using conventional light modulation techniques in this field. Creating a classic phase or amplitude modulator requires excessively large crystal sizes to form the basis of the modulator. One way to achieve modulation in the terahertz frequency range is to optically modify the modulation properties of the modulator material. Photogeneration of media by a beam of optical radiation, which lies in the field of absorption of the material leads to a change in their mobility and, as a consequence, to a change in the conductivity. Such a change contributes to the modulation process when the terahertz radiation passes through the material.

Bismuth germanate (BGO) crystals are high-ohmic semiconductor electro-optical crystals sensitive to optical radiation in the field of absorption of this crystal [2]. The possibility of modulation of sub-terahertz radiation in the frequency range 200 ÷ 300 GHz by a modulator based on BGO crystal was investigated. The modulator consists of a 500 μm polished BGO plate, the surface of which was parallel to the plane [111]. A transparent conductive ITO coating was applied on the opposite polished faces by vacuum deposition. The plate was placed in a Teflon housing. Welded contact conductors were welded to the opposite faces of the plate where the conductive coating is located outside the housing. The modulation characteristics of the modulator are studied depending on the illumination time and the applied voltage. The obtained results of the measurements are analyzed.

[1] Terahertz Techniques, Springer:Verlag Berlin Heidelberg, 2012, p.310.
[2] Determination of the mobility and transport properties of photocarriers in $Bi_{12}GeO_{20}$ by the time-of-flight technique, Journal of Applied Physics, 1993, 74(4), p.2180 – 2191.

Optically Stimulated Luminescence of MgB_4O_7 Doped with Ce^{3+} and Gd^{3+}

W. Abusaid[1], V. Altunal[1*], A. Ozdemir[2], V. Guckan[1], A. Ekicibil[1], F. Karadag[1] and Z. Yegingil[1]

[1]*Cukurova University, Art Sciences Faculty, Department of Physics, 01330 Adana, TURKEY*
[2]*Kahramanmaras Istiklal University, Elbistan Vocational High School of Health Service, Elbistan, Kahramanmaras, Turkey*
[*]*Corresponding E-mail: valtunal@cu.edu.tr*

This work aims to investigate the luminescent signals of $MgB_4O_7:Ce^{3+},Gd^{3+}$ phosphors at different molar concentrations and to improve the radiation sensitivity of the material. MgB_4O_7 samples were prepared and doped with Ce^{3+} and Gd^{3+} by the solid-state synthesis method. Luminescent signals from the $MgB_4O_7:Ce^{3+},Gd^{3+}$ powders were characterized by the Optically Stimulated Luminescence (OSL) and Thermoluminescence (TL) techniques. After the concentration quenching study, results showed that the highest OSL and TL sensitivities were obtained from the 0.1 % dopant concentration of Ce^{3+} and 3 % dopant concentration of Gd^{3+}. While the TL glow curve of the $MgB_4O_7:Ce^{3+},Gd^{3+}$ sample exhibited the four TL peaks, the OSL decay curve had two decay components. As a result of step annealing experiments, it was found that the origin of the OSL signals is associated with the TL traps located between 150 and 250 °C. With the superior properties, such as, the dose linearity up to 100 Gy beta doses, reusability in 20 experimental cycles, and minimal fading in 1 month, $MgB_4O_7:Ce^{3+},Gd^{3+}$ samples are candidate dosimeters for radiation dosimetry in 2D applications.

Acknowledgements. This work was supported by the NATO SPS MYP program under project number G5647 and Cukurova University Research Projects Development and Coordination Unit under the project numbers FDK-2018-10190, FAY-2019-11571, and FAY-2020-12932, FBA-2020-13126. The authors thank NATO and Cukurova University for supporting this research.

OSL Properties of $CaSO_4$:Tb,Eu Phosphor for Dosimetric Purpose

S. Bereket[1], V. Guckan[1*], V. Altunal[1], W. Abusaid[1], A. Ozdemir[2] and Z. Yegingil[1]

[1]*Cukurova University, Art Sciences Faculty, Department of Physics, 01330 Adana, TURKEY*
[2]*Kahramanmaras Istiklal University, Elbistan Vocational High School of Health Service, Elbistan, Kahramanmaras, Turkey*
[*]*Corresponding E-mail: veysiguckan@gmail.com*

In this study, Tb and Eu doped $CaSO_4$ luminescent phosphor was synthesized using the precipitation method. The rare earth elements Tb and Eu were used as doping ions to enhance the OSL properties. The structure analysis of $CaSO_4$:Tb,Eu was examined by X-ray diffraction (XRD) and Scanning Electron Microscope (SEM) methods to ensure that the product matched with the planned material and to have an idea about the morphology of the synthesized material. Spectroscopic analysis was carried out using radioluminescence (RL) technique. We recorded the thermoluminescence (TL) glow curve, and optically stimulated luminescence (OSL) decay signal and studied the luminescence characterization. The reusability of the samples was confirmed within an acceptable range of deviation (±4% for 20 cycles). The dose-response curve of the samples was tested and a linear increase up to 20 Gy was observed. The stability of the OSL signal in the dark environment of the samples was tested and it was observed that at the end of one month it showed a decrease of 11% compared to the initial signal. In addition to dosimetric analyses, we investigated the relationships between the Thermoluminescence and OSL trap group of the $CaSO_4$:Tb,Eu sample using step-annealing measurement. In this study, the basic dosimetric properties of newly doped $CaSO_4$:Tb,Eu phosphor were investigated and it was shown that this material is a candidate dosimeter for applications in medicine.

Acknowledgements. Financial assistance from the NATO SPS MYP under the research contract number G5647 and the Cukurova University Research Projects Development and Coordination Unit under contract numbers FUA-2021-13936, FAY-2020-12932 and FBA-2020-13126 are gratefully acknowledged.

Afterglow Peculiarities of YAP:Mn Crystal Irradiated by X-Ray and Visible Radiation

O. Poshyvak[1], D. Afanassyev[1], A. Luchechko[1,2], Ya. Zhydachevskyy[1,3] and S. Ubizskii[1]

[1]*Lviv Polytechnic National University, Lviv, S. Bandera St, 12, 79013, Ukraine,*
[2]*Ivan Franko National University of Lviv, Universytetska St., 1, Lviv, 79000, Ukraine,*
[3]*Institute of Physics of the Polish Academy of Sciences, Al. Lotników, 32/46, Warsaw, 02-668, Poland*

Optically stimulated luminescence (OSL) is used last decades as novel method of passive luminescence dosimetry and an alternative to the traditional thermo-luminescence dosimetry [1]. One of the promising material for this application is crystalline $YAlO_3:Mn^{2+}$(YAP:Mn) [2,3]. But despite the similarity of physical processes during irradiation and stimulated luminescence the OSL has a number of features. In particular, in contrast to thermo-luminescence, in which thermal activation of shallow traps makes them inactive when deeper dosimetric traps start empting, the charge carriers released from the latter during optical stimulation can be recaptured not only on deep traps but also on shallow ones. This peculiarity leads to long-lasting afterglow. It was previously reported [4] that glow initiated by optical stimulation of pre-irradiated YAP:Mn has a hyperbola-like kinetics being described by Becquerel's empirical decay function [5].

The present work is devoted to investigation of the afterglow in YAP:Mn after X-ray irradiation in comparison with that occurred after blue light stimulation of the preliminary irradiated by the X-ray sample, i.e. at measurement of OSL. Experiments have shown that the afterglow can last and registered up to almost 5 days just after 30 s of X-ray irradiation (45 kV, 0.3 mA). Its initial level is saturating if the exposure time becomes more than 300 s. In both cases (X-ray irradiation and visible light stimulation) of the Becquerel-type kinetics of glowing take place in the time scale of seconds up to thousands of seconds. At the same time the initial part of OSL response in milliseconds range has different character. The ways for elimination of the afterglow phenomenon influence on the absorbed dose estimation from the OSL response are analyzed and discussed.

Acknowledgments. This work was supported by the NATO Science for Peace and Security Program (project G5647), National Research Foundation of Ukraine (grant 2020.01/0248) and Ministry of Education and Science of Ukraine (project 0119U002249).

[1] E.G. Yukihara, S.W.S. McKeever, Optically Stimulated Luminescence: Fundamentals and Applications, Willey (2011).

[2] Ya. Zhydachevskii, A. Suchocki, M. Berkowski, Ya. Zakharko, *Radiation Measurements*, 42 (2007) 625-627.

[3] Ya. Zhydachevskii, A. Luchechko, D. Maraba et al., *Radiation Measurements*, 94 (2016) 18-22.

[4] S. Ubizskii, D. Afanassyev, Ya. Zhydachevskii, et al., *2019 International Conference on Information and Telecommunication Technologies and Radio Electronics* (*UkrMiCo-2019*), Odesa, Ukraine.

[5] M.N. Berberan-Santos, E.N. Bodunov, B. Valeur, Chemical Physics, 317 (2005) 57-62.

Optical Characterization of Rare-Earth Doped Bi-Modified Borate Glasses

P. Zięba[1], P. Reizer[1], J. Mirus[1], B. Mahlovanyi[1], J. Szlęzak[1], J. Cebulski[1] and Y. Shpotyuk[1,2]

[1]*University of Rzeszow, 35-959, Rzeszow, Poland*
[2]*Ivan Franko National University of Lviv, 79000, Lviv, Ukraine*

The silica-based glasses such as 45S5 and S53P4 are well-known candidates for different biomedical applications including bone-bonding, due to their high biocompatibility [1]. In addition, these glasses are often employed for rare-earth doping and further use in photonic applications [2]. Nowadays, high attention is paid for scientific and technological development in seeking for new materials with improved properties and lower production cost. In this regard, borate glasses become of high interest due to the preferential thermodynamic properties. Thus, the main advantage of borate glass in comparison to silica is significantly lower glass transition, crystallization and melting points. In the case of borate glass, the glass transition temperature T_g is usually below 500-600 ^oC, while in the case of silica glass it is often above 900-1000 ^oC [3]. Moreover, the difference between the glass transition and crystallization temperatures is higher in certain borate glasses. Above mentioned advantages allow cost-effective and easier shaping of the borate glasses into different forms (fibers, etc). To significantly extend the application field of borate glasses the rare-earth doping should be applied. Due to numerous *4f-4f* and *4f-5d* electronic transitions of rare-earth ions, it is possible to obtain the emission in the wide range from *UV* to *IR*.

In this work, Bi-modified borate glass of $(B_2O_3)_{50-x}(AO)_{20}(Na_2O)_{30}(Bi_2O_3)_x$ composition (A=Ca, Sr, Mg) doped with rare-earth ions were prepared by the conventional melt-quenching method. Optical and luminescent properties were investigated. The shift of both bandgap and multiphonon cut-off edge was observed due to Bi-addition and alkaline earth metals substitution. The absorption and luminescence spectra were recorded for Er^{3+}, Dy^{3+} and Eu^{3+} doped glasses. The feasibility of photoluminescence enhancement by glass composition modification was demonstrated. The relationship between the glass structure and its optical properties was established.

[1] F. Baino, S. Hamzehlou, S. Kargozar, *J. Funct. Biomater.* **9** (2018) 1-26.
[2] G.C. Righini, C. Armellini, S. Berneschi, et al., *J. Non-Cryst. Solids* **353** (2007) 753-756.
[3] N.M. Bobkova, *Glass Phys. Chem.* **29** (2003) 501–507.

Optical and Luminescence Properties of Ce, Dy-Doped Lithium Borate Glasses

B. Mahlovanyi[1,2], A. Ozimek[1], A. Wnęk[1], A. Warchoł[1], A. Luchechko[2], J. Cebulski[1] and Y. Shpotyuk[1,2]

[1]*Institute of Physics, University of Rzeszow, 35-959, Rzeszow, Poland*
[2]*Ivan Franko National University of Lviv, 79000, Lviv, Ukraine*

Rare earth ions are widely used in lasers, scintillators, and phosphors. Depending on the application, there are different demands on the properties of the activator ions and on the host matrix. This work is devoted to the study of new luminescent materials, which consist of oxide glasses doped with rare earth ions of cerium and dysprosium in the valence state 3+.

Optical and luminescence properties of lithium borate glasses (B_2O_3)-(MO)-(Li_2O)–(Bi_2O_3) doped with Dy and Ce rare earth (RE) ions have been investigated. Three systems of these glasses with various oxides of alkaline-earth metals (M = Mg, Ca, Sr) doped with Dy_2O_3 and CeO_2 were obtained using a standard melt-quenching technique in the air atmosphere. The doping by RE ions was performed as single doping (glass with 1.0 mol. % of Dy_2O_3 or glass with 1.0 mol. % of CeO_2) and co-doping (glass with 0.5 mol. % of Dy_2O_3 and 0.5 mol. % of CeO_2).

The optical and luminescent properties of obtained RE-doped glasses were studied using UV/Vis/NIR spectroscopy (optical transmission and absorption spectra) as well as photoluminescence spectroscopy (excitation and emission spectra). The substitution of alkaline-earth metals (M) by Mg, Ca or Sr leads to the shift of optical bandgap which is observed in the region between 315 and 390 nm depending on the glass composition. The photoluminescence spectra of Dy – doped glasses reveal two intensive emission bands, which correspond to $^4F_{9/2} \rightarrow {}^6H_{15/2}$ (around 486 nm) and $^4F_{9/2} \rightarrow {}^6H_{13/2}$ (around 580 nm) transitions of Dy^{3+} ions. Ce-doped glasses show one broadband, which corresponds to $^2D \rightarrow {}^2F_{5/2}$ (around 340 nm) transition of Ce^{3+} ions. Peculiarities of excitation energy transfer between RE activator ions are established. These glasses are shown to be a promising host matrix for rare earth doping.

Effect of Metal Oxides on Structure and Properties of the Borate-Phosphate Glasses

N. Stus[1], S. Nedilko[1], S. Yablochkov[1], P. Teselko[1], V. Scherbatskii[1], M. Androulidaki[2], A. Papadopoulos[2], A. Manousaki[2], V. Sheludko[3] and O. Gomenyuk[3]

[1]*Taras Shevchenko National University of Kyiv, Kyiv, Ukraine*
[2]*Institute of Electronic Structure & Laser (IESL) of Foundation for Research & Technology Hellas (FORTH), Heraklion 711 10 Crete, Greece*
[3]*O. Dovzhenko Hlukhiv National Pedagogical University, Hlukhiv, Ukraine*

Materials and composites, which possess luminescent properties, have various fields of application: industry, science and technology, everyday life, etc. Some of them now are developed for advanced opto-electronic devices, white light-emitting diodes (WLED) and solar cells.

The alkali borate and alkali phosphate-borate glasses, containing glass-forming oxides B_2O_3 and P_2O_5, have lower melting points, than silicate glasses. These glasses have been studied for a long time; however, new applications require new compositions of glasses with appropriate properties. In particular, this concerns the search for new fluorescent coatings for diode sources of white radiation, etc.

It is common knowledge that oxides of polyvalent metals alter structure and properties of various oxide glasses and this concerns borate and phosphate-borate glasses too. That is why, the series of glasses with compositions of the common formulae $m$$Na_2O$ - $n$$B_2O_3$ -$k$$P_2O_5$: xMO - yRE (M = Mn, Zn, Ge, Pb; RE = Eu, Pr) were prepared and studied by us. The molar composition of alkali phosphate-borate glass-forming matrix was close to 40% Na_2O - 20% P_2O_5 40 % B_2O_3. The amount of the Mn, Zn,Ge or Pb was in the range of 1 – 25 mol%, while the RE ions content was 1 – 5 mas %.

All the samples were made by the melt-quenching procedure and we have found that melting temperature depends mainly on the $m/n/k$ ratio, while amount of the Mn, Zn,Ge or Pb influences microstructure and quality of the glasses.

Microstructure and local composition of the samples were studied by SEM. The glasses were characterized by XRD, DTA, IR- and UV-VIS spectroscopy, their luminescent properties were studied.

It was found that luminescence spectra are complex and they range from 400 up to 750 nm. Luminescence kinetic is complex too, and decay time differs for different spectral components.

The glasses doped with rare – earth elements also showed the luminescence caused by radiation transitions in the *f-f* shell of the $Eu^{3+}$and Pr^{3+} ions. So, the luminescence spectra of such samples are the superposition of the wide bands related with luminescence of the glass matrix and linear spectra caused by intrinsic radiation transitions in the RE ions.

The conclusion was made that glasses of mentioned compositions can be suitable for development of glass - ceramic luminescent coatings for WLEDs and other devices.

Optical Properties and Phase Transformation of Bismuth Phosphate-Molybdate Glasses

V. Chornii[1,2], S.G. Nedilko[2], K. Terebilenko[2], O. Alekseev[2], M. Lazarenko[2] and M. Slobodyanyk[2]

[1]*National University of Life and Environmental Sciences of Ukraine, 15 Geroiv Oborony st., 03041, Kyiv, Ukraine*
[2]*Taras Shevchenko National University of Kyiv, 64/13 Volodymyrska st., 01301, Kyiv, Ukraine*

Oxide glass and glass-ceramics have been considered as prospective functional materials for applications in up-conversion laser, optical display devices, and fiber amplifiers, light emitting diodes, etc [1, 2]. Molybdate glasses among oxide glasses of various compositions have relatively low glass transition temperature (T_g) and are quite transparent in the range of visible light. These characteristics are valuable for elaboration of optical glass-ceramics on the base of those glasses by low-temperature co-sintering procedure. Unfortunately, the molybdate glasses are highly prone to crystallization at temperatures close to T_g because MoO_3 does not belong to glass-forming oxides. That is why, some glass-forming oxides (e.g. P_2O_5) incorporation to initial composition can assist in avoiding of unwanted glass crystallization.

The sets of undoped and Eu^{3+}- doped glasses of xK_2O-yP_2O_5-$zMoO_3$-$(100-x-y-z)Bi_2O_3$ composition (x = 26.85 – 48.41, y = 23.01 – 40.31, z = 13.55 – 46.02) were prepared by fast cooling of the molten salts. The calculated amounts of the analytically pure KH_2PO_4, Bi_2O_3, MoO_3 and Eu_2O_3 reagents were thoroughly grinded in agate mortar. Obtained mixtures were heated to 950 °C, kept at the temperature during 3 hours, the homogeneity of the each melt has been reached up to this time. Then, the melts were poured on a cooper sheet. The obtained in such way pieces of glasses were optically homogenous “on eye”, quite transparent with yellowish or orange undertones. The samples were characterized by means of optical, SEM and scanning force microscopy. The X-ray powder diffraction, differential scanning calorimetry, thermogravimetric analysis, IR and luminescence spectroscopy were also used under study.

The XRD patterns consist of three wide bands near 18°, 28° and 48° of 2Θ, respectively. The thermogravimetric analysis has shown that samples loss up to 4% of initial mass during heating to 600 °C. The highest loss of mass was observed for the samples with the highest P_2O_5 content (40.31 mol. %) and was related with moisture of the samples, which is inherent for some classes of phosphate-based glasses [3]. It was found that glassing temperature for the samples lie in 392 – 469 °C and the crystallization peaks are in 425 – 498 °C temperature range. Un-doped glasses reveal weak luminescence at room temperature when excited by laser radiation with λ_{ex} = 405 nm. The photoluminescence (PL) spectra of the all un-doped samples consist of wide two-component band with maxima near 580 and 660 nm. The peaks of the $^5D_0 \rightarrow {}^7F_2$ radiation transitions in the Eu^{3+} ions dominates in the PL spectra of Eu - doped glasses when the PL was excited in the 250 – 560 nm spectral range and at room temperature. The most intensive band in PL excitation spectra corresponds to the $^7F_0 \rightarrow {}^5D_2$ electronic transitions in Eu^{3+} ions. The results have showed that studied glasses are perspective for elaboration of oxide glass-ceramic materials of good luminescence characteristics.

[1] D. Chen, et al. *Journal of the European Ceramic Society* 35 (2015) 859-869.
[2] I. Khan, et al. *Journal of Alloys and Compounds* 805 (2019) 896-903.
[3] R.K. Brown, et al. *MRS Bulletin* 23 (1998) 63-67.

Spectral and Kinetic Characteristics of the Cathodoluminescence of Thin Films Y_2O_3:Eu

O.M. Bordun, I.O. Bordun, I.M. Kofliuk, I.Yo. Kukharskyy and I.I. Medvid

Ivan Franko National University of L'viv,Ukraine,79005, Lviv, Dragomanova str. 50.
e-mail: bordun@electronics.lnu.edu.ua

Among materials for optoelectronics, luminescent materials that are used to create displays, scintillators, and means for recording and visualizing information are of particular importance. One of the most common crystalline phosphor matrices in the red luminescence region is Y_2O_3:Eu, which is studied in this work in the thin-film state. For the study, the cathodoluminescence (CL) method was used, which is characterized by high sensitivity to changes in the electronic structure of the material (impurity and structural defects).

Thin films of Y_2O_3:Eu with a thickness of 0.2 - 1.0 μm obtained by radio-frequency (RF) ion-plasma sputtering in an atmosphere of argon or oxygen. The activator concentration was 5 mol%, which according to [1] provides the maximum luminescence yield. After the deposition of the films, they were heat-treated in air at 950–1050 °C. X-ray diffraction studies showed the presence of a polycrystalline structure of films with a predominant orientation in the (222) plane. The form of the obtained diffraction patterns is practically similar to the diffraction patterns of pure Y_2O_3 films, which we showed in [2]. In this case, in the Y_2O_3:Eu films obtained under an argon atmosphere, the reflex from the (440) plane has a somewhat higher intensity. The investigation of CL properties was carried out in the regime of pulsed electronic excitation

The luminescence spectra and kinetic characteristics of CL decay in thin Y_2O_3:Eu films were studied. Narrow luminescence bands appear in the CL spectra of the films, due to internal internally center transitions between the electron shells within the Eu^{3+} activator. These bands are associated with the allowed magnetic dipole transitions $^5D_0$-$^7F_1$ (for Eu^{3+} ions in C_2 and C_{3i} sites of crystal lattice Y_2O_3:Eu) and the allowed electric dipole transitions $^5D_0$-$^7F_2$ (for Eu^{3+} ions only in C_2 sites). The wavelength of the maximum radiation is λ_{max} = 612nm, which corresponds to the red color of the glow. The investigation of the dependence of the intensity of CL from the energy of the excited electrons was carried out at different pulse durations of electron irradiation. Based on the shape of the CL spectra at various energies and current densities of electronic excitation, the possibility of the formation of irregular solutions of yttrium and europium oxide and the structural features of surface and bulk layers are shown. The CL decay time constant for a glow of 612 nm was determined, the value of which is in the range (1,8 – 4,1) ms. The obtained values of the constant CL decay time indicate that the luminescence of Y_2O_3:Eu in the region of 612 nm is due to the electric dipole transition between the energy levels $^5D_0$ – $^7F_2$. It is shown that this value is a complex function of the type of atmosphere of the film deposition, the duration of the exciting pulses and the exposure time. From an analysis of the obtained decay times, it was shown that the surface layers are structurally heterogeneous than the bulk layers.

[1] I.O. Bordun, O.M. Bordun, I.Yo. Kukharskyy, Zh.Ya. Tsapovska // Acta Physica Polonica A.- **133**, №4 (2018) 914 - 917.
[2] O.M. Bordun, I.O. Bordun, I.Y. Kukharskyy // *J. Appl. Spectrosc*.- **82,** №3 (2015) 390 - 395.

Anodic Alumina Membranes: Light Scattering Intensity Along the Pores as a Function of Incidence Angles

V. Yakovtseva, D. Shimanovich and V. Shulgov

Belarusian State University of Informatics and Radioelectronics

1. Introduction – Nanochannel-array materials have attracted considerable scientific and commercial attention due to their potential utilization in magnetic, electronic, and optoelectronic structures, and devices. Nanoporous anodic alumina was originally considered as insulating component of semiconductor silicon microchips with metal aluminum conductors. It can be developed by electrochemical anodizing of aluminum to get free membranes with thickness up to 1 mm. Depending on the anodization regimes, pore size can be made from a few nanometers to hundreds of nanometers. Though structural properties and basic electrochemical routes are subject of extensive research during last five decades, only in the recent years unique optical properties of nanoporous anodic alumina have been discovered: a high transmission along pores with simultaneous high reflection from cut-edges [1], an optical birefringence [2], etc. So, nanoporous anodic alumina films are promising to control a light propagation in liquid crystal display devices.

2. Experimental - The 100 μm thick 40×48 mm^2 sized aluminum foils were used as initial substrates. The back side of the samples was protected with a masking layer. The two-stage porous anodization was made from the front side of the sample. The pore diameter and spacing are dictated by parameters of the anodization process, specifically by the electrolyte composition and the anodization voltage. The masking layer was removed from the back side and the rest of aluminum foil was etched to get free-standing films of porous alumina. Then the light transmission through porous anodic alumina membranes was studied. For comparison, a commercial Kimoto PF-90S M/M (K) holographic scattering film was used.

3. Results and Discussion - Figure 1shows the intensity of light scattering along the pores of alumina membranes for different angles of incidence. It can be seen that varying the membrane formation conditions makes it possible to obtain both samples that are similar in characteristics to a commercial scattering film, and samples with a pronounced predominance of scattering along pores. The latter property characterizes the possibility of using aluminum oxide films as passive brightness amplifiers for illuminating liquid crystal indicators and displays.

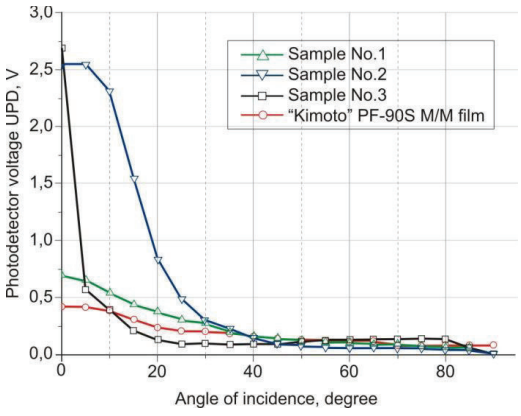

Fig. 1. The intensity of light scattering along the normal to the surface at different angles of incidence

4. Conclusions - The results obtained show that nanoporous structure of electrochemical anodic alumina films can be purposefully used to control light propagation, namely, to perform anisotropic light scattering in LCD backlight systems as well as the luminance enhancement.

[1] A. Lutich, etc. NanoLett. 4, No.9, 1755 (2004).
[2] A. Lutich, etc, Applied Physics B – Lasers and Optics **84**, Issue 1–2, 327–331 (2006).

Extrinsic Luminescence Quenching in ZnSe Crystals

N.Yu. Pavlova[1], V.Ya. Degoda[2], I.Yu. Doroshenko[2] and G.P. Podust[2]

[1]*National Pedagogical Dragomanov University, Kyiv, Ukraine*
[2]*Taras Shevchenko Kyiv National University, Physics Department, 03680 Kyiv, Ukraine*

Zinc selenide (ZnSe) is a promising material for the manufacture of ionizing radiation detectors of indirect (scintillators) and direct conversion of the energy of high-energy quanta and particles flow into electric current (semiconductor detectors) that does not require cooling. Particular interest in the luminescence band with a maximum at 630 nm in high-resistance ZnSe crystals is caused by the following factors.

Firstly, this luminescence band is used in scintillation crystals. Secondly, a feature of the luminescence center, which causes the 630 nm band, is that in the case of interband excitation, both - electron and hole - recombination mechanisms are realized at this center.

Therefore, spectroscopic studies of this luminescence center under intra-center excitation are necessary. The aim of the work was to study the temperature quenching of the luminescence band with a maximum at 630 nm under intra-center excitation in ZnSe single crystals.

Un-doped high-resistance (10^{10}-10^{14} Ω·см) ZnSe single crystals were investigated. Intra-center excitation was carried out using a light emitting diode (LED SN-HP3W-520) with a radiation maximum at 520 nm and FWHM 25 nm. Photoluminescence spectra were obtained at temperatures from 85 to 300 K.

In the temperature range from 85 to 400 K, the temperature dependence of the luminescence intensity of the 630 nm band under intra-center excitation was studied. At the same time, the conductivity of the sample was recorded. For this, two sprayed parallel strips of 5×1 mm at a distance of 5 mm were used as ohmic contacts. The use of LED provided uniform illumination of the sample in the region between the electrical contacts.

The luminescence band with a maximum at 630 nm arising under intra-center excitation was compared with the corresponding bands arising under x-ray and ultraviolet excitation of the studied samples. FWHM of 630 nm band under intra-center excitation was noticeably smaller than FWHM of 630 nm bands under X- and UV-excitation. The spectral position of the band maximum upon intra-center excitation is the same in all samples.

Under intra-center excitation of the luminescence band with a maximum of 630 nm in the temperature range T > 250 K, a rapid decrease in the luminescence intensity to almost zero was observed (temperature quenching). In the same region, simultaneously with luminescence quenching, a sharp increase of the conduction current in the samples was observed.

This clearly indicates that the quenching of the band with a maximum at 630 nm observed in the indicated temperature range is an extrinsic luminescence quenching, i.e. thermal ionization of the excited luminescence center and the appearance of a free electron in the conduction band occur.

The Parameters of Deep Traps Causing the Dark Conductivity of ZnSe Single Crystals

G.P. Podust[1], V.Ya. Degoda[1], N.Yu. Pavlova[2] and N.V. Martynyuk[3]

[1] *Taras Shevchenko National University of Kyiv, Kyiv, Ukraine*
[2] *National Pedagogikal Dragomanov University, Kyiv, Ukraine*
[3] *Lviv Polytechnic National University, Lviv, Ukraine*

One of the main characteristics of semiconductor detectors is the value of dark conductivity. In high-resistant zinc selenide samples (with resistivity ~ 10^{10}-10^{14} Ω·см), there is a very weak dark current at room temperature. This makes the material promising for use as semiconductor detector. However, it is necessary to know the nature of the observed dark conductivity. It was previously established [1] that the dark conductivity in ZnSe single crystals has electronic nature and is due to the delocalization of electrons from very deep traps. There is a need to determine not only the depth of these traps, but also their concentration and occupation degree.

To determine the depth, concentration, and occupation degree, it is necessary to study the temperature dependencies of dark conductivity at different voltages, as well as the current-voltage characteristics of photoconductivity at a known value of the electron-hole pairs generation in the sample (to determine the lifetime of free carriers). Such studies for high-resistance samples of single-crystal ZnSe are the subject of this work.

The ZnSe un-doped crystals were grown from the pre-purified charge. The two three-layered metal contacts were sprayed on the single crystals by a resistive method to study the conductivity. The stabilized voltage up to 1000 V was applied to one of the electrodes, while the other one was earthed through nano-ammeter. For photo-excitation, seven ultraviolet light-emitting diodes of UF-301 type with radiation maximum at 395 nm were used, i.e. the energy of UV-quanta was greater than the width of the ZnSe bandgap.

A method for determining the concentration of deep traps causing dark conductivity and for estimating their occupation degree was proposed. As a result, for several high-resistant samples of single-crystal ZnSe, the depths and concentrations were determined, and the occupation degree of traps providing dark conductivity at room and higher temperatures was estimated.

[1] Degoda, V.Y., Podust, G.P. Semiconductors (2014) 48: 273. https://doi.org/10.1134/S1063782614030087.

Materials with High Permittivity Based on Ferroelectric and Ion-Conducting Systems

T.O. Plutenko, O.I. V'yunov, L.L. Kovalenko, O.P. Fedorchuk and A.G. Belous

V.I. Vernadsky Institute of General and Inorganic Chemistry of the NAS of Ukraine, Palladina ave., 32/34, Kyiv - 03142, Ukraine

The miniaturization and high degree of integration of electronic devices and printed circuit boards is one of the strategies of "system in a box" technology and requires the development of dielectric capacitors based on materials with a high dielectric constant ($\varepsilon \geq 1000$). Several types of such materials are being developed. At first, these are solid solutions based on barium titanate, which large dielectric constant at room temperature associated with the ferroelectric properties. Partial reduction of titanium and an increase in the average grain size during sintering leads to an increase in dielectric losses and a relaxation contribution to the dielectric constant. The additives of 3d metal oxide MnO_2 to ceramics can prevent partial reduction of Ti. The AST (Al_2O_3 - SiO_2 - TiO_2) additive helps to reduce sintering temperature. It is interesting to study dielectric materials obtained using these additives. Secondly, a high dielectric constant was observed in $La_{0.67}Li_xTi_{1-x}Al_xO_3$ system, where a high dielectric constant can be associated with a barrier layer capacitor effect at the grain boundary. Nevertheless, dielectric properties of ceramic samples were investigated only for the orthorhombic structure, which is formed during fast quenching after sintering. Whereas materials obtained by slow cooling still remain unstudied.

Thereby, the aim of this work was to investigate the effect of MnO_2 and AST (Al_2O_3 –SiO_2–TiO_2) additives on the electrical properties and formation of $Ba(Ti,Sn)O_3$ solid solutions, as well as to study the effect of structure of partially substituted $La_{0.67}Li_xTi_{1-x}Al_xO_3$ (where $0.15 \leq x \leq 0.3$) solid solutions on their electrical properties.

The solid solutions of barium titanate stannate $Ba(Ti,Sn)O_3$ have been investigated. The sequence of phase transformations during the synthesis of the solid solution with the formation of intermediate barium orthotitanate (Ba_2TiO_4) and tetratitanate ($BaTi_4O_9$) has been established. Crystallographic and microscopic studies of ceramics based on $Ba(Ti,Sn)O_3$ have been carried out. It was found that the grain size does not change with the addition of manganese and grows with the addition of AST. It was found that the addition of manganese oxide and a low-melting additive AST can improve the dielectric parameters and reduce the sintering temperature of ceramics. Ceramics obtained at 1100 °C are characterized by high values of dielectric constant ($\varepsilon \sim 7000$) at 1 MHz and low dielectric values $tg\,\delta \sim 0.05–0.06$ at room temperatures.

$La_{0.67}Li_xTi_{1-x}Al_xO_3$ solid solutions ($0.15 \leq x \leq 0.3$) have been synthesized by solid-state reaction technique. To obtain the samples, they were sintered at 1200 ºC, single-phase solid solutions were formed for all x values. The samples had rhombohedral perovskite-related structure symmetry (space group R-3c, no. 167), while the properties for samples with perovskite-related orthorhombic symmetry are already known. Light-optical microscopy showed that the grain size of the $La_{0.67}Li_xTi_{1-x}Al_xO_3$ ceramics slightly increases with the concentration of lithium. Solid solutions $La_{0.67}Li_xTi_{1-x}Al_xO_3$ exhibit a high dielectric constant $\varepsilon' > 10^4$ in a relatively wide frequency range ($10^{-2} \leq f \leq 10^4$ Hz) without an explicit dependence on x. An impedance spectroscopy study indicates three semicircles in the Cole-Cole diagram that can be attributed to electrically different regions of the ceramic grain.

Comparing materials based on ferroelectric and ion-conducting systems we can conclude that both materials exhibit high dielectric permittivity in wide frequency range ($1 \leq f \leq 10^5$ Hz) but at the same time the dielectric properties of barium titanate are temperature dependent while the dielectric properties in lithium lanthanum titanate are thermally stable.

The Possibility of Selenium Application in THz Range

A. Bendak and N. Andrushchak

Lviv Polytechnic National University, 12 S. Bandery str., Lviv, 79013, Ukraine,
email: andrii.v.bendak@lpnu.ua

The investigation of terahertz radiation possibilities dynamically increases for the last two decades. The THz range falls between microwaves and far-infrared radiation, known as the "terahertz gap" due to generation, manipulation, and detection challenges. In particular, THz waves manipulation, modulation, and beam steering are relevant in a scientific field. An active search of usable and cost-effective materials and devices for solving of "terahertz gap" problem continues.

In [1], several materials for THz modulation are described, such as Silicon, with the 1.12 eV energy gap and high resistivity, Gallium Arsenide with 1.42 bandgap, Graphen as attracted of extraordinary career mobility, Vanadium Dioxide, etc. However, it still an actual question of semiconductor dielectric function investigation in the range of terahertz radiation. The other direction of possible studies is developing metamaterials, thin films, and heterostructures with tunable transmission and dielectric function and the influence of acousto- and electro-optical effects on diffraction efficiency [2].

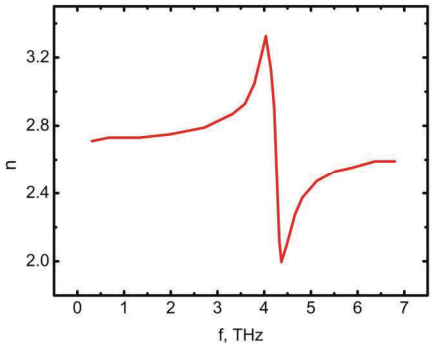

Fig.1. Refractive index for Selenium in 0.3-7 THz region [3]

The devices that operate at THz frequency ranges are typically built on semiconductor materials, which properties can be controlled by the magnetic field, temperature, mechanical methods, external electrical field, and all-optical. Analyzing the prospective materials for "terahertz gap" problem solving, Selenium should be proposed as one of the presumably promising materials for THz-waves modulation. The high photoconductivity of this element can become the basis of a tunable THz device. Many works deal with structure, electrical and optical properties of amorphous and different types of crystal Selenium. Still, there is not much information about the THz range's transmittance, reflectance, and refraction of Se material. In paper [3] it is presented a spectrally intense terahertz source based on triangular Selenium. Also, the authors correspond about very little refractive index dispersion of Se in 1-10μm range and small dispersion in electro-optic coefficient. Moreover, the index of refraction for Selenium in the 0.3-7 THz region (see Fig. 1) is relatively low with anomaly behavior at 4-4.3 THz frequencies, which is a promising factor for THz application.

The actual question is a study of amorphous and crystalline Se at different thicknesses up to nanometers, as Se-thin films, considering simple thermal-evaporation obtaining method [4]. Because Se is characterized as piezo-electric material, it would be a valuable study of THz waves' transmittance through mechanically-excited "diffraction grating" of a photo-induced electron gas in Selenium. Such tunable devices can be realized as interdigital transducers and have great potential for further application as Se-based devices operating at THz range. Thus, in our work, we propose the in-depth investigation of Selenium material for its applications in devices that can efficiently operate at THz ranges.

Acknowledgment: This work was supported by the Ministry of Education and Science of Ukraine in the frame of the "SubTera" project number 0119U100609.

[1] Yang Bai, et al. Review About the Optical-Controlled Terahertz Waves Modulator, *Applied Spectroscopy Reviews*, Vol.50, Issue 9, pp.707-727, 2015.
[2] Ranu Nayak, et.al. Enhanced acousto-optic diffraction efficiency in a symmetric $SrTiO_3/BaTiO_3/SrTiO_3$ thin-film heterostructure, *Applied Optics*, Vol. 39, No. 31, pp.5847-5853, 2000.
[3] Mostafa Shalaby, et al. Spectrally intense terahertz source based on triangular Selenium, *Scientific Reports*, Vol. 5, pp. 8059(1-4), 2015.
[4] Mahmoud H. et al. Determination of Optical Properties of Undoped Amorphous Selenium (*a*-Se) Films by Dielectric Modeling of Their Normal-Incidence Transmittance Spectra, *Applied Physics Research*, Vol. 6, No. 6, pp.10-44, 2014.

Optical Recharging of Complex Color Centers and Cobalt Ions in $Gd_3Ga_5O_{12}$:Co Crystals

D. Sugak[1,2], I.I. Syvorotka[1,2], M. Kushlyk[3,4], U. Yakhnevych[1], Ya. Zhydachevskyy[1,3], A.I. Popov[5], O. Buryy[1], S. Kachan[1], S. Ubizskii[1] and A. Suchocki[3]

[1]*Lviv Polytechnic National University, 12 Bandera st., Lviv, Ukraine.*
[2]*Scientific Research Company "Electron-Carat", 202 Stryjska st., Lviv, Ukraine*
[3]*Institute of Physics PAS, 32/46 Al. Lotników, Warsaw, Poland*
[4]*Ivan Franko National University of Lviv, 107 Tarnavskoho st., Lviv, Ukraine*
[5]*Institute of Solid State Physics, University of Latvia, 8 Kengaraga st., Riga, Latvia*
E-mail: suchy@ifpan.edu.pl

It is known that presence of Ca^{2+} or Mg^{2+} ions leads to appearance in GGG of photochromic properties. Co ions in GGG can be present both in the 2+ and 3+ oxidation states. Therefore photochromic properties can be also a feature of GGG:Co The work is devoted to studying of photochromic properties of GGG:Co (0.2 at.%). The attention was paid to the absorption changes under exposure to laser light of 266, 325, 440 and 625 nm depending on the radiation power and exposition. Under exposure with $\lambda = 325$ nm, the crystal coloration is observed as a result of appearance of the bands at 282, 406 and 620 nm with clearness at 336 nm. An exposure of the crystal with λ of 440 or 625 nm leads to bleaching of the bands at 282, 406 and 620 nm. An exposure with $\lambda = 266$ nm has a dual effect. Simultaneously with the changes in the visible region of the spectrum, there are changes in the IR absorption bands of Co ions. The nature of the color centers and the role of Co recharging in these processes are discussed.

Correlation Between Optical and Electrical Properties in β-Ga_2O_3 Single Crystals

V. Vasyltsiv, A. Luchechko, L. Kostyk, R. Lys, O. Tsvetkova, M. Kushlyk and B. Pavlyk

Department of Sensor and Semiconductor Electronics, Ivan Franko National University of Lviv, Tarnanavskogo Str. 107, Lviv 79017, Ukraine
andriy.luchechko@lnu.edu.ua

Gallium oxide (β-Ga_2O_3) is a wide band-gap oxide semiconductor (E_g =4.9 eV), which has unique conduction and tunable optical properties. The β-Ga_2O_3 is a promising material for application in different areas [1-3] including power electronic devices, solar-blind UV photodetectors, gas sensors, and transparent electrodes. Due to the perfect luminescence properties, β-Ga_2O_3 has attracted considerable attention for application in flat panel displays and UV phosphors. Moreover, it can emit luminescence from visible to near IR light when doped with different impurities.

The investigation results of the absorption, excitation and luminescence spectra, electrical conductivity, as well as thermostimulated luminescence (TSL) and depolarization (TSD) of UID and magnesium doped gallium oxide single crystals are presented in this work. The β-Ga_2O_3 crystals were grown by the floating zone technique with radiation heating. The luminescent properties of as-grown crystals as well as annealed in oxygen were investigated to determine the influence of intrinsic point defects or impurities on the luminescence yield and conductivity of β-Ga_2O_3 crystals. It was established, that as-grown β-Ga_2O_3 crystals have high conductivity and a high yield of blue luminescence band. Annealing in an oxygen atmosphere leads to an increase in both the resistivity of the crystals and the yield of the UV band of host luminescence. The additional doping with magnesium impurity leads to even stronger growth of the β-Ga_2O_3 crystals resistivity. TSL and TSD studies have shown that doping creates additional trap levels in the band-gap of the β-Ga_2O_3 crystal.

It should be noted, that the Fermi level is located near the bottom of the conduction band in as-grown crystals, so impurity and trap levels are populated by electrons. As a result, the concentration of active luminescence centers changes.

The role of intrinsic point defects and impurities in the creation of energy levels that determine the optical and electrical properties of gallium oxide crystals is discussed.

[1] M. Higashiwaki, K. Sasaki, A. Kuramata, T. Masui, and S. Yamakoshi, Development of gallium oxide power devices, *Phys. Status Solidi (A)*, 211 (2014) 21–26.
[2] A. Luchechko, V. Vasyltsiv, L. Kostyk, B. Pavlyk, Dual channel solar-blind UV photodetector based on β-Ga_2O_3, *Phys. Status Solidi (A)*, 216 (2019) 1900444.
[3] D. Guo, Q. Guo, Z. Chen, Z. Wu, P. Li, W. Tang, Review of Ga_2O_3 based optoelectronic devices, *Materials Today Physics*, 11 (2019) 100157.

The Growth and Properties of Sub-Micron Thin YIG-Based LPE Films Using Different Fluxes

I. Syvorotka[1], H. Savytskyy[2] and S. Ubizskii[3]

[1]*Scientific Research Company "Electron-Carat", Lviv, Ukraine*
[2]*Ya.S. Pidstryhach Institute for Applied Problems of Mechanics and Mathematics NASU, Lviv, Ukraine*
[3]*Lviv Polytechnic National University, Lviv, Ukraine*

The yttrium iron garnet $Y_3Fe_5O_{12}$ (YIG) is a well-known ferrimagnetic material having the smallest microwave losses and YIG films are famous materials for microwave devices [1]. Moreover, it has been shown the YIG films are a prospective material for nowadays applications such as spintronics, magnonics, data processing, etc. [2-5]. For majority novel applications the high-quality YIG films of sub-micrometer thickness are required.

This work is focused on investigation of growth process for substituted YIG films with sub-micron thickness grown by LPE method both from different fluxes and comparison of their magnetic properties.

The La, Lu and Sc- substituted yttrium iron garnet films were grown by liquid phase epitaxy (LPE) method using two types of fluxes – $PbO\text{-}B_2O_3$ and $Li_2MoO_4\text{-}Y_2(MoO_4)_3$. The processes of in-plane reversal magnetization and ferromagnetic resonance (FMR) were investigated. Typical in-plane magnetization hysteresis loops and typical FMR spectra of grown thin and thick YIG-based films are shown in Fig. 1.

Obtained parameters are compared with parameters of microns thickness films with the same compositions. The 100 nm thin films demonstrate small in-plane saturations field and low Gilbert damping constant (~10^{-4}).The prospects of using lead-free flux are shown.

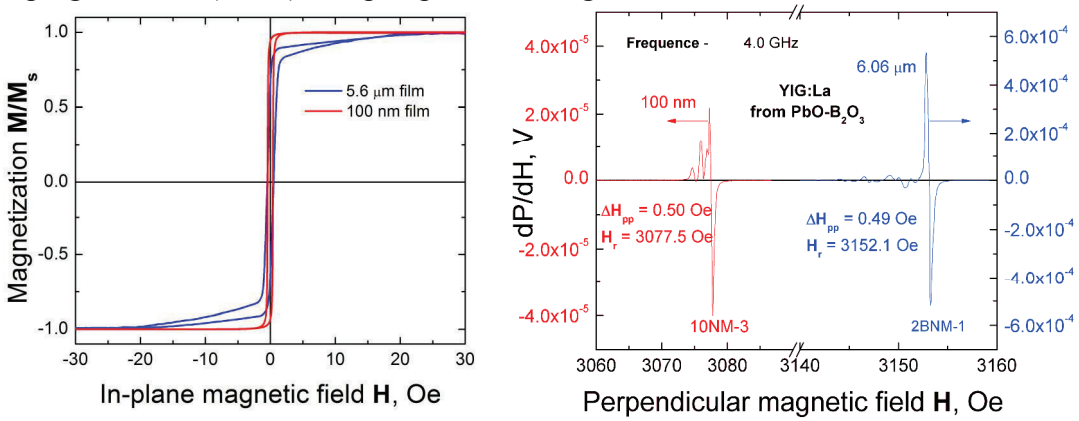

Fig. 1. Typical in-plane magnetization hysteresis loops (a) and FMR spectra (b) of YIG:La film with different thickness at room temperature.

[1] V.G. Harris, A. Geiler, Y. Chen, S.D. Yoon, M. Wu, A. Yang, Z. Chen, P. He, P.V. Parimi, X. Zuo, C.E. Patton, M. Abe, O. Acher, C. Vittoria, "Recent advances in processing and applications of microwave ferrites," J. Magn. Magn. Mater., vol. 321, pp. 2035–2047, 2009.

[2] A.V. Chumak, V.I. Vasyuchka, A.A. Serga and B. Hillebrands, "Magnon spintronics," Nat. Phys., vol. 11, pp. 453-461, 2015.

[3] H. Yu, J. Xiao and P. Pirro, "Magnon Spintronics," J. Magn. Magn. Mater., vol. 450, pp. 1-2, 2018.

[4] A.A. Serga, A.V. Chumak and B. Hillebrands, "YIG magnonics," J. Phys. D. Appl. Phys., vol. 43, 264002 (16 pp), 2010.

[5] T. Fischer, M. Kewenig, D.A. Bozhko, A.A. Serga, I.I. Syvorotka, F. Ciubotaru, C. Adelmann, B. Hillebrands and A.V. Chumak, "Experimental prototype of a spin-wave majority gate," Appl. Phys. Lett., vol. 110, 152401 (4 pp), 2017.

SECTION 6

INNOVATIVE OPTICAL/QUASIOPTICAL TECHNOLOGIES AND NANO ENGINEERING OF ANISOTROPIC MATERIALS

Liquid Crystal Nanocomposites: Optical Anisotropy, Dynamical Properties and Symmetry Aspects

A.V. Kityk[1], P. Huber[2], A. Andrushchak[3], R. Wielgosz[4], B. Sahraoui[5], M. Lelonek[6], P. Göring[6], N. Andrushchak[7], Ya. Shchur[8] and P. Pawlik[9]

[1]*Faculty of Electrical Engineering, Czestochowa University of Technology, Al. Armii Krajowej 17, 42-200 Czestochowa, Poland*
[2]*Technische Universität Hamburg, TUHH, Eißendorfer Str. 42, 21073 Hamburg, Germany*
[3]*Lviv Polytechnic National University, 12 Bandery Str., Lviv 79013, Ukraine*
[4]*Energia Oze Sp. z o.o., ul. Czestochowska 7, 42-274 Konopiska, Poland*
[5]*University of Angers, 2 Bd. Lavoisier, 49045 Angers Cedex 01, France*
[6]*SmartMembranes GmbH, Heinrich-Damerow-Str. 4, 06120 Halle (Saale), Germany*
[7]*Lviv Polytechnic National University, 12 Bandery Str., Lviv 79013, Ukraine*
[8]*Institute for Condensed Matter Physics, 1 Svientsitskii str., 79011, Lviv, Ukraine*
[9]*Faculty of Production Engineering and Materials Science, Czestochowa University of Technology, Al. Armii Krajowej 19, 42-200 Czestochowa, Poland*

Advances in optoelectronics and photonics during the last decade owe much to nanomaterials and relevant composite technologies. Mesoporous anodic alumina or silica membranes with electrochemically etched tubular nanochannels as hosts composed with guest liquid crystals embedded into their nanoporous network form inorganic-organic nanocomposite materials. They continue to be in the focus of numerous studies inspired both fundamental science and technological reasons. While the tubular structure of relevant mesoporous substrates already causes both optical and dielectric anisotropy, liquid crystals embedded into the nanochannels may change them considerably. We explore that in the dielectric spectroscopy, polarimetry and electrooptical experiments. Such anisotropy is defined much by the type of guest liquid crystal as well as interfacial host-guest molecular interactions which appear to be strongly dependent on the molecular anchoring and may be therefore modified by employing proper polymer channel-surface grafting [1]. Accordingly, the linear or circular birefringence, similarly as dielectric properties, may be tuned in a wide range opening thus new prospects in the technology of efficient functional materials. Our dielectric spectroscopy and electrooptical experiments evidently demonstrate that the relaxation dipolar dynamics of guest molecules is quite inhomogeneous inside the pores. It is of several orders faster in the core region of pore filling compared to the one revealed near the channel wall. Slow molecular dynamics in that case is explained by interfacial interactions leading also to a breaking of the macroscopic inversion symmetry. Due to this reason nematic liquid crystals confined into nanochannels demonstrate linear (Pockels) electrooptic effect forbidden in the bulk state [2]. Obtained experimental results are considered within the phenomenological approach based on the Landau-de Gennes free energy completed by the coupling terms arising from the interactions between the orientational (nematic) order parameter, electric and geometrical constraint fields.

Acknowledgment: These results are part of a project that has received funding from the EU Horizon 2020 research and innovation programme under the Marie Skłodowska-Curie grant agreement No 778156. This work was also supported by the Ministry of Education and Science of Ukraine in the frame of project 'Nanocrystalit' (0119U002255).

[1] A.V.Kityk, P.Huber, K.Senkter, A.Andrushchak, *et al,* Molecular ordering of nematic liquid crystals in tubular nanopores: Tailoring of optical anisotropy at the nanoscale by polymer pore-surface grafting, NAP 2018, 2018 IEEE 8th International Conference on Nanomaterials: Applications & Properties, art. 01SPN82.
[2] A.V.Kityk, M.Nowak, M.Reben, P.Pawlik, *et al*, Dynamic Kerr and Pockels electro-optics of liquid crystals in nanopores for active photonic metamaterials, arXiv:2107.01363v1.

Investigation of the Millimeter Wave Coplanar Waveguide (CPW) Modulator Based on Semiconductor Substrates

J. Sobolewski[1], P. Bajurko[1], D. Vynnyk[2], V. Haiduchok[3] and Y. Yashchyshyn[1]

[1]*Warsaw University of Technology, Institute of Radioelectronics and Multimedia Technology, Poland*
[2]*Lviv Polytechnic National University, Ukraine*
[3]*Scientific Research Company «Electron-Carat», Ukraine*

Due to rapid progress in telecommunication technology currently there is a growing demand for modulation techniques allowing to superimpose the high speed digital signals on the millimeter wave (mm-wave) carrier. The most common approach is to use semiconductor integrated circuits [1], however there are also concepts of combining electrical and optical domains allowing direct modulation of mm-waves from fiber optics systems [2, 3]. One of the ideas is to use photosensitive materials to change the properties of transmission line. In this work we investigate the possibility of using photosensitive semiconductor materials as a tunable substrate for coplanar waveguide (CPW).

Among other transmission lines, the CPW is distinguished by relatively low losses at mm-wave frequencies and by being straightforward to carry out measurements using on-wafer measurement setup. Another aspect important for this application is that the electromagnetic field in CPW is concentrated in small region close to the surface of the substrate. This facilitates the construction of the modulator, since changing the substrate material properties in this region can affect the electromagnetic wave propagation in the CPW. In this work we have chosen materials which conductivity can be changed with optical illumination, i.e. Ge and Se. Increasing the substrate conductivity introduces losses to the transmitted mm-wave and therefore changes the signal amplitude at the output.

Electromagnetic simulation techniques were used to evaluate this concept. The models of two types of structures were prepared in CST software. First one is constructed on bulk germanium substrate and the second one is based on thin selenium film deposited on germanium or gallium arsenide substrate. Metallization of the CPW line is made of 0.5 μm copper. Computer simulations allowed us to investigate the transmission through the CPW with different values of substrate conductivity and to determine the optimum conductivity ranges. Also different areas of the illuminated part of the CPW were examined in order to find required light spot size.

Acknowledgment: This work is part of a project that has received funding from the European Union's Horizon 2020 research and innovation programme under the Marie Skłodowska-Curie grant agreement No 778156.

[1] T. S. Rappaport, J. N. Murdock and F. Gutierrez, "State of the Art in 60-GHz Integrated Circuits and Systems for Wireless Communications," in *Proceedings of the IEEE*, vol. 99, no. 8, pp. 1390-1436, Aug. 2011, doi: 10.1109/JPROC.2011.2143650.

[2] Sung Tae Choi, Ki Seok Yang, S. Nishi, S. Shimizu, K. Tokuda and Yong Hoon Kim, "A 60-GHz point-to-multipoint millimeter-wave fiber-radio communication system," in *IEEE Transactions on Microwave Theory and Techniques*, vol. 54, no. 5, pp. 1953-1960, May 2006, doi: 10.1109/TMTT.2006.873617.

[3] J. Lasri *et al*., "A two heterojunction bipolar photo-transistor configuration for millimeter wave generation and modulation," *International Topical Meeting on Microwave Photonics MWP 2000 (Cat. No.00EX430)*, 2000, pp. 62-65, doi: 10.1109/MWP.2000.889786.

Properties of $CaWO_4$ and $CaMoO_4$ Crystals in the Subterahertz Frequency Range

P. Bajurko[1], J. Sobolewski[1], D. Vynnyk[2], V. Haiduchok[3], N. Andrushchak[2] and Y. Yashchyshyn[1]

[1]*Warsaw University of Technology, Institute of Radioelectronics and Multimedia Technology, Poland*
[2]*Lviv Polytechnic National University, Ukraine*
[3]*Scientific Research Company «Electron-Carat», Ukraine*

Calcium tungstate ($CaWO_4$) and calcium molybdate ($CaMoO_4$) materials have been used for construction of ionizing radiation detectors and as working elements for acousto-optical devices. In addition, $CaWO_4$ crystals have been used as materials for laser radiation generators. However, there are very few studies on the properties and applications of these materials in the subterahertz frequency range [1, 2]. In this work we investigate their electric properties in the frequency range from 220 GHz to 320 GHz.

The samples for the measurement were formed as rectangular z-cut plates. The samples were placed in the free space measurement setup composed of two transmitting/receiving modules with horn antennas, two PTFE lenses and a sample holder. The setup allows measurement of transmission and reflection of the subterahertz wave illuminating the sample. Dielectric parameters of the samples (permittivity ε_r and loss tangent tgδ) were extracted from the measured characteristics using the method described in [3, 4]. Refraction index n and absorption coefficient α, more common in publications in the field of optics, can be determined as well as they are related to ε_r and tgδ by equations (1) and (2).

$$n = \sqrt{\varepsilon_r} \tag{1}$$

$$\alpha \overset{\mathrm{tg}\delta \to 0}{\approx} \frac{\pi}{\lambda}\sqrt{\varepsilon_r}\,\mathrm{tg}\delta, \tag{2}$$

where λ is the wavelength.

As a result we obtained broadband frequency characteristics of the materials parameters. Samples were measured in ordinary and extraordinary polarization to evaluate their anisotropy. $CaWO_4$ does not exhibit anisotropic properties in the 220–320 GHz range. However, for $CaMoO_4$ the anisotropy is clearly pronounced. This behaviour can be used to develop bulk polarizers of subterahertz waves based on $CaMoO_4$. Moreover, the results show that both materials have low losses, which is important for construction of efficient high frequency devices.

Acknowledgment: This work is part of a project that has received funding from the European Union's Horizon 2020 research and innovation programme under the Marie Skłodowska-Curie grant agreement No 778156.

[1] J. Sobolewski and Y. Yashchyshyn, "Application of acousto-optical materials for modulation of sub-terahertz signal in coplanar structures," *2020 IEEE 15th International Conference on Advanced Trends in Radioelectronics, Telecommunications and Computer Engineering (TCSET)*, 2020, pp. 272-275.

[2] N. Andrushchak *et al.*, "Estimation of the Diffraction Efficiency of Oxide Single Crystals Acousto-Optic Devices in the Sub-Terahertz Frequency Range," *2020 IEEE 15th International Conference on Advanced Trends in Radioelectronics, Telecommunications and Computer Engineering (TCSET)*, 2020, pp. 829-833.

[3] P. R. Bajurko, "Millimeter wave permittivity and loss tangent measurements of LTCC materials," *2016 21st International Conference on Microwave, Radar and Wireless Communications (MIKON)*, 2016, pp. 1-4.

[4] P. Bajurko, K. Godziszewski, Y. Yashchyshyn, D. Vynnyk, V. Haiduchok and I. Solskii, "Determination of $Bi_{12}SiO_{20}$ permittivity and loss tangent in the 220–325 GHz band and the influence of UV exposure on these parameters," *2020 IEEE 15th International Conference on Advanced Trends in Radioelectronics, Telecommunications and Computer Engineering (TCSET)*, 2020, pp. 576-579.

On the Issue of Nanoscale KH_2PO_4 and $Ba(NO_3)_2$ Crystals Grown in Porous SiO_2 Matrix: Raman Spectroscopy, X-Ray Diffraction and *Ab Initio* Lattice Dynamics Analysis

Ya. Shchur[1], A.V. Kityk[2], V.V. Strelchuk[3], A.S. Nikolenko[3], G. Beltramo[4], S. Vitusevich[5], N. Andrushchak[6], V. Adamiv[7], I. Teslyuk[7], P. Huber[8] and A.S. Andrushchak[6]

[1]*Institute for Condensed Matter Physics, 1 Svientsitskii str., 79011, Lviv, Ukraine*
[2]*Czestochowa University of Technology, Al. Armii Krajowej 17, 42-200, Czestochowa, Poland*
[3]*V.E. Lashkaryov Institute of Semiconductor Physics, NASU, 41 Prosp. Nauky, 03028 Kyiv, Ukraine*
[4]*Institute of Biological Information Processing Mechanobiology (IBI-2), FZJ, 52425 Juelich, Germany*
[5]*Institute of Bioelectronics (IBI-3), FZJ, 52425 Juelich, Germany*
[6]*Lviv National Polytechnic University, 12 S. Bandery str., 79013, Lviv, Ukraine*
[7]*O.G. Vlokh Institute of Physical Optics, 23 Dragomanova str., 79005, Lviv, Ukraine*
[8]*Institute of Materials Physics and Technology, Hamburg University of Technology, Eissendorferstr. 42, 21073 Hamburg, Germany*

Combining dielectric crystals with mesoporous solids allows a versatile design of functional nanomaterials, where the porous host provides a mechanical rigid scaffold structure and the molecular filling adds the functionalization. Here, we report a study of the complex lattice dynamics of a SiO_2:KH_2PO_4 nanocomposite consisting of a monolithic, mesoporous silica glass host with KH_2PO_4 nanocrystals embedded in its tubular channels ~12 nm across. A micro-Raman investigation performed in the spectral range of 70-1600 cm^{-1} reveals the complex lattice dynamics of the confined crystals. Their Raman spectrum resembles the one taken from bulk KH_2PO_4 crystals and thus, along with X-ray diffraction experiments, corroborates the successful solution-based synthesis of KH_2PO_4 nanocrystals with a structure analogous to the bulk material. We succeeded in observing not only the high-frequency internal modes (~900-1200 cm^{-1}), typical of internal vibrations of the PO_4 tetrahedra, but, more importantly, also the lowest frequency modes typical of bulk KH_2PO_4 crystals. The experimental Raman spectrum was interpreted with a group theory analysis and first-principle lattice dynamics calculations.

We have studied the lattice dynamics of nanoscale $Ba(NO_3)_2$ crystals embedded in monolithic, mesoporous silica glass host, SiO_2, with non-regular system of 10-12 nm diameter pores. To interpret the Raman scattering of SiO_2: $Ba(NO_3)_2$ nanocomposite the polarized Raman spectra of bulk $Ba(NO_3)_2$ single crystal were investigated. Since the cubic symmetry (sp.gr. Pa-3, No.20)) is inherent for $Ba(NO_3)_2$, the special geometry of Raman scattering experiment was utilized to separate the phonon modes of A_g and E_g species. Combining group-theory analysis and *ab initio* lattice dynamics calculation we performed the detailed interpretation of all Raman lines of bulk single crystal. The Raman scattering of SiO_2: $Ba(NO_3)_2$ nanocomposite reveals an existence of comparatively large, ~10-20 μm, single crystalline regions of $Ba(NO_3)_2$ which are of near three orders of magnitude larger than the average spacing of SiO_2 pores. A thorough analysis of Raman lines shape has showed that the peak positions and normalized peak intensities of Raman spectra of the bulk $Ba(NO_3)_2$ single crystal and its nanoscale counterpart embedded in SiO_2 host are very similar. The full widths at half maximum (FWHM) of Raman lines below ~150 cm^{-1} of nanosized $Ba(NO_3)_2$ are mainly larger than those of monolithic bulk single crystal. Such increase of FWHM is the result of spatial confinement effect relevant for nanoconfined crystals embedded in porous SiO_2 matrix.

Acknowledgment: These results are part of a project that has received funding from the EU Horizon 2020 research and innovation programme under the Marie Skłodowska-Curie grant agreement No 778156. This work was also supported by the Ministry of Education and Science of Ukraine in the frame of project 'Nanocrystalit' (0119U002255).

Phase-Matched Magnetization-Induced Second-Harmonic Generation in Epitaxial Iron Garnet Thin Films

I.I. Syvorotka[1], D. Guichaoua[2], I. Solskyy[1], N.Ya. Syvorotka[1], K. Waszkowska[2] and B. Sahraoui[2]

[1]*Scientific Research Company "Electron-Carat", 202 Stryjska St., 79031 Lviv, Ukraine*
[2]*University of Angers, MOLTECH-Anjou Laboratory, UMR CNRS 6200, 2 bd Lavoisier, 49045 Angers, France*

The development of optoelectronic devices for communications, optical switching, information processing and storage requires the materials with exceptional optical and non-linear optical (NLO) properties. One of the suitable materials for such kinds of applications is iron garnets, which combine magnetic and magneto-optical properties and has high optical transmittance in infrared region.

The optical second harmonic generation (SHG) is a one of the nonlinear optical methods for investigation of surface and interface structures and using as tool for studying magnetically ordered crystals and thin solid films on substrate.

It is well known the bulk iron garnets are described by the centro-symmetrical point group O_h. So the optical SHG is forbidden by the symmetry. However, for the thin films grown on substrate these symmetry conditions are changing. Crystal lattice-mismatch strain deforms the cubic structure of the iron garnet lowering its inversion symmetry and producing strain-induced SHG [1].

In the present work the SHG of series of Bi-doped and Bi-free iron garnet films grown by liquid phase epitaxy (LPE) method was studied using Maker fringe technique, which widely used to study second-order NLO properties in non-centrosymmetric materials [2]. It was found that SHG is observed only in some Bi-doped iron garnets films. Moreover, SHG signals also depend of films magnetic properties due to the difference in the magnetic anisotropy. Investigation results are shown the total absence of nonmagnetic crystallographic SHG contribution and only a presence of magnetic SHG contribution.

The magnetization-induced enhancement of SHG in epitaxial iron garnet films and phase matching conditions are discussed.

Acknowledgment: These results are part of a project that has received funding from the EU Horizon 2020 research and innovation programme under the Marie Skłodowska-Curie grant agreement No 778156.

[1] P. Kumar, A. Maydykovskiy, L. Miguel, N. Dubrovina, and O. Aktsipetrov, Second harmonic generation study of internally-generated strain in bismuth-substituted iron garnet films, Opt. Express 18 (2010) 1076-1084.

[2] B Sahraoui, J Luc, A Meghea, R Czaplicki, J-L Fillaut and A Migalska-Zalas, Nonlinear optics and surface relief gratings in alkynyl–ruthenium complexes, J. Opt. A: Pure Appl. Opt. 11 (2009) 024005 (26pp)

The Optimal Vector Phase Matching Conditions for Second Harmonic Generation in Biaxial Non-Linear Optical Crystals

O. Buryy[1], N. Andrushchak[2], A. Danylov[3], B. Sahraoui[4] and A. Andrushchak[3]

[1]*Department of Semiconductor Electronics, Lviv Polytechnic National University, Lviv, Ukraine*
[2]*Department of Computer-Aided Design Systems, Lviv Polytechnic National University, Lviv, Ukraine*
[3]*Department of Applied Physics and Nanomaterials Science, Lviv Polytechnic National University, Lviv, Ukraine*
[4]*University of Angers, Institute of Sciences and Molecular Technologies of Angers, Angers, France*

The optimal geometries of vector phase matching (PM) are determined for second harmonic generation (SHG) in biaxial non-linear optical crystals of orthorhombic symmetry – CsB_3O_5 (CBO), $LiRbB_4O_7$ (LRB4), LiB_3O_6 (LBO), $KB_5O_8{\cdot}4H_2O$ (KB5), $KNbO_3$, $KTiOAsO_4$ (KTA), $KTiOPO_4$ (KTP). The directions of wave vectors ensuring the highest possible efficiency of SHG are defined by the extreme surface method [1]. Both the first (*ssf*) and the second (*sff*) type PM are considered. The examples of extreme surfaces are shown in Fig. 1. As followed from our calculations, the highest achievable SHG efficiencies for vector PM are not higher than the ones for scalar PM in the cases of CBO (*ssf*), LRB4 (*ssf*), KTP (*sff*) and LBO (both types of PM). Besides, the *sff* PM is absent in KB5, $KNbO_3$ and KTA crystals at the considered wavelengths of initial beams. The increase of the SHG efficiency ensured by *ssf* vector PM in comparison with the scalar one is equal to 145% for KB5, 39% for $KNbO_3$, 17% for KTA, 49% for KTP crystals, whereas for *sff* PM it is remarkably lower: 1.7% for CBO and 7.4% for LRB4.

Acknowledgment: These results are part of a project that has received funding from the EU Horizon 2020 research and innovation programme under the Marie Skłodowska-Curie grant agreement No 778156. This work was also supported by the Ministry of Education and Science of Ukraine in the frame of project 'OPTIMA' (0120U102204).

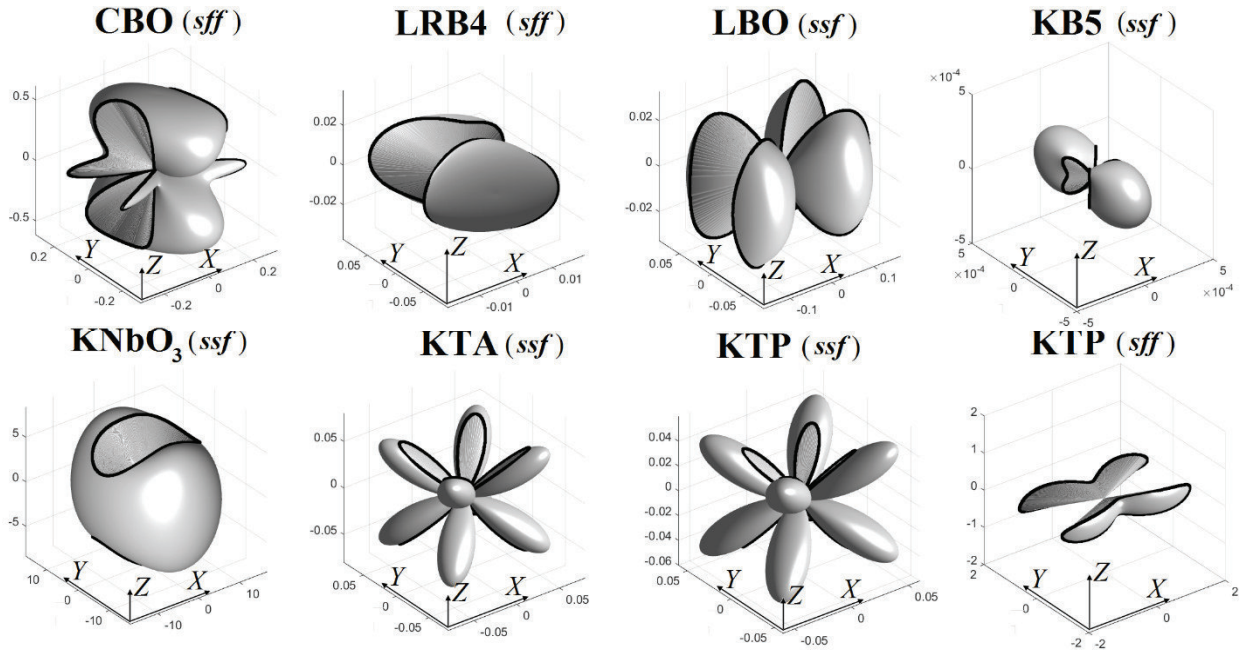

Fig. 1. The examples of extreme surfaces for considered crystals.

[1] N. Andrushchak, O. Buryy, A. Danylov, A. Andrushchak, B. Sahraoui, Opt. Mat., 2021, 120, 111420.

Luminescence Spectroscopy of Oxide Nanoparticles under Synchrotron Radiation Excitations

V. Pankratov[1]

[1]*Institute of Solid State Physic, University of Latvia, Kengaraga iela 8, LV-1063 Riga, Latvia*

Luminescence nanoparticles and nanomaterials (nanophosphors) are relevant in all applications as bulk luminescence materials. However, nanophosphors have found their most notable applications as luminescent markers in molecular biology and medical diagnosis and therapy. These range from non‐invasive in vivo whole‐body diagnosis to in vitro examination of individual organs or cells. It is well known that luminescence properties of nanophosphors suffer from surface defects of nanoparticles [1, 2]. On the other hand, surface states of nanoparticles induce new properties which are absent in bulk materials [2-5]. In the current talk unique surface‐dependent properties have been reviewed in popular nanophosphors ($Y_3Al_5O_{12}$:Ce; $LaPO_4$:Ce,Tb; YVO_4:Eu; $ZnWO_4$; CaF_2:Pr,Mn; etc.). The experimental results have been obtained by means of luminescence and VUV excitation spectroscopy technique utilizing synchrotron radiation excitations. The advantages of the experimental methods elaborated in two European synchrotron facilities at DESY (Hamburg, Germany) [6] and MAX IV (Lund, Sweden) [7, 8] will be discussed in details. It is also demonstrated that size-dependent luminescence properties of nanophosphors are significant if the electron thermalization length or the length of free electron pass becomes larger than the size of nanoparticles. Both surface and size-dependent properties play a crucial role in energy transfer processes in nanophosphors clearly elucidated by VUV excitation spectroscopy.

[1] V. Pankratov**,** V. Osinniy, A. Nylandsted Larsen, B. Bech Nielsen, Si Nanocrystals in SiO_2: Optical Studies in the Vacuum Ultraviolet Range, Phys. Rev. B, **83** (2011) 045308

[2] L. Shirmane, V. Pankratov, C. Feldmann, Comparing the luminescence processes of YVO_4: Eu and core-shell YVO_4@YF_3 nanocrystals with bulk-YVO4: Eu, Physica B: Condensed Matter **504** (2017) 80–85

[3] L. Shirmane, V. Pankratov**,** Emerging Blue-UV Luminescence in Cerium Doped YAG Nanocrystals, Physica Status Solidi Rapid Research Letters **10** (6) (2016) 475-479

[4] V. Pankratov, A.I. Popov, L. Shirmane, A. Kotlov, C. Feldmann, $LaPO_4$:Ce,Tb and YVO_4:Eu nanophosphors: Luminescence studies in the vacuum ultraviolet spectral range, J. Appl. Phys. **110** (2011) 053522

[5] A. Kuzmanoski, V. Pankratov**,** C. Feldmann, Energy transfer of the quantum-center couple Pr^{3+}-Mn^{2+} in CaF_2:Pr^{3+}, Mn^{2+} nanoparticles, Journal of Luminescence **179** (2016) 555–561

[6] G. Zimmerer, SUPERLUMI: A unique setup for luminescence spectroscopy with synchrotron radiation, Radiation Measurements **42** (2007) 859–864

[7] R. Pärna, R. Sankari, E. Kukk, et al., FinEstBeaMS - a wide-range Finnish-Estonian Beamline for Materials Science at the 1.5 GeV storage ring at the MAX IV Laboratory, Nuclear Inst. and Methods in Physics Research A **859** (2017) 83-89

[8] V. Pankratov, R. Pärna, M. Kirm, et al., Progress in development of a new luminescence setup at the FinEstBeAMS beamline of the MAX IV laboratory, Radiation Measurements **121** (2019) 91-98

Modulation of Subterahertz Radiation by Bismuth Germanate Crystals

N. Andrushchak[1], D. Vynnyk[1], M. Melnyk[2], P. Bajurko[3], J. Sobolewski[3], V. Haiduchok[4], A. Andrushchak[1] and Y. Yashchyshyn[3]

[1]*Lviv Polytechnic National University, Ukraine*
[2]*Lviv Center for Space Research Institute of the National Academy of Sciences of Ukraine*
[3]*Warsaw University of Technology, Institute of Radioelectronics and Multimedia Technology, Poland*
[4]*Scientific Research Company «Electron-Carat», Ukraine*

Nowadays, the electromagnetic radiation in subterahertz frequency range gains considerable interest [1] with increasing number of its possible applications in science and technology. Consequently, there is a growing demand for devices operating in subterahertz range. One of the essential components of subterahetrz systems are modulators – the devices controlling amplitude, frequency, phase or polarization of the electromagnetic waves. Development of the effective subterahertz modulators employing conventional light modulation techniques is challenging due to excessively large crystal size requirements. One way to achieve modulation in the subterahertz frequency range is using a material which transmission properties can be modified optically. In some materials photogeneration of charge carriers occurs as a result of illumination by optical radiation at wavelenghts within the absorption band of the material. This phenomenon leads to a change of carriers mobility and, as a consequence, change in the material conductivity. Such changes affect the transmission of the subterahertz wave passing through the material and therefore can be used for modulation.

Bismuth germanate (BGO) crystal is a high-resistivity semiconductor electro-optical material sensitive to optical radiation in it's absorption band [2]. The possibility of modulation of subterahertz radiation in the 200–300 GHz frequency range by a modulator based on BGO crystal was investigated. The modulator consists of a 500 μm polished BGO plate, the surface of which is parallel to the plane [111]. A transparent conductive ITO coating was applied on the opposite polished faces by vacuum deposition. The plate was placed in an insulating PTFE housing with a window. Polarisation voltage was applied with conductors attached to the conductive coatings on opposite faces of the plate, outside of the housing window. The modulation characteristics of the modulator as well as influence of illumination time and the polarization voltage were examined. The obtained results of the measurements are presented and analyzed.

Acknowledgment: This work is part of a project that has received funding from the European Union's Horizon 2020 research and innovation programme under the Marie Skłodowska-Curie grant agreement No 778156.

[1] Erik Bründermann, Heinz-Wilhelm Hübers, Maurice FitzGerald Kimmitt, *Terahertz Techniques*, Springer:Verlag Berlin Heidelberg, 2012, p.310.

[2] A. Ennouri, M. Tapiero, J. P. Vola, and J. P. Zielinger, "Determination of the mobility and transport properties of photocarriers in $Bi_{12}GeO_{20}$ by the time‐of‐flight technique", *Journal of Applied Physics*, 1993, 74(4), pp. 2180–2191.

Research of Nanocrystallites Based on Al_2O_3 Nanoporous Membranes from Saturated Aqueous Solutions of KH_2PO_4

V. Adamiv[1], O. Yaremko[2], I. Teslyuk[1] and A. Andrushchak[2]

[1]*Vlokh Institute of Physical Optics, 23 Dragomanov St., Lviv, Ukraine, 79005*
[2]*Lviv Polytechnic National University, 12 Bandera St., Lviv, Ukraine, 79013*

The issue of obtaining and using nanocomposite materials for radio networks of the optical and terahertz frequency bands is considered. Prepared nanoporous structures of anodized aluminum oxide Al_2O_3 (AOA) with pore diameters of 40 and 75 nm. A study of crystalline material KH_2PO_4 (KDP) in the form of nanowires and nanotubes was obtained and carried out in various growth options based on an Al_2O_3 membrane from a saturated aqueous solution of KDP, which is confirmed by the obtained images on an electron microscope, as well as using the focused ion beam technique. As a result, the formed structures can be used as an active medium in the optical range, as well as to create decelerating structures and elements of antenna-feeder devices of radio networks.

A series of papers dealing with nanoporous Al_2O_3 aluminum oxide (AOA) suggest various pathways to its applications [1-4]. These applications take into account various features of AOA: ordered structure, optical and physical properties, biocompatibility. Structures based on AOA are of great applied interest in the fields of biomedicine, sensor and filter design, optics, micro- and nanoelectronics.

By adjusting the residence time of AOA nanoporous matrices in a saturated aqueous solution of KH_2PO_4, it is possible to practically obtain crystalline compounds in the form of nanorods or nanotubes, as confirmed by electron microscope images and the focused ion beam technique. Increasing the crystallization time produces mainly nanorods of the corresponding structure (KDP). Depending on which conditions are chosen, partial or complete pore filling can be achieved, and hence nanotubes/nanorods of different shapes and sizes can be obtained. As a result, the formed structures can be used as an active medium in the optical range. It is nanocomposites that are worthy of attention in the quasi-optical range, where by introducing inhomogeneities, such as changes in dielectric conductivity, retarding structures can be formed, creating conditions for the construction of antenna-feeder devices of radio networks.

Acknowledgment: These results are part of a project that has received funding from the EU Horizon 2020 research and innovation programme under the Marie Skłodowska-Curie grant agreement No 778156. This work was also supported by the Ministry of Education and Science of Ukraine in the frame of project 'Nanocrystalit' (0119U002255).

[1] Yaremko O., Andrushchak N., Adamiv V., Rosa T., Lelonek M., Andrushchak A. / Research of Nanocomposite Materials for Telecommunication Networks // 3rd International Conference on Advanced Information and Communications Technologies, AICT 2019 – Proceedings, Pages 96-100.

[2] Atkinson R., Hendren W.R., Wurtz G.A. [et al.] / Anisotropic optical properties of arrays of gold nanorods embedded in alumina // Proceedings of SPIE. – 2006. – Vol.73. – №23. – P.2354021–235402-8.

[3] Sangar A., Merlen A., Torchio P. [et al.] / Fabrication and characterization of large metallic nanodots arrays for organic thin film solar cells using anodic aluminum oxide templates // Solar Energy Materials and Solar Cells. – 2013. – Vol.117. – P.657–662.

[4] Yaremko O., Kyryk M., Adamiv V., Zhukovska D., Teslyuk I., Vistak M., Shchur Ya., Vitusevich S., Neumann E., Andrushchak A. / Ma nufacture technology of nanocrystallites based on Al2O3 nanoporous membranes with saturated aqueous solution KH_2PO_4 for telecommunication systems // 2020 IEEE 15th International Conference on Advanced Trends in Radioelectronics, Telecommunications and Computer Engineering (TCSET), Pages 882-885, 2020.

Preliminary Studies of Second Harmonic Generation in Crystalline Nanocomposites

A. Danylov, I. Sen'ko and A. Andrushchak

Lviv Polytechnic National University, 12, S. Bandera Str.,79013, Lviv, Ukraine

The results of preliminary studies of nonlinear optical response in different anisotropic materials are presented. The investigation was carried out by means of equipment presented in Fig. 1. The installation verification was performed by the series of measurements in $LiNbO_3$ single crystals and comparison of the experimental results with model calculations by the scheme proposed in [1] and based on reference data [2].

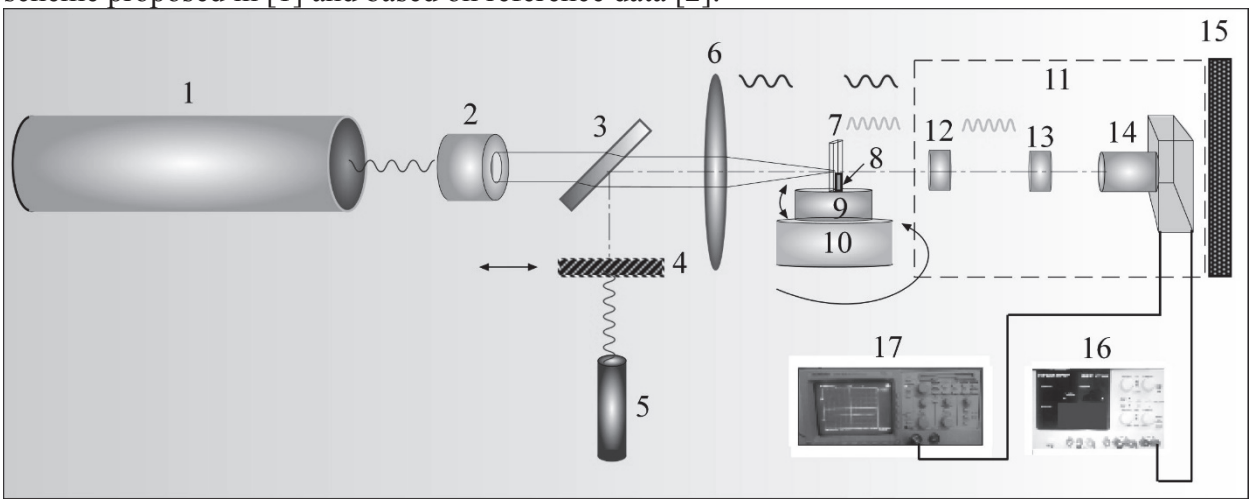

Figure 1. Optical arrangement of installation for nonlinear optical coefficient measurement in single crystals and nanocomposites by the method of Maker fringes (1 – 1.06-μm pulse laser, 2 – diaphragm, 3 – . Beam splitter, 4 – opaque screen, 5 – supplementary He-Ne laser, 6 – focussing lens, 7 – measuring sample, 8 – fastening, 9 – vertical rotation unit; 10 – horizontal rotation unit, 11 – photodetector unit with filters, 12 – infrared filter, 13 – interference filter, 14 – photodetector, 15 – light absorber, 16 – power supply unit, 17 – oscillograph).

The signal of second harmonic generation (SHG) in nanoporous matrix of Al_2O_3 and SiO_2 with incorporated nanocrystallites of ADP, KDP, HJO_3 and $CuSO_4$ crystals was analyzed by oscillograph. The range of exciting lamp voltage suitable for SHG and lower than material destruction threshold was determined. As nanoporous Al_2O_3 destruction threshold is lower than signal power of main frequency for SH effective generation we concentrated our attention on SiO_2 matrix with imbedded nanocrystallites. The relative value of SHG power with regard to the main frequency signal measured after signal reflection from the samples were determined. Next step of our studies consists in determination of nonlinear coefficients for the above mentioned crystalline nanocomposite structures.

Acknowledgment: These results are part of a project that has received funding from the EU Horizon 2020 research and innovation programme under the Marie Skłodowska-Curie grant agreement No 778156. This work was also supported by the Ministry of Education and Science of Ukraine in the frame of project 'Nanocrystalit' (0119U002255).

[1] Jerphagnon J., Kurtz S. K. J. Appl. Phys. –1970. – V. 41, – P. 1667-1681.
[2] Nikogosyan D.N., Nonlinea Optical Crystals: A Complete Survey. Springer Science+Business Media, Inc., New York. 2005.

The Peculiarities of Piezo-Optic Effect in Crystals with Periodical Change of Refractive Index

B. Mytsyk[1], N. Demyanyshyn[1], O. Buryy[2] and A. Andrushchak[2]

[1]*Karpenko Physico-Mechanical Institute of NAS of Ukraine, Naukova str. 5, 79060 Lviv, Ukraine; nmdem@ipm.lviv.ua*
[2]*Lviv Polytechnic National University, Bandery str. 12, 79013 Lviv, Ukraine*

For effective functioning of the devices of light beam modulation and control, the crystalline materials with high piezo-, elasto- and electro-optic coefficients are required for their sensitive elements. At that even with the use of such known photoelastic or electro-optical materials as gallium phosphide, quartz or lithium niobate [1] and applied real allowable mechanical or electrical stresses, it is possible to induce and fix a change of optical path based on registering the motion of light and dark interference bands only on a half-wave (λ/2). The creation of an interferometric device for modulation of optical radiation, in which it would be possible to fix the change of the optical path on a value higher than λ/2, is still an important task. This task can be solved by using of crystalline cells with periodical change of refractive index or striped structure.

The striped structure, which is formed due to the peculiarities of the chemical composition and technology of crystal growth, is revealed by crystals of the langasite group and doped crystals of the triglycine sulfate group. Crystalline bands (zones) in such crystals alternate and have different refractive indices. The thickness (width) of bands is mainly in the range of 10-100 μm. Due to the periodic change of the refractive index in the volume of the sample (from band to band) and the propagation of the light beam in the plane of the band, light diffraction occurs. The interference pattern formed by the Mach-Zehnder interferometer is characterized by a different value of the control voltage in each of the diffraction orders. For example, the piezo-optical effect (POE) in lanthanum-gallium silicate crystals is relatively small and commensurate with the one in the known lithium niobate crystal ($LiNbO_3$ or $LiNbO_3$:MgO). However, in the direction of beam propagation in the plane of the bands, when light diffraction is observed, the value of POE of these crystals in different diffraction orders is large and, i.e. for $+1^{st}$, 0^{th}, -1^{st} and -2^{th} orders is respectively equal to -4, +0.3, +18 and +34 Br (1 Br = 1 Brewster = 10^{-12} m^2/N). Therefore, the half-wave voltages decrease by two orders of magnitude from zero to –2nd diffraction maximum.

It should be emphasized, that the value of POE with a value of 34 Br is unique – it is more than 3 times higher than the value of POE in other unique from this point of view ammonium sulfate crystal (maximum POE is equal to 11.0 Br [2]). Thus, the use of crystalline materials with a striped structure is promising for the creation of effective cells for photo-elastic (or electro-optic) modulators of electromagnetic radiation and requires a detailed study of the peculiarities of this effect.

Acknowledgments: This work was supported by the National Research Foundation of Ukraine (Project 2020.02/0211). Furthermore, the work was partially supported by the European Union's Horizon 2020 research and innovation program under the Marie Skłodowska-Curie grant agreement No.778156 and the Ministry of Education and Science of Ukraine in the frame of project 'OPTIMA' (0120U102204).

[1] Acoustic crystals. Handbook. Ed. by M.P. Shaskolskaya. Science, Moscow, 1982.
[2] B. Mytsyk, V. Stadnyk, N. Demyanyshyn, Ya. Kost., P. Shchepanskyi, Photoelasticity of ammonium sulfate crystals. Opt. Mat., 2019, V. 88, P. 723-728.

LabVIEW-Powered Instrumentation for Accurate Interferometric Measurements of Refractive Indices

A. Ratych, I. Karbovnyk and N. Andrushchak

[1]*Lviv Polytechnic National University, Bandery str. 12, 79013 Lviv, Ukraine*
[2]*Ivan Franko National University of Lviv, Universytetska str, 1, 79000 Lviv, Ukraine*

We present a fully automated interferometric setup that is designed for highly precise measurements of refractive indices of bulk crystalline samples. The concept and physical background behind this setup are provided in [1]. The present setup is a next step toward higher accuracy and faster measurements and involves a number of hardware and software improvements.

The setup uses a 633 nm laser as a light source and is based on the Michelson interferometer that is mounted on the mechanically stable Thorlabs optical breadboard. Resulting interference pattern is focused onto Thorlabs Si Switchable Gain Detector PDA100A2 which is sensitive to the wavelengths in the range of 320 - 1100 nm. Brushless DC-servomotor Faulhaber 4490H024BS is responsible for the rotation of the sample and precise angle control is ensured by Faulhaber Motion Controller MC 5010 S with external speed controllers SC 5008 S. Motion control system allows communication via RS232/USB interface. Arduino Nano controller is connected to MC 5010 S serial port and reads raw angle data in binary format. After pre-processing angle values are sent through Arduino Nano serial/USB port as strings.

We use NI LabVIEW 2019 virtual instrument as a primary experiment controller. For the purpose of detector data acquisition, NI multifunctional I/O USB-6210 device is employed. Sample position data are collected via USB/serial interface using an implementation of the Virtual Instrument Software Architecture (VISA) I/O standard.

Early experimental results on reference samples of optical glass indicate that the setup can provide accuracy of the fourth decimal place. Example of wire measurements on the test sample are shown in Fig.1.

Acknowledgment: These results are part of a project that has received funding from the EU Horizon 2020 research and innovation programme under the Marie Skłodowska-Curie grant agreement No 778156. This work was also supported by the Ministry of Education and Science of Ukraine in the frame of project ‘OPTIMA’ (0120U102204).

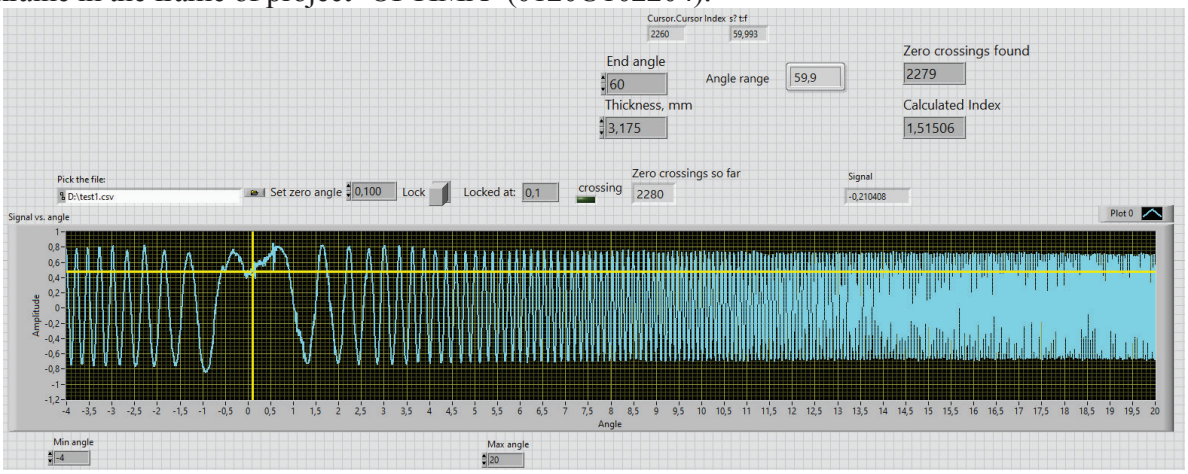

Fig. 1. Examples of wire measurements on the test sample

[1] N. Andrushchak, I. Karbovnyk. LabVIEW-Based Automated Setup for Interferometric Refractive Index Probing. https://doi.org/10.1177/2472630319891133

Experimental Measurements of Electo-Optic Coefficients for $LiTaO_3$ Crystals

Z. Kohut[1,2], O. Korneyev[1], B. Olkhovyk[1], B. Mytsyk[3] and A. Andrushchak[1]

[1]*Lviv National Polytechnic University, 12 S. Bandery str., 79013, Lviv, Ukraine*
[2]*Czestochowa University of Technology, Al. ArmiiKrajowej 17, 42-200, Czestochowa, Poland*
[3]*Karpenko Physico-Mechanical Institute of NAS of Ukraine, Naukova str. 5, 79060 Lviv, Ukraine; nmdem@ipm.lviv.ua*

Lithium tantalite possesses ferroelectric properties with Curie temperature near 660°C and represents itself as a colorless crystal of trigonal crystal family with spatial group R3c and its lattice constants are: a = 0,5154 nm; c = 1,3781 nm; Z = 6. This crystal can be used as an infrared detector, for excitation of surface acoustic waves, and also for generation and detection of oscillations in terahertz range of electromagnetic waves.

Experimental research of spatial anisotropy of linear electro-optic effect was conducted and electro-optic coefficients for possible directions of polarized light propagation in $LiTaO_3$ crystals with straight cut were defined.

Results were obtained with help of modernized optical setup based on Michelson`s interferometer (see Fig.1), which contains electronic control and measurement systems.

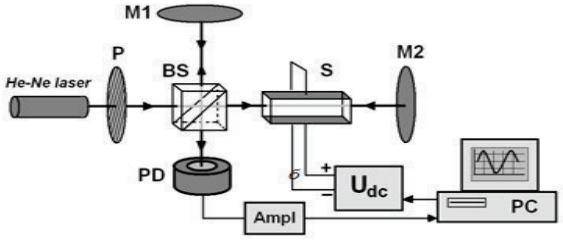

Fig. 1. Experimental setup based on Michelson`s interferometer.

Electro-induced change $\delta\Delta_{ik\ell}$ in optical path of light beam, which passes through sample in case of two-pass interferometer, occurred due to change of refraction index (electro-optic effect) and sample size (inverse piezoelectric effect) of researched crystal in direction of light propagation influenced by electric filed and it can be calculated with equation [1, 2]:

$$\delta\Delta_{ikl} = -\frac{r_{il}n_i^3}{2}E_l t_k + (n_i - 1)d_{lk}E_l t_k$$

Suggested experimental method and mathematic dependences allows us to define and calculate all electro-optic coefficients for $LiTaO_3$ crystals which are relying on measurements of change in optical path induced by applied electric field. Defined matrix of electro-optic coefficients allows to build the indicative surfaces for 3D analysis of spatial anisotropy of the electro-optic effect.

Acknowledgment: These results are part of a project that has received funding from the EU Horizon 2020 research and innovation programme under the Marie Skłodowska-Curie grant agreement No 778156. This work was also supported by the Ministry of Education and Science of Ukraine in the frame of project 'OPTIMA' (0120U102204).

[1] Andrushchak A.S. Spatial anisotropy of linear electro-optic effect for crystal materials: I. Experimental determination of electro-optic tensor by means of interferometric technique / A.S. Andrushchak, B.G. Mytsyk, N.M. Demyanyshyn, M.V. Kaidan, O.V. Urkevych, I.M. Solskii, A.V. Kityk, W.Schranz // Opt.Lasers.End.-2009-Vol.47.-P.31-38.

[2] Anrushchak A.S. Spatial anisotropy of induced optic effects in crystal materials / A.S. Andrushchak, O.A. Buryy, N.A. Andrushchak, N.M. Demyanyshyn, Lviv: Prostir-M, 2019.-200 P. (in Ukrainian).

The Effect of Nanoconfinement in Functional Materials for Electrical Energy Storage Devices

B. Venhryn, O. Balaban, I. Yidak and A. Andrushchak

Lviv Polytechnic National University, S. Bandery Str. 12, Lviv 79013, Ukraine

Recently, considerable attention in the scientific literature has been focused on technological approaches to obtaining and activation modification of the thermodynamic and kinetic properties of functional materials for electrical energy storage devices [1-4]. An urgent topic in world science is the study of nanoscale effects, which are manifested in the nanometer range of measurement, which opens the world to new properties of substance [5-6].

For the practical implementation of potentially useful properties of low-dimensional structures, new technological approaches that would allow the manufacture of structures with predetermined characteristics, strictly controlled sizes, and shapes are required.

A number of recent scientific studies show that the nanoconfinement is the most noticeable in electrochemical reactions, important in the manufacture of anode materials for lithium batteries in order to modify their thermodynamic and kinetic properties, affects the properties of heat storage in case of materials with variable phase composition, increases the reversibility of redox reactions in redox capacitors. In addition, the nanoconfinement effect is observed in nanoporous materials. In addition, the transition to nanoscale materials dimensions contributes to the growth of adsorption and selectivity of ions.

Due to the effect of nanoconfinement, we have synthesized several high-quality functional materials for use in devices of generation, conversion, and accumulation of electrical energy. Based on the research, it can be stated that the effect of nanoconfinement must be taken into account when obtaining low-dimensional structures with the predicted physicochemical properties and new functional characteristics.

Acknowledgment: These results are part of a project that has received funding from the EU Horizon 2020 research and innovation programme under the Marie Skłodowska-Curie grant agreement No 778156. This work was also supported by the Ministry of Education and Science of Ukraine in the frame of project 'OPTIMA' (0120U102204).

[1] B.P. Bakhmatyuk, B.Ya. Venhryn, I.I. Grygorchak, M.M. Micov, S.I. Mudry, Intercalation pseudo-capacitance in carbon systems of energy storage, *Reviews on Advanced Materials Science*, **14** (2007) 151-156.

[2] B.Ya. Venhryn, I.I. Grygorchak, Z.A. Stotsko, Yu.O. Kulyk, S.I. Mudry, V.V. Strelchuk, S.I. Budzulyak, G.I. Dovbeshko, O.M. Fesenko, Changes in the fractal and electronic structures of activated carbons produced by ultrasonic radiation and the effect on their performance in supercapacitors, *Archives of Materials Science and Engineering*, **57** (2012) 28-37.

[3] B.Ya. Venhryn, I.I. Grygorchak, Yu.O. Kulyk, S.I. Mudry, Improvement of Supercapacitor Parameters by Nickel Ion Intercalation into Activated Carbon, *Materials Science-Poland*, **31** (2013) 126-132, https://doi.org/10.2478/s13536-012-0072-6.

[4] B.Ya. Venhryn, I.I. Grygorchak, Yu.O. Kulyk, S.I. Mudry, V.V. Strelchuk, S.I. Budzulyak, G.I. Dovbeshko, O.M. Fesenko, Fe^{2+}- and Er^{2+}-intercalative modification of porous and electron structure of activated carbon and its influence on supercapacitor parameters, *Materials Science-Poland*, **32** (2014) 272-280, https://doi.org/10.2478/s13536-013-0178-5.

[5] Minjee Seo, Taek Dong Chung, Nanoconfinement effects in electrochemical reactions, *Current Opinion in Electrochemistry*, **13** (2019) 47-54, https://doi.org/10.1016/j.coelec.2018.10.011.

[6] F. Maximilian, Nanoconfinement effects in energy storage materials, *Physical Chemistry Chemical Physics*, **13** (2011) 21186-21195, https://doi.org/10.1039/C1CP22547B.

Study of the Process of Acoustic Wave Wear in Monocrystalline Materials

I.V. Stasyshyn[1,2], T.I. Vorovyak[1,2], I. Martynyuk-Lototska[3] and A.S. Andrushchak[2]

[1]*Karpenko physico-mechanical institute of the NAS of Ukraine*
[2]*Lviv National Polytechnic University, 12 S. Bandery str., 79013, Lviv, Ukraine*
[3]*Vlokh Institute of Physical Optics, 23 Dragomanov St., Lviv, Ukraine, 79005*

During the study of the acousto-optical parameter of different crystals there is a problem of finding diffraction responses. This problem can be caused by two parameters. The first of them is the parallelism of the faces of the manufactured samples. An interference approach can be used to find non-parallel faces. With the help of a Mach-Zender interferometer, in which a sample is installed on one face, the interference pattern is registered. The next step is to select the angle of the interferometer, which is close to zero between the two arms of the interferometer. The change in angle is caused by the investigated crystal and there is a non-parallelism under study.

The second parameter that affects the study of acousto-optical quality is the wear of the acoustic wave in the plane of the crystal. An optical scheme has been proposed and developed to determine the wear angle. The idea of the study is to select +1 order of diffraction in the crystal caused by an acoustic wave. To do this, an extended beam of laser radiation was applied to the crystal. After the crystal, the beam passes through the Fourier lens and zero-order filtering is performed in the focus of the lens. The inverse Fourier transform is then performed and recorded by a photosensor.

Such studies were performed on CaWO4 crystals and set wear angles. The maximum values of the wear of the acoustic wave in the plane 001 for the transverse wave is 45˚, and for the longitudinal 18˚.

Acknowledgment: These results are part of a project that has received funding from the EU Horizon 2020 research and innovation programme under the Marie Skłodowska-Curie grant agreement No 778156. This work was also supported by the Ministry of Education and Science of Ukraine in the frame of project ‘OPTIMA’ (0120U102204).

Nanoporous Characterization of Eu^{3+} Doped $BaGa_2O_4$ Ceramics

H. Klym[1], Yu. Kostiv[1], A. Ingram[2], L. Luchechko[3] and I. Karbovnyk[3]

[1]*Lviv Polytechnic National University, 12, Bandera str., Lviv, 79013, Ukraine*
[2]*Opole University of Technology, 75, Ozimska str., Opole, 45370, Poland*
[3]*Ivan Franko National University of Lviv, 107 Tarnavskogo str., Lviv, 79000, Ukraine*

The $BaGa_2O_4$ ceramics are materials for different applications in optoelectronic devices, as a potential candidate for secondary electron emission coatings in plasma display panels, for proton ceramic fuel cells, etc. [1]. Doping of $BaGa_2O_4$ ceramics by rare-earth ions results in modification of their structural properties. The aim of this work is study of nanopores evolution in the $BaGa_2O_4$ ceramics doped with Eu^{3+} ions in different concentration using positron annihilation lifetime (PAL) spectroscopy method in comparison scanning electron microscopy (SEM) methods.

The $BaGa_2O_4$ ceramics were prepared using solid-state reaction method from $BaCO_3$ and Ga_2O_3 components with purity of 99.99%. Powders with 0, 1, 3 and 4 mol.% of Eu_2O_3 (99.99%) were mixed in an agate mortar for 6 h with further pressing in a steel mold. Prepared pellets were annealed at 1200 ºC for 12 h in air. After that, the annealing of ceramic samples was carried out at 1300 ºC for 4h. PAL measurements were performed with an ORTEC spectrometer (^{22}Na source) placed between two sandwiched samples. PAL spectra were fitted on three components with positron lifetimes τ_1, τ_2, τ_3 and corresponding unity-normalized intensities I_1, I_2, I_3.

It is established that $BaGa_2O_4$ ceramics are characterized by branched structure of grains, grain boundaries and pores. Un-doped $BaGa_2O_4$ ceramics contain three phase, samples with 3 and 4 mol.% of Eu_2O_3 are two-phases ($BaGa_2O_4$ and Eu_3GaO_6 phases), while $BaGa_2O_4$ ceramics with 1 mol.% of Eu_2O_3 contain only one $(Ba,Eu)Ga_2O_4$ phase on own structural type. Samples of the polycrystalline undoped $BaGa_2O_4$ ceramics exhibit the greatest deviation from the stoichiometric composition. Such processes are obviously caused by the evaporation of the constituent powders of synthesis during annealing process at high temperatures.

It is shown that in Eu^{3+} doped $BaGa_2O_4$ ceramics two channels of PAL should be considered – the positron trapping and o-Ps decaying as for other functional ceramics [2]. The first component in PAL spectra for studied ceramics with parameters τ_1 and I_1 reflects their mainly microstructure specificity. The intermediate lifetime τ_2 is related to the size of free-volume defects near grain boundaries formed by addition phases, and I_2 intensity reflects their amount. The third component (τ_3, I_3) originate from annihilation of ortho-positronium o-Ps atoms in intrinsic nanopores of Eu^{3+} doped $BaGa_2O_4$ ceramics.

It is established that the τ_2 lifetime increases with rises of Eu^{3+} ions (from 1 to 3 mol.%) in $BaGa_2O_4$ ceramics, while its intensity I_2 decreases. These changes are in correlation with phases located near grain boundaries. The lifetime τ_3 and intensity I_3 increases. These changes correspond to expanded of nanopore size and increased of their amount at doping of base matrix. It is shown, that radius of nanopores calculated within Tao-Eldrup model from lifetime of the third component are centered near 0.3 nm.

This work was supported by the Ministry of Ministry of Education and Science of Ukraine.

[1] Kodu M., Avarmaa T., Mändar H., Jaaniso R. (2008). Pulsed laser deposition of $BaGa_2O_4$. Applied Physics A 93(3): 801-805.

[1] Klym H., Ingram A., Hadzaman I., Shpotyuk O. (2014) Evolution of porous structure and free-volume entities in magnesium aluminate spinel ceramics. Ceramics International 40:8561–8567.

Structural Peculiarities of Multilevel Thick Films for Active Media of Sensor Systems

H. Klym[1], I. Hadzaman[2], O. Shpotyuk[3] and I. Vasylchyshyn[4]

[1]*Lviv Polytechnic National University, 12 Bandera str., Lviv, 79013, Ukraine*
[2]*Drohobych Ivan Franko State Pedagogical University, 24 Ivan Franko str., Drohobych, 82100, Ukraine*
[3]*Vlokh Institute of Physical Optics, 23 Dragomanova str., Lviv,79005, Ukraine*

It is known that performance of spinel ceramics in the form of thick films has a number of advantages over other types of functional electroceramics, especially in combination of different levels. Transformation of all the functional properties of bulk materials in a thick-film multilevels (or multilayers) is needed to further miniature device applications [1]. The aim of this work is study of structural peculiarities of temperature- and humidity-sensitive thick-film multilevel structures.

Temperature-sensitive thick films and multilevel structures based on $Cu_{0.1}Ni_{0.8}Co_{0.2}Mn_{1.9}O_4$ with p-type electrical conductivity. $Cu_{0.1}Ni_{0.1}Co_{1.6}Mn_{1.2}O_4$ with p^+- type of electrical conductivity and dielectric $MgAl_2O_4$ (*i*-type) [2] were investigated. The humidity-sensitive thick films was applied to pre-formed temperature-sensitive level. Formation of p-p^+, p-p^+p, thick-film structures and integrated temperature-humidity-sensitive p-i-p^+ structures was carried out within one technological process.

It is established that the $Cu_{0.1}Ni_{0.8}Co_{0.2}Mn_{1.9}O_4$ thick films on the Rubalit substrate consist tree phases. There are diffraction lines of the spinel phase, aluminum oxide from the substrate and a low intensity line from a solid solution $(Ni_{1-x}Mn_x)O$ based on a NiO phase with a NaCl cubic structure. The $MgAl_2O_4$ thick films on Rubalit substrate contain two phases - a spinel and an aluminum oxide from a substrate. In the case of $Cu_{0.1}Ni_{0.1}Co_{1.6}Mn_{1.2}O_4$- and $Cu_{0.1}Ni_{0.8}Co_{0.2}Mn_{1.9}O_4$-based thick films, an amorphous halo is observed at the angle of 20-33° 2θ, which is also due to the diffraction from the cuvette material.

In accordance with results of topological investigations, thickness of temperature-sensible p- and p+-layers was 43.75 μm and 46.88 μm, accordingly. The of two-layered p^+-i thick-film structure is 139.06 μm, p^+-p – 110.16 μm, and integrated p-i-p+ thick-film structures with conductive Ag layer – 193.73 μm (thickness of Ag layer is 45.31 μm).

Structure of humidity-sensitive thick films is especially expressly selected on a background of Al_2O_3 substrate with conductive Ag layer. Evidently, that material contains the far of shallow pores, which serve as ducting for the receipt of water to nanopores, where processes of capillary condensation takes place, and also macropores which provide the effective receipt of water in the inner structure of material from an environment.

The $Cu_{0.1}Ni_{0.8}Co_{0.2}Mn_{1.9}O_4$-based thick films contain a greater amount of macropores formed in clusters. A similar structure is also characteristic for bulk material of the same composition. Thus, the structural features of ceramics can be transformed into thick films of similar compositions. The use of ceramic with a spinel structure as the main output component for preparation of thick films provided the density of the multilevel structure and contact of their levels.

This work was supported by the Ministry of Ministry of Education and Science of Ukraine.

[1] Tymecki L., Glab S., Koncki R. (2006) Miniaturized, planar ion-selective electrodes fabricated by means of thick-film technology. Sensors. 6(4):390-396.

[2] Hadzaman I., Klym H., Shpotyuk O. (2014). Nanostructured oxyspinel multilayers for novel high-efficient conversion and control. International Journal of Nanotechnology. 11(9-1011):843-853.

Authors Index

A

Abusaid W.. 96, 104,120,121
Adamiv V. 140, 145
Adamiv V.T. 107
Adanur I. 27
Afanassyev D. 122
Aksimentyeva O. 66, 82
Akyol M. 27
Alekseev O. 58, 126
Alekseev V. 98
Altinkok A. 14, 97
Altunal V. 96, 104, 120, 121
Androulidaki M. 45, 59, 125
Andrushchak A. 20, 47, 119, 137, 143, 144, 145, 146, 147, 149, 150
Andrushchak A.S. 118, 140, 151
Andrushchak N. 20, 119, 132, 137, 139, 140, 143, 144, 148
Arhipov P. 98
Arias-Serrano B.I. 43
Arslan H. 23
Artiukh E. 93
Aydınoğlu H.S. 38

B

Badalyan G.R. 16
Bagday S.R. 86
Bajurko P. 119, 138, 139, 144
Balaban O. 19, 150
Baran M. 39
Baranov V. 108
Barbash V. 58
Bartosiewicz K. 99, 100
Barvitskyi P. 11
Belous A. 60
Belous A.G. 55, 61, 69, 131
Beltramo G.. 140
Bendak A. 132
Bendikienė R. 51
Bereket S. 121
Berkowski M. 109, 110
Bilski P. 111, 112
Blazhivskyi K. 83
Bochkova T. 40
Bodnaruk A.V. 55
Bogatyrev V. 82
Boichyshyn L. 87
Bondar D. 40
Bordun I.O. 127
Bordun O.M. 127
Bortnitskaya M.A. 11
Borysiuk V. 65
Boyarintsev A. 80
Boyaryntseva Ya. 98
Boyko V. 35
Brezvin R. 117
Brvitskyi P. 57
Bulyk L.-I. 102
Buryy O. 103, 133, 143, 147

C

Cabioc`h T. 11
Çavdar T. 46, 53
Cebulski J. 123, 124
Čeh M. 79
Chaika M. 94
Chornii V. 34, 35, 58, 126
Chukova O. 59, 63
Ciepielewski P. 102
Corradi G. 56

D

Danylov A. 143, 146
Defferiere T. 75
Degoda V.Ya. 129, 130
Demchenko P. 42
Demyanyshyn N. 147
Derkowska-Zielinska B. 13, 106
Diachenko A.O. 88
Diduszko R. 109
Dluzewski P. 94
Doroshenko I.Yu. 129
Douissard P.A. 113
Drzewiecki A. 107
Dubovik O. 34
Duriagina Z. 26
Dutka V. 64
Dzeryn M. 82

E

Ekicibil A. 27, 38, 104, 120
Enhessari M. 74

F

Feder R. 77
Fedorchuk O.P. 131
Fedorov A. 95, 99, 111
Filipsonov R. 66
Fink-Finowicki J. 109
Fritze H. 75, 76, 77, 78
Ftomyn N. 116

G

Galenin E. 98
Galunov N. 91
Gerasimov Ya. 91
Gerasymov Ia. 98

Gerlach G. 93
Gieszczyk W. 111, 112
Gladyshevskii R. 41
Gladyshevskii R.E. 86
Głowacki M. 109, 110
Godlewski M. 9
Gokov S.P. 37
Gomenyuk O. 125
Gorbacheva T. 91
Gorbenko V. 12, 90, 95, 99, 100, 101, 102
Göring P. 137
Greshchuk O.M. 61
Grinyov B. 80
Gritsyna V.T. 37
Grygorchak I. 19
Gryn L. 108
Gryshchouk G.V. 86
Guckan V. 96, 104, 120, 121
Güçkan V. 46
Guichaoua D. 141

H

Hadzaman I. 153
Haiduchok V. 119, 138, 139, 144
Halbedel B. 57
Hizhnyi Yu. 34, 65, 110
Hofmann M. 29
Horbenko Yu. 82
Hreb V. 17, 18, 48, 49, 50, 62, 71, 83
Hrytsan V. 41
Huber P. 137, 140

I

Ingram A. 152
Izhyk O. 19

J

Johnson W. 76

K

Kachan S. 25, 133
Kaczmarek M. 95
Kaidan M.V. 118
Kalendarev R. 23
Kalita V.M. 55
Kalychak Ya.M. 86
Kamada K. 90, 95, 100
Kapustyanyk V. 114
Karadag F. 27, 104, 120
Karavaeva N. 91
Karbovnyk I. 147, 152
Karpets M.V. 11
Kaya D. 27, 38
Kazarinov Yu.G. 37
Khalameida S. 17, 84
Khomenko V.G. 69
Khromiuk I. 91
Khrushchyk K. 87
Khyzhun O. 84
Kildiyarov R. 117
Kindrat I.I. 107
Kiose T.A. 67, 68
Kissabekova A. 39
Kityk A.V. 137, 140
Klym H. 152, 153
Klyndyuk A.I. 16
Klysko Yu. 81
Kochtetov V. 29
Kocsor L. 56
Kofanov D. 91
Kofliuk I.M. 127
Kogut I. 78
Kohut Z. 149
Kondyr A. 48
Konieczny J. 51
Koptiev M. 45
Kordan V. 42
Korneyev O. 149
Kostiv Yu. 152
Kostyk L. 114, 134
Kotomin E.A. 92
Kotynska L. 85
Kovács L. 56
Kovalenko L.L. 131
Kovalskyi Ya. 64
Kovbasiuk T. 26
Kozlovskyi A. 24
Kozłowska A. 94
Krasnikov A. 39
Krech A. 80, 91
Krolenko K. 58
Krutyak N. 115
Kucerkova R. 95
Kudrjavtseva I. 102
Kukharskyy I.Yo. 127
Kukliński B. 107
Kulyk V. 26
Kulyk Yu. 36
Kumar Somakumar A. 102
Kuprin A.S. 11
Kurt K. 46, 53
Kurtsev D. 98
Kushlyk M. 133, 134
Kuzanyan A.S. 15, 16
Kuznetsova L. 85
Kuzovkov V.N. 92
Kvartskhava I.G. 15, 16

L

Labisz K. 51
Lazarenko M. 58, 126
Lelonek M. 137
Lengyel K. 56
Lesniewski T. 12
Levchuk L. 91
Levytska S. 85
Lisovskyi I.V. 69

Luchechko A. 48, 49, 122, 124, 134
Luchechko L. 152
Lushchik A. 32, 39, 92, 102
Lutsyuk I. 18, 49, 71, 83
Lys R. 134
Lyutyy P. 26

M

Mahlik S. 12
Mahlovanyi B. 123, 124
Majewska N. 12
Majewski-Napierkowski A. 113
Maksymovych N. 84
Malynych S. 66
Manousaki A. 45, 63, 125
Mares J.A. 90, 95, 101
Margiani N.G. 15, 16
Marinko Ž. 79
Martynyuk-Lototska I. 151
Markovskyi A. 90, 99
Martin T. 113
Martynyuk G. 66
Martynyuk N.V. 130
Mateichenko P. 22
Matovic B. 11
Matsenko O.V. 11
Matushko I. 84
Matviiv R. 117
Medvid I.I. 127
Melnyk M. 119, 144
Minikayev R. 59
Mirus J. 123
Mitina N. 19
Monastyrov M. 57
Moos R. 78
Moshchil V. 57
Moshchil V.B. 11
Mrozik A. 111
Mudry S. 36
Mühlbauer M.J. 29
Mumladze G.A. 15, 16
Mykhaylyk V.B. 18, 31, 83
Mytsyk B. 146, 149

N

Nagirnyi V. 115
Nahurskyy O. 25
Nakonechna O.I. 55
Naumovich Y. 30
Navrotska I.P. 86
Nazar A.P. 68
Nedilko S. 34, 45, 58, 65, 125
Nedilko S.A. 59, 63
Nedilko S.G. 35, 59, 63, 110, 126
Nepokupnaya T. 80
Nevliudov I. 80
Nikl M. 90, 95, 100, 101
Nikolenko A.S. 140
Nizankovskiy S. 22, 90, 99
Nizankovsky S. 108
Nizankovskyi S. 24, 94
Novosad I. 114
Novosad S. 114
Nowak E. 13

O

Oleksenko L. 84
Olenych I. 82
Olkhovyk B. 149
Olutas M. 14, 97
Ostash O.P. 11
Ovsianyk R. 36
Ozdemir A. 96, 104, 120, 121
Ożga M. 9
Ozimek A. 124

P

Padlyak B.V. 107
Pankratov V. 143
Papadopoulos A. 45, 63, 125
Paprocki K. 111
Parandiy P. 72
Pashko Yu. 36
Paszkowicz W. 59
Pavlova N.Yu. 129, 130
Pavlyk B. 134
Pawlik P. 137
Péter L. 56
Petrenko O. 35
Pietruszka R. 9
Pinto R.G. 43
Pirko I. 25
Plutenko T.O. 131
Podhurska V.Ya. 11
Podust G.P. 129, 130
Ponomarov S.S. 11
Popov A.I. 92, 133
Popov V. 91
Popruha Yu.I. 67
Poshyvak O. 122
Prikhna T. 57
Prikhna T.A. 11
Prokopets V. 35
Prysiazhna O. 57
Purans J. 23

R

Rahimi Mosafer H.S. 59
Rakitskaya T.L. 67, 68
Ratych A. 47, 148
Razumov-Fryziuk I. 80
Reizer P. 123
Revo S. 58
Romanenko A. 108
Rudko M. 72, 114
Ryabchenko S.M. 55

S

Sahraoui B. 137, 141, 142
Salapak L. 25
Salapak V. 25
Salehabadi A. 73
Samsonenko M. 84
Savva K. 59
Savytskyy H. 135
Schegeda M. 58
Scherbatskii V. 45, 58, 125
Schmidt H. 76
Schökel A. 29
Schröder S. 75
Sedzicki P. 13
Senko I. 20
Sen'ko I. 146
Senyshyn A. 29
Serbenyuk T.B. 11
Seweryn A. 9
Shakhno A. 12, 112
Sharay I.V. 55
Shchepanskyi P. 117
Shchur Ya. 137, 140
Sheludko V. 125
Shimanovich D. 128
Shlapa Yu. 60
Shlapa Yu.Yu. 55
Shopa Y. 116
Shpotyuk M. 44
Shpotyuk O. 44, 153
Shpotyuk Y. 123, 124
Shtablavyi I. 36
Shulgov V. 21, 128
Shved V. 50
Sibilieva T. 80
Sidelnikova N. 24
Sidletskiy O. 90, 98
Siryk Yu. 22, 24, 108
Skowronski L. 106
Skvortsova V. 23
Slobodyanyk M. 35, 126
Sobolewski J. 119, 138, 139, 144
Sokur N.V. 105
Solopan S. 60
Solopan S.A. 69
Solopan S.O. 55
Solskyy I. 141
Sorokin B. 76
Sotnikov A. 76
Spassky D. 115
Stadnik V. 48, 62
Stadnyk V. 117
Stasiv V. 109
Stasyshyn I. 20
Stasyshyn I.V. 150
Steiner C. 78
Stratakis E. 59
Strelchuk V.V. 140
Strykhaluik B.M. 118
Stus N. 125
Suchaneck G. 93
Suchocki A. 102, 109, 110, 133
Sugak D. 103, 133
Suhadolnik L. 79
Suhak Yu. 76
Sverdun V.B. 11
Sybilski P. 110
Sydorchuk V. 17, 84, 85
Sypniewska M. 106
Syrotych Y. 90, 95
Syrotyuk S. 81
Syrotyuk S.V. 52
Syvorotka I. 135
Syvorotka I.I. 103, 133, 141
Syvorotka N.Ya. 141
Szczesny R. 106
Szlęzak J. 123
Szybowicz M. 13

T

Terebilenko K. 35, 126
Teselko P. 125
Teslyuk I. 140, 145
Teslyuk I.M. 107
Timashkov I. 60
Tkachenko S. 98
Tolmachova G.N. 11
Torchyniuk P.V. 61
Tovstolytkin A.I. 55
Tovstyuk C. 70
Truba A.S. 68
Trubitsyn M. 40, 45
Trubitsyn M.P. 88
Tsiumra V. 39
Tsizh B. 82
Tsvetkova O. 134
Tuller H.L. 75
Tupitsyna I. 34
Turchak S. 18
Turko B. 72
Tüzemen E.Ş. 38

U

Ubizskii S. 17, 48, 103, 110, 122, 133, 135

V

V'yunov O.I. 61, 131
Vasylechko L. 17, 18, 39, 48, 49, 50, 62, 71, 83
Vasylechko V.O. 86
Vasyliv B. 26
Vasyliv B.D. 11
Vasyltsiv V. 134
Vasylchyshyn I. 153
Vavrukh V. 26
Venhryn B. 36, 47, 150
Vira V. 26
Vistovskiy V. 111
Vitusevich S. 140
Voitenko T. 59, 63

Volianiuk K. 19
Volkova V.Y. 68
Volnianskii M. 45, 88
Voloshinovskii A. 111
Volynets D.V. 88
Voronyak T. 20
Vorovyak T.I. 151
Vovk O. 24, 108
Vovk O.M. 94
Vovk O.O. 22, 138, 139, 144
Vynnyk D. 20, 47, 119
Vynnyk D.M. 118

W

Warchoł A. 124
Waszkowska K. 141
Wielgosz R. 137
Witkiewicz-Łukaszek S. 12, 90, 98, 101, 113
Witkiewicz-Łukaszyk S. 95
Witkowski B.S. 9
Wnęk A. 124
Wollbrink A. 78
Wulfmeier H. 75, 77

Y

Yablochkov S. 125
Yakhnevych U. 103, 133
Yakovtseva V. 128
Yakubovskaya G. 34
Yaremchenko A. 33
Yaremchenko A.A. 43
Yaremko O. 144
Yashchyshyn E. 119
Yashchyshyn Y. 138, 139, 144
Yegingil Z. 96, 104, 120, 121
Yeğingil Z. 46
Yidak I. 47, 150
Yiğit Ö. 46, 53
Yoshikawa A. 90, 95, 100
Yukhymchuk V.O. 61

Z

Zadneprovski B. 115
Zaichenko A. 19
Zakutayev A. 10
Zaremba O. 41, 42
Zazubovich S. 39
Zelenskaya O. 98
Zelinskiy A. 71
Zhao L. 77
Zhghamadze V.V. 15, 16
Zhydachevskii Ya. 62
Zhydachevskyy Ya. 18, 39, 48, 49, 83, 102, 109, 110, 122, 133
Zięba P. 123
Zorenko T. 12, 90, 95, 98, 99, 100, 101, 111, 112, 113
Zorenko Yu. 12, 90, 95, 98, 99, 100, 101, 102, 111, 112, 113
Zubkins M. 23

TABLE OF CONTENTS

Preface 5

Conference Boards 6

Abstracts 7

Section 1. TECHNOLOGY OF FUNCTIONAL MATERIALS FABRICATION 8

M. Godlewski, R. Pietruszka, A. Seweryn, M. Ożga and B.S. Witkowski, Oxides by Atomic Layer Deposition - from Applications in Nano-Electronics to Photovoltaics 9

A. Zakutayev, Wide Band Gap Oxide Semiconductors for Electronics that Can Operate at High Temperature and High Power 10

T.A. Prikhna, O.P. Ostash, A.S. Kuprin, V.Ya. Podhurska, T. Cabioc`h, T.B. Serbenyuk, M.V. Karpets, B. Matovic, S.S. Ponomarov, V.B. Sverdun, B.D. Vasyliv, V.E. Moshchil, G.N. Tolmachova, M.A. Bortnitskaya, P. Barvitskyi and O.V. Matsenko, High-Temperature Oxidation of Ti-Al-C MAX Phases-Based Bulk Materials and Coatings, Variation of Their Electrical Conductivity 11

V. Gorbenko, T. Zorenko, A. Shakhno, S. Witkiewicz-Łukaszek, N. Majewska, T. Lesniewski, S. Mahlik and Yu. Zorenko, Growth and Optical Properties of Ce^{3+} Doped $Y_{3-x}Ca_xAl_2Al_{3-x}Si_xO_{12}$ (x=0-0.5) and $Gd_{3-x}Ca_xGa_2Al_{3-x}Si_xO_{12}$ (x=0-0.3) Single Crystalline Films 12

P. Sedzicki, E. Nowak, M. Szybowicz and B. Derkowska-Zielinska, Influence of Thermal Treatment on the Elimination of Impurities in ZnO Thin Films on Glass 13

A. Altinkok and M. Olutas, Structural Properties of Transparent IGZO Thin Films Produced by Thermal Evaporation Technique 14

G.A. Mumladze, I.G. Kvartskhava, V.V. Zhghamadze, N.G. Margiani and A.S. Kuzanyan, Effect of $Pb(BO_2)_2$ Doping on Power Factor of $Bi_2Sr_2Co_{1.8}O_y$ Thermoelectric Ceramics 15

V.V. Zhghamadze, N.G. Margiani, A.I. Klyndyuk, G.A. Mumladze, A.S. Kuzanyan, I.G. Kvartskhava and G.R. Badalyan, Improvement of $Bi_2Ca_2Co_{1.7}O_y$ Thermoelectric Properties by $Pb(BO_2)_2$ Doping 16

V. Sydorchuk, V. Hreb, S. Ubizskii, S. Khalameida and L. Vasylechko, Hydrothermal Synthesis, Structure and Luminescence of Cr^{3+}-Doped Stannates Li_2SnO_3, Na_2SnO_3 and Li_8SnO_6 17

I. Lutsyuk, V. Hreb, S. Turchak, Ya. Zhydachevskyy, V.B. Mykhaylyk and L. Vasylechko, Sol-Gel and Solid State Synthesis of Cation-Deficient Perovskites Formed in $CaTiO_3$-$La_{2/3}TiO_3$ Pseudo-Binary System 18

O. Izhyk, N. Mitina, A. Zaichenko, K. Volianiuk, I. Grygorchak and O. Balaban, Unexpected Conductivity of Anionic and Cationic Polyelectrolyte Nanobrushes on Flat Ceramic Surfaces 19

T. Voronyak, D. Vynnyk, N. Andrushchak, I. Stasyshyn, I. Senko and A. Andrushchak, The Peculiarities of Experimental Determination of the Acousto-Optic Efficiency of Oxide Crystals 20

V. Shulgov, Investigation of the Electrophysical Properties of Dense Anodic Aluminum Oxide Films 21

O.O. Vovk, S. Nizhankovskiy, Yu. Siryk and P. Mateichenko, Diffusion of Cobalt Ions into Crystals of Non-Stoichiometric Magnesium Aluminate Spinel $MgO{\bullet}xAl_2O_3$ 22

V. Skvortsova, M. Zubkins, R. Kalendarev, H. Arslan and J. Purans, Zinc-Iridium Oxide Thin Films Fabrication and Properties 23

S. Nizhankovskyi, A. Kozlovskyi, O. Vovk, N. Sidelnikova and Yu. Siryk, Optical Properties of $MgAl_2O_4$ Crystals Grown by Iridium-Free Technology 24

V. Salapak, S. Kachan, O. Nahurskyy, I. Pirko and L. Salapak, Theoretical Study of the Effectiveness of Radiation Coloring of the Thallium-Containing Fluorite Crystals 25

V. Kulyk, Z. Duriagina, B. Vasyliv, T. Kovbasiuk, P. Lyutyy, V. Vira and V. Vavrukh, The Effect of Sintering Temperature on Crack Growth Resistance Characteristics of Yttria-Stabilized Zirconia Determined by Various Test Methods 26

D. Kaya, I. Adanur, M. Akyol, F. Karadag and A. Ekicibil, Chemically Synthesized Binary Pd-Co Alloys: Structural and Magnetic Properties 27

Section 2. MATERIALS FUNDAMENTALS: CRYSTAL STRUCTURE, DEFECTS, INTERACTIONS 28

A. Senyshyn, V. Kochtetov, M.J. Mühlbauer, A. Schökel and M. Hofmann, Diffraction Computed Tomography and Its Applications 29

Y. Naumovich, Quantitative Description of Oxygen Non-Stoichiometry in Mixed Ionic and Electronic Conductors Based on a Non-Ideal Solution Approach 30

V.B. Mykhaylyk, Foray into Non-Contact Luminescence Cryothermometry Enabled by Oxides 31

A. Lushchik, Characterization of Radiation-Induced Point Defects via EPR and Optical Spectroscopy in Oxides 32

A. Yaremchenko, Thermochemical Expansion: Constraints for the High-Temperature Processing and Operation of Perovskite-Related Oxides 33

Yu. Hizhnyi, S. Nedilko, V. Chornii, I. Tupitsyna, O. Dubovik and G. Yakubovskaya, Revealing the Luminescence Mechanisms in Li_2MoO_4 Scintillation Crystals by Complex Experimental and Computational Studies 34

V. Chornii, V. Boyko, S.G. Nedilko, O. Petrenko, V. Prokopets, K. Terebilenko and M. Slobodyanyk, Synthesis and Luminescence Properties of Pure and Doped with Europium(III) $A_{0.5x}Bi_{1-0.5x}Mo_xV_{1-x}O_4$ (A – Na, K) Compounds 35

I. Shtablavyi, R. Ovsianyk, S. Mudry, B. Venhryn, Yu. Pashko and Yu. Kulyk, Temperature Dependence of Nickel Oxide Wetting with Liquid Tin 36

Yu.G. Kazarinov, V.T. Gritsyna and S.P. Gokov, Optical Absorption of the Transparent Spinel Ceramics after High Energy Electron Irradiation and Thermal Annealing 37

D. Kaya, H.S. Aydınoğlu, E.Ş. Tüzemen and A. Ekicibil, Formation of p-Type NiO Thin Films on Different Substrates: Structural, Electrical, Optical, and Magnetic Properties 38

V. Tsiumra, M. Baran, A. Kissabekova, A. Krasnikov, A. Lushchik, Ya. Zhydachevskyy, L. Vasylechko and S. Zazubovich, Luminescence and Energy Transfer Processes in $LuNbO_4$:Bi,Eu 39

D. Bondar, T. Bochkova, M. Trubitsyn and M. Volnyanskii, Photoinduced Effects in the Single Crystals of PbO – MoO_3 System 40

O. Zaremba, V. Hrytsan and R. Gladyshevskii, Four-Component Perovskites in the *A*–*R*–Fe–O Systems at 1200°C (*A* – Alkaline-Earth, *R* – Rare-Earth Metal) 41

V. Kordan, O. Zaremba and P. Demchenko, Electrochemical Synthesis of $Li_yCa_{1-x}Nd_xMnO_3$ Solid Solution 42

R.G. Pinto, B.I. Arias-Serrano and A.A. Yaremchenko, Ionic and Electronic Transport in Acceptor-Doped $PrVO_4$ 43

M. Shpotyuk and O. Shpotyuk, Theoretical Estimation of Compositional Variations in Glass-Transition Temperature of Chalcogenide Glass Systems from Stochastic Agglomeration Theory and Covalent Bond Approach 44

M. Trubitsyn, M. Koptiev, M. Volnianskii, S. Nedilko, V. Scherbatskii, M. Androulidaki, A. Papadopoulos and A. Manousaki, Growth, Optical Properties and Conductivity of the Lithium Heptagermanate Crystals Doped with Rare - Earth and 3d Ions 45

T. Çavdar, V. Güçkan, Ö. Yiğit, Z. Yeğingil and K. Kurt, Influence of Dy^{3+} on Luminescence Spectra Emission of $CaSO_4$ under X-Ray Excitation 46

D. Vynnyk, B. Venhryn, A. Ratych, I. Yidak and A. Andrushchak, Features of Experimental Determination of the Coefficient of Acousto-Optical Quality of Crystalline Materials 47

V. Hreb, V. Stadnik, S. Ubizskii, A. Kondyr, A. Luchechko, Ya. Zhydachevskyy and L. Vasylechko, Structure and Luminescence Properties of Cr-Doped $CaAl_4O_7$ and $CaGa_4O_7$ Crystalophosphors 48

V. Hreb, I. Lutsyuk, A. Luchechko, Ya. Zhydachevskyy and L. Vasylechko, Influence of Synthesis Conditions on Luminescence Properties of Cr/Er/Yb Co-Doped $LiGa_5O_8$ Spinel-Type Materials 49

V. Shved, V. Hreb and L. Vasylechko, Electronic Structure and Magnetic Properties of $SmCo_{0.5}Cr_{0.5}O_3$ from First Principles 50

K. Labisz, R. Bendikienė and J. Konieczny, Influence of Electron Beam Alloying on Structure and Properties of Cast Aluminium Surface 51

S.V. Syrotyuk, The Spin-Polarized Electronic Structure in the Crystal ZnTe:Cr without and with a Cationic Vacancy 52

K. Kurt, T. Çavdar and Ö. Yiğit, Influence of Lanthanides on Luminescence Spectrum Emission of BeO under X-Ray Excitation 53

Section 3. NANOPARTICLES, NANO-CERAMICS AND NANO-COMPOSITES 54

A.I. Tovstolytkin, O.I. Nakonechna, I.V. Sharay, A.V. Bodnaruk, V.M. Kalita, S.M. Ryabchenko, Yu.Yu. Shlapa, S.O. Solopan and A.G. Belous, Advanced Magnetic Nanostructures for Biomedical Applications 55

L. Kovács, K. Lengyel, L. Kocsor, L. Péter and G. Corradi, Lithium Niobate: from Single Crystals to Nanocrystals 56

T. Prikhna, M. Monastyrov, O. Prysiazhna, B. Halbedel, V. Moshchil and P. Brvitskyi, Properties and Application of Nanopowders of Polyvalent Iron Oxides Obtained by Electroerosion Dispersion 57

S. Nedilko, O. Alekseev, V. Barbash, V. Chornii, K. Krolenko, M. Lazarenko, S. Revo, M. Schegeda and V. Scherbatskii, Structure and Properties of Micro and Nanostructured Cellulose Films Incorporated with Oxides and Carbon Particles 58

O. Chukova, S.A. Nedilko, S.G. Nedilko, T. Voitenko, M. Androulidaki, K. Savva, E. Stratakis, H.S. Rahimi Mosafer, R. Minikayev and W. Paszkowicz, Pulsed Laser Deposition of Luminescent Downshifting Coatings on Silicon Solar Cells 59

Yu. Shlapa, S. Solopan, I. Timashkov and A. Belous, Synthesis of CeO_2 Nanoparticles by Precipitation in the Solutions and Their Physical-Chemical Properties 60

P.V. Torchyniuk, O.I. V'yunov, V.O. Yukhymchuk, O.M. Greshchuk and A.G. Belous, Phase Transformations at the Synthesis of Organic-Inorganic Perovskites $CH_3NH_3PbI_3$ 61

V. Stadnik, V. Hreb, Ya. Zhydachevskii and L. Vasylechko, Sol-Gel Combustion Synthesis, Crystal Structure and Luminescence of Cr- and Mn-Doped $SrAl_4O_7$ Nanopowders 62

O. Chukova, S.A. Nedilko, S.G. Nedilko, T. Voitenko, A. Manousaki and A. Papadopoulos, Development of the Borate Glasses Incorporated with La-Vanadate Nanoparticles 63

V. Dutka and Ya. Kovalskyi, Features of Obtaining Polymer Composites Based on Disperse Oxides and Vinyl Polymers 64

Yu. Hizhnyi, S. Nedilko and V. Borysiuk, Interaction of Chromate Oxyanions with Carbon Nanostructures: TD-DFT Calculations of Excited Electronic States and Possibility of the Optical Monitoring 65

R. Filipsonov, G. Martynyuk, S. Malynych and O. Aksimentyeva, Bifunctional Polymer-Magnetite Composites 66

T.L. Rakitskaya, T.A. Kiose and Yu.I. Popruha, Nanocatalysts for Carbon Monoxide Oxidation Based on the Acid Modified Polyphase Aluminosilicate Support and Contained Palladium(II) and Copper(II) Salts 67

T.L. Rakitskaya, A.S. Truba, A.P. Nazar, T.A. Kiose and V.Y. Volkova, Synthesis, Phase Transformations of Polymorphous Nanooxidic Forms of Iron and Their Interaction with Sulfur Dioxide 68

I.V. Lisovskyi, S.A. Solopan, A.G. Belous and V.G. Khomenko, Hybrid Solid Electrolyte Based on the Combination of $Li_{1.3}Al_{0.3}Ti_{1.7}(PO_4)_3$ Ceramic and Liquid Solution with $LiPF_6$ for Li-Ion Batteries 69

C. Tovstyuk, Dynamic Dielectric Function of Two-Dimensional Electron Gas 70

I. Lutsyuk, V. Hreb, A. Zelinskiy and L. Vasylechko, Sol-Gel Synthesis of $ZnAl_2O_4$, $MgGa_2O_4$ and $LiGa_5O_8$ Nanopowders Co-Doped with Cr^{3+}, Er^{3+} and Yb^{3+} Ions 71

M. Rudko, P. Parandiy and B. Turko, Porous Silicon Surface Modified and Incorporated by ZnO 72

M. Enhessari and A. Salehabadi, Synthesis and Characterization of $CuMn_2O_4$ Nanoparticles: a Potential Semiconductor for Photoelectric Devices 73

Section 4. MATERIALS FOR SENSING AND CATALYSIS 74

H. Fritze, H. Wulfmeier, T. Defferiere, S. Schröder and H.L. Tuller, Nonstoichiometry and Chemical Expansion of Cerium Oxide Based Thin Films 75

Yu. Suhak, W. Johnson, A. Sotnikov, H. Schmidt, B. Sorokin and H. Fritze, Contributions to Acoustic Loss in Piezoelectric CTGS ($Ca_3TaGa_3Si_2O_{14}$) Resonators 76

H. Wulfmeier, R. Feder, L. Zhao and H. Fritze, High-Temperature Stable Thin-Film Oxide Electrodes for Langasite and Catangasite Resonators 77

I. Kogut, A. Wollbrink, C. Steiner, R. Moos and H. Fritze, Non-Stoichiometry of Thin-Film $Ce_{1-x}Zr_xO_{2-\delta}$ Characterized by a Resonant Nanobalance 78

M. Čeh, L. Suhadolnik and Ž. Marinko, TiO_2-Nanotubes-Based Reactors for Highly Efficient Photocatalytic and Photoelectrocatalytic Degradation of Organic Compounds 79

T. Sibilieva, A. Boyarintsev, B. Grinyov, A. Krech, T. Nepokupnaya, I. Nevliudov and I. Razumov-Fryziuk, 3D-Printed Scintillators with Inorganic Powders for X-Ray Imaging 80

Yu. Klysko and, Guest-Tuned Spin Crossover in Metal-Organic Frameworks 81

Yu. Horbenko, B. Tsizh, M. Dzeryn, I. Olenych, O. Aksimentyeva and V. Bogatyrev, Sensitive Elements of Gas Sensors Based on Poly-*o*-Toluidine/Silica Nanoparticles Composite 82

V. Hreb, I. Lutsyuk, K. Blazhivskyi, Ya. Zhydachevskyy, V.B. Mykhaylyk and L. Vasylechko, Cr-Doped Solid Solutions $La(Ga_{1-x}Al_x)O_3$ and $(La_{1-x}Sr_x)(Al_{1-x}Ti_x)O_3$ for Possible Luminescence Temperature Sensor Application 83

I. Matushko, S. Khalameida, M. Samsonenko, V. Sydorchuk, L. Oleksenko, N. Maksymovych and O. Khyzhun, Effect of Mechanochemical and Microwave Modification of SnO_2 Nanomaterials on Properties of Hydrogen Sensors 84

V. Sydorchuk, S. Levytska, L. Kotynska and L. Kuznetsova, Modification of Zn-Al Hydrotalcite as Potential Photocatalyst 85

V.O. Vasylechko, G.V. Gryshchouk, Ya.M. Kalychak, R.E. Gladyshevskii, I.P. Navrotska and S.R. Bagday, Sorption of Lead on Na-Modified Transcarpathian Clinoptilolite 86

K. Khrushchyk and L. Boichyshyn, Oxide-Hydroxide Layers on the Surface of Al-Gd-Ni(Fe) Amorphous Alloy Ribbons and Their Capacitive Properties 87

A.O. Diachenko, M.P. Trubitsyn, M. Volnianskii and D.V. Volynets, Electrical Properties of Lithium-Sodium Tetragermanate Single Crystal 88

Section 5. MATERIALS FOR QUANTUM AND OPTO-ELECTRONICS AND DETECTORS OF RADIATION 89

V. Gorbenko, A. Markovskyi, Y. Syrotych, S. Witkiewicz-Lukaszek, T. Zorenko, J.A. Mares, M. Nikl, O. Sidletskiy, S. Nizhankovskiy, K. Kamada, A. Yoshikawa and Yu. Zorenko, Development of Advanced Composite Scintillators and LED Converters Based on the Epitaxial Structures of Garnet Compounds 90

N. Galunov, Ya. Gerasimov, N. Karavaeva, A. Krech, T. Gorbacheva, I. Khromiuk, D. Kofanov, L. Levchuk and V. Popov, Oxide Composite Scintillation Materials for High-Energy Radiation Detectors 91

A.I. Popov, E.A. Kotomin, V.N. Kuzovkov and A. Lushchik, Thermal Annealing of Point Defects in Irradiated Functional Ceramics for Nuclear Applications 92

G. Suchaneck, E. Artiukh and G. Gerlach, The Different Magnetoresistance Mechanisms of $Sr_2FeMoO_{6-\delta}$ Ceramics 93

O.M. Vovk, S. Nizhankovskyi, P. Dluzewski, A. Kozłowska and M. Chaika, YAG:Ce-Al_2O_3 Eutectics Grown by Horizontal Directed Crystallization as Luminescent Converter of White SSL Driven by High Power Laser Diodes 94

Y. Syrotych, V. Gorbenko, S. Witkiewicz-Łukaszyk, T. Zorenko, M. Kaczmarek, A. Yoshikawa, K. Kamada, J.A. Mares, M. Nikl, R. Kucerkova, A. Fedorov and Yu. Zorenko, Scintillation Properties of Composite Scintillators Based on TAG:Ce Single Crystalline Films and GAGG:Ce Crystal Substrates 95

V. Guckan, V. Altunal, W. Abusaid, A. Ozdemir and Z. Yegingil, Study of Enhancement the TL/OSL Intensities of $KMgF_3$ Perovskites 96

A. Altinkok and M. Olutas, Electrothermal Properties in Highly Transparent and Resistive Thin Film of Thermally Evaporated Indium-Tin-Oxide 97

Ia. Gerasymov, O. Sidletskiy, Ya. Boyaryntseva, S. Tkachenko, P. Arhipov, E. Galenin, D. Kurtsev, O. Zelenskaya, V. Alekseev, S. Witkiewicz-Lukaszek, T. Zorenko and Yu. Zorenko, Alkaline Earth and Alkali Metals Impurities Effect on Optical and Scintillation Properties of YAG:Ce Single Crystals 98

A. Markovskyi, V. Gorbenko, K. Bartosiewicz, T. Zorenko, S. Nizhankovskiy, A. Fedorov and Yu. Zorenko, Development of Novel Film and Composite Color Converters for White LEDs Based on the Epitaxial Structures of $Lu_{3-x}Tb_xAl_5O_{12}$:Ce (x = 1-2) Garnet Using Liquid Phase Epitaxy Growth Method 99

K. Bartosiewicz, V. Gorbenko, T. Zorenko, M. Nikl, K. Kamada, A. Yoshikawa and Yu. Zorenko, Growth and Luminescent Properties of the Single Crystalline Films and Single Crystals of $Lu_{3-x}Gd_xAl_5O_{12}$:Ce Garnets 100

S. Witkiewicz-Lukaszek, V. Gorbenko, T. Zorenko, J.A. Mares, M. Nikl and Yu. Zorenko, Three-Layered Composite Scintillator Based on the Ce^{3+} and Sc^{3+} Doped YAG and LuAG Garnets for Simultaneous Registration of α-, β-Particles and γ-Quanta 101

L.-I. Bulyk, A. Kumar Somakumar, P. Ciepielewski, Yu. Zorenko, Ya. Zhydachevskyy, I. Kudrjavtseva, V. Gorbenko, A. Lushchik and A. Suchocki, High-Pressure Studies of Ce^{3+} Luminescence in Epitaxial $LuAlO_3$ Single Crystalline Film 102

U. Yakhnevych, D. Sugak, I.I. Syvorotka, O. Buryy and S. Ubizskii, Determination of the Diffusion Incorporation Mechanism of Cu Ions into LiNbO3 by Studying of Spatial Changes of Crystal Properties 103

V. Altunal, V. Guckan, A. Ozdemir, W. Abusaid, A. Ekicibil, F. Karadag and Z. Yegingil, Luminescence Characterization of BeO:$Na_{5\%}$,$Ce_{0.01\%}$,$Er_{0.01\%}$ Ceramic 104

N.V. Sokur, AMoRE: a Low Temperature Bolometric Experiment to Search for Double Beta Decay of ^{100}Mo with Molybdate Crystal Scintillators 105

M. Sypniewska, R. Szczesny, L. Skowronski and B. Derkowska-Zielinska, Optical and Structural Properties of ZnO:Alq_3 Thin Layers Dispersed in Various Polymer Matrices 106

B.V. Padlyak, I.I. Kindrat, B. Kukliński, A. Drzewiecki, V.T. Adamiv and I.M. Teslyuk, Luminescence Properties of the Sm^{3+} Centres in the Sm-Ag Co-Doped Glasses with $Li_2B_4O_7$ Composition 107

Yu. Siryk, O. Vovk, L. Gryn, A. Romanenko, V. Baranov and S. Nizhankovsky, Eutectic Composites in Al_2O_3–Y_2O_3 System Solidified by Horizontal Directed Crystallization Method 108

M. Głowacki, J. Fink-Finowicki, V. Stasiv, Ya. Zhydachevskyy, R. Diduszko, M. Berkowski and A. Suchocki, (Y,Gd)AlO_3 Perovskite Solid Solution Single Crystals Doped with Mn and Hf Grown by the Czochralski and Floating Zone Methods 109

Ya. Zhydachevskyy, Yu. Hizhnyi, S.G. Nedilko, M. Głowacki, P. Sybilski, M. Berkowski, S. Ubizskii and A. Suchocki, Optical Properties and Electronic Structure of $R$$AlO_3$ (R = La, Gd, Y, Yb, Lu) Perovskite 110

W. Gieszczyk, P. Bilski, A. Mrozik, V. Vistovskiy, A. Voloshinovskii, A. Fedorov, K. Paprocki, T. Zorenko and Yu. Zorenko, Luminescent and Scintillation Properties of Sc^{3+} and La^{3+} Doped $LuAlO_3$ Crystals 111

A. Shakhno, W. Gieszczyk, P. Bilski, T. Zorenko and Yu. Zorenko, Luminescent Properties and Multi-Centres Formation in Ce-Doped $Ca_3Sc_2Si_3O_{12}$ Single Crystals 112

A. Majewski-Napierkowski, P.A. Douissard, T. Martin, T. Zorenko, S. Witkiewicz-Łukaszek and Yu. Zorenko, Energy Transfer Processes in LuAG:Ce,Pr Single Crystalline Film Scintillators 113

L. Kostyk, V. Kapustyanyk, S. Novosad, I. Novosad and M. Rudko, Recombination Luminescence of Zinc Tungstate Crystals Doped with Lithium, Terbium and Neodymium 114

N. Krutyak, V. Nagirnyi, D. Spassky and B. Zadneprovski, Luminescent Properties of $Zn_xCd_{1-x}WO_4$ Solid Solutions 115

N. Ftomyn and Y. Shopa, Investigation of the Optical Activity of $Ca_3Ga_2Ge_4O_{14}$ Crystals 116

R. Matviiv, V. Stadnyk, R. Brezvin, P. Shchepanskyi and R. Kildiyarov, Refractive and Dilatometric Properties of Doped K_2SO_4 Crystals 117

D.M. Vynnyk, M.V. Kaidan, A.S. Andrushchak and B.M. Strykhaluik, Spatial Anisotropy of Electromechanical Coupling in $Li_2B_4O_7$ Crystals 118

N. Andrushchak, D. Vynnyk, M. Melnyk, P. Bajurko, J. Sobolewski, V. Haiduchok, A. Andrushchak and E. Yashchyshyn, Modulation of Terahertz Radiation by Bismuth Germanate Crystals 119

W. Abusaid, V. Altunal, A. Ozdemir, V. Guckan, A. Ekicibil, F. Karadag and Z. Yegingil, Optically Stimulated Luminescence of MgB_4O_7 Doped with Ce^{3+} and Gd^{3+} 120

S. Bereket, V. Guckan, V. Altunal, W. Abusaid, A. Ozdemir and Z. Yegingil, OSL Properties of $CaSO_4$:Tb,Eu Phosphor for Dosimetric Purpose 121

O. Poshyvak, D. Afanassyev, A. Luchechko, Ya. Zhydachevskyy and S. Ubizskii, Afterglow Peculiarities of YAP:Mn Crystal Irradiated by X-Ray and Visible Radiation 122

P. Zięba, P. Reizer, J. Mirus, B. Mahlovanyi, J. Szlęzak, J. Cebulski and Y. Shpotyuk, Optical Characterization of Rare-Earth Doped Bi-Modified Borate Glasses 123

B. Mahlovanyi, A. Ozimek, A. Wnęk, A. Warchoł, A. Luchechko, J. Cebulski and Y. Shpotyuk, Optical and Luminescence Properties of Ce, Dy-Doped Lithium Borate Glasses 124

N. Stus, S. Nedilko, S. Yablochkov, P. Teselko, V. Scherbatskii, M. Androulidaki, A. Papadopoulos, A. Manousaki, V. Sheludko and O. Gomenyuk, Effect of Metal Oxides on Structure and Properties of the Borate-Phosphate Glasses 125

V. Chornii, S.G. Nedilko, K. Terebilenko, O. Alekseev, M. Lazarenko and M. Slobodyanyk, Optical Properties and Phase Transformation of Bismuth Phosphate-Molybdate Glasses 126

O.M. Bordun, I.O. Bordun, I.M. Kofliuk, I.Yo. Kukharskyy and I.I. Medvid, Spectral and Kinetic Characteristics of the Cathodoluminescence of Thin Films Y_2O_3:Eu 127

V. Yakovtseva, D. Shimanovich and V. Shulgov, Anodic Alumina Membranes: Light Scattering Intensity Along the Pores as a Function of Incidence Angles 128

N.Yu. Pavlova, V.Ya. Degoda, I.Yu. Doroshenko and G.P. Podust, Extrinsic Luminescence Quenching in ZnSe Crystals 129

G.P. Podust, V.Ya. Degoda, N.Yu. Pavlova and N.V. Martynyuk, The Parameters of Deep Traps Causing the Dark Conductivity of ZnSe Single Crystals 130

T.O. Plutenko, O.I. V'yunov, L.L. Kovalenko, O.P. Fedorchuk and A.G. Belous, Materials with High Permittivity Based on Ferroelectric and Ion-Conducting Systems 131

A. Bendak and N. Andrushchak, The Possibility of Selenium Application in THz Range 132

D. Sugak, I.I. Syvorotka, M. Kushlyk, U. Yakhnevych, Ya. Zhydachevskyy, A.I. Popov, O. Buryy, S. Kachan, S. Ubizskii and A. Suchocki, Optical Recharging of Complex Color Centers and Cobalt Ions in $Gd_3Ga_5O_{12}$:Co Crystals 133

V. Vasyltsiv, A. Luchechko, L. Kostyk, R. Lys, O. Tsvetkova, M. Kushlyk and B. Pavlyk, Correlation Between Optical and Electrical Properties in β-Ga_2O_3 Single Crystals 134

I. Syvorotka, H. Savytskyy and S. Ubizskii, The Growth and Properties of Sub-Micron Thin YIG-Based LPE Films Using Different Fluxes 135

Section 6. INNOVATIVE OPTICAL/QUASIOPTICAL TECHNOLOGIES AND NANO ENGINEERING OF ANISOTROPIC MATERIALS 136

A.V. Kityk, P. Huber, A. Andrushchak, R. Wielgosz, B. Sahraoui, M. Lelonek, P. Göring, N. Andrushchak, Ya. Shchur and P. Pawlik, Liquid Crystal Nanocomposites: Optical Anisotropy, Dynamical Properties and Symmetry Aspects 137

J. Sobolewski, P. Bajurko, D. Vynnyk, V. Haiduchok and Y. Yashchyshyn, Investigation of the Millimeter Wave Coplanar Waveguide (CPW) Modulator Based on Semiconductor Substrates 138

P. Bajurko, J. Sobolewski, D. Vynnyk, V. Haiduchok, N. Andrushchak and Y. Yashchyshyn, Properties of $CaWO_4$ and $CaMoO_4$ Crystals in the Subterahertz Frequency Range 139

Ya. Shchur, A.V. Kityk, V.V. Strelchuk, A.S. Nikolenko, G. Beltramo, S. Vitusevich, N. Andrushchak, V. Adamiv, I. Teslyuk, P. Huber and A.S. Andrushchak, On the Issue of Nanoscale KH_2PO_4 and $Ba(NO_3)_2$ Crystals Grown in Porous SiO_2 Matrix: Raman Spectroscopy, X-Ray Diffraction and *Ab Initio* Lattice Dynamics Analysis 140

I.I. Syvorotka, D. Guichaoua, I. Solskyy, N.Ya. Syvorotka, K. Waszkowska and B. Sahraoui, Phase-Matched Magnetization-Induced Second-Harmonic Generation in Epitaxial Iron Garnet Thin Films 141

O. Buryy, N. Andrushchak, A. Danylov, B. Sahraoui and A. Andrushchak, The Optimal Vector Phase Matching Conditions for Second Harmonic Generation in Biaxial Non-Linear Optical Crystals 142

V. Pankratov, Luminescence Spectroscopy of Oxide Nanoparticles under Synchrotron Radiation Excitations 143

N. Andrushchak, D. Vynnyk, M. Melnyk, P. Bajurko, J. Sobolewski, V. Haiduchok, A. Andrushchak and Y. Yashchyshyn, Modulation of Subterahertz Radiation by Bismuth Germanate Crystals 144

V. Adamiv, O. Yaremko, I. Teslyuk and A. Andrushchak, Research of Nanocrystallites Based on Al_2O_3 Nanoporous Membranes from Saturated Aqueous Solutions of KH_2PO_4 145

A. Danylov, I. Sen'ko and A. Andrushchak, Preliminary Studies of Second Harmonic Generation in Crystalline Nanocomposites 146

B. Mytsyk, N. Demyanyshyn, O. Buryy and A. Andrushchak, The Peculiarities of Piezo-Optic Effect in Crystals with Periodical Change of Refractive Index 147

A. Ratych, I. Karbovnyk and N. Andrushchak, LabVIEW-Powered Instrumentation for Accurate Interferometric Measurements of Refractive Indices 148

Z. Kohut, O. Korneyev, B. Olkhovyk, B. Mytsyk and A. Andrushchak, Experimental Measurements of Electo-Optic Coefficients for $LiTaO_3$ Crystals 149

B. Venhryn, O. Balaban, I. Yidak and A. Andrushchak, The Effect of Nanoconfinement in Functional Materials for Electrical Energy Storage Devices 150

I.V. Stasyshyn, T.I. Vorovyak, I. Martynyuk-Lototska and A.S. Andrushchak, Study of the Process of Acoustic Wave Wear in Monocrystalline Materials 151

H. Klym, Yu. Kostiv, A. Ingram, L. Luchechko and I. Karbovnyk, Nanoporous Characterization of Eu^{3+} Doped $BaGa_2O_4$ Ceramics 152

H. Klym, I. Hadzaman, O. Shpotyuk and I. Vasylchyshyn, Structural Peculiarities of Multilevel Thick Films for Active Media of Sensor Systems 153

Authors Index 154

PHOTONICS

перший професійний каталог оптоелектроніки

- оптика, оптомеханіка
- лазери
- спектрометри оптичні, аксесуари
- раманівська спектрометрія
- системи вимірювань, аналізу та реєстрації
- аналітичне обладнання

ТОВ «СЕЛТОК ФОТОНІКС»
тел.: (044)351 16 05
office@seltokphotonics.com
www. seltokphotonics.com

ЕЛЕКТРОННЕ НАУКОВЕ ВИДАННЯ

Збірник тез

Міжнародної наукової конференції “Оксидні матеріали електронної техніки – отримання, властивості, застосування”

OMEE-201

28 вересня – 2 жовтня, 2021
Львів, Україна

Режим доступу:

http://science.lpnu.ua/omee-2021/book-abstracts-omee-2021

Відповідальний за випуск *М. В. Шпотюк*

Видавець і виготівник: Видавництво Львівської політехніки
Свідоцтво суб’єкта видавничої справи ДК № 4459 від 27.12.2012 р.

вул. Ф. Колесси, 4, Львів, 79013
тел. +380 32 2584103, факс +380 32 2584101
vlp.com.ua, ел. пошта: vmr@vlp.com.ua